Gravity and the Hierarchical Universe: The Milky Way Lights the Way

Richard Reade Lane

A thesis submitted for the degree of
Doctor of Philosophy
at the University of Sydney

July 2010

Abstract

Despite recent advancements in instrumentation and analysis techniques, galactic evolution is poorly understood. It has become apparent that observations of our own Milky Way can be extremely useful in tackling this long-standing problem; due to our location within the Milky Way we have the perfect vantage point for detailed observations of various phenomena which may not be apparent in distant galaxies. This thesis is comprised of a series of papers published in various astronomical journals over the years 2007–2009. The overarching motive is the understanding of galactic, and subgalactic hierarchical merging, its relation to the evolution of spiral galaxies, and how this relates to to the Λ Cold Dark Matter structure formation paradigm at small scales. This thesis is divided into two separate, but intimately related sections, each divided into subchapters to form a coherent structure. The focus of Chapter 2 is testing Newtonian gravity in the weak acceleration regime and quantifying the dark matter content of globular clusters, which are analysed in the context of structure formation. Other important properties of globular clusters are also investigated, including their isothermal rotations, metallicities, and tidal heating by the Milky Way disc. Chapter 3 centres around the Monoceros Ring, a ring of stellar material which encircles the plane of the Milky Way, and its involvement in the evolution of the Milky Way disc. The largest pinhole survey of the Monoceros Ring is presented, with ten new detections tracing the Ring almost entirely around the Milky Way plane. The results presented are strongly indicative of its origin being external to the Milky Way, and that it is, therefore, most likely the only known, extant, in-plane accretion event in the Milky Way system.

Statement of Originality

This thesis describes work carried out in the Sydney Institute for Astronomy, within the School of Physics, University of Sydney, between March 2006 and December 2009. The work presented in this thesis is, to the best of my knowledge and belief, original except as acknowledged in the text. I hereby declare that I have not submitted this material, either in full or in part, for a degree at this or any other institution.

....
Richard Reade Lane Date

Publications Included in this Thesis

The original research contained in this thesis is presented in the form of journal articles published by peer-reviewed journals. All of the papers consist of research conducted by myself, in consultation with my supervisor Geraint Lewis, co-supervisor Rodrigo Ibata, and other collaborators. Details of my contribution to each work are provided in the introductions to each subchapter, immediately preceding the paper.

"Halo globular clusters observed with AAOmega: dark matter content, metallicity and tidal heating." **Richard R. Lane**, László L. Kiss, Geraint F. Lewis, Rodrigo A. Ibata, Arnaud Siebert, Timothy R. Bedding, Péter Székely, Zoltán Balog and Gyula M. Szabó, 2010, *MNRAS, DOI: 10.1111/j.1365-2966.2010.16874.x*

"AAOmega observations of 47 Tucanae: evidence for a past merger?" **Richard R. Lane**, Brendon J. Brewer, László L. Kiss, Geraint F. Lewis, Rodrigo A. Ibata, Arnaud Siebert, Timothy R. Bedding, Péter Székely and Gyula M. Szabó, 2010, *ApJ Letters, 711, L122-L126*

"Testing Newtonian gravity with AAOmega: mass-to-light profiles and metallicity calibrations from 47 Tuc and M55." **Richard R. Lane** , László L. Kiss, Geraint F. Lewis, Rodrigo A. Ibata, Arnaud Siebert, Timothy R. Bedding and Péter Székely, 2010, *MNRAS, 401, 2521-2530*

"Testing Newtonian gravity with AAOmega: mass-to-light profiles of four globular clusters." **Richard R. Lane**, László L. Kiss, Geraint F. Lewis, Rodrigo A. Ibata, Arnaud Siebert, Timothy R. Bedding and Péter Székely, 2009, *MNRAS 400, 917-923*

"The Anglo-Australian Telescope/Wide Field Imager survey of the Monoceros Ring and Canis Major dwarf galaxy - II. From $l = (280 - 025)^{\circ}$." Blair C. Conn, **Richard R. Lane**, Geraint F. Lewis, Mike J. Irwin, Rodrigo A. Ibata, Nicolas F. Martin, Michele Bellazzini and Artem V. Tuntsov, 2008, *MNRAS 390, 1388-1398*

"The AAT/WFI survey of the Monoceros Ring and Canis Major dwarf galaxy - I. From $l = (193 - 276)^{\circ}$." Blair C. Conn, **Richard R. Lane**, Geraint F. Lewis, Rodrigo Gil-Merino, Mike J. Irwin, Rodrigo A. Ibata, Nicolas F. Martin, Michele Bellazzini, Robert Sharp, Artem V. Tuntsov and Annette M. N. Ferguson, 2007, *MNRAS 376, 939-959*

Publications Not Included in this Thesis

"Surveying the Monoceros Ring: locations, velocities and a contentious dwarf." Blair C. Conn, Geraint F. Lewis, **Richard R. Lane**, Rodrigo A. Ibata, Nicolas F. Martin and Mike J. Irwin, 2008, *Galaxies in the Local Volume, Astrophysics and Space Science Proceedings, pp283-284, Springer Netherlands*

Acknowledgements

I would first like to thank my supervisor, Geraint F. Lewis, for his fantastic support throughout my candidature, including (but certainly not restricted to) his insistence on the pronunciation of various names ending in “ies” and “ees”. Thanks also to my associate supervisor Rodrigo Ibata for expert advice and guidance, as well as his hospitality during a stay at Observatoire Astronomique de Strasbourg. I would like to thank Blair Conn and Mike Irwin for their help with wide field camera observations and data reduction. Thanks must also go to László Kiss and Arnaud Siebert for their velocity extractions and their helpful/thoughtful input on all things globular cluster. Without László, in particular, this thesis would not have the focus that it does.

I need to give **big** thanks to Margaret King. Without her amazing support none of this could have possibly happened.

Thank you Virginia and Dad, my bro’ Marc, and various friends for helping get me through; most notably (but in no specific order) Martine, Emily (in particular for proofreading my Conclusions and Distractions sections), Dan, Ryan, Greg, Mark and Lauren (although admittedly she didn’t help much toward the end).

To the various and varied people I have been privileged to share an office with, I would like to thank them all for: their interest in cricket (and introducing me to the wonders of cricinfo when I couldn’t watch TV), their often important discussions on my thesis work, proofreading and code debugging skills, and their love of all things ridiculous. These include, but are not necessarily restricted to: Brendon Brewer, Juliana Kwan, Chris Hales, Madhura Killedar (in particular for proofreading my Introduction), Matthew Francis, Daniel Yardley, Luke Barnes and Berian James.

I have been financially supported during my thesis through a scholarship, travel allowances and conference fees by the School of Physics at the University of Sydney, which also deserves thanks.

I also must thank Shaun Micallef, Randall Munroe, Jorge Cham, Luke Surl, Jessica Hagy, Zach Weiner, the Abstruse Goose, the Onion and the Australian cricket team for all their wonderful distractions.

> *If you try and take a cat apart to see how it works, the first thing you have on your hands is a non-working cat.*
>
> *- Douglas Adams*

Contents

Chapter 1

Introduction

The Sun and you and me, and all the stars that we can see, are moving at a million miles a day, in an outer spiral arm at forty thousand miles an hour of the Galaxy we call the Milky Way.

- Monty Python (Galaxy Song)

Galaxies and globular clusters fall into a gap between two scales of Universal structure: the large-scale structure and stellar sized objects, the formation of which are fairly well understood. This gap is slowly being filled, however many characteristics of galaxy formation are still poorly understood. For example, too few satellites orbit large spirals to reconcile observations with the widely accepted paradigm describing the large-scale structure of the Universe, Λ Cold Dark Matter (ΛCDM), and it is not well understood how, or where, globular clusters form. Do they form with their host galaxy, in galactic mergers, or as the product of some entirely different process? Can observations of structures within spiral galaxies reproduce a realistic evolutionary scenario?

The substructure within galaxies forms as the result of processes which are individual to each galaxy, since each galaxy evolves in its own unique environment. Analysis of this unique substructure should allow the evolutionary history of a particular galaxy to be determined, if enough information is available. Therefore, to build this picture accurately for a specific galaxy, it is important to obtain as much age, composition, kinematic and spatial information as possible on the stellar content of that galaxy. Although there are two main types of large galaxies in the Universe, elliptical and spiral, this study focuses on the evolution of the Milky Way (MW), so the discussion throughout will focus almost exclusively on spiral galaxies. For the interested reader, there are detailed discussions by Bender & Saglia (1999) and Mirabel (2001) on the formation and evolution of elliptical galaxies.

Globular clusters, nearly spherical clusters of stars in the mass range $\sim 10^4 - 10^6$ solar masses ($M_\odot$), reside in the halo of every large nearby galaxy, and in many nearby dwarf galaxies as well. It is the current understanding that, in fact, all large galaxies contain globular clusters in their haloes. These clusters are some of the smallest objects that have been probed with N-body simulations of ΛCDM structure formation (e.g. Cen *et al.*, 2003; Weil & Pudritz, 2002; Abadi, 2009), furthermore, because they reside at differing distances from the centre of the host, they make ideal testing grounds for gravitational phenomena. Although they are well studied, many questions remain unanswered with regard to these objects. To form a comprehensive understanding of galaxies themselves we must also understand these fascinating halo structures.

1.1 The Birth of Galaxies

There is still no consensus on exactly how spiral galaxies initially form, and it has taken many years to arrive at the current understanding. An early, and highly influential, paper on this topic

(Eggen *et al.*, 1962) studied kinematics and metallicities[1] of stars in the solar neighbourhood and advocated that either the MW had a violent formation history or that most of the low metallicity stars did not form in the centrifugally supported disc (see sections 1.2.1, 1.2.2 and 1.2.3 for discussions on the separate components of spiral galaxies). This led the authors to the conclusion that the Galaxy[2] was formed via the monolithic collapse of a proto-galactic gas cloud. This view changed substantially as a result of several studies, most notably Searle & Zinn (1978), who showed that a scenario in which the hierarchical merger of small fragments built up the Galactic halo agreed with their observations of the wide distribution of metallicities among Halo globular clusters, and White & Rees (1978) who argued for a two stage formation process. Furthermore, the relatively small distances between galaxies compared to their physical dimensions (as opposed to the large separation between stars in comparison with their size), naturally leads to the assumption that galaxy interactions and mergers play a major role in the evolution of these objects (e.g. Conselice *et al.*, 2009). The understanding of the formation of elliptical galaxies has changed in a similar fashion, beginning with the monolithic collapse of gas scenario (e.g. Larson, 1974; Carlberg, 1984), and moving toward a combination of hierarchical and monolithic collapse to reconcile with the observed structure and kinematics.

1.2 Spiral Galaxies

Most, if not all, spiral galaxies are composed of four major components: the bulge, an old stellar population clustered about the centre (similar in morphology to a globular cluster; see Section 1.2.3); a dense gaseous disc undergoing star formation; a large, nearly spherical, diffuse stellar halo (which generally contains between one hundred and several hundred globular clusters; Section 1.2.3); and a large dark matter (DM) halo. All three visible components can be seen clearly in the Sombrero Galaxy (NGC 4594) and the Two Micron All Sky Survey (2MASS; Skrutskie *et al.*, 2006) view of the MW (Figure 1.1). The disc is generally further separated into thin and thick components (Figure 1.2). The 2MASS view of the MW (Figure 1.1) also shows this division; the thin Disc is visible as the dark dust lane running though the centre and the thick Disc as the more diffuse stellar population surrounding this dark dust lane.

Since these components are present in all spiral galaxies (although some spiral galaxies, such as M33, have very small and non-luminous bulges – see Section 1.2.1 and Figure 1.3), decomposition into the separate components is beneficial for both photometric and kinematic studies of galactic structure, and is also useful when producing statistical models (see Section 1.2.3). The photometric separation of bulge and disc components began with de Vaucouleurs (1948) who determined that the bulges of early- and late-type galaxies had cuspy and exponential surface brightness profiles respectively (see Section 1.2.3 for a description of the de Vaucouleurs profile). Furthermore, since each component has distinct properties, this separation is fairly clean (although some overlap exists between thin and thick disc populations, for example) and each component can effectively be treated separately. Stellar populations can be separated in several ways, namely by age, kinematics and elemental abundances (metallicity). The age of the population provides separation between components since each component undergoes star formation at different epochs; the kinematics of each component are distinct, as is their metallicity distribution (which is related to the age of a population and its stellar masses). Stars

[1] Metallicity ([M/H]) is the abundance of all elements heavier than helium (which are synthesised in the nuclear fusion processes in stellar cores) compared to hydrogen, normalised to the solar value (i.e. $[M/H]=\log(Z/Z_{\odot})$, where Z is the ratio of all metal atoms to hydrogen atoms). Often iron is used as a proxy for 'all metals' and is represented as [Fe/H]. In this case $[Fe/H]=\log(N_{Fe}/N_{H}) - \log(N_{Fe}/N_{H})_{\odot} \approx [M/H]$.

[2] Hereafter, the capitalisations of Galactic, Galaxy, Bulge, Plane, Disc, Halo, Warp and Flare refer to the Milky Way galaxy unless otherwise specified (e.g. "the Galactic plane" and "the Plane" both refer to the plane of the Milky Way). Lowercase galactic, galaxy, bulge, plane, disc, halo, etc refer to external galaxies, or galaxies in general.

Figure 1.1: Two examples of edge on spiral galaxies exhibiting the three major visible components: the bulge, disc and stellar halo. *Left:* The Sombrero galaxy (NGC 4594) and *right:* the 2MASS view of the MW. Image credits - *left:* NASA and the Hubble Heritage Team (STScI/AURA), *right:* the Two Micron All Sky Survey - http://www.ipac.caltech.edu/2mass/

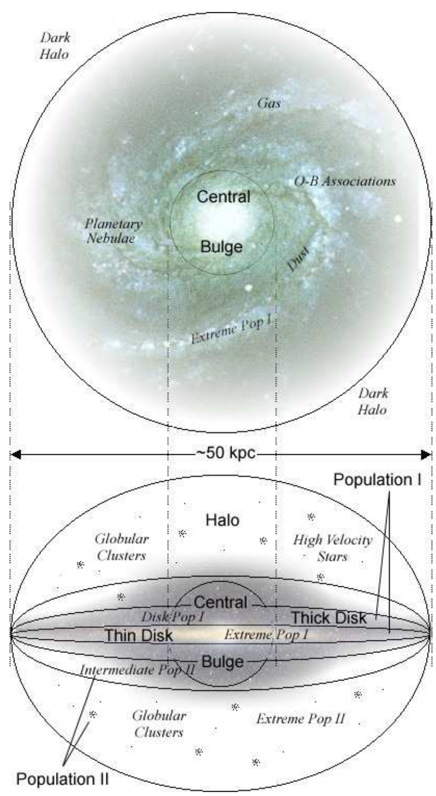

Figure 1.2: A schematic view of a spiral galaxy, overlaid with *top:* an image of NGC 4321, and *bottom:* the COBE (http://lambda.gsfc.nasa.gov/product/cobe/) satellite image of the Milky Way. Note the differentiation of components. Image credit: Dale E. Gary, New Jersey Institute of Technology - http://web.njit.edu/

with lower metallicities must have formed from gas clouds which had not been enriched with heavier elements and so are thought to be older, less massive and cooler stars. The exception are the "blue straggler" stars which are massive, hot stars with low metallicities, appearing much younger than other stars within a particular population, and are thought to be formed by mergers between old, low metallicity stars (e.g. Perets & Fabrycky, 2009).

Sections 1.2.1, 1.2.2 and 1.2.3 discuss, in detail, the individual components of spiral galaxies.

1.2.1 The Bulge

The Bulge consists almost exclusively of an old, metal-rich stellar population, with the metallicity of the Galaxy as a whole decreasing with Galactocentric radius (e.g. Najarro *et al.*, 2009). However, due to the uncertain nature of Galactic formation, it is unclear whether the Bulge formed hierarchically as a separate structure early, with the Disc forming later (Forbes & Spitler, 2008), or whether the Disc formed first and later formed a pseudobulge[3] through secular evolution, or the coalescence of dense clumps formed by instabilities in the Disc (e.g. Kormendy & Kennicutt, 2004; Elmegreen *et al.*, 2008, and references therein). Problems arise because a Bulge built from many individual fragments, which each have independent star formation histories, cannot account for the nearly uniform stellar population of the Bulge. It is apparent that the Bulge is at least as old as Halo globular clusters (Renzini, 1994), $\sim 12-14$ billion years (Gyr), and that the formation of the Bulge may have been part of the same dynamical process that formed the Halo (Ortolani *et al.*, 1995), but it is still unclear as to how this discrepancy can be resolved.

Another problem is that bulges vary greatly in size and shape, from virtually bulge-free, to barred bulges. Lütticke *et al.* (2000a,b) demonstrated that $\sim$45% of all bulges are boxy[4] or peanut-shaped and, furthermore, if barred the exact shape of the bulge depends on the angle of the observer to the bar. Their numerical simulations showed that peanut bulges are simply bars seen edge on, with the major axis of the bar perpendicular to the line of sight, and boxy bulges are those where bars are observed at smaller angles of inclination. In those cases where the galaxy contains a central bar the bulge can appear almost spherical if seen with the bar end on and, of course, bars can also vary greatly in size and shape. Despite these *observationally* different types of bulges having the same *actual* morphology, this can only be the case with edge on, barred spiral galaxies. Figure 1.3 shows two face on spiral galaxies, namely M33 (NGC 598) and M83 (NGC 5236), which exhibit vastly different galactic bulge morphologies; M33 has virtually no bulge and the bulge of M83 is extremely large and luminous. Because of the range of different bulges, it seems likely they are formed from processes that are independent of the formation of galactic discs.

Figure 1.3: Two spiral galaxies showing two extremes of bulge sizes and luminosities. *Left:* M33 (NGC 598) has a very small, compact bulge, whereas *right:* M83 (NGC 5236) has a much more obvious large, bright bulge. Image credits - *left:* N. Caldwell, B. McLeod, and A. Szentgyorgyi (SAO), *right:* FORS Team, European Southern Observatory - http://eso.org/

[3]A dense central component of a spiral galaxy with a similar morphology to classical, merger built bulges produced slowly from disc gas.

[4]Boxy bulges appear almost square from the observer's line of sight.

1.2.2 The Disc

Galactic discs are made of several components, namely the extreme thin-, thin- and thick-discs, however, the extreme thin- and thin-discs are generally treated as a single component, and this will also be the case throughout this thesis.

Thin Disc

This disc component typically has a radius ~10 kiloparsecs (kpc), is several hundred parsecs (pc) thick (*c.f.* the thin Disc has a scale height of $\sim 100 - 300\,\mathrm{pc}$; Kroupa, 1992; Kong & Zhu, 2008) and defines the plane of the galaxy (see Figures 1.1 and 1.2). In general, the thin discs of spirals are gaseous, the site of almost all star formation within the galaxy, blue and exhibit a spiral structure (Figures 1.2 and 1.3). Due to the blue colouring of most thin discs, it is often said that only young stars are found in the thin disc. However, Binney *et al.* (2000) show that stars up to ~12 Gyr old can be found in the solar neighbourhood. The majority of the stars in spiral galaxies reside on nearly circular orbits in the thin disc. The circular velocity of the stars is almost independent of the radius, indicating the presence of large quantities of dark matter within the galactic halo (see Section 1.2.3 and e.g. Rubin, 1983), with the rotational velocity of the Disc being $\sim 220\,\mathrm{km\,s^{-1}}$ (e.g. Bobylev *et al.*, 2008).

Thick Disc

A much more diffuse component than the thin disc, this appears in many ways to be an extension of the thin disc from images such as the right panel of Figure 1.1. Kinematic, age and metallicity data, however, have shown that these components contain distinct stellar populations with differing chemical histories (e.g. the abundances of α-elements[5], as well as Al, V, and Co, are greater for stars in the thick Disc compared to the thin Disc, for a given metallicity), with thick Disc stars being older (10–13 Gyrs) than those in the thin Disc (1–12 Gyrs; Binney *et al.*, 2000; Reddy, 2007), as well as dynamically warmer. The thick Disc has a scale height of $\sim 700 - 1200\,\mathrm{pc}$ (von Hippel & Bothun, 1993; Buser *et al.*, 1999), with two major processes having been put forward to account for the "thickness" of thick discs.

• **Migration of Thin Disc/Bulge Stars:** This migration can occur in two ways:

1 - Due to the kinematics of thin discs, it is certain that over long enough timescales, stars will migrate from the thin disc to populate a region surrounding it, producing a thick disc. This is because stellar populations in thin discs cannot, realistically, be on orbits that lie entirely in a perfect plane.

2 - The flattening of bulges by the gravitational potential of the thin disc may also create the appearance of a thick disc (e.g. Gilmore & Reid, 1983).

However, because the timescales for these migrations are very long, this scenario has been replaced by the more favourable merger hypothesis.

• **Minor/Intermediate Mergers:** Velazquez & White (1999) showed that dynamical heating during a single merger between a dense stellar object with a mass of $\sim 10-20\%$ of the disc mass and a Milky Way-like thin disc, produces a reasonably realistic thick disc. However, a more realistic scenario is the merger of several such objects because ΛCDM cosmologies predict large numbers of dark haloes surrounding galactic discs. With this constraint, N-body simulations

[5] Those elements produced via α-processes in stellar cores: C, N, O, Ne, Mg, Si, S, Ar, Ca and Ti.

by Kazantzidis *et al.* (2008) and Villalobos & Helmi (2008), showed that as few as a single DM halo, and as many as six, on realistic orbits and with masses $\sim 20 - 60\%$ of the thin disc mass ($\sim 10 - 20\%$ of the total galactic mass), crossing the disc over the past ~ 8 Gyr, will create a long-lived stable thick disc that remains extant until the present and has a complex vertical kinematic and morphological structure that is consistent with the thin-/thick-disc decomposition described above. The scale height of the thick disc created increases with the orbital inclination of the mergers, and also depends on other conditions such as a pro- or retro-grade orbital motion with respect to the disc. It is interesting to note that the simulations by Kazantzidis *et al.* (2008) and Villalobos & Helmi (2008) also leave a significant proportion of the thin disc in its original, kinematically cold state, allowing for the old stellar populations in the thin Disc described by Binney *et al.* (2000).

Warp and Flare in Galactic Discs

Although galactic discs usually appear close to planar, this is not necessarily the case. Many, including the MW disc itself, exhibit some measure of warping and flaring[6]. The extreme warping of the discs of UGC 3697 and ESO 510-G13 can be seen in the upper two panels of Figure 1.4, and the lower panel shows the warped/flared model of the Disc from 2MASS red clump star counts, originally presented as Figure 22 of López-Corredoira *et al.* (2002).

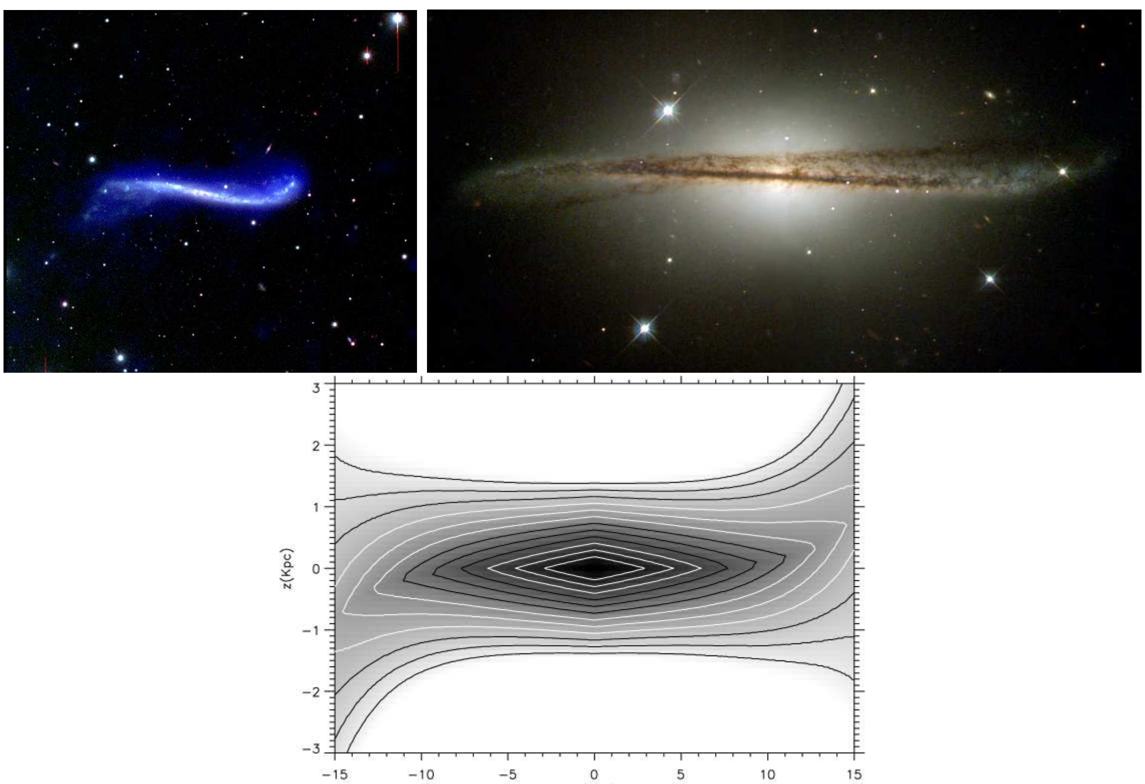

Figure 1.4: Both UGC 3697 (*upper left*), and ESO 510-G13 (*upper right*) exhibit unusually large warps in both their stellar and gaseous discs. *Bottom*: The López-Corredoira *et al.* (2002) model of the Galactic disc, produced from 2MASS red clump star counts, shows both distinct Warp and Flare (Figure 22 from that study). Image credits - *upper left:* L. D. Matthews (CfA), J. M. Uson (NRAO), *upper right:* NASA and the Hubble Heritage Team (STScI/AURA).

It is important to note that the amount of Warp and Flare measured is very much dependent

[6]The increase in scale height of the disc with increasing radius.

on the tracer used. The greatest Warp is in the dusty component of the Disc, and the least in pulsars (see Figure 1.5). The cause of the Warp is still unknown, but the four possible mechanisms put forward to-date are the tidal forces of a Galactic satellite (e.g. Kazantzidis *et al.*, 2009, and Figure 1.6, show the effect of an accreting satellite on the gaseous disc), asymmetric intergalactic magnetic fields interacting with ionised gas in the Disc, a misalignment of the Halo[7], or the direct accretion of material from the intergalactic medium onto the Disc (Castro-Rodríguez *et al.*, 2002, and references therein).

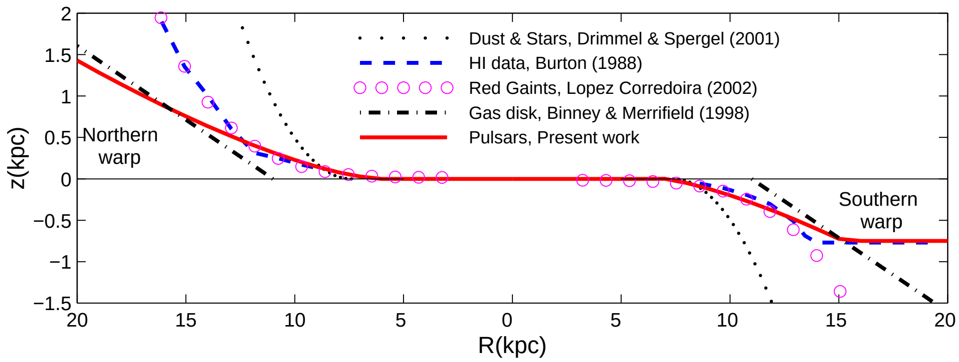

Figure 1.5: Galactic warp models originally presented as Figure 2 by Yusifov (2004), showing the correlation between the strength of the Warp and the tracer used to measure it.

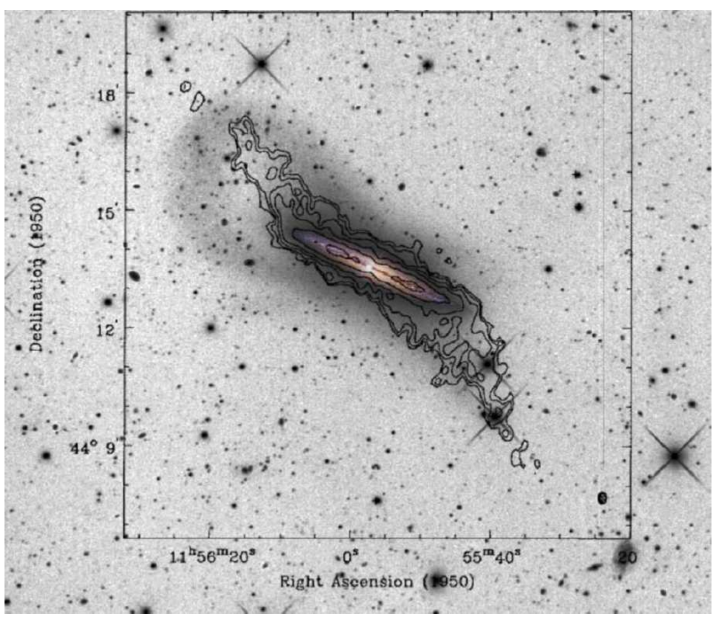

Figure 1.6: NGC 4013 and its warped gaseous disc. A giant stellar tidal stream (the remnants of a tidally destroyed satellite galaxy) is seen encircling this edge on spiral galaxy. The interaction with the satellite has deformed the neutral hydrogen in the disc of the host galaxy, leading to a warped gaseous disc (shown here as contours). This is clear evidence that warps in gaseous galactic discs can be created in such a manner. This is also good evidence for stellar haloes being formed via mergers (Section 1.2.3) Originally presented as Figure 7 by Martínez-Delgado *et al.* (2009).

[7]It is possible, for example, that the visible Galaxy is in orbit about the centre of the dark Halo (Blitz, L – private communication).

1.2.3 The Halo

As for the disc, the halo has two separate components, namely the stellar and dark haloes.

Stellar Halo

This galactic component is a nearly spherically symmetric collection of stars surrounding the galactic centre, and is populated by older, metal-poor stars (the metallicity range of Halo stars is $-4 \leq [Fe/H] \leq 0$, peaking at $[Fe/H] \sim -1.6$; Ryan & Norris, 1991) and globular clusters (GCs). The spatial density of the stellar Halo falls off as $\rho(r) \propto r^{-\alpha}$ for $r \lesssim 25\,\mathrm{kpc}$ (with $3 \leq \alpha \leq 3.5$), likely drops off more and more rapidly for $r > 25\,\mathrm{kpc}$ (Binney & Merrifield, 1998), and has a mass of $\sim 10^9\,\mathrm{M}_\odot$ (e.g. Carney *et al.*, 1990). Although the spatial extent of the stellar Halo is not known, the most distant Halo objects yet observed are 123 kpc (the distance to the furthest Halo globular cluster AM 1; Harris, 1996; Frommert, 2007), and 130 kpc (the most distant known Halo field stars; Clewley & Warren, 2003) from the Galactic centre. In comparison, recent work (Ibata *et al.*, 2001a, 2007; McConnachie *et al.*, 2009) has shown that the stellar halo of the nearest large spiral to the MW, the Andromeda galaxy (M31), extends to at least twice this distance and even envelopes the neighbouring galaxy M33 (Figure 1.7). It is likely through interactions with smaller galaxies (i.e. mergers) that these haloes are built up, and so these structures are very important for understanding galactic formation and evolution (see Helmi 2008 for a review of formation/evolution scenarios arising from the analysis of substructure in the Galactic stellar halo).

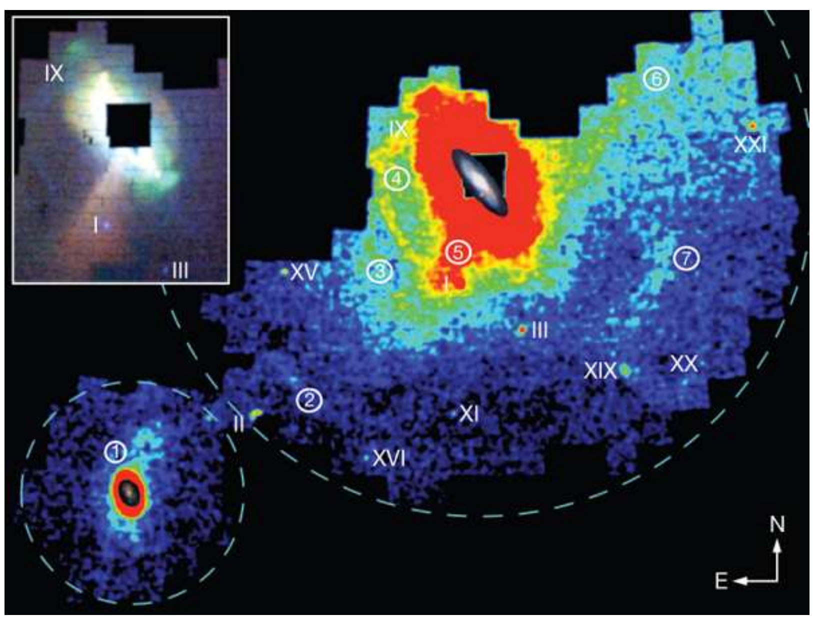

Figure 1.7: The density distribution of stellar sources surrounding M31 and M33 with the inset showing the central parts of the survey at higher resolution. The stars forming the density map all have colours and magnitudes consistent with red giant branch stars at the distance of M31. The dashed circles represent radii of 150 and 50 kpc from M31 and M33, respectively, and images of both galaxies are overlaid at their locations within the survey field. Visible dwarf satellites are indicated with roman numerals and the circled numbers indicate: 1, M33 structure; 2, 125-kpc stream (stream A); 3, stream C; 4, eastern arc (stream D); 5, giant stellar stream; 6, northwest minor-axis stream; 7, southwest cloud. Originally published as Figure 1 by McConnachie *et al.* (2009).

Extended stellar haloes may actually be very common surrounding large spiral galaxies, as should be expected since galaxies evolve through mergers (see Section 1.3 and Chapter 3). Evidence for this comes, in part, from the first ground-based observations of an extended stellar halo around a spiral galaxy outside the Local Group (Mouhcine, Ibata & Rejkuba, 2010, Figure 1.8 – also see Figure 1.6 for further evidence of stellar halo formation in progress; see Section 1.3 for an explanation of the Local Group). The common nature of extended stellar haloes surrounding spiral galaxies can also be inferred from the MW itself. The Monoceros Ring and Sagittarius dwarf tidal stream (see below for further discussion of these Galactic tidal features) are two large stellar streams which both appear to have been formed through interactions between the MW and external dwarf galaxies and represent a significant fraction of the mass of the stellar Halo.

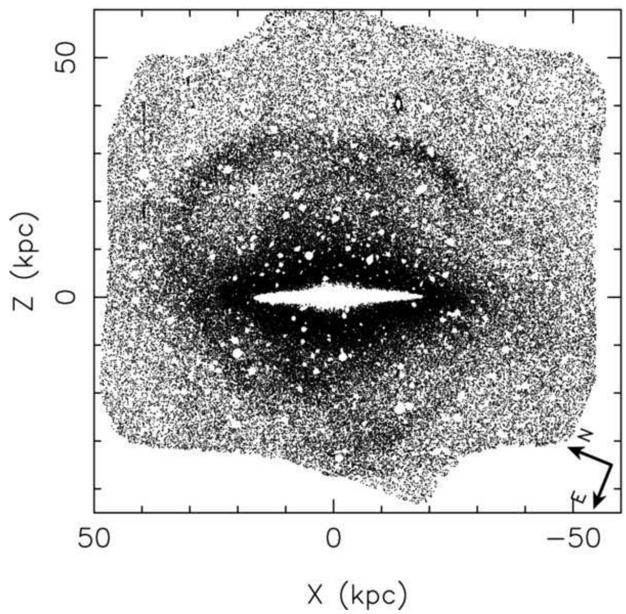

Figure 1.8: A surface density map of red giant branch stars surrounding NGC 891. A large system of tidal streams loop around the galaxy – the remnants of accretion events which are building up the stellar halo. Also visible is a dense stellar structure enveloping the disc and bulge. Originally published as Figure 1 by Mouhcine, Ibata & Rejkuba (2010).

The stellar Halo has long been considered a single Galactic component and thought to have little or no intrinsic rotation. Therefore, it was thought to be a gravitationally supported structure with stars on almost radial orbits about the Galactic centre. However, there is growing evidence that the Halo is made up of two distinct components which have different metallicity and density profiles, with the inner Halo having a net prograde rotation and the outer Halo having a net retrograde rotation (e.g. Carollo *et al.*, 2007).

Globular Clusters

As mentioned previously, GCs populate the halo of most, if not all, large galaxies. There are ∼160 known Galactic globular clusters (spherical clusters of stars whose density diminishes with radius, see Figure 1.9), which are usually separated into three categories, namely the Bulge (e.g. Valenti *et al.*, 2007), Disc (e.g. Casuso & Beckman, 2006) and Halo (e.g. Parmentier & Grebel, 2005) clusters, although catalogues such as Harris (1996) and Frommert (2007) do not differentiate between the different categories. No consensus has been reached on whether GCs form with their host galaxy (e.g. Bekki *et al.*, 2007), as the results of galactic mergers (e.g. Hancock *et al.*, 2009; Hartwick, 2009), or are formed through another process entirely (e.g. Hasegawa *et al.*, 2009).

Figure 1.9: The globular cluster 47 Tucanae (47 Tuc). Image credit: the Two Micron All Sky Survey - http://www.ipac.caltech.edu/2mass/.

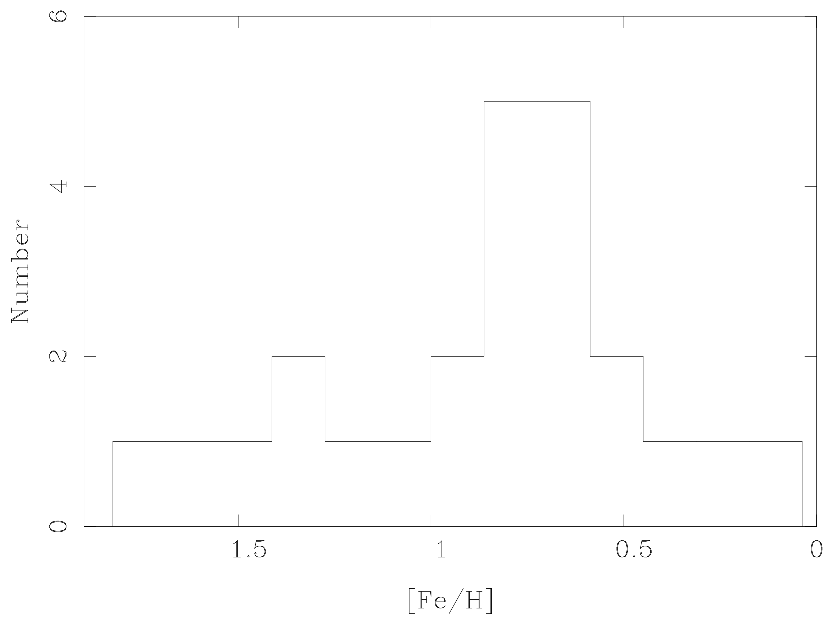

Figure 1.10: Histogram of the metallicity data of Bulge GCs published by Valenti *et al.* (2007). Note the large number with [Fe/H]~ -0.75 indicating the possibility of a unique population.

Halo GCs are the most numerous, and extend to large radii in a roughly spherical distribution about the Galactic centre. The Disc and Halo populations have distinct metallicity ranges, namely $-2.6 \lesssim$[Fe/H]$_{\mathrm{Halo}} \lesssim -0.8$ and $-0.8 \lesssim$[Fe/H]$_{\mathrm{Disc}} \lesssim -0.2$ (Binney & Merrifield, 1998), however, the Bulge population has a metallicity range that spans nearly this entire spectrum, $-1.7 \lesssim$[Fe/H]$_{\mathrm{Bulge}} \lesssim -0.2$ (Valenti *et al.*, 2007), indicating they may not be a separate population but a mixture of Disc and Halo clusters apparently located in the Bulge by chance, due to the current position along their orbital path. However, there is a clear peak in the metallicity distribution of Bulge GCs at [Fe/H]~ -0.75, right at the intersection of the Disc and Halo populations, so perhaps this population is truly separate but is mixed with a few Disc and Halo contaminant GCs in chance physical alignment with the Bulge (Figure 1.10).

As mentioned in Section 1.2, GCs are similar in morphology to classical galactic bulges[8] which, in turn, are similar to large elliptical galaxies. Furthermore, classical bulges and elliptical galaxies obey the same surface brightness profile, namely the Sérsic (1968) profile[9]:

[8]Those that are not boxy-, peanut- or pseudo-bulges.

[9]Since de Vaucouleurs (1948) originally proposed that the surface brightness profiles of galactic bulges closely

$$I(r) = I_e \exp\left\{-b_n\left[-\left(\frac{r}{r_e}\right)^{1/n}\right]\right\} \tag{1.1}$$

where I_e is defined as the surface brightness at the effective radius[10], and the parameter b_n ensures that r_e is the half light radius. Because of the similar morphologies, it should be no surprise that the Sérsic profile also fits the surface brightness profiles of GCs remarkably well. The Plummer (1911) profile:

$$I(r) = \frac{I_{\rm tot}}{\pi b^2}\left(1 + \frac{r^2}{b^2}\right)^{-2} \tag{1.2}$$

(here b is the scale radius, effectively the half-light radius) is a very close match to the Sérsic profile in the outer regions, but diverges at approximately the half-light (or half-mass) radius (Figure 1.11). However, because the Plummer model is physically motivated, that is it produces a stable physical distribution (the Plummer Sphere; e.g. Boily & Kroupa, 2003), the advantage of this model is that it can be used to estimate various observational parameters, including the scale radius, the total mass and the projected velocity dispersion profile, where this is not possible with the Sérsic profile (see Dejonghe, 1987, for details). Although it is recognised that the Plummer model is not a perfect representation of GCs, it fits both the surface brightness and velocity dispersion profiles of GCs remarkably well (see Figure 1.11 and Chapter 2), and the ability to determine physical parameters using this model makes it an incredibly useful tool. Equation 1.3 shows the projected Plummer velocity dispersion profile:

$$\sigma^2(R) = \frac{\sigma_0^2}{\sqrt{(1 + R^2/r_s^2)}}, \tag{1.3}$$

where σ is the projected velocity dispersion with radius R, σ_0 is the central velocity dispersion and r_s is the Plummer scale radius. The half-mass radius is equivalent to the scale radius in the projected Plummer model, as above, but is ≈ 1.305 times the scale radius for unprojected models (Haghi *et al.*, 2009). It should be noted that King (1966) models have been very successful in modelling the surface brightness and velocity dispersion profiles of GCs. These models come in several varieties, namely single and multiple component, both truncated and non-truncated. However, these models are no more accurate than the Plummer model when analysing data with velocity uncertainties of $\sim 1 - 2\,\mathrm{km\,s^{-1}}$ (approximately the accuracy of the individual stellar velocities, as well as velocity dispersions, analysed in this thesis) and are not solvable analytically. Therefore, the Plummer model has been chosen for the analysis throughout this work, for ease of use and with no reduction in accuracy.

Globular clusters are important tracers of both galactic formation and evolution (see Bassino, 2008; Harris, 2010, for reviews), the shape (e.g. Peñarrubia, Walker & Gilmore, 2010) and mass (e.g. Watkins, Evans & An, 2010) of the dark matter halo, and the formation and evolution of the individual stellar components of galaxies (i.e. the bulge and stellar halo – for example see Bica *et al.* 2006; Forbes & Spitler 2008). One great advantage of GCs is their intrinsic luminosity; bright GCs can be observed in galaxies beyond 100 Mpc and are generally found in large numbers. In addition, distribution functions of key parameters such as mass, age and metallicity can be constructed using GCs, rather than being restricted to the luminosity-weighted averages that can be extracted from unresolved field stars. Furthermore, Galactic GCs are located at small enough distances for individual stars to be resolved. This allows for accurate measurements

follow Equation 1.1 with a Sérsic index of 4 (also see Figure 1.11), it has been shown that there are many exceptions to this rule (e.g. Courteau *et al.*, 1996; MacArthur *et al.*, 2003) and that the generalised de Vaucouleurs profile, the Sérsic profile, fits a greater range of classical bulge morphologies (e.g. McDonald *et al.*, 2009).

[10]The radius which encloses 50% of the total luminosity.

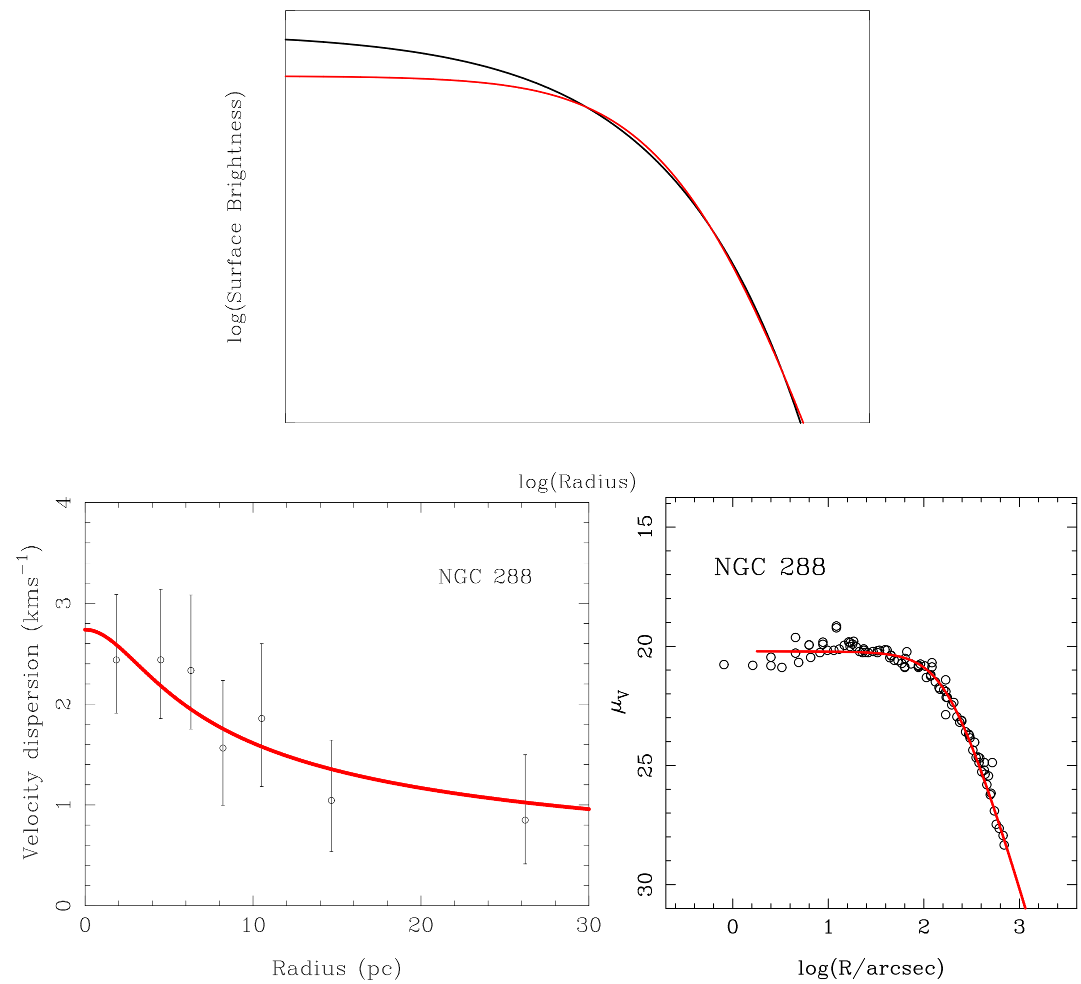

Figure 1.11: *Top:* A Sérsic profile of index 1 (black curve) overplotted with a Plummer profile with a scale length of 10.0 and a total luminosity of 2.2 (red curve). All units are arbitrary, the curves are presented here simply to show their functional forms. *Lower left:* Velocity dispersion data of NGC 288 overplotted with the best-fit Plummer model (see Section 2.3). *Lower right:* V-band surface brightness data of NGC 288, originally published by Trager *et al.* (1995) as part of their Figure 2 (open circles), overplotted (red curve) with a Plummer surface brightness profile (again, see Section 2.3). Note the quality of the Plummer model fits to both the velocity dispersion and surface brightness profiles.

of the internal dynamics of each cluster which is essential for calculating their masses, and, therefore, mass-to-light ratios and dark matter content (see Chapter 2).

The Monoceros Ring and Canis Major Overdensity

It is well known that galaxies are built up over time in a hierarchical manner (see Section 1.3), and observational evidence of tidal interactions is quite common; these interactions produce substructure in the halo of the galaxy. The Sagittarius dwarf galaxy is a good example of this in the Halo (Ibata *et al.*, 1994, also recall Figure 1.6). As relics of galactic evolution, analysing such galactic substructure is vital to our understanding of the evolutionary histories of galaxies. Our own Milky Way provides us with a unique opportunity to observe this substructure in fine detail.

While conducting a survey of the stellar Halo, analysing SDSS[11] F-type stars at their main sequence turnoff, Newberg *et al.* (2002) discovered an overdensity of stars originally observed to cover $\gtrsim 40°$ of sky toward the Galactic centre. This object has now been traced around the entire Galactic plane, and at two distinct distances from the Galactic centre (Crane *et al.*, 2003; Ibata *et al.*, 2003; Rocha-Pinto *et al.*, 2003; Yanny *et al.*, 2004; Conn *et al.*, 2005, 2007, 2008) and has become known as the Monoceros Ring (MRi). The accepted explanation for the existence of the MRi is that it is the only known, extant in-Plane accretion event in the MW system. As such, it provides a unique opportunity for studying the evolution of the Galactic disc; in-plane accretion events deposit material directly on to galactic discs, driving disc evolution. Recently there have been many new discoveries of tidal streams which are also apparently close to the Plane (see Grillmair, 2006, and references therein). Are Planar streams more common than previously realised, or can these new streams be attributed to the same accretion event that formed the MRi? Unlike the Sagittarius dwarf, the progenitor for the MRi is unknown, although the leading candidate is the purported Canis Major overdensity/dwarf galaxy (Martin *et al.*, 2004), which is thought to be the remnants of a tidally stripped dwarf galaxy in a nearly Planar orbit. It is possible, however, that the overdensity is only an *apparent* overdensity which is due to observers at our location in the Galaxy looking through the Galactic warp. The overdensity is located close to the maximum Warp, South of the Plane [at Galactic coordinates $(l,b)^\circ \approx (240,-9)^\circ$], so it may give the impression of a stellar overdensity because our line-of-sight cuts through more of the Disc in this region.

Currently two *N*-body models of the tidal destruction of the Canis Major dwarf have been produced (Martin *et al.*, 2005; Peñarrubia *et al.*, 2005), neither of which describe the observed structure of the MRi successfully. Note that of the two models, only the Martin *et al.* (2005) model represents the observed location of the Canis Major overdensity correctly. It is important, therefore, to test observations of the MRi to a Galaxy model so that the most accurate possible information can be obtained for the MRi. The Besançon Synthetic Galaxy model (Robin *et al.*, 2003) is a population synthesis model, and, as such, is extremely useful for comparisons to observations of the Milky Way because it allows for the separation of the various Galactic components (Halo, Bulge and Disc), mimicking our ability to dissect spiral galaxies themselves (see Section 1.2). The Besançon model potential is calculated in a self-consistent manner, in agreement with star counts from the HIgh Precision PARallax COllecting Satellite (HIPPARCOS; Mel'Nik & Dambis, 2009, and references therein), and the rotation curve of the Galaxy. It contains constraints on the structure of the Bulge, and, importantly, on the warping and flaring of the Disc. The model is designed to reliably predict star counts in photometric bands from visible (U) to near-infrared (K). Therefore, this is an excellent model for highlighting detections of the MRi within observational data.

Dark Halo

Dark matter was first proposed as a solution to a problem – that galaxies near the virial radius[12] of galaxy clusters have velocities which exceed that of a stable system if clusters were only comprised of visible material (Zwicky, 1933). In other words, the galaxies near the virial radius of a galaxy cluster would have escape velocities greater than that of the cluster if the only matter within the cluster was visible. This was later shown also to be true for the discs of spiral galaxies; the rotation curves of galactic discs are essentially flat, meaning that the circular velocity of the disc is approximately constant with radius (see Rubin, 1979, references therein,

[11] The Sloan Digital Sky Survey (York *et al.*, 2000)

[12] The radius of a sphere, centered on a galaxy or a galaxy cluster, within which virial equilibrium holds. Virial equilibrium occurs where $2 < T >= n < V >$ (here $< T >$ is the average total kinetic energy of the system and $< V >$ is the average total potential energy of the system) for some value of n.

and Figure 1.12). This could only be the case if galaxies have a large component of non-luminous mass extending out to large radii, the dark halo. Dark haloes appear to be ubiquitous among galaxies, from dwarfs to large ellipticals.

The nature of dark matter is unknown, however, it is by far the most massive component of galaxies, comprising more than 90% of the total mass. The dark Halo extends to at least 100 kpc with a density distribution $\rho \propto r^{-2}$, and within 50 kpc of the Galactic centre has a mass $\sim 5 \times 10^{11}$ $M_{\odot}$ (Kochanek, 1996). There is ongoing debate over whether the dark Halo is spherical (e.g. Ibata *et al.*, 2001b; Siebert *et al.*, 2008), oblate (e.g. Jurić *et al.*, 2008), prolate (e.g. Starkenburg *et al.*, 2009) or triaxial (e.g. Law *et al.*, 2009).

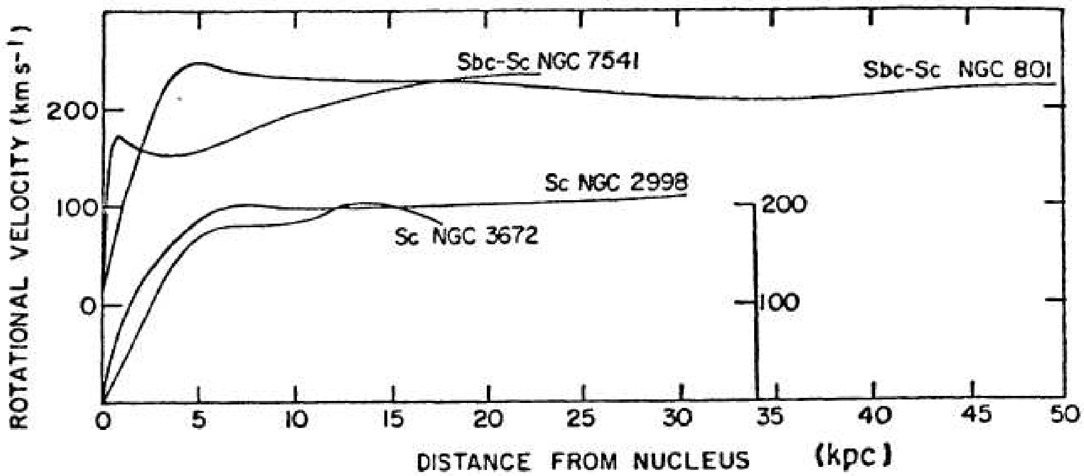

Figure 1.12: The rotation curves for the spiral galaxies NGC 801, NGC 2998, NGC 3672, and NGC 7541, originally published as Figure 2 by Rubin (1979). All show a steep increase in rotational velocity near the bulge (at radius = 0) which flattens out at small radii. This could only occur if there was a significant quantity of non-luminous mass extending to large radii.

1.3 Hierarchical Structure Formation, ΛCDM and the Gravitational Interaction

The Milky Way is one of two large spiral galaxies in the Local Group of galaxies, which contains approximately 30–40 galaxies in total. Although N-body analysis of structure formation in ΛCDM cosmology reproduces structure on the Local Group scale extremely well, below this scale it over-represents observed structure by ~ 2 orders of magnitude. This has become known as the "missing satellite problem" – too few dwarf galaxies and globular clusters are observed within the local Universe when compared with ΛCDM predictions (e.g. Diemand *et al.*, 2007). Despite many new faint, dwarf satellite galaxies in the Local Group being discovered recently (e.g. Willman *et al.*, 2005a,b; Zucker *et al.*, 2006; Martin *et al.*, 2006), the vast majority of the missing satellites are yet to be found. Some recent studies have attempted to shed light on this problem, for example by invoking luminosity bias (Tollerud *et al.*, 2008) or mass-dependent suppression of star formation in low-mass subhaloes (Koposov *et al.*, 2009), however, the debate surrounding the missing satellites is ongoing.

An important question to ask, then, is "do we understand gravity correctly?" Is it possible that in the ΛCDM predictions we are seeing the consequences of a fundamental flaw in our understanding of the gravitational interaction? Attempts to solve this problem abound, particularly with regard to removing the requirement for dark matter from gravitational theories. Of particular note is MOdified Newtonian Dynamics (MOND; Milgrom, 1983), which alters the strength of gravity below an acceleration threshold ($a_0 \approx 1.2 \times 10^{-10}\,\mathrm{m\,s^{-2}}$) and has seen some success with matching observations (e.g. for the Fornax dwarf galaxy; Łokas, 2001), however, many other modified gravity theories exist which can also claim some success (e.g. Moffat & Toth, 2008), and none can be applied universally.

MOND, which modifies Newtonian dynamical theory only when accelerations are very weak, describes well, without invoking dark matter, the relation between the rotation and luminosity of spiral galaxies, and also describes the rotation curves of galaxies. It does not, however, accurately replicate the orbits of galaxies within clusters, nor the rotations of galaxy clusters themselves. Moffat & Toth (2008) claim that their modified gravity theory explains galaxy rotation curves, galaxy cluster masses and velocity dispersions, lensing, and cosmological observations, as well as predicting accurate velocity dispersion profiles which are consistent with Newtonian theory for GCs. This, however is still not a universal gravitational theory and is, in any case, still debated. Furthermore Moffat & Toth (2008) only fit their model in the Newtonian regime with data from globular clusters by Scarpa *et al.* (2007), who claim that a modified version of gravity may be required to explain their data. These data do not agree with much of the literature and have not been replicated by other studies (e.g. Sollima *et al.*, 2009, see also Chapter 2). Recent extensions of General Relativity theory seem to be more universal, because, for example, they perform well when predicting large scale structure formation; they include “dark fields” that seed cosmological structure growth. They may also explain recent weak lensing data. However, the presence of these dark fields reduces calculability because it is unclear what these fields are or how they should behave. They also come at the cost of the original MOND premise, that the matter we see is the sole source of gravity (Ferreira & Starkman, 2009). It is clear, then, that empirical testing for non-Newtonian behaviour is vitally important to our understanding of the nature of the gravitational interaction.

Halo GCs are the perfect test-beds for studying the nature of the gravitational interaction, since they are thought to be virtually DM free. This is based on evidence from dynamical models (e.g. Phinney, 1993), *N*-body simulations (e.g. Moore, 1996), observations of GC tidal tails (e.g. Odenkirchen *et al.*, 2001), their dynamical and luminous masses (e.g. Mandushev *et al.*, 1991), and the lack of microlensing events from GC mass dark haloes (e.g. Navarro *et al.*, 1997; Ibata *et al.*, 2002). Because they are at differing distances to the Galactic centre and Galactic plane, Galactic influences cannot be the primary cause of any observed divergence from Newtonian predictions, and furthermore, the vast majority of Halo GCs have an ellipticity of ~ 1 (Han & Ryden, 1994) indicating that they have neither large rotations nor large tidal forces acting on them. In addition, the accelerations felt by the stellar members of GCs is often below a_0 (particularly the external members, e.g. Scarpa *et al.*, 2007, and also see Section 2.3 where it is shown that the most distant cluster members exhibit accelerations at least an order of magnitude below a_0). There is also evidence that the most massive Halo GC (ω Centauri) has recently undergone a merger (see Section 2.4), which makes GCs not only the ideal for testing ground for our understanding of the gravitational interaction, but for galaxy evolution via hierarchical merging at the subgalactic-scale as well.

The study by Scarpa *et al.* (2007) seems to show that the velocity dispersion profiles of several GCs flatten out well inside the tidal radius (where the external gravitational field matches that from the cluster itself), reminiscent of galaxy rotation curves (see Figure 1.13). If this were shown to be a real effect, this would place a sizable doubt on our understanding of the gravitational interaction at low accelerations. The authors claim specifically that a modification to gravity is required to explain their results, or, at least, that their data is evidence for a failure of Newtonian Dynamics for accelerations below a_0, and challenge the astronomical community to disprove or generalise their results. This is a vitally important challenge as the understanding of one of the fundamental forces of nature is in question.

Chapter 2 is dedicated to trying to replicate the results by Scarpa *et al.* (2007), i.e. to show whether GCs exhibit a flattening of their velocity dispersion profiles in the outer regions. If this could be replicated it would be further evidence that something is amiss with our understanding of gravity. For this Chapter ten GCs were selected for analysis. These clusters were chosen to be at varying distances to the Galactic Plane and Centre, and hence any consistent deviation from Newtonian gravity across all clusters (shown as a flattening of the velocity dispersion profiles which would be evident as a deviation from the Plummer model – see Section 1.2.3 and Equations 1.2 and 1.3 for details of the Plummer model) could not be primarily due to Galactic influences. Two clusters, namely M30 and NGC 288, were chosen to overlap with the Scarpa *et al.* (2007) study so those clusters could be compared directly. Further selection criteria for the clusters chosen are as follows. They are all bright ($M_V < -7$), with Heliocentric distances $< 30\,\mathrm{kpc}$ to facilitate observations, but with a large enough distance range from the Galaxy such that Galactic influences would be easy to rule out. Clusters were also chosen to have radial velocities greater than 2σ from the velocity peak of stars in the direction of the cluster, based on the Besançon model (to ensure the greatest probability of extracting cluster members with minimal Galactic contamination).

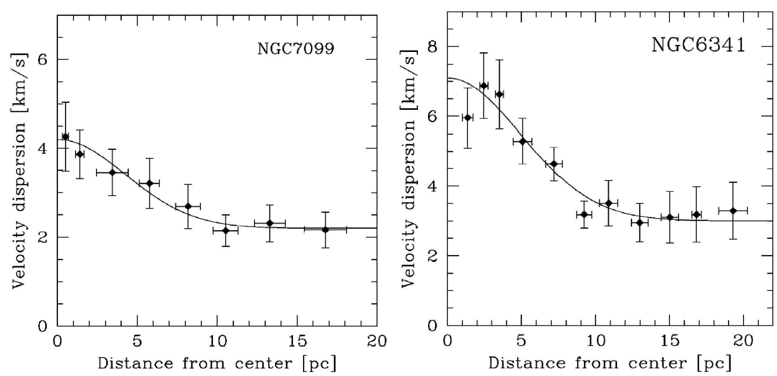

Figure 1.13: Originally published as two panels of Figure 2 by Scarpa *et al.* (2007), an obvious flattening of the velocity dispersion profiles of NGC 7099 and NGC 6341 is shown. These results have not been replicated by other studies.

Another important piece of this puzzle can be addressed by observing the remnants of hierarchical accretion within our own Galaxy, not just within the GCs in the Halo. Dwarf galaxies generally have masses at which merging is still predicted by ΛCDM to be on-going ($\gtrsim 10^7 \mathrm{M}_\odot$; again see Section 2.4). Accretion onto the Halo has been well-studied by analysing the Sagittarius dwarf interaction, however, the Sagittarius dwarf is, of course, only part of the evolutionary history of the Galaxy. Because the MRi may be driving the evolution of the Disc, defining its extent and distance, as well as searching for its progenitor, are vital to our understanding of the evolution of the Milky Way. The location of the MRi in the Galactic plane makes it much more difficult to study because it is obscured by the dust, gas and stars of the Disc itself. Disentangling the MRi from the Galactic disc has become a serious challenge to observers, but once this has been done a much clearer picture of Galactic evolution will become available. Producing this coherent picture of the evolution of the Milky Way is one of the greatest opportunities, and challenges, facing Galactic astronomy of this age.

1.4 Thesis Outline/Rationale

> *I think that it is much more likely that the reports of flying saucers are the results of the known irrational characteristics of terrestrial intelligence than of the unknown rational efforts of extra-terrestrial intelligence.*
>
> *- Richard Feynman*

The research described in this thesis comprises two distinct, yet closely related, topics. Therefore, this thesis is divided into two main sections, namely Chapters 2 and 3. Each of these Chapters contain individual, related subchapters, which could each be considered a chapter in its own right. The Chapters themselves comprise papers published by, or submitted to, *Monthly Notices of the Royal Astronomical Society* (MNRAS) and *Astrophysical Journal* (ApJ). Each subchapter is preceded by an introduction outlining the work presented in the paper to give context, as well as stating my specific involvement in the production of each paper. All papers presented in this thesis are listed beginning on page 1. The two Chapters comprise the majority of the work that has gone into this thesis, however, it is not necessarily in chronological order. Instead it has been organised by topic for readability and coherence.

The primary goal of the work presented in Chapter 2 is the understanding of GC dynamics and, hence, the dark matter content of these objects and the nature of the gravitational interaction, which is vital to our understanding of galactic evolution. Furthermore, if we do not understand the nature of the gravitational interaction, does the missing satellite problem have any relevance? GCs are used as test-beds for this work because of their low internal accelerations. However, if we are to use these objects to test our understanding of gravity, we must first quantify their dark matter content. Because modifications to Newtonian gravity generally take place at the approximate accelerations where dark matter is invoked to reconcile with observations, we must first rule out dark matter as the cause of any deviations to Newtonian predictions. The data from several surveys are analysed in a completely homogeneous manner, using the same data reduction and analysis techniques. Because of the homogeneous manner in which this work was performed it has been possible to make strong statements regarding the realism of modified gravity theories, as well as the dark matter content of Galactic GCs. This is extremely important to our understanding of gravity itself, as well as galactic evolution and small-scale structure formation. The hierarchical nature of Universal structure formation is further probed at the very low-mass scale with the first kinematic evidence for a merger history within the globular cluster 47 Tucanae.

Second, because we live within the MW, we have a unique platform from which to observe extant evolutionary processes at work on galactic scales. The only known in-Plane accretion event is probed in a large, deep pinhole survey of the outer Halo and thick Disc. This survey is used to to trace the MRi around the Galaxy, and calculate its distance from the Galaxy at each location, with the ultimate goal of determining its origin. The survey is presented in Chapter 3. Understanding the MRi is essential to our understanding of Galactic evolution because it is the only known extant Planar accretion event in the MW system, and planar accretions drive disc evolution by depositing material directly onto galactic discs.

The conclusions presented in Chapter 4 produce a coherent picture from all the material presented in this thesis, with the overall goal being the understanding galactic evolution via hierarchical merging, and the nature of the gravitational interaction. This Chapter also presents possibilities for future directions in this field, and outlines plans for future research.

Chapter 2

Globular Clusters, Dark Matter and the Gravitational Interaction

Every passing hour brings the Solar System forty three thousand miles closer to Globular Cluster M13 in Hercules – and still there are some misfits who insist that there is no such thing as progress.

- Kurt Vonnegut

2.1 Testing Newtonian Gravity with AAOmega: Mass-to-Light Profiles of Four Globular Clusters

Richard R. Lane, László L. Kiss, Geraint F. Lewis, Rodrigo A. Ibata, Arnaud Siebert, Timothy R. Bedding and Péter Székely, 2009, *Monthly Notices of the Royal Astronomical Society 400, 917-923*

The first paper in this thesis begins a series of three papers, with this first paper focusing on our understanding of the nature of the gravitational interaction. There have been several provocative studies published recently (Scarpa *et al.*, 2003, 2004a,b, 2007) in which the authors claim to have detected a flattening of the velocity dispersion profile in the outer regions of GCs. This exciting claim calls into question our understanding of gravity; because GCs are thought to contain little, or no, dark matter, their velocity dispersion profiles should drop off in a Keplerian-like fashion. A flattening of the dispersion profiles of GCs could indicate either a large dark matter component, or a flaw in our understanding of the nature of gravity itself. Both of these are extremely interesting scenarios.

Although GCs are *thought* to contain little dark matter, this is still under debate, so quantifying the dark matter content was necessary in order to rule out its effects in any deviation from Newtonian gravity that may be observed. It was also necessary to test for the claimed velocity dispersion profile flattening. These two tests were performed in a single step on four GCs, namely M22, M30, M53 and M68, using a Plummer (1911) profile fit to the velocity dispersion profile. As discussed in Section 1.2.3 the Plummer model is a very useful tool for determining physical parameters of GCs; because of the physical motivation behind the model, many physical parameters of these objects can be calculated from a well fitted model. The other important characteristic of the Plummer model is that it produces a monotonically decreasing function for the velocity dispersion profile – the expected Keplerian-like fall of with radius – which means that any flattening of the profile at large radii will be revealed as a deviation from the model.

The data analysed in this paper was obtained by myself (RRL) and László Kiss. The data reduction was performed by myself, and all code for the analysis of the reduced data, as well as the manuscript itself, was written by myself in consultation with László Kiss, my supervisors Geraint Lewis and Rodrigo Ibata, and collaborators.

Monthly Notices of the ROYAL ASTRONOMICAL SOCIETY

Mon. Not. R. Astron. Soc. **400,** 917–923 (2009) doi:10.1111/j.1365-2966.2009.15505.x

Testing Newtonian gravity with AAOmega: mass-to-light profiles of four globular clusters

Richard R. Lane,[1⋆] László L. Kiss,[1] Geraint F. Lewis,[1] Rodrigo A. Ibata,[2] Arnaud Siebert,[2] Timothy R. Bedding[1] and Péter Székely[3]

[1] *Sydney Institute for Astronomy, School of Physics, A28, The University of Sydney, NSW 2006, Australia*
[2] *Observatoire Astronomique, Universite de Strasbourg, CNRS, 67000 Strasbourg, France*
[3] *Department of Experimental Physics, University of Szeged, Szeged 6720, Hungary*

Accepted 2009 August 5. Received 2009 August 4; in original form 2009 July 8

ABSTRACT

Testing Newtonian gravity in the weak-acceleration regime is vital to our understanding of the nature of the gravitational interaction. It has recently been claimed that the velocity dispersion profiles of several globular clusters flatten out at large radii, reminiscent of galaxy rotation curves, even though globular clusters are thought to contain little or no dark matter. We investigate this claim, using AAOmega observations of four globular clusters, namely M22, M30, M53 and M68. M30, one such cluster that has had this claim made for its velocity dispersion, was included for comparison with previous studies. We find no statistically significant flattening of the velocity dispersion at large radii for any of our target clusters and, therefore, we infer that the observed dynamics do not require that globular clusters are dark matter dominated, or a modification of gravity. Furthermore, by applying a simple dynamical model we determine the radial mass-to-light profiles for each cluster. The isothermal rotations of each cluster are also measured, with M22 exhibiting clear rotation, M68 possible rotation and M30 and M53 lacking any rotation, within the uncertainties.

Key words: gravitation – stellar dynamics.

1 INTRODUCTION

Newtonian gravitation has been shown to describe the motions of bodies with intermediate accelerations (e.g. Solar system bodies) very accurately. The Newtonian theory of gravity breaks down in the presence of strong gravitational fields, where it has been successfully superseded by general relativity, but there is evidence that there are also discrepancies in the low-acceleration regime. Spiral galaxies, for example, require the invocation of dark matter (DM) to reconcile the discrepancy between their rotational velocities and our understanding of Newtonian gravity. Another indication is the so-called ‘Pioneer anomaly’: radiometric data from Pioneers 10 and 11 have shown that both are experiencing an unexplained constant acceleration of $a = (8.74 \pm 1.33) \times 10^{-10}\,\mathrm{m\,s^{-2}}$ towards the Sun (see de Diego 2008 and references therein). In fact, all spacecraft in the outer Solar system seem to be experiencing this anomalous acceleration (e.g. Anderson et al. 2002), potentially indicating a deviation from the Newtonian gravity at low accelerations.

It has been claimed that one of the leading versions of modified Newtonian dynamics (MOND; Milgrom 1983) can predict the kinematic properties of galaxies without invoking DM. MOND predicts a breakdown of Newtonian gravity at an acceleration scale $a_0 \approx 1.2 \times 10^{-10}\,\mathrm{m\,s^{-2}}$ (see Iorio 2009 and references therein). This is approximately the acceleration regime where DM becomes necessary to reconcile theoretical velocity profiles of galaxies with observation.

Globular clusters (GCs) are the ideal test bed for this divergence from Newtonian predictions, since they are thought to contain little or no DM. This is based on the evidence from dynamical models (e.g. Phinney 1993), *N*-body simulations (e.g. Moore 1996), observations of GC tidal tails (e.g. Odenkirchen et al. 2001), dynamical and luminous masses of GCs (e.g. Mandushev, Staneva & Spasova 1991) and the lack of microlensing events from GC-mass dark haloes (e.g. Navarro, Frenk & White 1997; Ibata et al. 2002). In addition, GCs at different distances from the Galactic Centre experience differing gravitational attractions from the Galaxy, so that any Galactic influence can be ruled out if all exhibit similar behaviour. Furthermore, the accelerations experienced by stars in GCs drop below a_0 well inside the tidal radius (e.g. Scarpa et al. 2007).

Recently, Scarpa et al. (2007) showed that there may be a flattening of the velocity profiles of several GCs in the Galactic halo (ω Centauri, M15, M30, M92 and M107), at or about the acceleration where DM is invoked to maintain stability in rotating galaxies. On the other hand, Moffat & Toth (2008) overlaid the Scarpa et al.

⋆E-mail: rlane@physics.usyd.edu.au

Table 1. Clusters selected for the current survey, based on the criteria outlined in the text, with the total number of fibre configurations, and spectra, obtained during the run. Note that the number of spectra quoted here is the total number of spectra obtained before Galactic contaminants were removed. For M68, three configurations were observed on the two observing runs in 2008 June and five subsequent configurations were observed during a service run in 2009 May.

Cluster	Fibre configurations	Total spectra
M22	10	3407
M30	2	620
M53	6	1727
M68	3+5	2650

(2007) results with a modified gravity (MOG) model and found little or no deviation from the Newtonian gravity for GCs with masses less than a few times 10^6 $M_{\odot}$. Because both groups used an identical set of measured velocity dispersions, there is an obvious discrepancy. If MOND were correct, it would mean that all gravitational interactions would diverge from the Newtonian gravitation in the predicted regime. Irrespective of MOND itself, testing the gravitational interaction at low accelerations is extremely important in the overall understanding of gravity. This paper continues this test, with four Galactic halo GCs, namely M22 (NGC 6656), M30 (NGC 7099), M53 (NGC 5024) and M68 (NGC 4590).

2 DATA ACQUISITION AND REDUCTION

We used the multi-object, double-beam spectrograph (AAOmega) on the 3.9-m Anglo-Australian Telescope at the Siding Spring Observatory in New South Wales, Australia, to obtain the spectra for this survey. AAOmega has 392 fibres covering a 2 deg^2 field of view, with each fibre capable of obtaining a single spectrum from a single star in this field. The 1500V grating (with a resolution of $R = 3700$) was used in the blue arm and the 1700D grating ($R = 10\,000$) was used in the red arm, with the central wavelengths set to 5200 and 8640 Å, respectively. This configuration was chosen to include the calcium triplet lines at 8498, 8542 and 8662 Å, for accurate velocity determination and proxy metallicities, as well as the swathe of iron and magnesium lines around 5200 Å for accurate metallicity measurements. The astrometric positions of the targets, taken from the Two-Micron All-Sky Survey (2MASS) Point Source Catalogue,[1] have accuracies of ∼0.1 arcsec.

The observations were taken over two observing runs, on 2008 June 5–8 and 14–19, with an average seeing of ∼1.5 arcsec. We obtained 3 × 1200 s exposures per fibre configuration to obtain signal-to-noise ratio ∼20–100, with several configurations per cluster (see Table 1 for actual numbers of spectra obtained for each cluster – note that for M68, three configurations were obtained in 2008 June, and five further configurations were obtained during a separate service run in 2009 May). In this study, we also made use of data for M30 obtained in a previous observing run in 2006 (originally published by Kiss et al. 2007). Flat fields, arc lamp exposures and ∼25 dedicated sky fibres were used for data reduction and calibration. FeAr, CuAr, CuHe, CuNe and ThAr arc lamps were used to ensure accurate wavelength calibration. Data reduction was performed using the 2DFDR pipeline,[2] designed specifically for the reduction of AAOmega data. The efficacy of the pipeline has been checked with a comparison of individual stellar spectra.

2.1 Cluster selection

We aimed to observe several hundred stars from each of the four GCs, namely M22 (NGC 6656), M30 (NGC 7099), M53 (NGC 5024) and M68 (NGC 4590). These four targets were selected by several criteria: they are bright ($M_V < -7$), nearby ($D < 30$ kpc) and have radial velocities $> 1.5\sigma$ from the peak velocity given by the Besançcon Galaxy Model[3] in that direction, for the ease of extracting the cluster members from Galactic contaminants. One cluster (M30) was included specifically because it was one of the targets of Scarpa et al. (2007), and it satisfied all other selection criteria. This allows a comparison with the results of that study.

We produced a colour–magnitude diagram for each cluster using data from the 2MASS Point Source Catalogue, and the red giant branch (RGB) was identified in colour–magnitude space. Selection of individual target stars was based on the $J - K$ colours and K magnitudes of the RGB of the cluster to minimize the number of stars selected from the Galactic population. Despite this selection process, a number of Galactic contaminant stars were still expected in the final sample, and it was therefore necessary to remove them before analysis. Section 2.1.1 describes this process.

2.1.1 Cluster membership

To select cluster members, it was necessary to determine several quantities for each observed star. Atmospheric parameters and radial velocities were determined using an iterative process, combining best fits to the synthetic spectra from the Munari et al. (2005) spectrum library, with χ^2 fitting, and cross-correlating this best-fitting model with the observed spectrum to calculate the radial velocity. This approach is very similar to that adopted by the radial velocity experiment (RAVE) project (Steinmetz et al. 2006; Zwitter et al. 2008), and is based on the same synthetic spectral library as RAVE. Kiss et al. (2007) outlined this method in detail.

For M22, M30 and M68, we used four parameters to identify members, namely metallicity ([m/H]), equivalent width of the calcium triplet lines, radial velocity and the distance from the centre of the cluster (terminating at the tidal radius as quoted by Harris 1996); only stars that matched using all criteria were judged to be members. Fig. 1 shows all the stars for which spectra were obtained, highlighting those determined to be cluster members. Note that spectra from observing runs over 2006–2008 were combined with the spectra of M22, M30 and M68 taken during the current survey to ensure greater statistical significance of the results.

M53, being closer to the Galaxy in both [m/H] and radial velocity, required a non-degenerate metallicity to determine membership. We used the method outlined by Cole et al. (2004) to calculate [Fe/H] from the equivalent widths of the calcium triplet lines for each star, resulting in a much cleaner selection for this cluster. Further cuts were made on temperature ($T_{\rm eff} < 9000$ K) and the quality of the synthetic spectral fit to produce the final sample used for analysis. Typical uncertainties in the radial velocities of our member stars

[1] http://www.ipac.caltech.edu/2mass/

[2] http://www2.aao.gov.au/twiki/bin/view/Main/CookBook2dfdr

[3] http://www.obs-besancon.fr/modele/

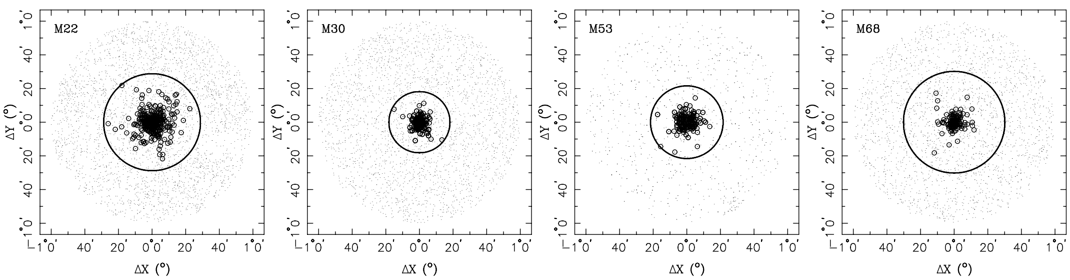

Figure 1. Members of each cluster used for analysis (circled dots), based on the selection method described in the text. The uncircled dots are the stars which were observed and determined not to be cluster members. The large circle is the tidal radius of the cluster from Harris (1996). In each panel, north is up and east is to the left.

are ∼3, ∼2, ∼3 and ∼2.5 km s^{-1} for M22, M30, M53 and M68, respectively. All stars have uncertainties less than 6 km s^{-1}.

The sample consisted of 345, 194, 180 and 123 RGB member stars for M22, M30, M53 and M68, respectively. Note that for M30, the 168 main-sequence turn-off (MSTO) and subgiant branch stars from the Scarpa et al. (2007) study were also included in our analysis, bringing the total number of members for that cluster to 362. The consequence of mixing stellar types in our analysis of M30 is discussed in Section 3.2.

3 RESULTS

3.1 Rotation

The radial velocities were used to determine the rotation of each cluster, assuming an isothermal rotation. The rotation was measured by dividing the cluster in half at a given position angle (PA) and calculating difference between the average velocities in the two halves. This was performed over PAs in steps of 10° for all clusters, except M53 which was done in 15° steps to avoid aliasing effects. The resulting data were then fit with a sine function. Fig. 2 shows the measured rotation for each cluster and the best-fitting sine function. Note that Scarpa et al. (2007) detected no rotation in M30 to a level of 0.75 km s^{-1}, and we corroborate their result; we detect no evidence for rotation to a level of 0.8 km s^{-1}. For M53, no rotation is evident to 0.5 km s^{-1}; however, it is clear that M22 is rotating, with a projected axis of rotation approximately north–south. M68 shows some indication of rotation, although additional data are required to confirm this.

3.2 Velocity dispersions

To determine the velocity dispersions of our samples, we first corrected all the four clusters for rotation, and then binned the stars by

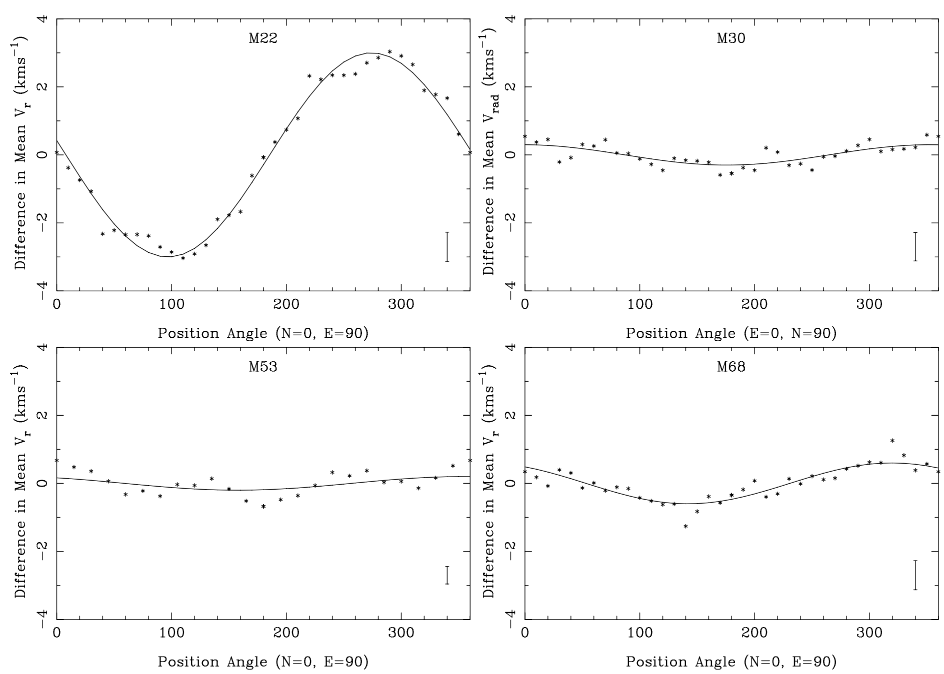

Figure 2. The rotation of each cluster calculated as the difference between the mean velocities from each side of the cluster along equal PAs, as described in the text. The best χ^2 fitting sine function is overplotted, and a typical error bar is represented in the lower right of each panel.

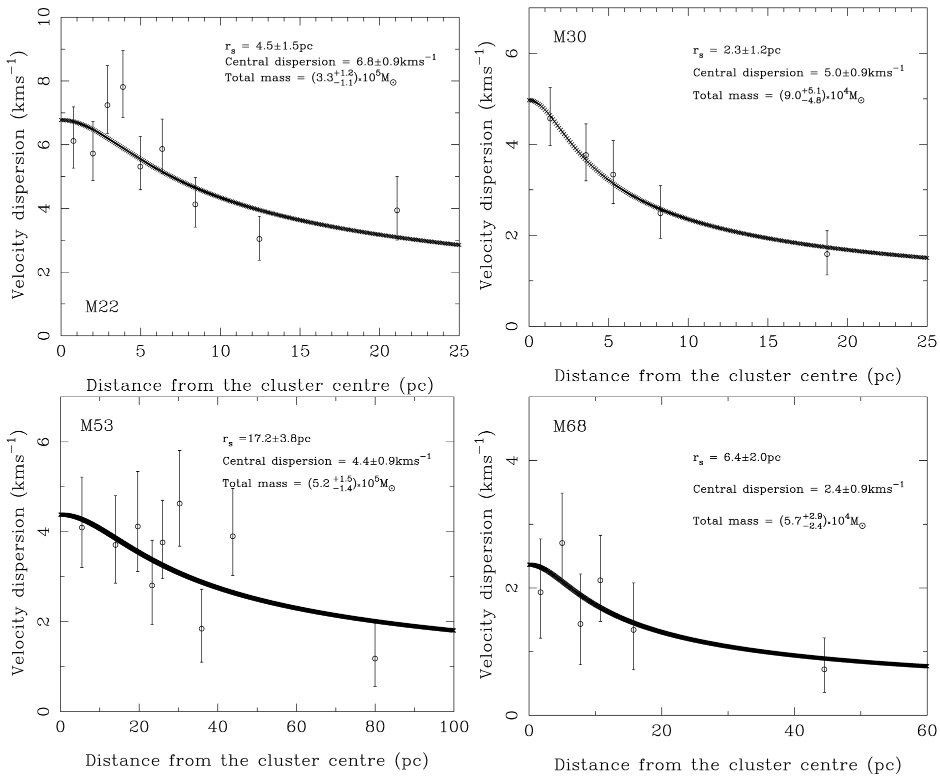

Figure 3. Velocity dispersion profiles of each cluster. The best-fitting Plummer (1911) model is overplotted, and the fitted parameters as well as the calculated total cluster mass are shown.

distance from the cluster centre (annuli), ensuring approximately equal numbers of stars per bin. The mean and standard deviation were calculated for the velocities in each bin. Our velocity dispersions were determined using a Markov Chain Monte Carlo (MCMC) maximum-likelihood method (see Gregory 2005 for an overview of the MCMC methodology), which takes into account the individual velocity uncertainties on the stars and provides the velocity dispersion in each bin with associated uncertainties.

The resulting velocity dispersion profiles were then overplotted with the best-fitting Plummer (1911) model, as shown in Fig. 3. The data points have been plotted at the mean radius of the stars in each bin. Because fewer cluster members exist at larger radii, the outermost bin is generally much larger than the inner bins. To ensure our Plummer model fits do not exhibit an artificial slope in the outskirts of the clusters, masking any possible flattening of the velocity dispersion profiles, we also performed fits to the profiles with the last bin excluded. The fits are nearly identical for M22, M30 and M68. For M53, a small discrepancy between the fits was observed due to the scatter in the velocity dispersions of the inner bins; however, this discrepancy has no impact on our overall results. The reduced χ^2 values for the Plummer fits shown in Fig. 3 are ∼2.3, ∼1.1, ∼2.0 and ∼1.5 for M22, M30, M53 and M68, respectively. We used two parameters in the fitting process, namely the central velocity dispersion and the scale radius (r_s; containing half the cluster mass). Due to the nature of the model, it is possible to calculate the total cluster mass from the central velocity dispersion (σ_0) and r_s (see Dejonghe 1987 for a detailed discussion of Plummer models and their application):

$$M_{tot} = \frac{64\sigma_0^2 r_s}{3\pi G}.$$

The total masses are shown in each panel of Fig. 3.

We chose the Plummer model to fit to our velocity dispersion profiles, because it is a monotonically decreasing function and, therefore, any flattening of the profiles would be clearly shown. The cluster in common between this study and that of Scarpa et al. (2007), M30, shows the best Plummer fit of the four. Note that our complete data set, which includes those data used by Scarpa et al. (2007), has been binned to ensure similar numbers of stars per bin. Because our binning is different to that used by Scarpa et al. (2007), a data point-by-data point comparison between the two studies is not possible here. Within the limits of the model, and the uncertainties in the data, the velocity dispersion does not exhibit any flattening at large radii, and therefore there is no indication that either DM or a modified theory of gravity is required to explain the velocity dispersion of M30. The same case can be made for the other three clusters we examined, and the velocity dispersion profiles along with best-fitting Plummer models (and parameters) are presented in Fig. 3.

Different stellar populations in GCs are known to have differing velocity scatters within the cluster ('velocity jitter'; see Gunn & Griffin 1979; Carney et al. 2003, for detailed discussions). This jitter is due to instabilities in the atmospheres of luminous giant stars. Since we included the MSTO and subgiant stars from the

Table 2. Comparisons between the radial velocities of each cluster in the Harris (1996) catalogue and those from this survey.

Cluster	V_r (Harris 1996)	V_r (This paper)
M22	-148.9 ± 0.4	-144.86 ± 0.34
M30	-181.9 ± 0.5	-184.40 ± 0.20
M53	-79.1 ± 4.1	-62.80 ± 0.31
M68	-94.3 ± 0.4	-94.93 ± 0.26

Scarpa et al. (2007) study with our RGB sample, this jitter should be evidenced as a slightly increased velocity dispersion from the result by Scarpa et al. (2007). This increase in dispersion will be smaller, however, than if we produced our velocity dispersions from our RGB stars alone. Comparing our dispersion profiles for M30 with those of Scarpa et al. (2007), we see some evidence for this increase in the inner regions of the cluster, although the difference is well within the uncertainties. No increase in dispersion is seen in the outer parts; Scarpa et al. (2007) quote a dispersion of $\sim$2.25 km s^{-1} at a radius of 25 pc, whereas our data show a dispersion of $\sim$1.6 km s^{-1} at this distance, although this discrepancy is still within the uncertainties.

The main result from the Scarpa et al. (2007) study was an apparent flattening of the velocity dispersion profiles of five of their six clusters, indicating a DM component or a need for an MOG theory to explain their results. Moffat & Toth (2008) overlaid the dispersion profiles of Scarpa et al. (2007) with an MOG dispersion profile and showed that the flattening of the profiles was consistent with the Newtonian gravity, although the authors did omit one data point from two of the clusters analysed. The Moffat & Toth (2008) MOG model differs from the Newtonian gravity for very massive objects (e.g. galaxy clusters and elliptical galaxies) but becomes Newtonian for masses below a few times $10^6\,M_{\odot}$, which is the mass range of GCs. The MOG fit proves to be an equivalently good fit to these data, indicating no deviation from the Newtonian gravity in these clusters, and a Gaussian with a flat tail has no physical significance. Because Scarpa et al. (2007) overlaid their data with a Gaussian with a flat tail, and Moffat & Toth (2008) overlaid the same data with an MOG model (which becomes Newtonian at low mass), and both are a similarly good fit, neither DM nor a modified version of gravity is required to explain their data, and our study confirms this. A similar conclusion was reached by Sollima et al. (2009) for Ω Centauri.

3.3 Systemic velocities

In addition to the velocity dispersions, the systemic velocity of each cluster was measured (using the Monte Carlo method described above) and compared to similar data in Harris (1996), the most comprehensive catalogue of GC parameters. This comparison is summarized in Table 2. Note especially M53, for which our calculated velocity is significantly different to that of Harris (1996), with the discrepancy well outside the error bars of both measurements. Since Harris (1996) quotes systemic velocity data for M53 from Webbink (1981), who examined a total of 12 stars, our systemic velocity calculation based on 180 stars is a more reliable measurement for this cluster.

3.4 Mass-to-light ratio

One important indicator of large quantities of DM in a dynamical system is a large mass-to-light ratio (i.e. $M/L_{\rm V} \gg 1$). Furthermore, this DM will cause the stars to have large accelerations and therefore inherently higher maximal velocities, and hence a larger velocity dispersion. An obvious way to determine whether or not a pressure-supported object like a GC is DM dominated is to measure its $M/L_{\rm V}$. Of course, this requires a surface brightness profile, for which we have used those by Trager, King & Djorgovski (1995). These profiles were converted to solar luminosities per parsec^2. The density profile was then calculated using (again see Dejonghe 1987):

$$\rho(r) = \frac{M_{\rm tot}}{\pi} \frac{r_{\rm s}^2}{\left(r_{\rm s}^2 + r^2\right)^2}.$$

The $M/L_{\rm V}$ profiles are shown in Fig. 4, along with the $M/L_{\rm V}$ ratios. The vertical line shows the value of $r_{\rm s}$. Because the central regions of GCs are highly concentrated, particularly in post-core-collapsed clusters, it is difficult to accurately determine the mass in the core. The $M/L_{\rm V}$ ratios have, therefore, only been calculated for radii greater than $r_{\rm s}$. Evstigneeva et al. (2007) showed that ultra-compact dwarf galaxies (UCDs) follow the same luminosity–velocity dispersion relation as old GCs. Since it has also been shown that UCDs with a dynamical $M/L_{\rm V}$ up to 5 do not require DM to explain these mass-to-light ratios (e.g. Haşegan et al. 2005; Evstigneeva et al. 2007), we see no requirement for any of our clusters, apart from M53, to contain any DM component. Haşegan et al. (2005) determined that a $M/L_{\rm V} > 6$ for UCDs may indicate some DM content, and since we estimate $M/L_{\rm V} \approx 6.7$ for M53 this may indicate a small DM component in this cluster. Note that if we take the lower limit of our uncertainties for the mass-to-light ratio of M53, we reach the regime where DM is not required, and none of our clusters shows $M/L_{\rm V} \gg 1$, indicating DM is not dominant.

Note that we have produced $M/L_{\rm V}$ *profiles* rather than simply deriving a single $M/L_{\rm V}$ value from the central velocity dispersion and central surface brightness. We suggest that determining $M/L_{\rm V}$ profiles is preferable because it describes the $M/L_{\rm V}$ of the entire cluster outside the core, rather than just its core. This is especially true for post-core-collapse clusters, such as M30, in which the core masses are highly uncertain. Furthermore, M30 is the only cluster in our sample known to have a collapsed core (e.g. Trager et al. 1995). This cluster also has a maximum in its $M/L_{\rm V}$ profile at about the scale radius $r_{\rm s}$, which may be due to mass segregation. The most massive stars are known to fall towards the core during the evolution of the cluster (see Spitzer 1985 for a review of mass segregation processes in GCs). The somewhat less pronounced maximum in the $M/L_{\rm V}$ profile of M68 may be the first evidence that this cluster is currently undergoing core collapse. It has been argued that a central concentration parameter $c \approx 2$ may indicate a collapsed core in certain GCs, and for M68 $c = 1.91$ (van den Bergh 1995). Note that, despite our calculation of the $M/L_{\rm V}$ ratio being restricted to $R > r_{\rm s}$, the profiles should be accurate for $R > r_{\rm c}$, the core radius, or $R \gtrsim r_{\rm s}/2$. Therefore, we argue that the peak in $M/L_{\rm V}$ is real, although a larger sample of cluster members for $R < r_{\rm s}$ will be required to test this and, therefore, to show whether M68 is truly undergoing core collapse.

4 CONCLUSIONS

We have studied four GCs to determine their velocity dispersion profiles, and found that neither DM nor MOG is required to reconcile the kinematic properties of these particular clusters. M53 may contain a small DM component, indicated by an $M/L_{\rm V} > 6$, but it is not dominant. Within the uncertainties, the $M/L_{\rm V}$ ratio

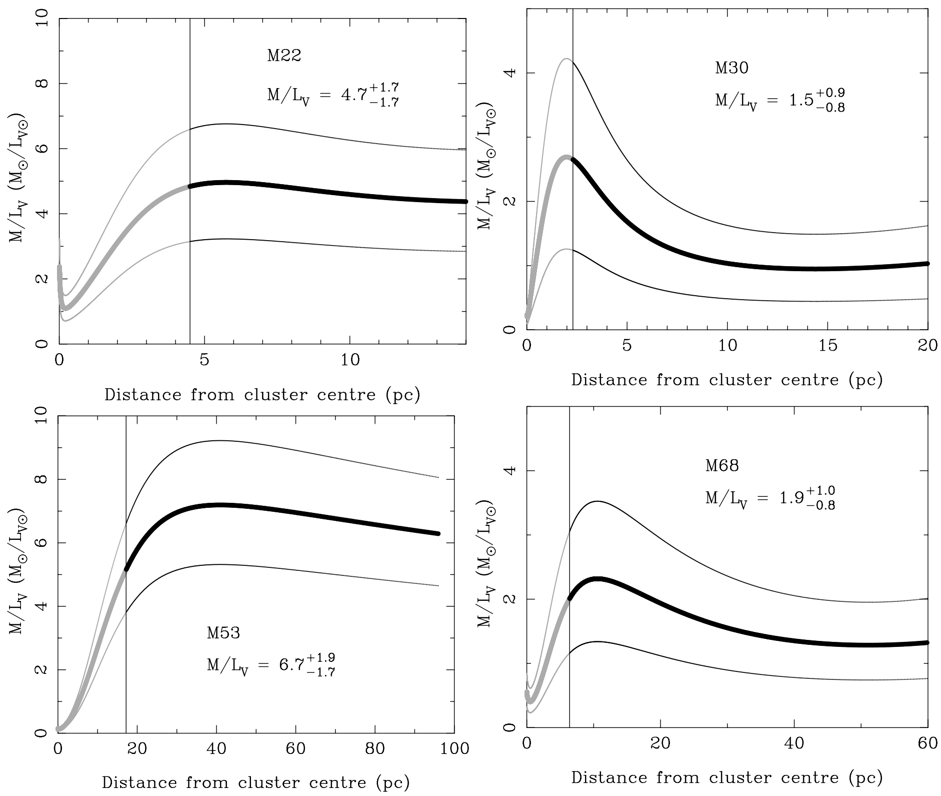

Figure 4. Mass-to-light profiles for each cluster (thick curve). The thin curves show the uncertainties on the M/L_{V}, calculated via the 1σ difference of r_{s} from its calculated value. The vertical line indicates the value of r_{s}. The M/L_{V} value given is only calculated for radii greater than r_{s} because the mass estimates are highly uncertain in the cores of GCs, particularly if they are post-core-collapsed clusters.

of M53 is still consistent with little, or no, DM content. The dynamics of all four clusters are well described by a purely analytic Plummer (1911) model, which indicates that the Newtonian gravity adequately describes their velocity dispersions, and shows no breakdown of Newtonian gravity at $a_0 \approx 1.2 \times 10^{-10}\,\mathrm{m\,s^{-2}}$, as has been claimed in previous studies.

Furthermore, the Plummer model was used to determine the total mass, scale radius (the radius at which half the mass is contained) and the M/L_{V} profile for each cluster. We find that none of our clusters has $M/L_{\mathrm{V}} \gg 1$, another indication that DM is not dominant. Within the uncertainties, our estimated cluster masses all match those in the literature (e.g. Meziane & Colin 1996), and the same is true for the M/L_{V} ratios (e.g. Pryor & Meylan 1993). We have produced M/L_{V} *profiles*, rather than quoting a single value based on the central velocity dispersion and central surface brightness. This method is preferred because it describes the M/L_{V} of the entire cluster, rather than only its core; this is particularly important for post-core-collapsed GCs for which the central mass is highly uncertain.

Because the only one of our clusters to have a collapsed core (M30) shows a peak in its M/L_{V} profile at approximately r_{s}, this may be an indication of the resulting mass segregation. If this is the case, then we may have the first evidence that M68, which also exhibits a M/L_{V} peak near r_{s} and has a central concentration of 1.91 (van den Bergh 1995), is currently undergoing core collapse. Further observations are required, both photometric and kinematic, to confirm this.

Another important result from this study is the measured rotations of our clusters. Of the four clusters studied here, one exhibits an obvious rotation, namely M22, with an axis of rotation approximately north–south. M68 may be rotating as well and additional data are required to confirm this. M53 and M30 do not show any rotation to the level of 0.5 and $0.8\,\mathrm{km\,s^{-1}}$, respectively.

While these results are strongly indicative of the current picture of GCs being DM poor, and their dynamics can be explained by standard Newtonian theory, we are currently undertaking robust dynamical modelling of GC systems to fully address the question of the influence of non-Newtonian physics in explaining our observations.

ACKNOWLEDGMENTS

This project has been supported by the Anglo-Australian Observatory, the Australian Research Council and the Hungarian OTKA grant K76816.

REFERENCES

Anderson J. D., Laing P. A., Lau E. L., Liu A. S., Nieto M. M., Turyshev S. G., 2002, Phys. Rev. D, 65, 082004
Carney B. W., Latham D. W., Stefanik R. P., Laird J. B., Morse J. A., 2003, AJ, 125, 293
Cole A. A., Smecker-Hane T. A., Tolstoy E., Bosler T. L., Gallagher J. S., 2004, MNRAS, 347, 367

de Diego J. A., 2008, Revista Mexicana Astron. Astrofis. Conf. Ser., 34, 35
Dejonghe H., 1987, MNRAS, 224, 13
Evstigneeva E. A., Gregg M. D., Drinkwater M. J., Hilker M., 2007, AJ, 133, 1722
Gregory P. C., 2005, Bayesian Logical Data Analysis for the Physical Sciences: A Comparative Approach with 'Mathematica' Support. Cambridge Univ. Press, Cambridge
Gunn J. E., Griffin R. F., 1979, AJ, 84, 752
Harris W. E., 1996, VizieR Online Data Cat., 7195, 0
Haşegan M. et al., 2005, ApJ, 627, 203
Ibata R. A., Lewis G. F., Irwin M. J., Quinn T., 2002, MNRAS, 332, 915
Iorio L., 2009, preprint (arXiv:0901.3011)
Kiss L. L., Székely P., Bedding T. R., Bakos G. Á., Lewis G. F., 2007, ApJ, 659, L129
Mandushev G., Staneva A., Spasova N., 1991, A&A, 252, 94
Meziane K., Colin J., 1996, A&A, 306, 747
Milgrom M., 1983, ApJ, 270, 384
Moffat J. W., Toth V. T., 2008, ApJ, 680, 1158
Moore B., 1996, ApJ, 461, L13
Munari U., Sordo R., Castelli F., Zwitter T., 2005, A&A, 442, 1127
Navarro J. F., Frenk C. S., White S. D. M., 1997, ApJ, 490, 493
Odenkirchen M. et al., 2001, ApJ, 548, L165
Phinney E. S., 1993, in Djorgovski S. G., Meylan G., eds, ASP Conf. Ser. Vol. 50, Structure and Dynamics of Globular Clusters. Astron. Soc. Pac., San Francisco, p. 141
Plummer H. C., 1911, MNRAS, 71, 460
Pryor C., Meylan G., 1993, in Djorgovski S. G., Meylan G., eds, ASP Conf. Ser. Vol. 50, Structure and Dynamics of Globular Clusters. Astron. Soc. Pac., San Francisco, p. 357
Scarpa R., Marconi G., Gilmozzi R., Carraro G., 2007, The Messenger, 128, 41
Sollima A., Bellazzini M., Smart R. L., Correnti M., Pancino E., Ferraro F. R., Romano D., 2009, MNRAS, 396, 2183
Spitzer L. Jr, 1985, in Goodman J., Hut P., eds, Proc. IAU Symp. 113, Dynamics of Star Clusters. Reidel, Dordrecht, p. 109
Steinmetz M. et al., 2006, AJ, 132, 1645
Trager S. C., King I. R., Djorgovski S., 1995, AJ, 109, 218
van den Bergh S., 1995, AJ, 110, 1171
Webbink R. F., 1981, ApJS, 45, 259
Zwitter T. et al., 2008, AJ, 136, 421

This paper has been typeset from a TEX/LATEX file prepared by the author.

2.2 Testing Newtonian Gravity with AAOmega: Mass-To-Light Profiles and Metallicity Calibrations From 47 Tuc and M55

Richard R. Lane , László L. Kiss, Geraint F. Lewis, Rodrigo A. Ibata, Arnaud Siebert, Timothy R. Bedding and Péter Székely, 2010, *Monthly Notices of the Royal Astronomical Society, 401, 2521-2530*

This second paper continues the test of Newtonian gravity in GCs from the first paper (Section 2.1) using 47 Tucanae and M55, with an important addition. Due to the very large datasets obtained for these two clusters (these are currently the largest spectral datasets available for both clusters), it was possible use these data to extend a previously published method for calculating the metallicities of GCs. The previous method using the luminosity of the Horizontal Branch (HB) and equivalent widths of the spectral lines of the infrared CaII triplet was calibrated to the luminosity of the Tip of the Red Giant Branch (TRGB). This has two major advantages: the TRGB is much brighter than the HB ($\sim$ 5 magnitudes) so this method can be used for much more distant objects, and it can also be used for objects with blue HBs since these stellar populations are too hot to exhibit strong CaII lines. This recalibration is, therefore, a significant improvement over the previous method.

Furthermore, an unexpected result was uncovered, a *rise* in the velocity dispersion profile of 47 Tuc at large radius! This is the first evidence for this anomaly in this cluster and may be the result of evaporation, or a past merger (see Section 2.4). As in the first paper, the rotational velocities of the clusters were measured, with 47 Tuc exhibiting a surprisingly large rotation. Could this also be the result of a merger?

Serendipitously, two GCs residing in the Small Magellanic Cloud, namely NGC 121 and Kron 3, lie close enough on the sky that they are in the same field as 47 Tucanae. Although very distant ($\sim 60\,\mathrm{kpc}$) it was possible to obtain data for several stars from each cluster, and hence determine their global metallicities. Furthermore, because M55 is located in front of the southern tidal tail of the Sagittarius dwarf galaxy, it was possible to extract some members from this stream, and again, determine the global metallicity of the stream in that location.

The data analysed in this paper were obtained, and reduced, by my collaborators. All code used for data analysis, as well as the manuscript itself, was written by myself (RRL) in consultation with László Kiss, my supervisors Geraint Lewis and Rodrigo Ibata, and collaborators.

Monthly Notices of the ROYAL ASTRONOMICAL SOCIETY

Mon. Not. R. Astron. Soc. **401,** 2521–2530 (2010) doi:10.1111/j.1365-2966.2009.15827.x

Testing Newtonian gravity with AAOmega: mass-to-light profiles and metallicity calibrations from 47 Tuc and M55

Richard R. Lane,[1⋆] László L. Kiss,[1,2] Geraint F. Lewis,[1] Rodrigo A. Ibata,[3] Arnaud Siebert,[3] Timothy R. Bedding[1] and Péter Székely[4]

[1]*Sydney Institute for Astronomy, School of Physics, A29, University of Sydney, NSW, Australia 2006*
[2]*Konkoly Observatory of the Hungarian Academy of Sciences, PO Box 67, H-1525 Budapest, Hungary*
[3]*Observatoire Astronomique, Universite de Strasbourg, CNRS, 67000 Strasbourg, France*
[4]*Department of Experimental Physics, University of Szeged, Szeged 6720, Hungary*

Accepted 2009 October 4. Received 2009 October 2; in original form 2009 September 1

ABSTRACT

Globular clusters (GCs) are an important test bed for Newtonian gravity in the weak-acceleration regime, which is vital to our understanding of the nature of the gravitational interaction. Recent claims have been made that the velocity dispersion profiles of GCs flatten out at large radii, despite an apparent paucity of dark matter (DM) in such objects, indicating the need for a modification of gravitational theories. We continue our investigation of this claim, with the largest spectral samples ever obtained of 47 Tucanae (47 Tuc) and M55. Furthermore, this large sample allows for an accurate metallicity calibration based on the equivalent widths of the calcium triplet lines and *K*-band magnitude of the Tip of the Red Giant Branch. Assuming an isothermal distribution, the rotations of each cluster are also measured with both clusters exhibiting clear rotation signatures. The global velocity dispersions of NGC 121 and Kron 3, two GCs in the Small Magellanic Cloud, are also calculated. By applying a simple dynamical model to the velocity dispersion profiles of 47 Tuc and M55, we calculate their mass-to-light profiles, total masses and central velocity dispersions. We find no statistically significant flattening of the velocity dispersion at large radii for M55, and a marked *increase* in the profile of 47 Tuc for radii greater than approximately half the tidal radius. We interpret this increase as an evaporation signature, indicating that 47 Tuc is undergoing, or has undergone, core-collapse, but find no requirement for DM or a modification of gravitational theories in either cluster.

Key words: gravitation – stellar dynamics – globular clusters: individual.

1 INTRODUCTION

The nature of the gravitational interaction is one of the most important concepts in astrophysics, yet complete comprehension of this interaction is still elusive. The so-called Pioneer and Fly-by anomalies, where spacecrafts exhibit behaviour that is unexpected from Newtonian and general relativity gravitation theories, outline this lack of understanding (see Anderson et al. 2002; de Diego 2008, and references therein), although these examples may have more mundane explanations. More importantly, it has been claimed that several globular clusters (GCs; ω Centauri, M15, M30, M92 and M107) exhibit a flattening of their velocity dispersion profiles at radii $R \sim \frac{r_t}{2}$, where r_t is the tidal radius of the cluster (Scarpa, Marconi & Gilmozzi 2003, 2004a,b). The authors claim that either dark matter (DM) or a modification of gravitational theory is required to explain their results.

Modified theories of gravity (MOG; see Durrer & Maartens 2008, for a review of modified gravity theories) and those of Newtonian dynamics (MOND; Milgrom 1983) have been shown to solve some of the discrepancies. However, these are not universal theories and to-date have only been applied to specific instances (e.g. the Bullet Cluster and galaxy rotation curves; see Angus, Famaey & Zhao 2006; Sanders & Noordermeer 2007, respectively). MOG theories diverge from Newtonian gravity in the high-acceleration regime and MOND diverges from Newton in the low-acceleration regime. Therefore, if either of these theories were correct, the effect should be measurable at the predicted accelerations. Independent of MOG or MOND theories, testing the gravitational interaction at low accelerations is essential to the overall understanding of gravity.

GCs are an ideal testing ground for weak-field gravitation because the accelerations experienced by stars at large radii are below

⋆E-mail: rlane@physics.usyd.edu.au

the limit where DM, or a modified gravitation theory, is required to explain observations in many dynamical systems ($a_0 \approx 1.2 \times 10^{-10}\,\mathrm{m\,s^{-2}}$; Scarpa et al. 2007). Furthermore, they are thought to contain little, or no, DM – indicated by dynamical models (Phinney 1993), N-body simulations (Moore 1996), observations of GC tidal tails (Odenkirchen et al. 2001), dynamical and luminous masses of GCs (Mandushev, Staneva & Spasova 1991) and the lack of microlensing events from GC-mass dark haloes (Navarro, Frenk & White 1997; Ibata et al. 2002), although this is still under debate. GCs are also located at varying distances from the centre of the Galaxy, so that if all exhibit similar behaviour, Galactic influences cannot be the primary cause.

In Lane et al. (2009) (hereafter Paper I), we calculated the velocity dispersions and mass-to-light profiles of M22, M30, M53 and M68. Our conclusions were that there is no requirement for significant quantities of DM, or a modification of Newtonian gravity, to explain the kinematics of any of these clusters. In the current paper, we continue this investigation with the largest spectroscopic data set to date of 47 Tucanae (47 Tuc) and M55. We begin by describing the data acquisition/reduction (Section 2) and the membership selection for each cluster (Section 2.2). Our large samples allow us to determine a metallicity calibration based on the Tip of the Red Giant Branch (TRGB; Section 3.1), as well as the rotations (Section 3.2), systemic velocities and velocity dispersions (Section 3.3) and mass-to-light profiles (Section 3.4) – where we also place limits on the DM content of each cluster from their velocity dispersions and mass-to-light profiles. Finally, our concluding remarks are presented in Section 4.

2 DATA ACQUISITION AND REDUCTION

AAOmega, a double-beam, multi-object spectrograph on the 3.9-m Anglo-Australian Telescope (AAT) at Siding Spring Observatory in New South Wales, Australia, was employed to obtain the data for this survey. AAOmega is capable of obtaining spectra for 392 individual objects over a two degree field of view. We used the D1700 grating, which has been optimized for the Ca II infrared triplet region, centred on 8570Å, with 30 sky fibres used for optimal sky subtraction, and 5–8 fibres for guiding. The positional information for our targets was taken from the Two Micron All Sky Survey (2MASS) Point Source Catalogue (Skrutskie et al. 2006) which has an accuracy of ∼0.1 arcsec, and we selected stars that matched the $J - K$ colour and K magnitude range of the red giant branch (RGB) of each cluster.

Our observations were performed over seven nights on 2006 August 12–18, and a further eight nights on 2007 August 30 to September 6. The mean seeing was ∼1.5 arcsec. Several fibre configurations were taken for each cluster with 3600–5400 s exposures giving a signal-to-noise ratio of $\sim 50 - 250$. To minimize scattered light cross-talk between fibres, each field configuration was limited to stars in a 3 mag range. In total, 4670 and 7462 spectra were obtained in the 47 Tuc and M55 regions, respectively. Flat field and arc lamp exposures were used to ensure accurate data reduction and wavelength calibration. The pointing accuracy of the AAT is ∼0.3 arcsec and the fibres have a ∼2 arcsec diameter. The offset due to the pointing uncertainty is azimuthally scrambled by the fibre, so has no effect on the zero-point of the wavelength calibration. Data reduction was performed with the 2DFDR pipeline,[1] which is specifically designed for AAOmega data. The efficacy of the pipeline has been checked with a comparison of individual stellar spectra.

Radial velocity and atmospheric parameters were obtained through an iterative process which takes the best χ^2 fits to synthetic spectra from the library by Munari et al. (2005) and cross-correlates this model with the observed spectra to calculate the radial velocity [a process very similar to that used by the Radial Velocity Experiment (RAVE; Steinmetz et al. 2006; Zwitter et al. 2008) project]. We used the same spectral library as the RAVE studies; Kiss et al. (2007) outline this process in detail.

[1] http://www2.aao.gov.au/twiki/bin/view/Main/CookBook2dfdr

2.1 Radial velocity and uncertainty estimates

To be sure that we are not under/overestimating the uncertainties, and that our radial velocity measurements, and estimates of the random uncertainties, are reproducible, we observed a single configuration of M68 (as part of the data obtained for Paper I), consisting of 317 spectra of the same stars on consecutive nights.

Radial velocities from the data for a single night were estimated using two independent pipelines to test the efficacy of our own software. For this, we compared the outputs of our own pipeline (again see Kiss et al. 2007 for a detailed description) with that from the pipeline written specifically for the RAVE project. The average difference in radial velocities between the two pipelines is $0.3 \pm 0.1\,\mathrm{km\,s^{-1}}$.

To test that our pipeline reproduces reliable velocities, and associated uncertainties, these were extracted from the data from consecutive nights. Subtracting one from the other results in a distribution with a mean of $-0.33\,\mathrm{km\,s^{-1}}$ and $\sigma \approx 0.97$. Therefore, 95 per cent of the stars observed have velocities within $\approx 2\,\mathrm{km\,s^{-1}}$ from one night to the next. This is within the systematics of the instrument (see Section 3.3) and is comparable to the quoted uncertainties for individual velocity estimates. Furthermore, because we used many fibre configurations for each cluster, it was necessary to test for systematic offsets between configurations. Therefore, we calculated the velocity dispersion of stars from four separate configurations within the same distance bin (13 stars were available from each configuration). The dispersions between configurations had a maximal difference of $0.3\,\mathrm{km\,s^{-1}}$, which is well within the uncertainties of the bin.

2.2 Cluster membership

We selected cluster members using four parameters, namely the equivalent width of the calcium triplet lines, surface gravity ($\log g$), radial velocity and metallicity ([m/H]). Only stars that matched all criteria were judged to be members. A further cut of $\log g < 3.25$ was applied to 47 Tuc to ensure as many Galactic stars were as possible were removed. This very probably removed some cluster members but was a necessary sacrifice to ensure our sample was as free of Galactic contaminants as possible. Fig. 1 shows the selection criteria of 47 Tuc. The selections of M55 are not shown because the velocity of the cluster ($\sim 175\,\mathrm{km\,s^{-1}}$) is far removed from the Galactic population ($\sim 0\,\mathrm{km\,s^{-1}}$), so the selections are very clean.

It should be noted that for several clusters studied in Paper I, a cut-off of $T_{\mathrm{eff}} \gtrsim 9000\,\mathrm{K}$ was necessary to remove hot horizontal branch (HB) stars with highly uncertain radial velocities because the calcium triplet in very hot stars is replaced by hydrogen Paschen lines (and also have intrinsic radial velocity variability, see Section 3.3). No cut was made on T_{eff} for either of the current clusters because no stars with $T_{\mathrm{eff}} \gtrsim 7050\,\mathrm{K}$ (for 47 Tuc) or $T_{\mathrm{eff}} \gtrsim 8500\,\mathrm{K}$ (for M55) remained after our selection process. Fig. 2 shows the

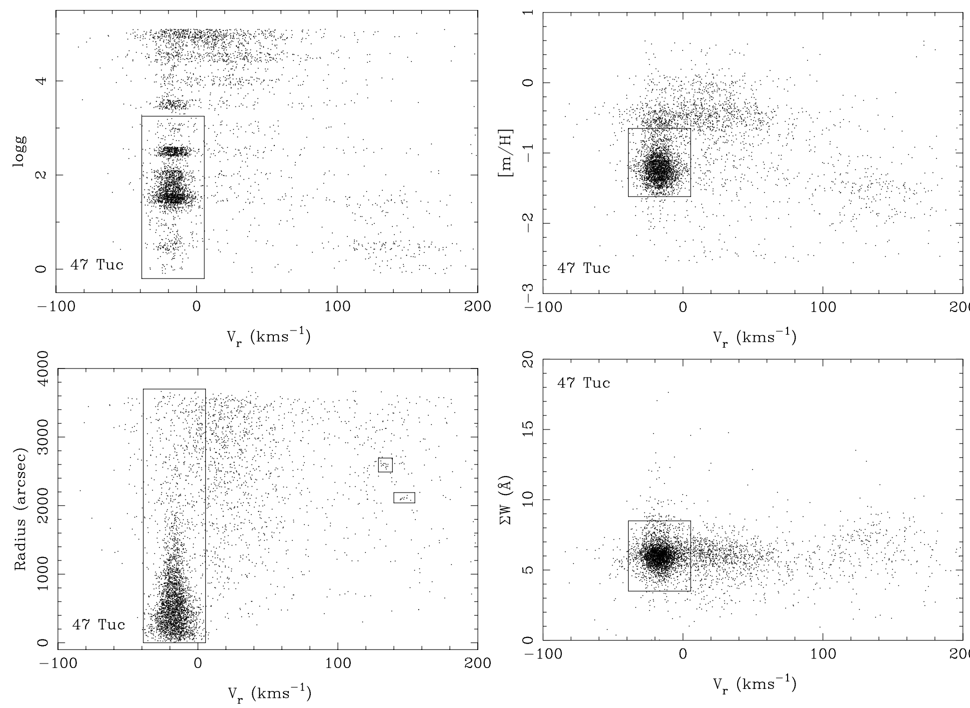

Figure 1. The selections made for 47 Tuc. The boxes indicate the selections on each parameter. The lower left panel also shows the selections for Kron 3 (at ∼2600 arcsec radius) and NGC 121 (at ∼2100 arcsec radius). The selection box for Kron 3 is centred on the cluster and was restricted to the cluster diameter (204 arcsec). For NGC 121, there were no stars outside 150 arcsec despite the diameter being similar to that of Kron 3.

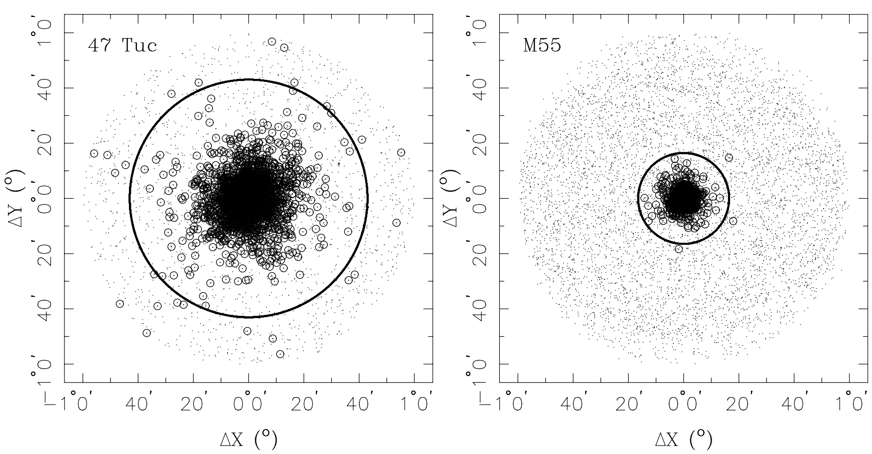

Figure 2. The uncircled points are the stars which were observed and determined not to be cluster members. The members used for analysis, based on the selection method described in the text, are circled points. The large circle is the tidal radius of the cluster from Harris (1996). In each panel, north is up and east is to the left.

relative locations of the observed stars and highlights those found to be members. Several member stars in each cluster were found beyond the tidal radius; the implications of this are discussed in Section 3.3.1.

Fig. 3 shows the colour–magnitude diagrams (CMDs) of the cluster members, with the extra-tidal stars as large points. These extra-tidal stars do not populate any specific region of the CMD, indicating that there is no systematic contributing to their selection as members. The HB, RGB bump and asymptotic giant branch (AGB) clump are all visible in 47 Tuc. A hint of the HB can be seen in M55 at $\sim 13 < J < 14$, however, it is not well populated because, unlike 47 Tuc, M55 has a blue HB, and these stars are too hot to exhibit strong calcium triplet spectra. A total of 2241 and 726 members were selected for 47 Tuc and M55, respectively. For 47 Tuc, 98.6 per cent of our final sample used for analysis (2210 out of 2241 stars) fall within the 99.7 per cent confidence level for

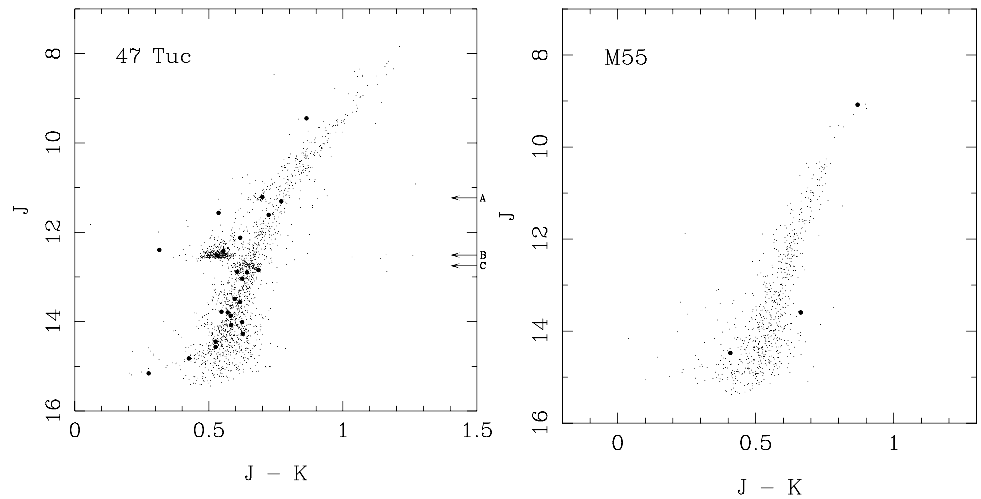

Figure 3. CMDs of selected members of 47 Tuc and M55 with extra-tidal stars shown as large points. Because these do not populate any particular part of the CMD, there is no systematic contributing to their selection as members. Note the AGB clump (A), horizontal branch (B) and RGB bump (C) in 47 Tuc. The HB of M55 at $\sim 13 < J < 14$ is sparsely populated because it has a blue HB whose stars are too hot for strong calcium triplet spectra.

cluster membership based on statistical analysis of each selection parameter.

2.2.1 *Sgr, NGC 121 and Kron 3*

M55 resides in front of the southern tidal tail of the Sagittarius dwarf galaxy (Sgr; Ibata, Gilmore & Irwin 1994) and 42 stars from that field were found to be part of Sgr (see Section 3.1 for details). These were removed from the sample and analysed separately. Two GCs from the Small Magellanic Cloud (SMC) are present in the 47 Tuc field, namely NGC 121 and Kron 3. When determining Kron 3 membership, we restricted our selection to a box centred on the cluster with a length of 204 arcsec, the diameter of the cluster as quoted by Bica & Dutra (2000) (Fig. 1). For NGC 121, we simply selected the clump of stars shown in Fig. 1 because there were no stars outside ∼150 arcsec, despite the diameter of this cluster being about the same as that of Kron 3 (Bica & Dutra 2000). We then overplotted the selections on the 2MASS region around 47 Tuc to ensure they fell in the same region of sky as the cluster and discarded those that did not (Fig. 4). A total of 10 and 11 stars were found to be members of NGC 121 and Kron 3, respectively.

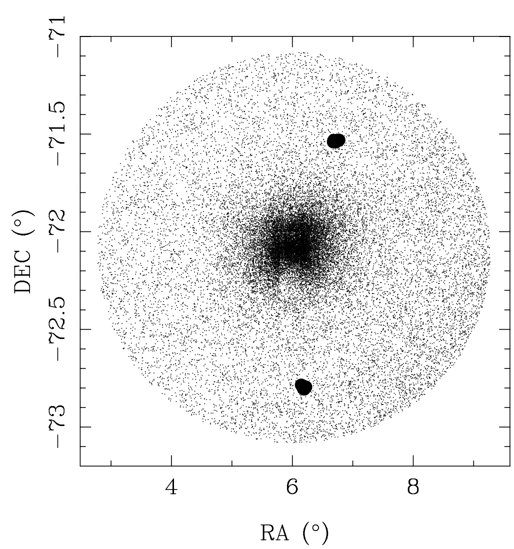

Figure 4. Selected members of Kron 3 [large points below 47 Tuc: (RA,Dec.) ≈ (6.19, −72.79)] and NGC 121 [large points above 47 Tuc: (RA,Dec.) ≈ (6.70, −71.54)].

3 RESULTS

3.1 Metallicity

Given the large sample sizes of both clusters, we were able to perform an accurate metallicity calibration in a similar way to that by Cole et al. (2004) and Warren & Cole (2009). Our method uses the TRGB K magnitude (K_{TRGB}), instead of the HB used by Cole et al. (2004) and Warren & Cole (2009). Both methods are robust, but the TRGB is brighter than the HB, allowing our method to be used for more distant clusters where the HB is not visible. In addition, only in the K band has a direct calibration of the TRG been made with *Hipparcos* parallaxes (Tabur, Kiss & Bedding 2009). The metallicity calibration was carried out in three steps. First, K_{TRGB} was subtracted from each star and plotted against the equivalent width of the calcium triplet lines (see Fig. 5), giving a distance independent measure of the luminosity. K_{TRGB} values were taken from Valenti, Ferraro & Origlia (2004) (47 Tuc, M30 M55 and M68), Marconi et al. (1998) (Sgr core) and 2MASS CMDs (Kron 3, NGC 121, M22 and M53; see below). Several stars from the M55 field overlapped the 47 Tuc region in this figure. Because the metallicity of 47 Tuc is similar to that of the tidal tails of Sgr (e.g. Chou et al. 2007), this overlap was expected; these stars belong to the southern tidal tail of Sgr and are highlighted in Fig. 5. All stars with $T_{\mathrm{eff}} > 6000$ K were removed from the M55 sample for the metallicity analysis because these hotter HB stars have the calcium triplet lines affected by hydrogen Paschen lines and, therefore, should not be used for metallicity analysis. This was not necessary for 47 Tuc since the

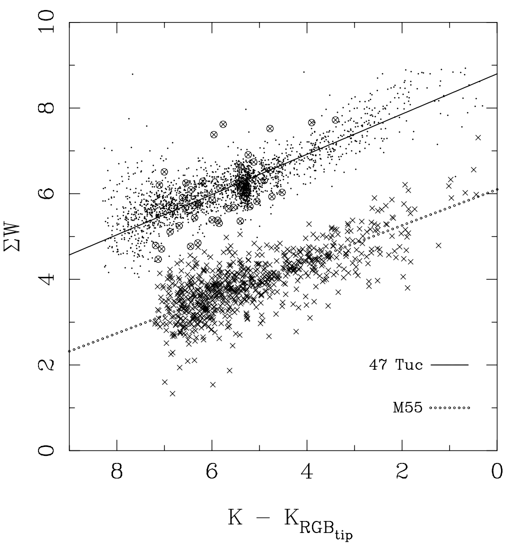

Figure 5. $K - K_{\rm TRGB}$ versus equivalent width of the calcium triplet lines. Crosses are M55 members, dots are 47 Tuc members and circled crosses are those stars determined to belong to the southern tidal tail of Sgr. These were analysed separately. The straight lines are the linear fits to the data once the Sgr members, and all stars having $T_{\rm eff} > 6000$ K, were removed.

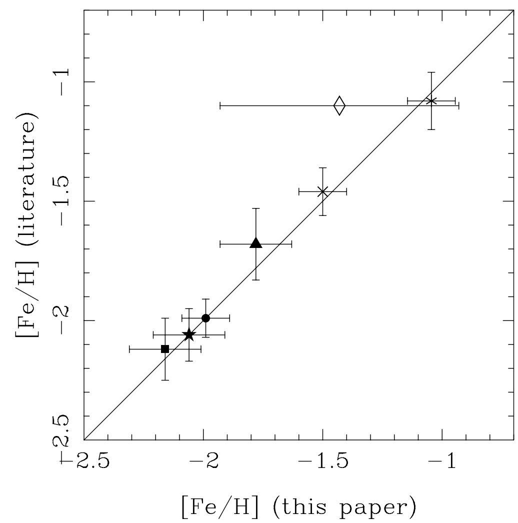

Figure 6. Calculated [Fe/H] for M30 (square), M68 (star), M53 (circle), M22 (triangle), NGC 121 (cross), Sgr (diamond), Kron 3 (asterisk) versus literature values (see text). The large uncertainty for Sgr is due to the difficulty in calculating the TRGB for this object. No consensus on an uncertainty estimate has been reached, hence none is shown here from the literature.

selections were restricted to stars with $\log g < 3.25$, because this cluster is closer to the Galaxy in $\log g$, which removed all the hotter HB stars.

The second step in the calibration process was to fit straight lines to the data (Fig. 5). Because our 47 Tuc sample contains many HB stars, and these were not expected to exhibit the same relation between calcium triplet line widths and $K - K_{\rm TRGB}$, these fits were also performed with the HB stars of 47 Tuc removed. No difference in the fits was found, so the HB stars are included in Fig. 5. The slope of these lines are 0.47 and 0.42 for 47 Tuc and M55, respectively (cf. 0.64 for V-band analysis of the HB by Cole et al. 2004 and 0.47 for K-band analysis of the HB Warren & Cole 2009).

Thirdly, by plotting [Fe/H] of the two clusters (from Harris 1996) versus $\Sigma W - AX$, where A is the gradient of the slope above and X is $K - K_{\rm TRGB}$, for these two clusters we have a calibrator on [Fe/H] (see Cole et al. 2004; Warren & Cole 2009, for a detailed discussion of this calibration methodology). $\Sigma W - AX$ can then be calculated for any cluster and therefore [Fe/H]. Fig. 6 shows [Fe/H] calculated by this method versus [Fe/H] from the literature: for Sgr (Chou et al. 2007), Kron 3 (Glatt et al. 2008b), NGC 121 (Glatt et al. 2008a) as well as the four clusters from Paper I, namely M22 (Monaco et al. 2004), M30 (Harris 1996), M53 (Harris 1996) and M68 (Harris 1996) (TRGB values for these final four clusters were all measured from 2MASS CMDs), showing this calibration for [Fe/H] to be robust. For clarity, the [Fe/H] values from this paper, and the literature, are also shown in Table 1.

The large uncertainty for Sgr is due to the difficulty in determining an accurate measure of the TRGB for this object, because the Sgr tidal tails are close to the Galaxy in colour–magnitude space (e.g. Marconi et al. 1998). Furthermore, there is a metallicity gradient along the tails. To determine the K magnitude of the TRGB for the southern Sgr tail at the location covered in the current survey, we produced a CMD from our data (Fig. 7) and found $K_{\rm TRGB} \approx 11.15$.

Table 1. [Fe/H] values from this paper and from the literature, in order of decreasing metallicity.

Cluster	[Fe/H] (this paper)	[Fe/H] (literature)
Kron 3	-1.05 ± 0.1	-1.08 ± 0.12
Sgr	-1.4 ± 0.5	~ -1.1
NGC 121	-1.5 ± 0.1	-1.46 ± 0.1
M22	-1.78 ± 0.15	-1.68 ± 0.15
M53	-1.99 ± 0.1	-1.99 ± 0.08
M68	-2.06 ± 0.15	-2.06 ± 0.11
M30	-2.16 ± 0.15	-2.13 ± 0.13

Note. The literature values are taken from Kron 3 (Glatt et al. 2008b), Sgr (Chou et al. 2007), NGC 121 (Glatt et al. 2008a), M22 (Monaco et al. 2004), M53 (Harris 1996), M68 (Harris 1996) and M30 (Harris 1996).

The paucity of stars in this CMD introduces large uncertainties into the calculated [Fe/H] for this object (Fig. 6).

Since no literature values of the $K_{\rm TRGB}$ are available for Kron 3, NGC 121, M22 or M53, we produced CMDs from 2MASS of stars within 2 arcmin of the cluster core (for M22 and M53) and within 10 arcsec for Kron 3 and NGC 121. Several hundred stars in the CMDs for M22 and M53, and ~100 for Kron 3 and NGC 121, meant that accurate values could be calculated.

3.2 Rotation

Assuming each cluster has an isothermal distribution, their rotations were measured by halving the cluster by position angle (PA) and calculating the mean radial velocity of each half. The two mean velocities were then subtracted. This was performed in steps of 10°, and the best-fitting sine function overplotted. The results are presented in Fig. 8.

This method gives an amplitude that is twice the actual measured rotation. Therefore, 47 Tuc exhibits rotation at $2.2 \pm 0.2\,{\rm km\,s^{-1}}$

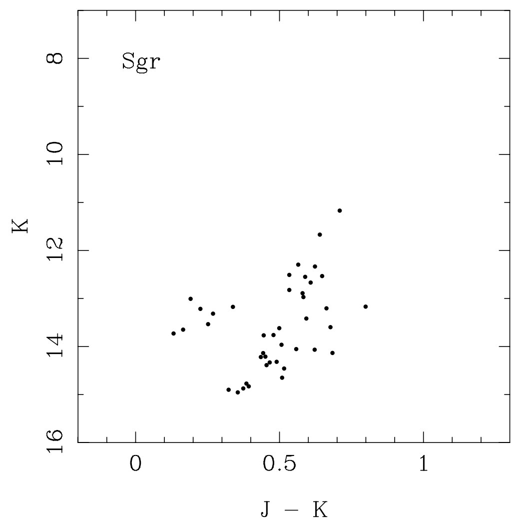

Figure 7. CMD of Sgr stars extracted from the M55 field showing the TRGB at $K \approx 11.15$.

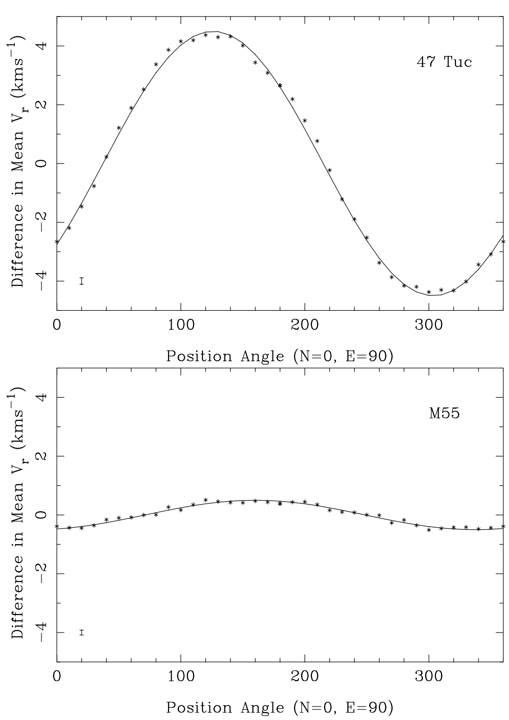

Figure 8. The rotation of each cluster calculated as the difference between the mean velocities on each side of the cluster along equal PAs, as described in the text. The best χ^2 fit sine function is overplotted, and a typical error bar is represented in the lower left of each panel.

with an approximate projected rotational axis along the line PA = 40°–220°, and M55 shows rotation at a level of 0.25 ± 0.09 km s^{-1} and an approximate axis of rotation along the line PA = 65°–245°. Our rotation measure for 47 Tuc corresponds to the value calculated by Meylan & Mayor (1986) at a radius of $\approx$20 pc and by Strugatskaya (1988) at $\approx$36 pc. Székely et al. (2007) showed that M55 is rotating with a velocity of $\sim$0.5 km s^{-1}. This discrepancy can probably be attributed to Székely et al. (2007) having a sample size approximately half that of the current study. For both clusters, we corrected the individual stellar velocity data for the measured rotation before the velocity dispersions, and M/L_V profiles, were calculated.

3.3 Velocity dispersions

Fig. 9 shows velocity versus *J* magnitude for the 47 Tuc data. It appears that the HB population (labelled 'B') has the greatest velocity dispersion of any stellar population in our sample. Stellar pulsations can alter the velocity dispersion profile of a GC, if pulsating stars are present in sufficient numbers, so it is important to check for this effect. 47 Tuc only has one single known RR Lyrae star (Bono et al. 2008), so this will not affect the dispersion profile; however, it is natural to expect that the large number of HB stars in this sample to have an effect, since HB stars are known to pulsate when located close to the instability strip. To test this, we calculated the velocity dispersion of the 47 Tuc sample in *J* magnitude bins. The bin containing the HB stars ($12.43 < J < 12.59$) has a velocity dispersion of 7.5 ± 0.3 and the overall dispersion is 7.5 ± 0.6. Because these stars do not show an increase in dispersion compared with the complete sample, and, furthermore, are distributed evenly throughout the cluster (Fig. 10), we see no reason to exclude the HB stars from the velocity dispersion analysis. Our M55 sample contains very few HB stars (see Fig. 3) so this effect is negligible in this cluster.

We measured the systemic velocity of each cluster, using a Markov Chain Monte Carlo (MCMC) maximum likelihood method (Gregory 2005), which takes into account the individual velocity uncertainties on the stars, providing the systemic velocity with associated uncertainties. A comparison between our values and those from the Harris (1996) catalogue are shown in Table 2. The velocities show systematic differences of the order of 2–3 km s^{-1} between our mean values and those in Harris (1996). These

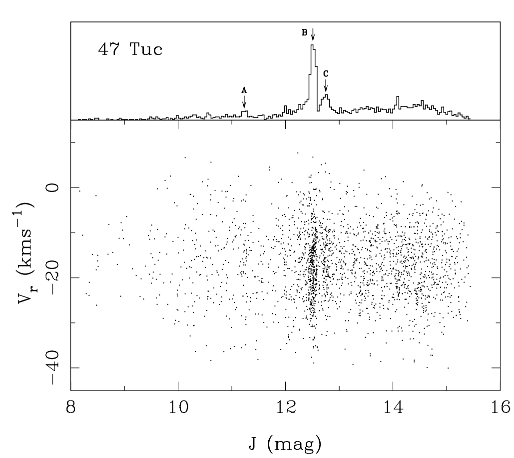

Figure 9. Velocity versus *J* magnitude of the members of 47 Tuc. The HB stars (B) appear to have the largest velocity dispersion of any stellar type. As per Fig. 3, the AGB clump is labelled 'A', the horizontal branch 'B' and the RGB bump 'C'.

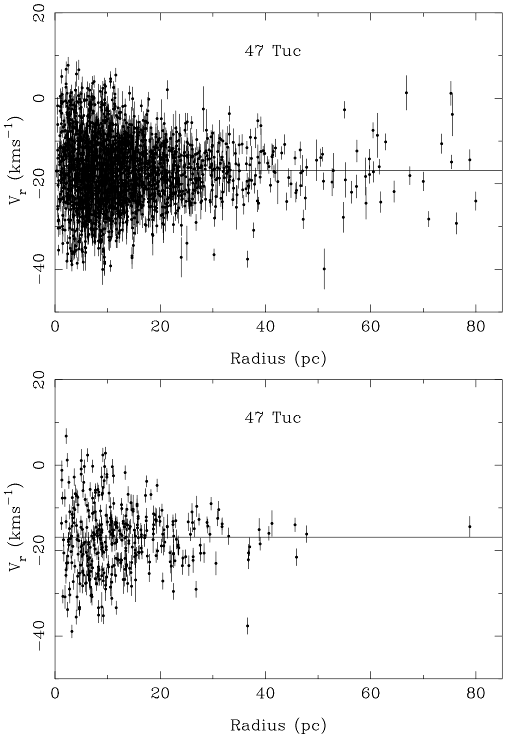

Figure 10. Velocities, and associated uncertainties, versus distance of 47 Tuc. Complete sample (top panel) and HB stars only (bottom panel). Note that the HB stars are evenly distributed throughout the cluster. The horizontal line denotes the measured systemic velocity.

Table 2. Comparisons between the systemic radial velocities of each cluster in the Harris (1996) catalogue and those from this survey.

Cluster	V_r (Harris 1996)	V_r (this paper)
47 Tuc	-18.7 ± 0.2	-16.85 ± 0.16
M55	174.8 ± 0.4	177.37 ± 0.13

Note. Velocities are in km s^{-1}.

differences are similar to what Balog et al. (2009) found for two open clusters, NGC 2451A and B, using the same instrument and analysis method and comparing data to velocities in the literature. Our interpretation is that there might be a systematic uncertainty in the zero-point of our velocity system.

To determine the velocity dispersions of our samples, we binned the stars in annuli centred on the cluster centre, ensuring approximately equal number of stars per bin (∼50 for M55 and ∼100 for 47 Tuc; see Table 3 for the bin dimensions). The MCMC method described above was then used to determine the dispersion in each bin, and the resulting velocity dispersion profiles were overplotted with the best-fitting Plummer (1911) model. The central velocity dispersion and the scale radius (r_s; containing half the cluster mass) were used for the fitting. The Plummer model allows for the calculation of the total cluster mass from the central velocity dispersion (σ_0) and r_s via (see Dejonghe 1987 for a discussion of Plummer

Table 3. Dimensions of the bins, and the number of stars in each, used in the velocity dispersion analysis.

47 Tuc		M55	
Inner bin edge	Stars per bin	Inner bin edge	Stars per bin
0.000	99	0.00	51
2.131	102	1.41	45
3.048	99	1.98	49
4.031	99	2.62	52
4.834	101	3.14	49
5.698	100	3.76	51
6.416	100	4.29	45
7.210	100	4.71	55
8.080	100	5.32	47
8.894	100	6.05	50
9.699	100	6.89	49
10.600	100	7.73	52
11.460	100	8.97	49
12.409	100	11.12	44
13.347	99	15.00	38
14.713	101		
15.849	100		
17.647	100		
19.484	100		
21.899	100		
25.069	100		
30.220	100		
46.704	41		

Note. Only the inner bin edges are shown. Values given are parsecs from the centre of the cluster. The final bin extends to 80 pc for 47 Tuc and 35 pc for M55.

models and their application):

$$M_{\rm tot} = \frac{64\sigma_0^2 r_s}{3\pi G}.$$

Twenty five extra-tidal stars were found to be members of 47 Tuc ($r_t \sim 56$ pc; Harris 1996). The velocity dispersion of 47 Tuc shows a marked increase for $R \gtrsim 28$ pc (this is discussed in Section 3.3.1). Because of this increase in velocity dispersion in the outer regions, the outer two bins were excluded from the Plummer model fitting to the dispersion profiles (Fig. 11), since including them in the fit would have created an artificial increase in the fit over the entire cluster, and hence artificially altered the total mass, scale radius and central dispersion estimates. For M55, only 3 extra-tidal stars were found to be members, and since there is no increase in the dispersion profile, these are not affecting the profile in the outskirts of the cluster. The total masses, scale radii and central velocity dispersions are presented in Table 4. Our mass estimates agree well with other studies (e.g. Meylan 1989; Pryor & Meylan 1993; Meziane & Colin 1996; Kruijssen & Mieske 2009), none of whom used Plummer models to calculate their estimates.

Scarpa et al. (2003, 2004a,b) showed an apparent flattening of the velocity dispersion profiles of five of the six GCs studied, indicating a significant DM component, or a modified theory of gravity, was required to explain their results. MOG models generally differ from Newtonian gravity for large accelerations (e.g. in galaxy clusters or elliptical galaxies) but become Newtonian for intermediate accelerations [e.g. for solar system bodies; see Moffat & Toth (2008) as an example]. MOND, however, becomes non-Newtonian for accelerations below about 1.2×10^{-10} m s^{-2} (Milgrom 1983), approximately the regime where DM is invoked to explain, for example, rotation curves of galaxies.

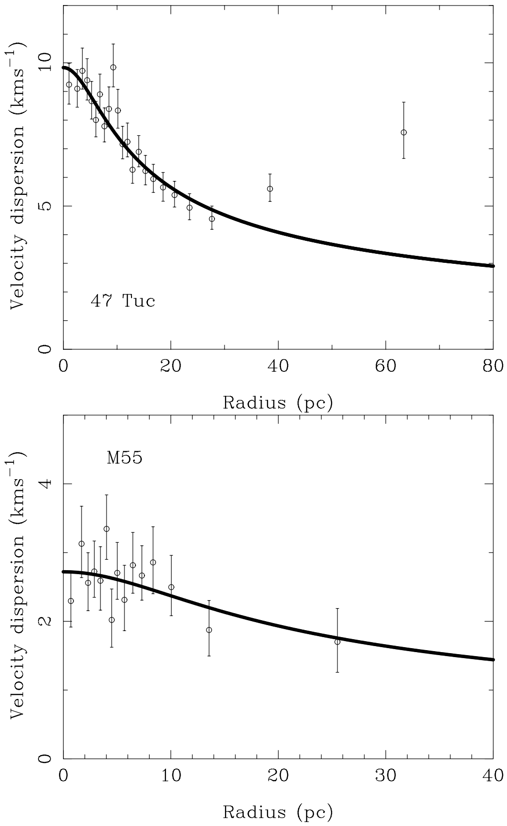

Figure 11. Velocity dispersion profiles of each cluster. The best-fitting Plummer (1911) model is overplotted. Note that for 47 Tuc the outermost two bins are not included during the fitting process to ensure no artificial increase in the estimates of total mass, r_s or central dispersion.

Table 4. Total masses, scale radii (r_s) and central velocity dispersions (σ_0) for 47 Tuc and M55.

Cluster	Total mass ($M_\odot$)	r_s (pc)	σ_0 (km s^{-1})
47 Tuc	$1.1 \pm 0.1 \times 10^6$	7.8 ± 0.9	9.6 ± 0.6
M55	$1.4 \pm 0.5 \times 10^5$	11.7 ± 4.2	2.7 ± 0.5

Plummer models have the advantage of being monotonically decreasing and, therefore, any flattening of the profiles would be discernible. Within the limits of the model, and the uncertainties in the data, neither velocity dispersion exhibits any flattening, although the profile of 47 Tuc exhibits an increase in its dispersion. This could not be called 'flattening' and a MOND/MOG model, or DM, is not required to explain this phenomenon, although a DM component may be one explanation (see Section 3.3.1). Therefore, we infer that neither DM nor a modification to the current understanding of gravitation is needed to explain the dynamics of either 47 Tuc or M55, corroborating earlier results in Paper I for M22, M30, M53 and M68, and similar conclusions by Sollima et al. (2009) for ω Centauri and Jordi et al. (2009) for Pal 14.

Because we only sampled 10 and 11 stars from NGC 121 and Kron 3, respectively, it was not possible to create a velocity dispersion *profile* for these objects. Instead, a single velocity dispersion value for the cluster was calculated, with NGC 121 having a velocity dispersion of 2.2 ± 1.1 km s^{-1} and Kron 3 of 1.8 ± 0.9 km s^{-1}.

3.3.1 Evaporation

GCs are known to be tidally destroyed by their host galaxy through tidal heating (e.g. Pal 5; Odenkirchen et al. 2003). The tidal stripping signature is evidenced by stars being stripped in two directions (the leading and trailing tidal streams). Because the sampled field around 47 Tuc does not reach far outside the tidal radius (Fig. 2), it is not possible to tell whether the extra-tidal stars exhibit a preferential direction. Therefore, an inspection of a 20° × 20° region centred on 47 Tuc was performed, using 2MASS data selected on the RGB and HB colours/magnitudes of 47 Tuc. No evidence for extended tidal structure was observed, independently confirming the result by Leon, Meylan & Combes (2000) who found no convincing statistical evidence of tidal tails.

Evaporation in GCs has been shown to occur due to internal two-body relaxation over the cluster lifetime (e.g. McLaughlin & Fall 2008), particularly during core-collapse, or in post-core-collapsed clusters. Importantly, N-body simulations have shown that this evaporation exhibits a signature in the velocity dispersion profile, increasing the dispersion at $r_t/2$, precisely the region where our 47 Tuc profile increases (Drukier et al. 2007; for 47 Tuc, $r_t/2 \approx$ 28 pc). Furthermore, the extra-tidal velocity distribution is symmetric about the systemic velocity (Fig. 10) implying that these stars are being accelerated in a symmetric way into the outer regions of the cluster. Drukier et al. (2007) pointed out that this evaporation is exacerbated by the collapse of a GC core, leading to greater numbers of two-body interactions. This leads to greater numbers of stars accelerated to the outer regions of the cluster, and beyond, increasing evaporation. It is this evaporation scenario that we infer for 47 Tuc, from its velocity dispersion at large radii, adding to the growing body of evidence that 47 Tuc is in a core-collapse, or post-core-collapse, phase (e.g. Gebhardt et al. 1995; Robinson et al. 1995; Howell, Guhathakurta & Gilliland 2000, and references therein).

To confirm that our interpretation is valid, and that we are not simply describing a chance phenomenon, we rebinned the data to have ~50 stars per bin. The velocity dispersion profile is unaltered by the different binning. Furthermore, we changed the bin boundaries to be sure that this increasing velocity dispersion is real, and, again, found no difference in the overall shape of the profile. Of course, alternative explanations exist for the increase in dispersion. For example, if GCs form in a similar fashion to Ultra Compact Dwarf galaxies, there may be a large quantity of DM in the outskirts of the cluster as discussed by Baumgardt & Mieske (2008). However, no evidence exists supporting GCs forming in this manner. A full MCMC analysis of the outermost, apparently evaporating, stars will be performed in a subsequent paper.

3.4 Mass-to-light profiles

In dynamical systems such as elliptical and dwarf galaxies, large quantities of DM are evidenced by high mass-to-light ratios ($M/L_V \gg 1$). DM causes higher stellar accelerations, leading to inherently higher maximal stellar velocities, and hence a larger velocity dispersion. Therefore, one method for determining whether a pressure-supported object like a GC is DM dominated is to measure its M/L_V from its velocity dispersion. For our M/L_V profiles, we have used the surface brightness profiles by Trager, King & Djorgovski (1995), converted to solar luminosities per square parsec and our density profiles were calculated using (Dejonghe

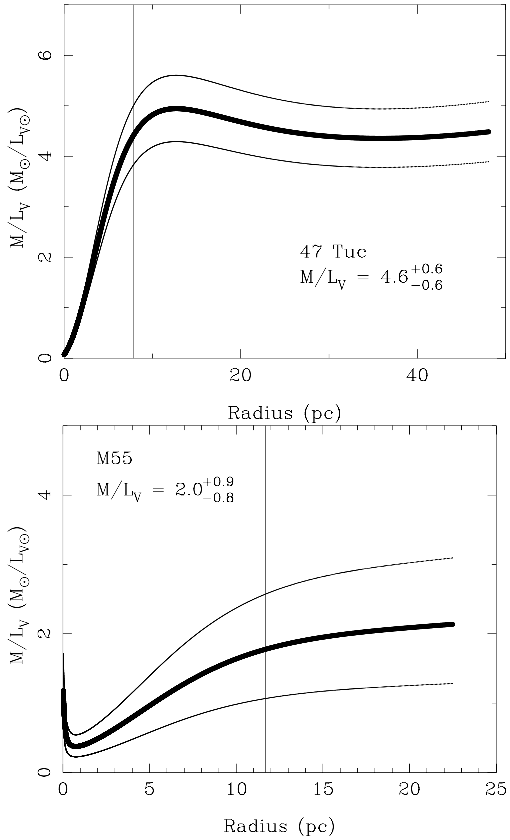

Figure 12. Mass-to-light profiles of 47 Tuc and M55. The thick line is the calculated M/L_V and the thin lines are the uncertainties. The vertical line is r_s, and the mean M/L_V is only calculated for $R > r_s$ due to the uncertainty in core mass. Neither cluster has $M/L_V \gg 1$, indicating DM is not dominant.

1987)

$$\rho(r) = \frac{M_{\text{tot}}}{\pi}\frac{r_s^2}{\left(r_s^2 + r^2\right)^2}.$$

The M/L_V profiles, and associated M/L_V values, are shown in Fig. 12. Because of the uncertainty in core mass, the stated M/L_V values are the mean mass-to-light for $R > r_s$. Our method for calculating M/L_V is preferable to the widely adopted method using the central mass and luminosity, due to the uncertainty in core mass. Despite its apparent superiority over other methods for measuring M/L_V, very few studies have adopted it. This technique has been used by Gebhardt & Fischer (1995) for 47 Tuc, but only for the inner 10 arcmin ($\lesssim r_s$). Because the mass estimates are highly uncertain at small radii, we do not claim to have any realistic data on the M/L_V for $R < r_s$, so no comparison between the current study and that by Gebhardt & Fischer (1995) can be made.

Neither cluster has $M/L_V \gg 1$, therefore DM cannot dominate, although the larger M/L_V of 47 Tuc may indicate a small DM component. However, it has been shown that Ultra-Compact Dwarf galaxies, which follow the same luminosity – velocity dispersion relation as old GCs, show no evidence of DM for $M/L_V <$ 5 (e.g. Haşegan et al. 2005; Evstigneeva et al. 2007). Because of this, we see no requirement for DM in either cluster.

4 CONCLUSIONS

Having the largest sample of spectra ever obtained for 47 Tuc and M55, we were able to produce a very accurate calibration of [Fe/H] based on the equivalent width of the calcium triplet lines and the K-band magnitude of the TRGB. This method is similar to that by Cole et al. (2004) and Warren & Cole (2009), except that we use the TRGB instead of the HB which means this method can be used for much more distant objects.

We calculated the rotation of our clusters assuming them to be isothermal. The rotation of 47 Tuc is $\sim$2.2 $\pm$ 0.2 with an approximate projected rotational axis along the line PA = 40°–220°, and M55 exhibits rotation at a level of 0.25 ± 0.09 km s^{-1} and has an approximate axis of rotation along the line PA = 65°–245°. For 47 Tuc, the rotation amplitude is in good agreement with previous work (e.g. Meylan & Mayor 1986). The only previous study estimating the rotation of M55 (Székely et al. 2007) found a value about twice that of the current work, but Székely et al. (2007) had a sample size approximately half that of ours, which may explain this discrepancy.

Our calculated velocity dispersion profiles of 47 Tuc and M55 provide no evidence that either DM or a modification of current gravitational theories are required to reconcile their kinematic properties, corroborating previous work in Paper I. The dynamics of M55 are well described by a purely analytic Plummer (1911) model, which indicates that Newtonian gravity adequately describes its velocity dispersions, and shows no breakdown of Newtonian gravity at $a_0 \approx 1.2 \times 10^{-10}$ ms^{-2}, as has been claimed for other GCs. The internal dynamics of 47 Tuc (for $R < r_t/2$) are also very well described by the Plummer model, however, the velocity dispersion profile of 47 Tuc exhibits a large increase for $R > r_t/2$, exactly the region where evaporation due to two-body interactions in the core should be observable, especially for GCs undergoing core-collapse or in a post-core-collapse state. We interpret this increase in velocity dispersion as evaporation, and hence that this cluster is either presently in a state of core-collapse, or is a post-core-collapse GC. This adds to the growing evidence that 47 Tuc is currently undergoing a dynamical phase change (e.g. Gebhardt et al. 1995; Robinson et al. 1995; Howell et al. 2000, and references therein). A full analysis of the outer regions of this apparently evaporating cluster will be performed in a subsequent paper.

We used a Plummer model to determine the total mass, scale radius (r_s) and the M/L_V profile for each cluster. We find that neither cluster has $M/L_V \gg 1$, indicating that DM is not dominant. Within the uncertainties, our estimated cluster masses match those in the literature well, as do the M/L_V ratios (e.g. Meylan 1989; Pryor & Meylan 1993; Meziane & Colin 1996; Kruijssen & Mieske 2009). The mass-to-light profiles produced by Gebhardt & Fischer (1995) cannot be compared to the current work because they sampled the inner 10 arcmin for which the mass is uncertain. Note that we consider using mass-to-light *profiles* is a more accurate method for calculating M/L_V than using the core mass and surface brightness, because of this uncertainty.

While our results strongly indicate that the current understanding of GCs being DM poor, and their dynamics explained by standard Newtonian gravity, more robust dynamical modelling is required for confirmation.

ACKNOWLEDGMENTS

This project has been supported by the University of Sydney, the Anglo-Australian Observatory, the Australian Research Council, the Hungarian OTKA grant K76816 and the Lendület Young Researchers Program of the Hungarian Academy of Sciences. We thank Roberto Gilmozzi for his helpful suggestions and feedback on both this paper and Paper I.

REFERENCES

Anderson J. D., Laing P. A., Lau E. L., Liu A. S., Nieto M. M., Turyshev S. G., 2002, Phys. Rev. D, 65, 082004
Angus G. W., Famaey B., Zhao H. S., 2006, MNRAS, 371, 138
Balog Z., Kiss L. L., Vinkó J., Rieke G. H., Muzerolle J., Gáspár A., Young E. T., Gorlova N., 2009, ApJ, 698, 1989
Baumgardt H., Mieske S., 2008, MNRAS, 391, 942
Bica E., Dutra C. M., 2000, AJ, 119, 1214
Bono G. et al., 2008, ApJ, 686, L87
Chou M.-Y. et al., 2007, ApJ, 670, 346
Cole A. A., Smecker-Hane T. A., Tolstoy E., Bosler T. L., Gallagher J. S., 2004, MNRAS, 347, 367
de Diego J. A., 2008, Rev. Mex. Astron. Astrofis., 34, 35
Dejonghe H., 1987, MNRAS, 224, 13
Drukier G. A., Cohn H. N., Lugger P. M., Slavin S. D., Berrington R. C., Murphy B. W., 2007, AJ, 133, 1041
Durrer R., Maartens R., 2008, preprint (arXiv:0811.4132)
Evstigneeva E. A., Gregg M. D., Drinkwater M. J., Hilker M., 2007, AJ, 133, 1722
Gebhardt K., Fischer P., 1995, AJ, 109, 209
Gebhardt K., Pryor C., Williams T. B., Hesser J. E., 1995, AJ, 110, 1699
Glatt K. et al., 2008a, AJ, 135, 1106
Glatt K. et al., 2008b, AJ, 136, 1703
Gregory P. C., 2005, Bayesian Logical Data Analysis for the Physical Sciences: A Comparative Approach with 'Mathematica' Support. Cambridge Univ. Press, Cambridge
Harris W. E., 1996, AJ, 112, 1487
Haşegan M. et al., 2005, ApJ, 627, 203
Howell J. H., Guhathakurta P., Gilliland R. L., 2000, PASP, 112, 1200
Ibata R. A., Gilmore G., Irwin M. J., 1994, Nat, 370, 194
Ibata R. A., Lewis G. F., Irwin M. J., Quinn T., 2002, MNRAS, 332, 915
Jordi K., Grebel E. K., Hilker M., Baumgardt H., Frank M., Kroupa P., Haghi H., Côtè P., Djorgovski S. G., 2009, AJ, 137, 4586
Kiss L. L., Székely P., Bedding T. R., Bakos G. Á., Lewis G. F., 2007, ApJ, 659, L129
Kruijssen J. M. D., Mieske S., 2009, A&A, 500, 785
Lane R. R., Kiss L. L., Lewis G. F., Ibata R. A., Siebert, Bedding T. R., Székely A., P., 2009, MNRAS, 400, 917
Leon S., Meylan G., Combes F., 2000, A&A, 359, 907
Marconi G., Buonanno R., Castellani M., Iannicola G., Molaro P., Pasquini L., Pulone L., 1998, A&A, 330, 453
Mandushev G., Staneva A., Spasova N., 1991, A&A, 252, 94
McLaughlin D. E., Fall S. M., 2008, ApJ, 679, 1272
Meylan G., 1989, A&A, 214, 106
Meylan G., Mayor M., 1986, A&A, 166, 122
Meziane K., Colin J., 1996, A&A, 306, 747
Milgrom M., 1983, ApJ, 270, 384
Moffat J. W., Toth V. T., 2008, ApJ, 680, 1158
Monaco L., Pancino E., Ferraro F. R., Bellazzini M., 2004, MNRAS, 349, 1278
Moore B., 1996, ApJ, 461, L13
Munari U., Sordo R., Castelli F., Zwitter T., 2005, A&A, 442, 1127
Navarro J. F., Frenk C. S., White S. D. M., 1997, ApJ, 490, 493
Odenkirchen M. et al., 2001, ApJ, 548, L165
Odenkirchen M. et al., 2003, AJ, 126, 2385
Phinney E. S., 1993, ASPC, 50, 141
Plummer H. C., 1911, MNRAS, 71, 460
Pryor C., Meylan G., 1993, in Djorgovski S. G., Meylan G., eds, ASP Conf. Ser. Vol. 50, Structure and Dynamics of Globular Clusters. Astron. Soc. Pac., San Francisco, p. 357
Robinson C., Lyne A. G., Manchester R. N., Bailes M., D'Amico N., Johnston S., 1995, MNRAS, 274, 547
Sanders R. H., Noordermeer E., 2007, MNRAS, 379, 702
Scarpa R., Marconi G., Gilmozzi R., 2003, A&A, 405, L15
Scarpa R., Marconi G., Gilmozzi R., 2004a, in Ryder S. D., Pisano D. J., Walker M. A., Freeman K. C., eds, Proc. IAU Symp. 220, Dark Matters in Galaxies. Astron. Soc. Pac., San Francisco, p. 215
Scarpa R., Marconi G., Gilmozzi R., 2004b, in Dettmar R., Klein U., Salucci P., eds, Proc. Sci. Vol. 55.1, Baryons in Dark Matter Halos. SISSA, http://pos.sissa.it
Scarpa R., Marconi G., Gilmozzi R., Carraro G., 2007, The Messenger, 128, 41
Skrutskie M. F. et al., 2006, AJ, 131, 1163
Sollima A., Bellazzini M., Smart R. L., Correnti M., Pancino E., Ferraro F. R., Romano D., 2009, MNRAS, 396, 2183
Steinmetz M. et al., 2006, AJ, 132, 1645
Strugatskaya A. A., 1988, Pis Astron. Zh., 14, 31
Székely P., Kiss L. L., Szatmáry K., Csák B., Bakos G. Á., Bedding T. R., 2007, Astron. Nachr., 328, 879
Tabur V., Kiss L. L., Bedding T. R., 2009, ApJ, 703, L72
Trager S. C., King I. R., Djorgovski S., 1995, AJ, 109, 218
Valenti E., Ferraro F. R., Origlia L., 2004, MNRAS, 354, 815
Warren S. R., Cole A. A., 2009, MNRAS, 393, 272
Zwitter T. et al., 2008, AJ, 136, 421

This paper has been typeset from a TEX/LATEX file prepared by the author.

2.3 Halo Globular Clusters Observed with AAOmega: Dark Matter Content, Metallicity and Tidal Heating

Richard R. Lane, László L. Kiss, Geraint F. Lewis, Rodrigo A. Ibata, Arnaud Siebert, Timothy R. Bedding, Péter Székely, Zoltán Balog and Gyula M. Szabó, 2010, *Monthly Notices of the Royal Astronomical Society, DOI: 10.1111/j.1365-2966.2010.16874.x*

This paper is the final paper in the series analysing Newtonian gravity, completing the analysis of the velocity dispersion profiles of GCs with M4, M12, NGC 6752 and NGC 288, bringing the total to ten. The original primary focus of this three-paper project was the understanding of the nature of the gravitational interaction. Therefore, it should be clearly stated here that no evidence was uncovered which could be used to infer any large dark matter component in any of our clusters, nor the requirement of a modification to Newtonian gravity. Out of these ten clusters, all at varying distances from the Galactic centre and Plane, only M4 showed any obvious flattening of its velocity dispersion profile at large radii. M4 has an orbit that is nearly Planar so this flattening can be attributed to tidal heating.

The number of clusters observed allowed some statistical predictions on the tidal field of the Milky Way. It is clear that the clusters close to the Plane are all tidally heated by the Disc. What is *not* clear, however, is why the stars in the outer regions of *all* these objects should cool down much more rapidly than their relaxation times. This was an unexpected puzzle that is, as yet, unanswered, but may be explained by stars escaping from the outskirts of the clusters, or due to outer GCs being on very circular orbits (which are, therefore, not heated significantly in their passage around the Galaxy). Analysis of data from the Radial Velocity Experiment (RAVE) is in progress to resolve this problem. Again, because of the number of GCs at varying distances from both the Galactic centre and Plane, it was also possible to make broad predictions about the the shape of the dark Halo by looking for tidal heating events in the most distant GCs. This is the first time analysis of GCs has been used in this manner.

As in the fields of 47 Tuc and M55 described in Section 2.2, the observed M4 field contained another cluster. This observation was intentionally offset slightly from the centre of M4 to allow the inclusion of NGC 6144 on the edge of the field, for which we obtained data on 19 stars. Despite this small number of stars we were able to determine the systemic radial velocity of this cluster with better accuracy than previous studies.

Other important things to come from this project included a rotation measurement for all clusters, a readjustment of literature values (e.g. Harris, 1996) of the tidal radius of NGC 6752, and the unresolved puzzle of the rapid cooling of distant cluster members following tidal shocks. All of these are discussed in this paper.

Again, the data analysed in this paper were obtained, and reduced, by collaborators. And again, all the code used in the data analysis, as well as the manuscript itself, was written by myself (RRL) in consultation with László Kiss, my supervisors Geraint Lewis and Rodrigo Ibata, and collaborators.

Monthly Notices of the Royal Astronomical Society

Mon. Not. R. Astron. Soc. (2010) doi:10.1111/j.1365-2966.2010.16874.x

Halo globular clusters observed with AAOmega: dark matter content, metallicity and tidal heating

Richard R. Lane,[1★] László L. Kiss,[1,2] Geraint F. Lewis,[1] Rodrigo A. Ibata,[3] Arnaud Siebert,[3] Timothy R. Bedding,[1] Péter Székely,[4] Zoltán Balog[5] and Gyula M. Szabó[2]

[1]*Sydney Institute for Astronomy, School of Physics, A28, The University of Sydney, NSW 2006, Australia*
[2]*Konkoly Observatory of the Hungarian Academy of Sciences, PO Box 67, H-1525 Budapest, Hungary*
[3]*Observatoire Astronomique, Universite de Strasbourg, CNRS, 67000 Strasbourg, France*
[4]*Department of Experimental Physics, University of Szeged, Szeged 6720, Hungary*
[5]*Max-Planck Institut für Astronomie, Königstuhl 17, D-69117 Heidelberg, Germany*

Accepted 2010 April 20. Received 2010 April 13; in original form 2009 November 18

ABSTRACT

Globular clusters (GCs) have proven to be essential to our understanding of many important astrophysical phenomena. Here, we analyse spectroscopic observations of 10 halo GCs to determine their dark matter (DM) content, their tidal heating by the Galactic disc and halo, describe their metallicities and the likelihood that Newtonian dynamics explains their kinematics. We analyse a large number of members in all clusters, allowing us to address all these issues together, and we have included NGC 288 and M30 to overlap with previous studies. We find that any flattening of the velocity dispersion profiles in the outer regions of our clusters can be explained by tidal heating. We also find that all our GCs have $M/L_V \lesssim 5$, therefore, we infer the observed dynamics do not require DM, or a modification of gravity. We suggest that the lack of tidal heating signatures in distant clusters indicates the halo is not triaxial. The isothermal rotations of each cluster are measured, with M4 and NGC 288 exhibiting rotation at a level of $0.9 \pm 0.1\,\mathrm{km\,s^{-1}}$ and $0.25 \pm 0.15\,\mathrm{km\,s^{-1}}$, respectively. We also indirectly measure the tidal radius of NGC 6752, determining a more realistic figure for this cluster than current literature values. Lastly, an unresolved and intriguing puzzle is uncovered with regard to the cooling of the outer regions of all ten clusters.

Key words: gravitation – stellar dynamics – globular clusters: individual.

1 INTRODUCTION

Globular clusters (GCs) are often used as tracers of the gravitational potentials of galaxies and galaxy clusters (e.g. Kissler-Patig et al. 1999; Côté et al. 2003; Wu & Tremaine 2006; Quercellini, Amendola & Balbi 2008; Gebhardt & Thomas 2009). Although this has been applied to theoretical Galactic potentials (e.g. Allen, Moreno & Pichardo 2006), the actual Milky Way (MW) potential has not yet been analysed in this way. The tidal forces of spiral galaxies are thought to be strongest near the disc because the concentrated mass in that region (gas and stars) has a larger density gradient than the more slowly varying density of the dark matter (DM) halo. Interestingly, many distant MW objects such as GCs and dwarf galaxies are known to be tidally stripped, despite being far enough from the disc that they should not directly interact with it. For example, NGC 7492 is ∼3 kpc further from the Galactic centre than the most distant detection of the Monoceros Ring, an object on the very outskirts of the disc (∼22 kpc; Conn et al. 2007), and exhibits clear evidence of tidal interaction with the Galaxy (Lee et al. 2004). In this paper, we consider 10 GCs at varying Galactocentric and Planar distances, allowing the inference of properties of the potential of the MW for the first time, by looking for signatures of tidal heating in these clusters.

Many GCs exhibit internal accelerations below $a_0 \approx 1.2 \times 10^{-10}\,\mathrm{m\,s^{-2}}$, the level at which either modified gravity such as Modified Newtonian Dynamics (MOND; Milgrom 1983) or DM is required to reconcile the observed kinematics of elliptical galaxies with theory. Near the tidal radius (r_t) it is likely that most stars in GCs feel accelerations below this level, making them an ideal testing ground for low-acceleration gravity (Sollima & Nipoti 2010, and references therein). Furthermore, if all GCs exhibit similar behaviour, Galactic influences cannot be the primary cause. In this final paper in the series [see also Lane et al. 2009 (hereafter Paper I) and Lane et al. 2010a (hereafter Paper II)], we present the velocity dispersions and mass-to-light profiles of four GCs, namely

★E-mail: rlane@physics.usyd.edu.au

Table 1. All parameters derived from the kinematics of the clusters in this project in order of decreasing metallicity (see text, Papers I and II for literature comparisons), as well as the tidal radius from Harris (1996) and the estimated acceleration, due to the cluster, for the most distant cluster member.

Cluster	[Fe/H]	$V_{\rm r}$	M/L$_{\rm V}$	$M_{\rm tot}$	$V_{\rm rot}$	$r_{\rm s}$	σ_0	$r_{\rm t}$	a
47 Tuc	–	-16.9 ± 0.2	$4.6^{+0.6}_{-0.6}$	11^{+1}_{-1}	2.2 ± 0.2	7.8 ± 0.9	9.6 ± 0.6	56.1	2.3×10^{-11}
Kron 3	-1.05 ± 0.10	–	–	–	–	–	–	–	–
M4	-1.16 ± 0.13	71.5 ± 0.3	$1.6^{+0.5}_{-0.5}$	$2.2^{+0.7}_{-0.6}$	0.9 ± 0.1	9.1 ± 2.3	3.9 ± 0.7	20.8	3.8×10^{-11}
NGC 288	-1.24 ± 0.13	-45.1 ± 0.2	$2.1^{+1.5}_{-1.3}$	$0.44^{+0.32}_{-0.26}$	0.25 ± 0.15	3.7 ± 2.0	2.7 ± 0.8	33.1	6.2×10^{-12}
Sgr	-1.40 ± 0.50	–	–	–	–	–	–	–	–
NGC 121	-1.50 ± 0.10	–	–	–	–	–	–	–	–
M12	-1.50 ± 0.13	-41.0 ± 0.2	$1.1^{+0.7}_{-0.6}$	$0.53^{+0.32}_{-0.30}$	0.15 ± 0.1	1.5 ± 0.8	4.7 ± 0.9	25.1	1.1×10^{-11}
NGC 6752	-1.62 ± 0.15	-26.2 ± 0.2	$3.6^{+1.1}_{-1.1}$	$2.0^{+0.6}_{-0.6}$	nil	3.8 ± 1.1	5.7 ± 0.7	64.4 (31.9 ± 2.0)	2.7×10^{-11}
M22	-1.78 ± 0.15	-144.9 ± 0.3	$4.7^{+1.7}_{-1.7}$	$3.3^{+1.2}_{-1.1}$	1.5 ± 0.4	4.5 ± 1.5	6.8 ± 0.9	27.0	6.4×10^{-11}
M55	–	174.8 ± 0.4	$2.0^{+0.9}_{-0.8}$	$1.4^{+0.5}_{-0.5}$	0.25 ± 0.09	11.7 ± 4.2	2.7 ± 0.5	25.1	1.9×10^{-11}
M53	-1.99 ± 0.10	-62.8 ± 0.3	$6.7^{+1.9}_{-1.7}$	$5.2^{+1.5}_{-1.4}$	nil	17.2 ± 3.8	4.4 ± 0.9	112.6	5.8×10^{-12}
M68	-2.06 ± 0.15	-94.9 ± 0.3	$1.9^{+1.0}_{-0.8}$	$0.57^{+0.29}_{-0.24}$	0.6 ± 0.4	6.4 ± 2.0	2.4 ± 0.9	90.0	1.9×10^{-12}
M30	-2.16 ± 0.15	-184.4 ± 0.2	$1.5^{+0.9}_{-0.8}$	$0.90^{+0.51}_{-0.48}$	nil	2.3 ± 1.2	5.0 ± 0.9	42.7	8.1×10^{-12}
NGC 6144	–	196.6 ± 0.8	–	–	–	–	–	82.2	–

Note. From left to right the columns are: cluster name, [Fe/H], systemic radial velocity, M/L$_{\rm V}$, total cluster mass, rotational velocity, Plummer scale radius, central velocity dispersion, tidal radius and acceleration due to the cluster. Some parameters were not calculated due to low sampling, and 47 Tuc and M55 do not have calculated values for [Fe/H] because they were used as calibrators (see Paper II). $V_{\rm r}$, $V_{\rm rot}$ and σ_0 are in km s^{-1}, $M_{\rm tot}$ is in 10^5 M$_\odot$, $r_{\rm s}$ and $r_{\rm t}$ are in pc and a is in m s^{-2}. The $r_{\rm t}$ value for NGC 6752 in parentheses is that derived in Section 3.1.

M4, M12, NGC 288 (chosen for comparison with earlier studies) and NGC 6752, bringing the total for this project to 10. This sample allows statistically significant conclusions to be made on the DM content of halo GCs, and on whether a modification of gravity is required to reconcile their internal kinematics with Newtonian gravitational theory.

Our sample of GCs contains three close to the Galaxy (M55, M12 and M22), four at intermediate distances (NGC 6752, M4, M30 and 47 Tuc) and three that are distant (M68, NGC 288 and M53). We define 'close' to be $R < 5$ kpc, 'intermediate' as $5 < R < 10$ kpc, and 'distant' to be $R > 10$ kpc, following Harris (1996). NGC 288 was chosen, in part, because it is one of the GCs analysed by Scarpa et al. (2007b) who found it to have a flat velocity dispersion profile, similar to that of low surface brightness galaxies which are thought to be DM dominated through to their cores. Our targets were then analysed in separate studies (Papers I and II and the current paper) ensuring a mix of nearby, intermediate and distant GCs to ensure any Galactic influences, if any, would be clearly observed. See Table 1 for the estimated acceleration, due to the cluster, of the most distant cluster member for all 10 clusters analysed in this project. Note that the three distant clusters all experience accelerations due to the Galaxy of $\sim a_0$.

2 DATA ACQUISITION AND REDUCTION

We used AAOmega, a double-beam, multi-object spectrograph on the 3.9-m Anglo-Australian Telescope (AAT) at Siding Spring Observatory in New South Wales, Australia, to obtain the data for this survey. AAOmega covers a two-degree field of view, and is capable of obtaining spectra for 392 individual objects over this field. We used 30 sky fibres used for optimal sky subtraction and 5–8 fibres for guiding. The positional information for our targets was taken from the Two Micron All Sky Survey (2MASS) Point Source Catalogue (Skrutskie et al. 2006) which has an accuracy of $\sim$0.1 arcsec.

Observations of M4 were performed on 2008 February 15–17, 2008, with 1.5–2.5 arcsec seeing. The data for M12 were taken over two observing runs: seven nights on 2006 August 12–18, and a further eight nights on 2007 August 30 – 2007 September 6, both with mean seeing of $\sim$1.5 arcsec. NGC 288 was observed during the 2006 run and NGC 6752 during the 2007 run. For all observations, we used the 2500V grating in the blue arm, resulting in spectra between 4800 and 5150 Å with $\lambda/\Delta\lambda = 8000$. In the red arm, we used the 1700D grating, which is optimized for the Ca II IR triplet region. The red spectra cover $8350 - 8790$ Å, with $\lambda/\Delta\lambda = 10\,000$. This set-up returns the highest spectral resolution available with AAOmega, and is suitable for measuring stellar radial velocities. We selected targets for this campaign by matching the $J - K$ colour and K magnitude range of the red giant branch (RGB) of each cluster. To minimize scattered-light cross-talk between fibres, each configuration was limited to 3 mag in range.

We obtained 718, 2826, 1223 and 3664 spectra in the M4, M12, NGC 288 and NGC 6752 fields, respectively. Flat-field and arc-lamp exposures were used to ensure accurate data reduction and wavelength calibration. Data reduction was performed with the 2DFDR pipeline,[1] which was specifically developed for AAOmega data. We checked the efficacy of the pipeline with a comparison of individual stellar spectra.

Radial velocities and atmospheric parameters were obtained through an iterative process, taking the best fits to synthetic spectra from the library by Munari et al. (2005), degraded to the resolution of AAOmega, and cross-correlating this model with the observed spectra to calculate the radial velocity [a process very similar to that used by the Radial Velocity Experiment (RAVE; Steinmetz et al. 2006; Zwitter et al. 2008) project]. We used the same spectral library as the RAVE studies; this process is outlined in detail by Kiss et al. (2007).

2.1 Cluster membership

We determined cluster membership using four parameters: the equivalent width of the calcium triplet lines, surface gravity, radial velocity and metallicity ([m/H]). Stars matching all criteria were

[1] http://www2.aao.gov.au/twiki/bin/view/Main/CookBook2dfdr

judged to be members. Only stars having $\log g < 4.0$ and $\log g < 4.6$ were selected for NGC 6752 and M12, respectively, ensuring the majority of Galactic contaminants were removed before further selection criteria were applied. This probably removed some genuine cluster members but was necessary to ensure our sample was as free from Galactic field stars as possible.

For several clusters studied in Paper I, a cut-off of $T_{\rm eff} \gtrsim 9000$ K was necessary to remove hot horizontal branch (HB) stars. These have radial velocities with large uncertainties due to the calcium triplet in very hot stars being replaced by hydrogen Paschen lines. No cuts were made on $T_{\rm eff}$ for any of the current clusters because no stars with $T_{\rm eff} \gtrsim 7425$ K (for M4), $T_{\rm eff} \gtrsim 5600$ K (for M12), $T_{\rm eff} \gtrsim 7000$ K (for NGC 288) or $T_{\rm eff} \gtrsim 5500$ K (for NGC 6752) remained after our selection process. In total, 200, 242, 133 and 437 stars were found to be members of M4, M12, NGC 288 and NGC 6752, respectively. Fig. 1 shows the relative locations of the observed stars and highlights those found to be members. Note that 19 stars in the M4 field were found to be members of the GC NGC 6144. For M4,

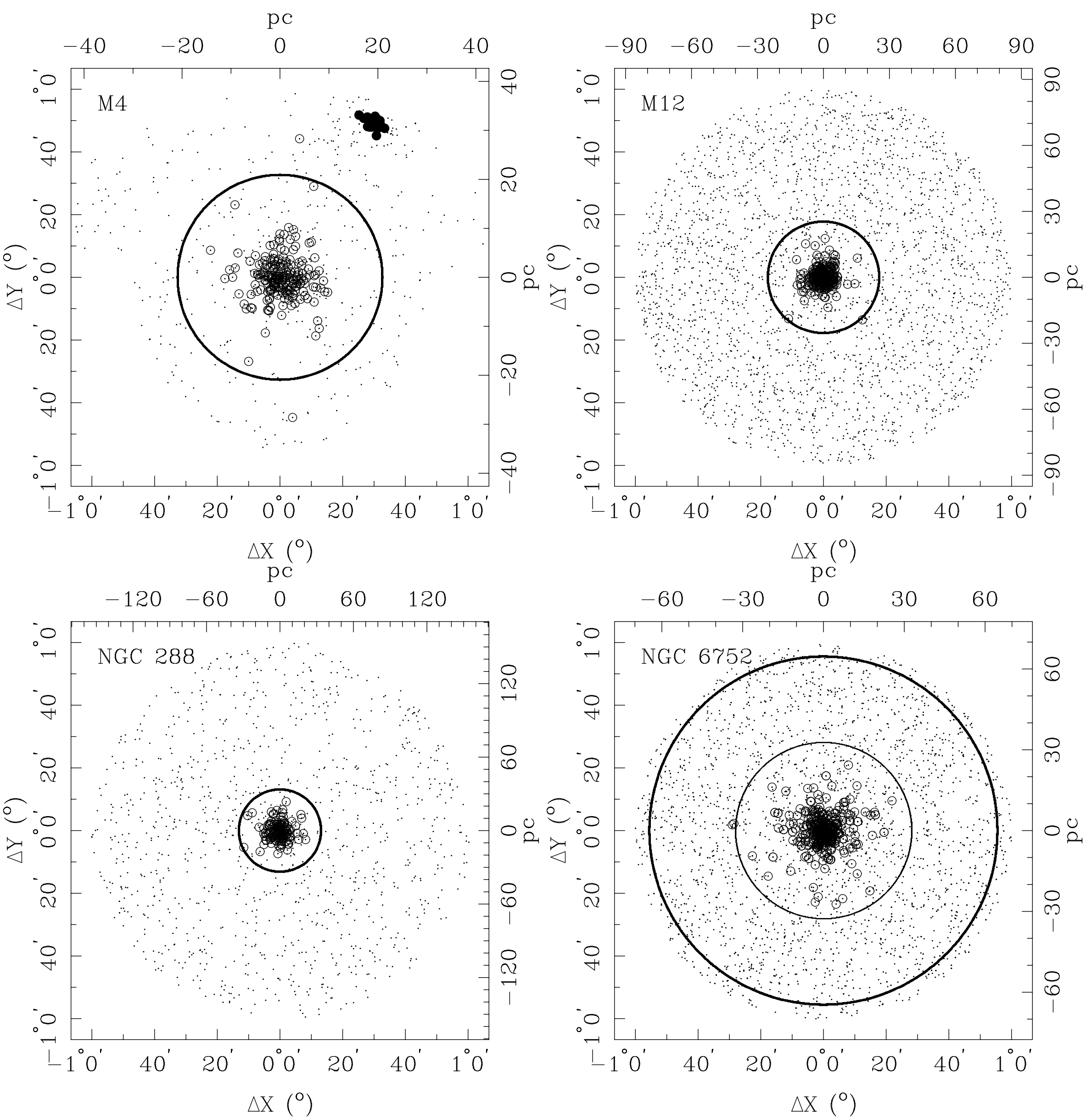

Figure 1. Distribution on the sky of the stars observed in the four fields, with axes in both degrees and parsecs from the cluster centre. Circled points indicate stars that we determined to be cluster members (see text). The large circle is the tidal radius of the cluster from Harris (1996), with the smaller thinner circle in the lower right-hand panel being our derived value for $r_{\rm t}$ for NGC 6752 (see text). The large points in the upper right of the M4 field are the stars we determined to be members of NGC 6144. In each panel, north is up and east is to the left.

we find that 88.0 per cent of the selected members fall within 2σ of *all* selection parameters and 100 per cent within 3σ. For M12, these values are 94.2 and 100 per cent; for NGC 288, 89.5 and 100 per cent; and for NGC 6752, 97.5 and 100 per cent. Based on this, we see no statistical reason to think there is significant Galactic contamination in our final samples.

3 RESULTS

3.1 Tidal radius of NGC 6752

The tidal radius of NGC 6752 in the Harris (1996) catalogue is 55.34 arcmin (shown as the large thick circle in the right-hand panel of Fig. 1), however, this GC is known to have a collapsed core (e.g. Rubenstein & Bailyn 1997) and Harris (1996) warns against using tidal radii calculated from core parameters for such GCs. The most distant of our selected members throughout this project have, generally, been very close to the tidal radius. NGC 6752 is a clear outlier, with members only found to within $\sim 1/2$ of the value of r_t quoted by Harris (1996). Therefore, we propose an updated value of r_t for NGC 6752 based on our membership selections. Note that M30 and 47 Tuc were not used to determine r_t for NGC 6752 because of a paucity of stars observed in M30, and because stars were found out to the edge of the field of view of AAOmega for 47 Tuc.

Based on the membership selections of the remaining seven clusters, the tidal radius is located 94.1 $\pm$ 2.1 per cent of the distance to the most distant member from the cluster centre. Our most distant member for NGC 6752 is located at 33.87 pc, or 29.11 arcmin, therefore, $r_{t_{6752}} = 27.4 \pm 1.7$ arcmin. The quoted uncertainty is based only on the standard deviation of the distance between the outermost member and the tidal radii of our clusters, so the true uncertainty in the value of r_t is likely to be much greater than this. The large thin circle in the right-hand panel of Fig. 1 represents our derived value for r_t. It should be stressed that this value is not a robust measure of r_t, but we suggest it is a more realistic value than that in the Harris (1996) catalogue.

3.2 Metallicity

Our metallicity ([Fe/H]) calibration method, discussed in detail in Paper II, was used to determine the metallicities of each cluster. Briefly, the K magnitude of the Tip of the RGB (K_{TRGB}) was subtracted from the K magnitudes of each star and plotted against the equivalent width of the calcium triplet lines to give a distance independent measure of luminosity. For M4, the K_{TRGB} value was taken from a $J - K$ versus K colour magnitude diagram based on 2MASS data within 5 arcmin of the cluster centre ($K_{\mathrm{TRGB}} = 5.3$), for M12 from Paust (2006) ($K_{\mathrm{TRGB}} = 9.1$), for NGC 288 from Davidge & Harris (1997) and Valenti, Ferraro & Origlia (2004) ($K_{\mathrm{TRGB}} = 8.5$) and for NGC 6752 from Valenti et al. (2004) ($K_{\mathrm{TRGB}} = 7.4$). Linear fits to these data, combined with plotting [Fe/H] values versus $\Sigma W - AX$ for 47 Tuc and M55 ([Fe/H] from Harris 1996, with A being the gradient of the slope above and X being $K - K_{\mathrm{TRGB}}$), allow a calibrator on [Fe/H] for other clusters.

Fig. 2 displays the robustness of this technique, with [Fe/H] values from this project plotted against those from the literature. Solid points are the clusters analysed in Papers I and II. From the current paper, the cross is M4, the square is M12, the triangle is NGC 288 and the diamond is NGC 6752; the [Fe/H] literature values are from Kanatas et al. (1995), Johnson & Pilachowski (2006), Chen et al. (2000) and Zinn (1985), respectively. This method is similar to that outlined by Cole et al. (2004) and Warren & Cole (2009), except we use the TRGB rather than the HB so it can be used for much more distant objects. A recent photometric study of 47 Tuc has revised the metallicity of 47 Tuc to -0.83 (Bergbusch & Stetson 2009). If this new value is adopted for our calibration, a maximum change in our calculated [Fe/H] values is -0.05 (Kron 3), which is well within our uncertainty estimates. Calculated [Fe/H] values are also shown in Table 1.

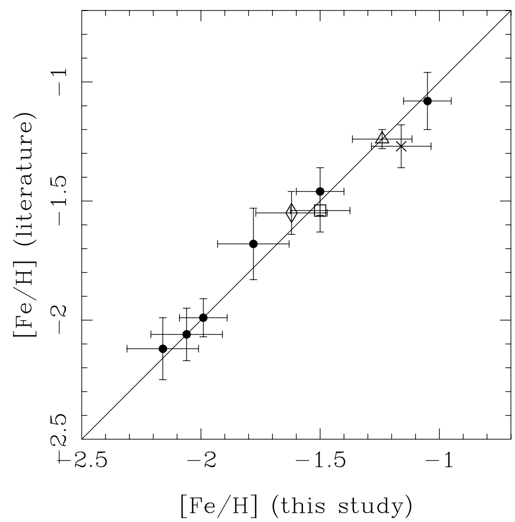

Figure 2. [Fe/H] values derived from our method outlined in the text versus those from the literature. Solid points are those GCs from Papers I and II, and those from the current paper are: M4 (cross), M12 (square), NGC 288 (triangle) and NGC 6752 (diamond). The [Fe/H] literature values are from Kanatas et al. (1995), Johnson & Pilachowski (2006), Chen et al. (2000) and Zinn (1985), respectively.

3.3 Rotation

To measure the projected rotation of each cluster, we assumed an isothermal distribution. The rotations were measured by halving each by position angle (PA) and subtracting the mean stellar velocity of one half from the other. This was repeated in steps of 10° and the best-fitting sine function overplotted (Fig. 3). Note that, for NGC 6752, it was necessary to perform this in steps of 30° to avoid aliasing effects. The method results in an amplitude that is twice the projected rotation. Therefore, M4 exhibits rotation at 0.9 $\pm$ 0.1 km s^{-1}, with an approximate axis of rotation of PA = 70°–250°, M12 at 0.15 $\pm$ 0.1 km s^{-1}, with an approximate axis of rotation of PA = 40°–220° (although this is effectively consistent with no rotation), NGC 288 at 0.25 $\pm$ 0.15 km s^{-1}, with an approximate axis of rotation of PA = 0°–180°, and NGC 6752 shows no rotation to a level of 0.2 km s^{-1}. Our rotation measurement for M4 agrees well with that by Peterson, Rees & Cudworth (1995), who quoted an amplitude of 0.9 ± 0.4 km s^{-1} with an axis along the line PA = 100°–280°, although only for the inner 15 arcmin ($\sim r_t/2$, about 1/3 of the radius of our most distant member).

For all clusters, we corrected the individual stellar velocity data for the measured rotation before calculating the velocity dispersions and M/L$_V$ profiles.

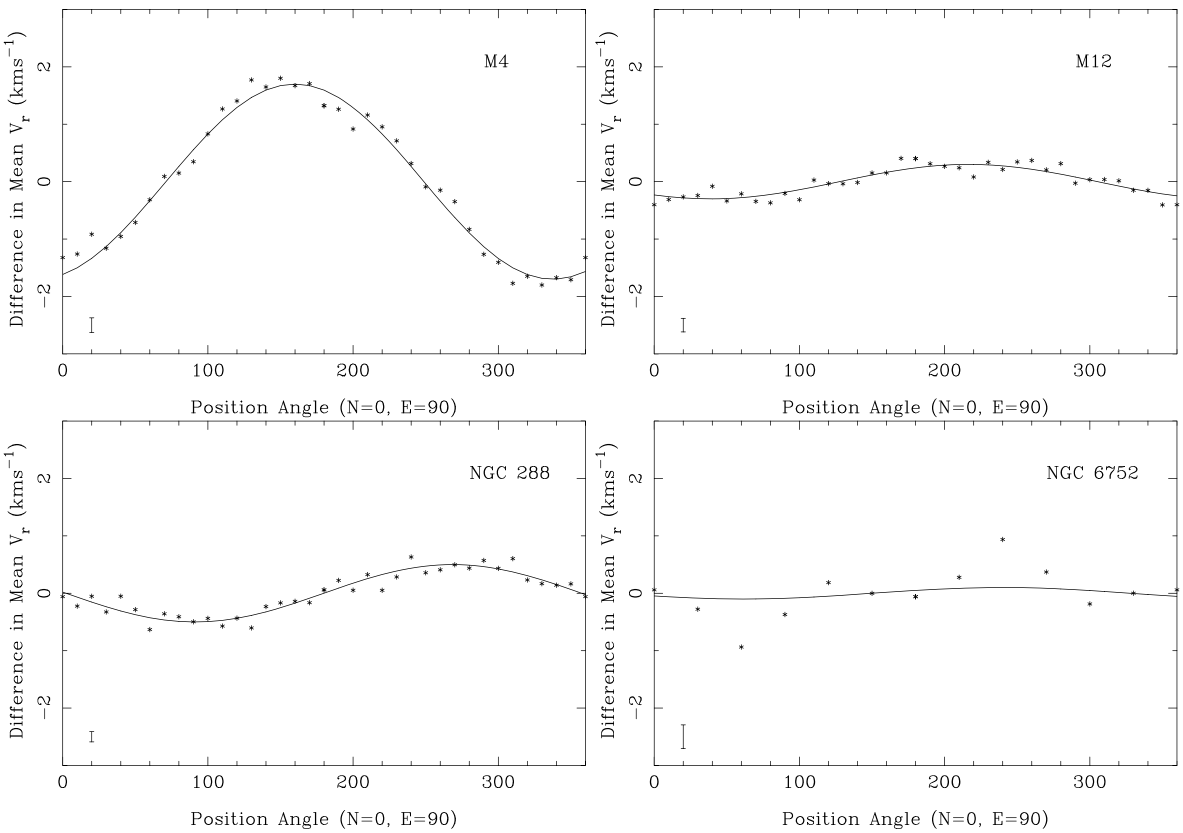

Figure 3. The rotation of each cluster calculated as the difference between the mean velocities on each side of the cluster along equal PAs, as described in the text. The best-fitting sine function is overplotted, and a typical error bar is represented in the lower left of each panel.

3.4 Velocity dispersions

The systemic velocities of each cluster were measured using a Markov Chain Monte Carlo (MCMC) method (Gregory 2005), taking into account the individual velocity uncertainties on the stars, and providing the systemic velocities with associated uncertainties. A simple combination of the stellar velocities in each bin can provide a measure of systemic velocity and dispersion, although this does not take into account the individual velocity uncertainties. To fully incorporate these, we used a Bayesian MCMC-based analysis to provide a measure of realistic uncertainties of the velocity properties as a function of radius. Our systemic velocities agree very well with those from the literature (V_r for all 10 clusters from this project are shown in Table 1), except for NGC 6144. Our survey did not sample this cluster well (19 stars were found to be members), however, only seven stars were analysed by Geisler et al. (1995) which may explain the discrepancy between the two values. The literature values are taken from Suntzeff et al. (1993) (M4 and M12), Rutledge et al. (1997) (NGC 288 and NGC 6752) and Geisler et al. (1995) (NGC 6144).

The velocity dispersions of our samples were calculated for annular bins centred on the cluster, each containing a similar number of stars (M4 $\approx$ 20, M12 $\approx$ 30, NGC 288 $\approx$ 20 and NGC 6752 $\approx$40), centred on the cluster. The MCMC method described above was used to determine the dispersion in each bin, with the resulting velocity dispersion profiles overplotted with the best-fitting line-of-sight Plummer (1911) model:

$$\sigma^2(R) = \frac{\sigma_0^2}{\sqrt{\left(1 + R^2/r_s^2\right)}}.$$

Here, σ_0 is the central velocity dispersion and r_s is the Plummer scale radius (for projected Plummer models, r_s is equivalent to the projected half-mass radius; Haghi et al. 2009). The Plummer model is advantageous for our analysis because it is monotonically decreasing, so any flattening of the profiles would be discernible. It also allows for the calculation of the total mass of the cluster from the central velocity dispersion (σ_0) and r_s via (see Dejonghe 1987 for a discussion of Plummer models and their application):

$$M_{\rm tot} = \frac{64\sigma_0^2 r_s}{3\pi G}. \tag{1}$$

Note that this model assumes the velocity distributions of the clusters are isotropic. How this assumption affects the overall conclusions of this paper regarding MOND and DM within GCs is far from obvious, and is a very complex problem which is beyond the scope of the current study (see Spurzem et al. 2005; Giersz 2006; Kim et al. 2008, and references therein, for detailed discussions of the problem of isotropy in GCs). However, the anisotropies in each of the 10 clusters analysed in Papers I, II and the current study are likely to vary greatly due to the large variation in Galactocentric distances and rotational velocities. Because all our clusters exhibit similar kinematic morphologies, with the possible exception of M4 (Section 4), the anisotropy issue seems to have little impact on our results.

We have chosen a Plummer model that does not include a tidal cut-off, over a more sophisticated Plummer model which includes a limiting tidal radius, because the tidal radii of many GCs are not well known (e.g. NGC 6752 and 47 Tuc; see Section 3.1 and Paper II, respectively). Indeed, for many clusters we have found cluster members well outside literature values of r_t. This means that our model includes velocity dispersion information outside the tidal radii of our clusters. We have, therefore, not removed any velocity information for $R > r_t$, which would reduce the accuracy of the model at large radii where $a < a_0$.

The velocity dispersion profiles, along with the total masses, scale radii and central velocity dispersions, are presented in Fig. 4. Except for M4, our mass estimates agree well with other studies (e.g. Meylan 1989; Pryor & Meylan 1993; Kruijssen & Mieske 2009), none of whom used Plummer models to calculate their estimates. For M4, we find a total mass about twice that of those studies [although this is reduced to a ∼69 per cent difference if the extremes of the uncertainties of Kruijssen & Mieske (2009) and the current paper are taken]. Despite the Plummer profile fit being within the uncertainties, it is apparent that the outer five bins of M4 have nearly the same measured velocity dispersions. This increases the value of r_s in the fitting of the profile, which is used to calculate the total mass (equation 1), which, in turn, leads to an inflated mass estimate. We attribute this apparent flattening of the dispersion profile to tidal heating (see Section 4).

Except for M4, none of the clusters discussed here have shown the apparent flattening of the velocity dispersion profiles reported by Scarpa, Marconi & Gilmozzi (2003), Scarpa et al. (2007a) and Scarpa et al. (2007b), indicating that neither a significant DM component nor a modified theory of gravity is required to explain their kinematic properties. This corroborates earlier results for 47 Tuc, M22, M30, M53, M55 and M68 in Papers I and II, and similar conclusions are drawn by Sollima et al. (2009) for ω Centauri, by Jordi et al. (2009) for Pal 14 and by Sollima & Nipoti (2010) for MOND theories in general. Through studies such as these, it is becoming increasingly apparent that neither DM nor modified gravity theories are necessary to explain the internal kinematics of GCs.

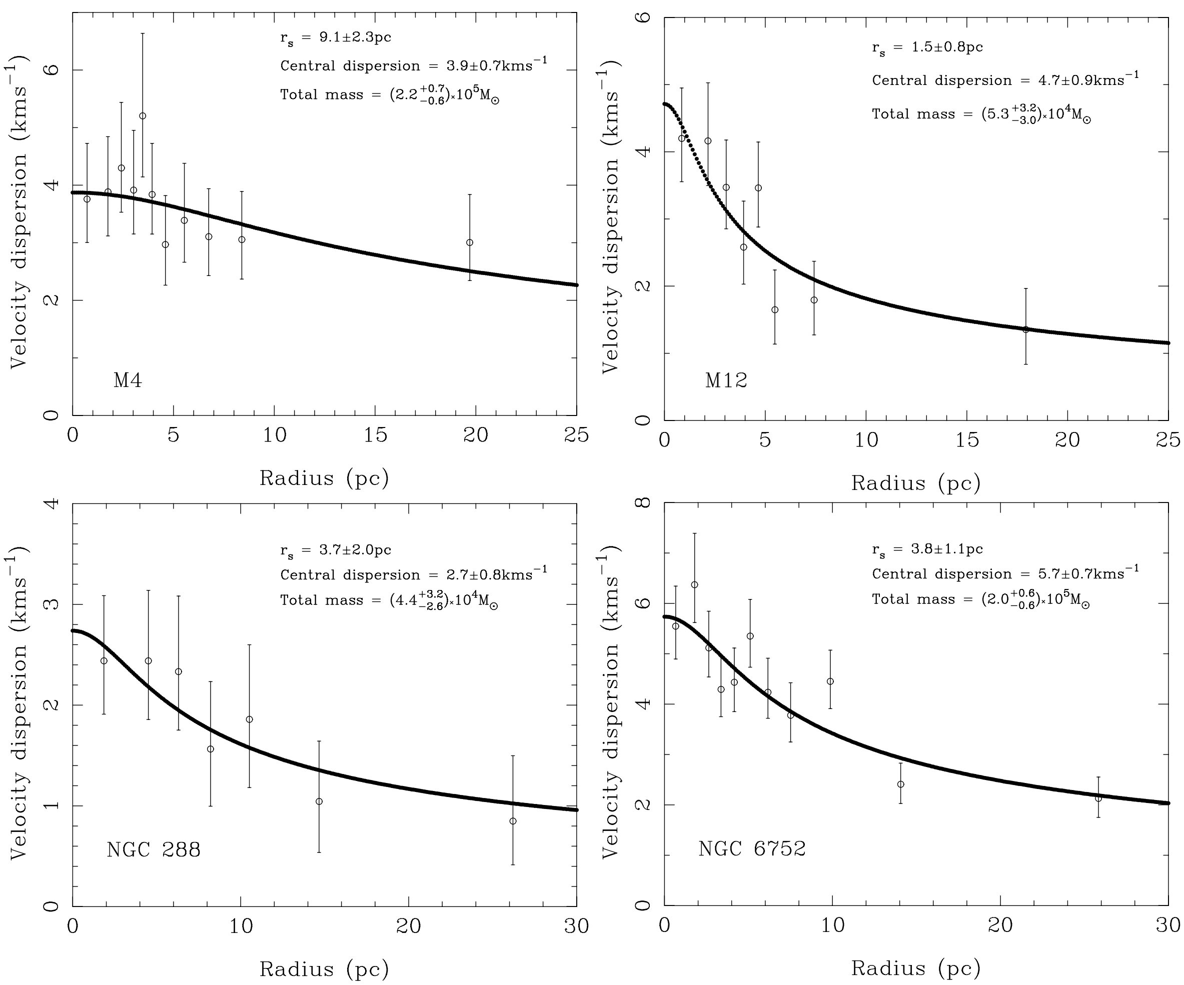

Figure 4. Velocity dispersion profiles of each cluster from the current paper. The best-fitting Plummer (1911) model is overplotted and the derived scale radius, central dispersion and total mass is shown in each panel.

3.5 Mass-to-light profiles

DM causes larger stellar accelerations, and hence higher maximal stellar velocities, therefore a good indication of whether a pressure-supported object like a GC is DM dominated is to measure its mass-to-light ratio. To calculate the M/L$_V$ for our clusters, we have used the surface brightness data by Trager, King & Djorgovski (1995, see Fig. 5) to which projected Plummer surface brightness profiles,

$$L(R) = \frac{L_{\rm tot}}{\pi r_{\rm s}^2}\left(1+\frac{R^2}{r_{\rm s}^2}\right)^{-2},$$

have been fitted (Fig. 5). These Plummer profiles were converted to solar luminosities per square parsec. Projected mass density profiles (Dejonghe 1987),

$$\rho(R) = \frac{M_{\rm tot}}{\pi}\frac{r_{\rm s}^2}{\left(r_{\rm s}^2+R^2\right)^2},$$

in units of solar masses per square parsec, were then divided by the surface brightness profiles to produce radial mass-to-light profiles. The Plummer fits to the surface brightness data do not include tidal cut-offs, for the reasons discussed in Section 3.4. Note that the kinematic and surface brightness models have been fitted independently, which allows a radial M/L$_V$ profile to be calculated.

The M/L$_V$ profiles and mean values are shown in Fig. 6; the thick line is the calculated M/L$_V$ and the thin lines are their uncertainties. The M/L$_V$ profiles at small radii deviate significantly from the mean. We interpret this as being due to the uncertainty in the measured luminosities and kinematics near the cores of the clusters. Crowding and confusion effects are inherent in luminosity and kinematic measurements of dense stellar fields, such as those near the cores of GCs; it is clear in Fig. 5 that there is a large spread of surface brightness measurements near the cores of all four clusters. Because of this uncertainty in core luminosities and kinematics, our mean M/L$_V$ values were calculated for $R > r_{\rm s}$ to ensure that these effects were removed.

DM-dominated dynamical systems (e.g. elliptical and dwarf galaxies) exhibit high mass-to-light ratios (M/L$_V \gtrsim 10$), whereas

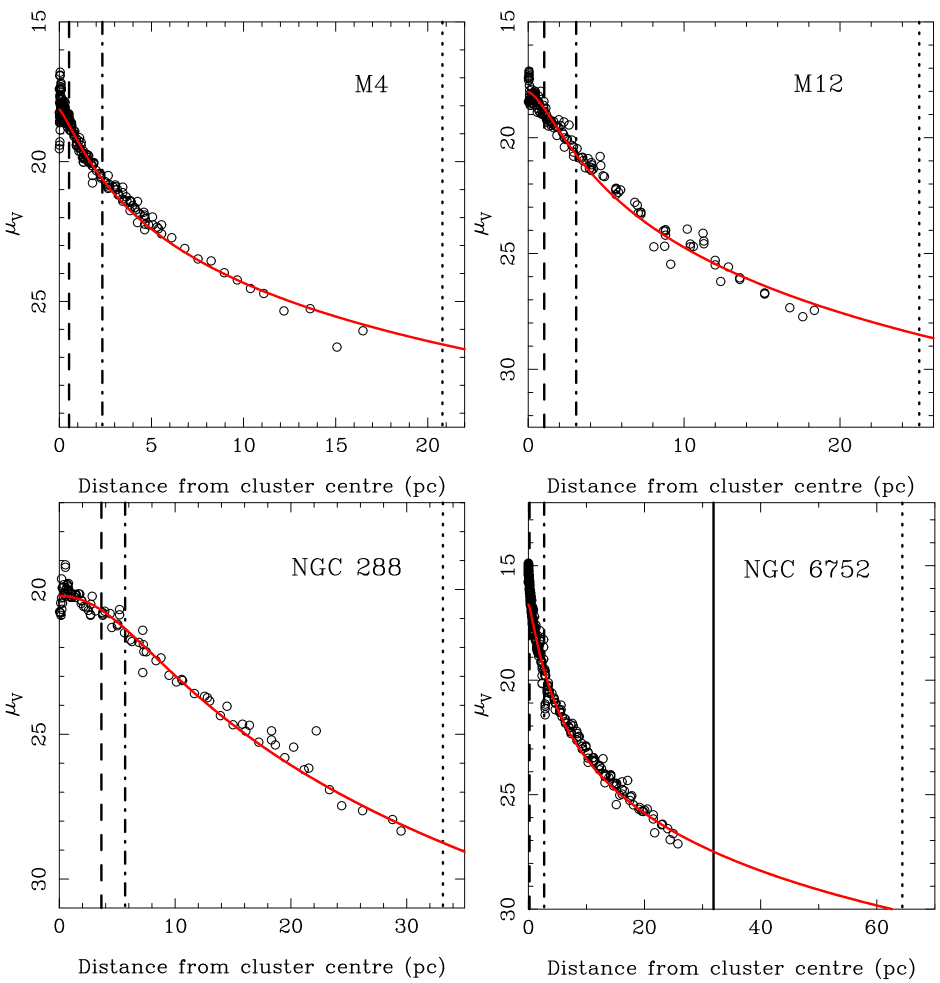

Figure 5. Surface brightness data by Trager et al. (1995) overplotted with our Plummer profiles. The vertical lines represent the core radius (dashed), half-mass radius (dot–dashed) and tidal radius (dotted) from Harris (1996). The solid vertical line in the lower right-hand panel (NGC 6752) is the tidal radius we derived in Section 3.1.

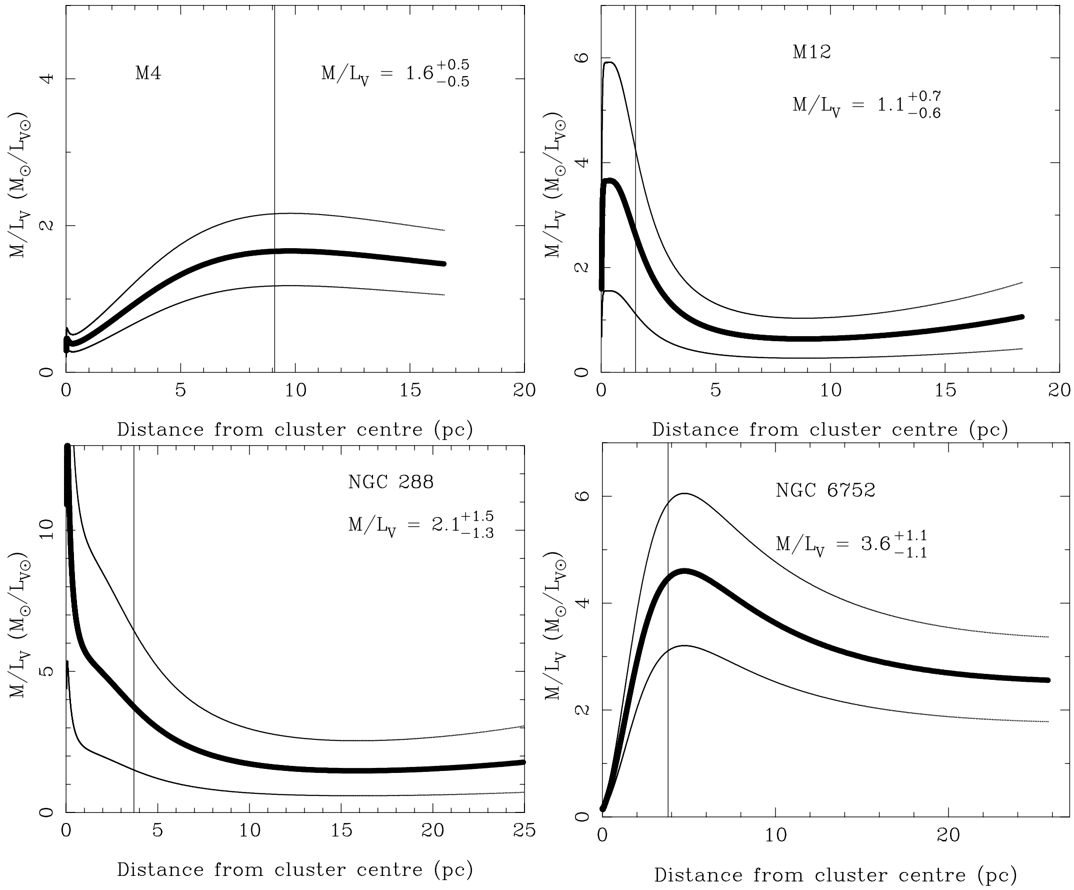

Figure 6. Mass-to-light profiles of the four clusters analysed in the current paper. The thick line is the calculated M/L_V, the thin lines are their uncertainties and the vertical line is the value of r_s. The quoted M/L_V value is only calculated for $R > r_s$. None of these clusters have $M/L_V \gg 1$, furthering the argument that DM is not dominant. The deviation from a purely Plummer profile (Fig. 5) has the effect of decreasing the M/L_V of NGC 6752 by ~0.8 from its calculated value.

ultra compact dwarfs, which have the same velocity dispersion–luminosity relation as GCs (Haşegan et al. 2005; Evstigneeva et al. 2007), show no evidence for DM for $M/L_V \lesssim 5$. None of our clusters have $M/L_V \gg 1$, therefore DM cannot dominate, and because none have $M/L_V > 5$, we see no need for any DM component. Similar conclusions were reached for all six clusters studied in Papers I and II. All results from this project indicate strongly that, in general, GCs do not contain large quantities of DM. We thought it important to mention that Baumgardt & Mieske (2008) have shown that dynamically more evolved GCs exhibit lower M/L_V values, so the larger M/L_V of NGC 6752 should indicate that this cluster is dynamically 'young'. However, this is in direct contradiction with the current understanding of NGC 6752 having a collapsed core (Rubenstein & Bailyn 1997).

It is interesting to note that Ferraro et al. (2003) discussed the possibility of a large M/L_V value (~6–7) for the inner 0.08 pc of NGC 6752, because of the observed accelerations of millisecond pulsars near the core. Since we do not claim any knowledge of the M/L_V at those radii, this indeed remains a possibility, should the M/L_V increase further from r_s towards the core. This intriguing possibility should be pursued by extracting more information on the kinematics of the core of NGC 6752, particularly in light of a newly recognized correlation that may be useful for accurately estimating the masses of GC cores (Leigh, Sills & Knigge 2009).

3.5.1 Correlation between M/L_V and luminosity

47 Tuc is well known as having a bimodal distribution of various line strengths in both MS and giant stars (e.g. Norris & Freeman 1979; Cannon et al. 1998; Harbeck, Smith & Grebel 2003). The most popular explanation for this phenomenon is that the cluster has undergone multiple episodes of star formation. In Paper II, we reported a rise in the velocity dispersion of 47 Tuc for $R \gtrsim r_t/2$, which we interpreted as evidence for evaporation. Here, we present an alternative scenario for this signature: a past merger, which explains both the rise in velocity dispersion and the bimodality in line strengths, as well as its anomalously high luminosity compared with its M/L_V (see Fig. 7).

The clusters from this project exhibit a clear trend between M/L_V and total luminosity (Fig. 7; a trend which is generally attributed to low-mass star depletion, e.g. Kruijssen & Portegies Zwart 2009, and references therein), with 47 Tuc being an apparent outlier. Since there is no reason to think that 47 Tuc has a large DM component, a simple explanation is that 47 Tuc merged with another object of

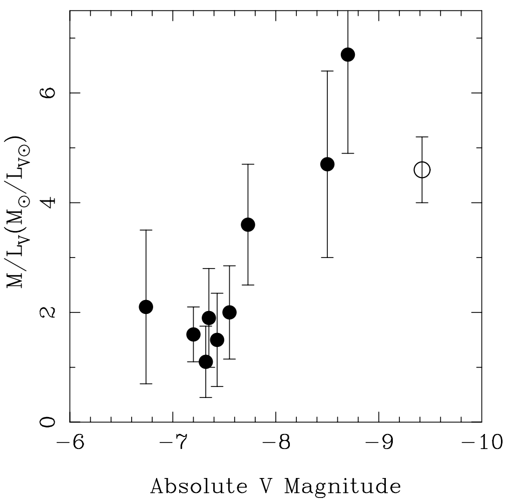

Figure 7. M/L_V from this study versus absolute *V*-band magnitude (taken from Harris 1996) for all 10 clusters. Note the trend to higher M/L_V with increased luminosity. The open circle is 47 Tuc.

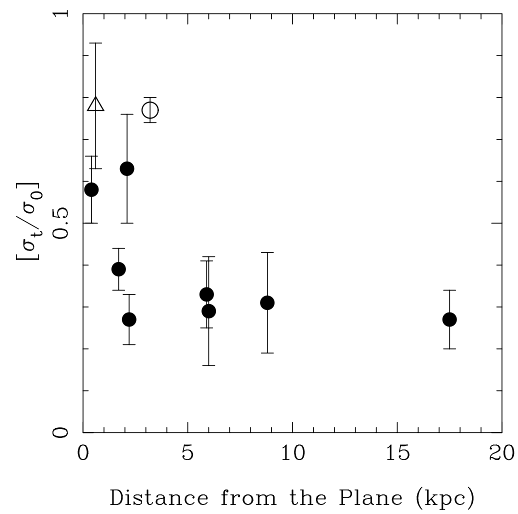

Figure 8. The ratio between velocity dispersions at the tidal radius and the core versus distance from the plane (taken from Harris 1996) for the 10 clusters. Note the trend towards higher values of $[\sigma_t/\sigma_0]$ towards the Galactic plane. The open circle is 47 Tuc and the open triangle is M4.

similar metallicity in its past. This merger would have increased the total luminosity of the cluster without altering its M/L_V significantly and caused bimodalities in both line strengths and velocities. If there has not yet been enough time for the two populations to mix thoroughly, this may be the cause of the observed rise in velocity dispersion. A detailed analysis of this scenario was presented by Lane et al. (2010b).

4 EVIDENCE FOR TIDAL HEATING

When attempting to determine the reality of MOND using GCs, it is generally agreed that GCs at large distances from the Galaxy are most useful because the external acceleration imparted by the Galactic tidal field is below a_0 (Sollima & Nipoti 2010, and references therein). An important question to ask, then, is at what Galactocentric distance does the external field become 'negligible'. Furthermore, does the shape of the halo have an effect on the GC dynamics, whereby distant GCs in certain regions of the halo are affected above this threshold? One clear theoretical prediction is that the external field should heat the external parts of the GCs, thus increasing the velocity dispersion, which can lead to the complete tidal disruption of the cluster (as can be seen with Pal 5; e.g. Odenkirchen et al. 2001). This is especially true during disc crossings and at perigalacticon where tidal shocks strongly affect the dynamics of the cluster for short periods. We present here an examination of our data as an analysis of the Galactic tidal field.

Fig. 8 shows how the ratio between the velocity dispersions at the tidal radius and core varies with distance from the plane. The closer to the plane, the greater the tidal effects from the Galaxy, and the larger the ratio. It is clear that for $R_Z \gtrsim 3$ kpc, the tidal effects of the Galaxy are essentially equivalent at all radii. From this, we can infer that the DM halo exerts the dominant tidal force for $R_Z \gtrsim 3$ kpc. Furthermore, because the four clusters beyond $R = 5$ kpc (in increasing distance these are M30, M68, NGC 288 and M53) are in different locations in the halo (Harris 1996) and on orbits with vastly different orientations to the halo (Allen et al. 2006), this indicates the possibility of a non-triaxial DM halo (see Peñarrubia, Walker & Gilmore 2009, for a discussion of the effects of halo triaxiality on the dynamics of GCs). Note that this is not strong evidence for the shape of the dark halo, however, it is worth mentioning.

M4 has a fairly flat velocity dispersion profile in the outer regions (Fig. 4). This cluster is also very close to the plane (600 pc; Harris 1996) and has the largest value of $[\sigma_t/\sigma_0]$ of any of our clusters (Fig. 8). Furthermore, its 3D space velocity, with respect to the local standard of rest (Dinescu, Girard & van Altena 1999), indicates that it is continuously interacting with the disc because its orbit is nearly planar. This, combined with its low M/L_V, strongly indicates that tidal heating is the cause of the flattening of the velocity dispersion in the outskirts of M4 rather than a substantial DM component.

Fig. 8 seems to indicate that GCs are tidally shocked within $\sim$3 kpc of the plane, then cool down, and stay cool, beyond that distance. However, the orbital periods calculated by Dinescu et al. (1999) are about an order of magnitude shorter than the relaxation times in the Harris (1996) catalogue for all of our clusters. Since the outskirts of GCs are much less dense than the cores, two-body interactions could not cause the outer regions to cool in less than the relaxation time of the cluster. In fact, no mechanism known to the authors can account for this rapid cooling in the outskirts of our GCs. Based on the M/L_V and velocity dispersion profiles of all 10 clusters, a large DM component is very unlikely. It is also very unlikely that we are seeing a MONDian effect in these outer regions because of the Newtonian nature of the velocity dispersion profiles. It is possible that the evaporation of high velocity stars accelerated by disc shocks in the outer regions of the GCs could explain the cooling of the clusters; however, addressing this problem is beyond the scope of this paper and more work is required to solve this intriguing puzzle.

5 CONCLUSIONS

In the current paper, we have analysed four GCs (M4, M12, NGC 288 and NGC 6752) to determine their velocity dispersion and M/L_V profiles, bringing the total to 10 for this project. We have included GCs that have external accelerations extending from above a_0 down to a_0 and we find no deviation from our Plummer models at lower accelerations. Therefore, we see no indication that DM, or a modified version of gravitational theory, is required to reconcile GC dynamics with Newtonian gravity. This adds to the growing body of evidence that GCs are DM-poor, and that our understanding of weak-field gravitation is not incomplete. Within the stated uncertainties, the dynamics of all these clusters are well described by purely analytic Plummer (1911) models, which indicates that Newtonian gravity adequately describes their velocity dispersions, and we observe no breakdown of Newtonian gravity at $a_0 \approx 1.2 \times 10^{-10}$ m s^{-2}, as has been claimed in previous studies.

Despite this, we see the intriguing possibility of an unknown cooling process in the outskirts of GCs; the external regions of our GCs seem to cool much faster following tidal disc shocks than the relaxation time of the clusters. Because it is highly unlikely that a MONDian process, or a significant DM component, is the cause of this cooling (based on our velocity dispersion and M/L_V profiles), further work is required to solve this puzzle. Furthermore, the lack of tidal heating events in the distant clusters provides some indication that the dark halo is not triaxial.

The Plummer model was also used to determine the total mass, scale radius and M/L_V profile for each cluster. We find that none of our clusters have $M/L_V \gg 1$, further evidence that DM does not dominate. We have produced M/L_V profiles, rather than quoting a single value based on the central velocity dispersion and central surface brightness. This method is used because it describes the M/L_V of the entire cluster, rather than only its core. This is particularly important for post-core-collapsed GCs, where crowding and confusion effects introduce significant uncertainty into luminosity and kinematic measurements at small radii. Within the uncertainties, our estimated cluster masses all match those in the literature except for M4, which we calculate to have a total mass about twice that of the literature values. The reason for this discrepancy is that the tidally heated cluster has an increased velocity dispersion in its outer regions, flattening the Plummer fit, increasing the value of r_s, and, therefore, increasing the mass estimate.

Another important result from this study is the measured rotations of our clusters. Of the four clusters studied here, M4 and NGC 288 show clear rotation, M12 may have some rotation, and NGC 6752 displays no rotation signature.

Throughout this project we have found similar results for the DM content, and Newtonian kinematics, of our 10 GCs, all at varying distances from the Galactic centre and disc, including three that experience external accelerations due to the Galaxy of $\sim a_0$. All data were acquired using the same instrument (AAOmega on the AAT), reduced using the same pipeline (2DFDR), and analysed in the same way. This homogeneous approach is vital to a large project, such as this, to ensure all systematics are accounted for in a similar fashion. Because of all these factors, our results from the three papers are *strongly* indicative that the current picture of GCs being DM poor, and with dynamics explained by standard Newtonian theory, is correct.

ACKNOWLEDGMENTS

This project has been supported by the University of Sydney, the Anglo-Australian Observatory, the Australian Research Council, the Hungarian OTKA grant K76816, the Lendület Young Researchers Program of the Hungarian Academy of Sciences and the Bólyai János Research Fellowship of the Hungarian Academy of Sciences (GyMSz). RRL thanks Martine L. Wilson for her support during the writing of this paper. The authors thank Dean McLaughlin for his helpful comments.

REFERENCES

Allen C., Moreno E., Pichardo B., 2006, ApJ, 652, 1150
Baumgardt H., Mieske S., 2008, MNRAS, 391, 942
Bergbusch P. A., Stetson P. B., 2009, AJ, 138, 1455
Cannon R. D., Croke B. F. W., Bell R. A., Hesser J. E., Stathakis R. A., 1998, MNRAS, 298, 601
Chen A. B.-C., Tsay W.-S., Tsai W.-S., Lu P. K., 2000, AJ, 120, 2569
Cole A. A., Smecker-Hane T. A., Tolstoy E., Bosler T. L., Gallagher J. S., 2004, MNRAS, 347, 367
Conn B. C. et al., 2007, MNRAS, 376, 939
Côté P., McLaughlin D. E., Cohen J. G., Blakeslee J. P., 2003, ApJ, 591, 850
Davidge T. J., Harris W. E., 1997, ApJ, 475, 584
Dejonghe H., 1987, MNRAS, 224, 13
Dinescu D. I., Girard T. M., van Altena W. F., 1999, AJ, 117, 1792
Evstigneeva E. A., Gregg M. D., Drinkwater M. J., Hilker M., 2007, AJ, 133, 1722
Ferraro F. R., Possenti A., Sabbi E., Lagani P., Rood R. T., D'Amico N., Origlia L., 2003, ApJ, 595, 179
Gebhardt K., Thomas J., 2009, ApJ, 700, 1690
Geisler D., Piatti A. E., Claria J. J., Minniti D., 1995, AJ, 109, 605
Giersz M., 2006, MNRAS, 371, 484
Gregory P. C., 2005, Bayesian Logical Data Analysis for the Physical Sciences: A Comparative Approach with 'Mathematica' Support. Camb. Univ. Press, Cambridge, United Kingdom
Haghi H., Baumgardt H., Kroupa P., Grebel E. K., Hilker M., Jordi K., 2009, MNRAS, 395, 1549
Harbeck D., Smith G. H., Grebel E. K., 2003, AJ, 125, 197
Harris W. E., 1996, AJ, 112, 1487
Haşegan M. et al., 2005, ApJ, 627, 203
Johnson C. I., Pilachowski C. A., 2006, AJ, 132, 2346
Jordi K. et al., 2009, AJ, 137, 4586
Kanatas I., Griffiths W. K., Dickens R. J., Penny A. J., 1995, MNRAS, 272, 265
Kim E., Yoon I., Lee H. M., Spurzem R., 2008, MNRAS, 383, 2
Kiss L. L., Székely P., Bedding T. R., Bakos G. Á., Lewis G. F., 2007, ApJ, 659, L129
Kissler-Patig M., Grillmair C. J., Meylan G., Brodie J. P., Minniti D., Goudfrooij P., 1999, AJ, 117, 1206
Kruijssen J. M. D., Mieske S., 2009, A&A, 500, 785
Kruijssen J. M. D., Portegies Zwart S. F., 2009, ApJ, 698, L158
Lane R. R., Kiss L. L., Lewis G. F., Ibata R. A., Siebert A., Bedding T. R., Székely P., 2009, MNRAS, 400, 917 (Paper I)
Lane R. R., Kiss L. L., Lewis G. F., Ibata R. A., Siebert A., Bedding T. R., Székely P., 2010a, MNRAS, 401, 2521 (Paper II)
Lane R. R. et al., 2010b, ApJ, 711, L122
Lee K. H., Lee H. M., Fahlman G. G., Sung H., 2004, AJ, 128, 2838
Leigh N., Sills A., Knigge C., 2009, MNRAS, L318
Meylan G., 1989, A&A, 214, 106
Milgrom M., 1983, ApJ, 270, 365
Munari U., Sordo R., Castelli F., Zwitter T., 2005, A&A, 442, 1127
Norris J., Freeman K. C., 1979, ApJ, 230, L179
Odenkirchen M. et al., 2001, ApJ, 548, L165
Paust N. E. Q., 2006, PhD thesis, Dartmouth College
Peñarrubia J., Walker M. G., Gilmore G., 2009, MNRAS, 399, 1275
Peterson R. C., Rees R. F., Cudworth K. M., 1995, ApJ, 443, 124
Plummer H. C., 1911, MNRAS, 71, 460
Pryor C., Meylan G., 1993, Struct. Dyn. Globular Clusters, 50, 357
Quercellini C., Amendola L., Balbi A., 2008, MNRAS, 391, 1308
Rubenstein E. P., Bailyn C. D., 1997, ApJ, 474, 701
Rutledge G. A., Hesser J. E., Stetson P. B., Mateo M., Simard L., Bolte M., Friel E. D., Copin Y., 1997, PASP, 109, 883

Scarpa R., Marconi G., Gilmozzi R., 2003, A&A, 405, L15
Scarpa R., Marconi G., Gilmozzi R., Carraro G., 2007a, A&A, 462, L9
Scarpa R., Marconi G., Gilmozzi R., Carraro G., 2007b, The Messenger, 128, 41
Skrutskie M. F. et al., 2006, AJ, 131, 1163
Sollima A., Nipoti C., 2010, MNRAS, 401, 131
Sollima A., Bellazzini M., Smart R. L., Correnti M., Pancino E., Ferraro F. R., Romano D., 2009, MNRAS, 396, 2183
Spurzem R., Giersz M., Takahashi K., Ernst A., 2005, MNRAS, 364, 948
Steinmetz M. et al., 2006, AJ, 132, 1645
Suntzeff N. B., Mateo M., Terndrup D. M., Olszewski E. W., Geisler D., Weller W., 1993, ApJ, 418, 208
Trager S. C., King I. R., Djorgovski S., 1995, AJ, 109, 218
Valenti E., Ferraro F. R., Origlia L., 2004, MNRAS, 351, 1204
Warren S. R., Cole A. A., 2009, MNRAS, 393, 272
Wu X., Tremaine S., 2006, ApJ, 643, 210
Zinn R., 1985, ApJ, 293, 424
Zwitter T. et al., 2008, AJ, 136, 421

This paper has been typeset from a TEX/LATEX file prepared by the author.

2.4 AAOmega Observations of 47 Tucanae: Evidence for a Past Merger?

Richard R. Lane, Brendon J. Brewer, László L. Kiss, Geraint F. Lewis, Rodrigo A. Ibata, Arnaud Siebert, Timothy R. Bedding, Péter Székely and Gyula M. Szabó, 2010, *The Astrophysical Journal Letters, 711, L122-L126*

Evidence for subgalactic-scale hierarchical merging is rare, however, the predictions of ΛCDM indicate that hierarchical clustering processes at scales $\sim 10^7 M_\odot$ should still be occurring today (e.g. Moore *et al.*, 1998), which is still an order of magnitude larger than the masses of GCs. At even smaller scales it is reasonable to suspect that extant relics of mergers may also exist, although it is also reasonable to assume they are rare, and may only exist in the largest clusters. Until the the discovery of two distinct kinematic populations within ω Centauri by Ferraro *et al.* (2002), no kinematic evidence had been found for hierarchical merging at such small scales. Given that ω Centauri is the most massive GC in the MW system, no other remnants of such small-scale accretion may be observable, and this discovery may have been the only one of its kind possible in the Halo.

Although there have been hints from photometric surveys that 47 Tucanae may also contain relics of a past merger (e.g. the mixed stellar populations reported by Anderson *et al.*, 2009), no evidence had been found in velocity space to support the claim, and the mixed stellar populations were thought to be due to self enrichment processes. In this fourth paper we report the first *kinematic* evidence for a merger event in 47 Tucanae, an extremely important find.

The discovery came from the velocity dispersion profile of 47 Tuc presented in Section 2.2. The rise in the velocity dispersion beyond approximately half the tidal radius was an unexpected result and, as discussed in Sections 2.2 & 2.3 may be the result of several competing scenarios. All of these are presented in this paper together with other possibilities. The most plausible scenario appears to be a merger between two smaller GCs that both formed from the same protocluster cloud. This merger hypothesis may seem unlikely because the probability of two objects of such similar metallicity and mass passing close enough to each other to merge in the Halo seems very small. However, this problem is removed if the two clusters form from the same protocluster cloud, which inevitably orbit the barycentre of the system. Through dynamical friction the two protoclusters shed angular momentum which eventually necessitates coalescence.

Again, the data analysed in this paper were obtained, and reduced, by collaborators. The Bayesian code used in the modelling (Section 2) was written by Brendon Brewer. The manuscript itself was written by myself (RRL) in consultation with Brendon Brewer, László Kiss, my supervisors Geraint Lewis and Rodrigo Ibata, and collaborators, and I am also responsible for the interpretation of the modelling (Sections 3 and 4).

The Astrophysical Journal Letters, 711:L122–L126, 2010 March 10 doi:10.1088/2041-8205/711/2/L122

AAOMEGA OBSERVATIONS OF 47 TUCANAE: EVIDENCE FOR A PAST MERGER?

Richard R. Lane[1], Brendon J. Brewer[2], László L. Kiss[1,3], Geraint F. Lewis[1], Rodrigo A. Ibata[4], Arnaud Siebert[4], Timothy R. Bedding[1], Péter Székely[5], and Gyula M. Szabó[3]
[1] Sydney Institute for Astronomy, School of Physics, A28, The University of Sydney, NSW 2006, Australia
[2] Department of Physics, University of California, Santa Barbara, CA 93106-9530, USA
[3] Konkoly Observatory of the Hungarian Academy of Sciences, P.O. Box 67, H-1525, Budapest, Hungary
[4] Observatoire Astronomique, Université de Strasbourg, CNRS, 67000 Strasbourg, France
[5] Department of Experimental Physics, University of Szeged, Szeged 6720, Hungary
Received 2009 November 21; accepted 2010 February 3; published 2010 February 23

ABSTRACT

The globular cluster 47 Tucanae (47 Tuc) is well studied but it has many characteristics that are unexplained, including a significant rise in the velocity dispersion profile at large radii, indicating the exciting possibility of two distinct kinematic populations. In this Letter, we employ a Bayesian approach to the analysis of the largest available spectral data set of 47 Tuc to determine whether this apparently two-component population is real. Assuming the two models were equally likely before taking the data into account, we find that the evidence favors the two-component population model by a factor of $\sim 3 \times 10^7$. Several possible explanations for this result are explored, namely, the evaporation of low-mass stars, a hierarchical merger, extant remnants of two initially segregated populations, and multiple star formation epochs. We find the most compelling explanation for the two-component velocity distribution is that 47 Tuc formed as two separate populations arising from the same proto-cluster cloud which merged $\lesssim 7.3 \pm 1.5$ Gyr ago. This may also explain the extreme rotation, low mass-to-light ratio, and mixed stellar populations of this cluster.

Key words: globular clusters: individual (47 Tucanae)

Online-only material: color figure

1. INTRODUCTION

As one of the closest and most massive Galactic globular clusters (GCs), 47 Tucanae (47 Tuc) is a test-bed for Galaxy formation models (Salaris et al. 2007, and references therein), distance measurement techniques (e.g., Bono et al. 2008), and metallicity calibrations (e.g., McWilliam & Bernstein 2008; Lane et al. 2010a). This close examination, however, has left several unresolved conundrums. While not unique in this respect (see Gratton et al. 2004, for a review of elemental abundance variations in GCs), 47 Tuc has a bimodal distribution of carbon and nitrogen line strengths (e.g., Harbeck et al. 2003). Furthermore, 47 Tuc has a complex stellar population, exhibiting, for example, multiple sub-giant branches (e.g., Anderson et al. 2009). Although multiple red giant and horizontal branches can also be found in other GCs, and may be due to chemical anomalies (e.g., Ferraro et al. 2009; Lee et al. 2009), 47 Tuc is particularly unusual in many respects. It has an extreme rotational velocity (a property it shares only with M22 and ω Centauri, e.g., Merritt et al. 1997; Anderson & King 2003; Lane et al. 2010a) and an apparently unique rise in its velocity dispersion profile at large radii (Lane et al. 2010a).

Furthermore, the mass-to-light ratio (M/L_V) of 47 Tuc is very low for its mass (Lane et al. 2010b), that is, it does not obey the mass–M/L_V relation described by Rejkuba et al. (2007). Note that this mass–M/L_V relation is not due to the presence of dark matter but because of dynamical effects (Kruijssen 2008). Explanations for these unusual properties may be intimately linked to its evolutionary history. In this Letter, we describe and analyze various explanations for the rise in velocity dispersion in the outer regions of 47 Tuc initially reported by Lane et al. (2010a).

Lane et al. (2010a) provided a complete description of the data acquisition and reduction, radial velocity uncertainty estimates, the membership selection process, and statistical analysis of cluster membership for all data presented in this Letter.

2. PLUMMER MODEL FITS

The Plummer (1911) model (see also Dejonghe 1987) predicts that the isotropic, projected velocity dispersion σ falls off with radius r as

$$\sigma(r; \{\sigma_0, r_0\}) = \frac{\sigma_0}{\left(1 + \left(\frac{r}{r_0}\right)\right)^{1/4}}, \quad (1)$$

where σ_0 is the central velocity dispersion and r_0 is the scale radius of the cluster. We now describe how we fitted Plummer profiles to the 47 Tuc radial velocity data to infer the values of the parameters σ_0 and r_0, and also to evaluate the overall appropriateness of the Plummer hypothesis (H_1) by comparing it to a more complex double Plummer model (H_2).

The mechanism for carrying out this comparison is Bayesian model selection (Sivia & Skilling 2006). Suppose we have two (or more) competing hypotheses, H_1 and H_2, with each possibly containing different parameters θ_1 and θ_2. We wish to judge the plausibility of these two hypotheses in light of some data D and some prior information. Bayes' rule provides the means to update our plausibilities of these two models, to take into account the data D:

$$\begin{aligned}\frac{P(H_2|D)}{P(H_1|D)} &= \frac{P(H_2)}{P(H_1)}\frac{P(D|H_2)}{P(D|H_1)} \\ &= \frac{P(H_2)}{P(H_1)} \times \frac{\int_{\theta_1} p(\theta_1|H_1)p(D|\theta_1, H_1)\,d\theta_1}{\int_{\theta_2} p(\theta_2|H_2)p(D|\theta_2, H_2)\,d\theta_2}. \quad (2)\end{aligned}$$

Thus, the ratio of the posterior probabilities for the two models depends on the ratio of the prior probabilities and the ratio of the *evidence* values. The latter measure how well the models predict the observed data, not just at the best-fit values of the parameters, but averaged over all plausible values of the parameters. It should be noted that we rely solely on the velocity information for our Plummer model fits. Taking the stellar density as a function of radius into account would be useful in further constraining the models.

2.1. Single Plummer Model

The data are a vector of radial velocity measurements $\mathbf{v} = \{v_1, v_2, \ldots, v_N\}$ of N stars, along with the corresponding distances from the cluster center $\mathbf{r} = \{r_1, r_2, \ldots, r_N\}$ and observational uncertainties on the velocities $\sigma_{\rm obs} = \{\sigma_{\rm obs,1}, \ldots, \sigma_{\rm obs,N}\}$. We will consider $\mathbf{v}$ to be the data, whereas $\mathbf{r}$ and $\sigma_{\rm obs}$ are considered part of the prior information. In this case, the probability distribution for the data given the parameters is the product of independent Gaussians, whose standard deviations vary with radius,

$$p(\mathbf{v}|\mu, \sigma_0, r_0) = \prod_{i=1}^{N} \left(\frac{1}{\sqrt{2\pi\sigma_i^2}} \exp\left(-\frac{1}{2} \left(\frac{v_i - \mu}{\sigma_i} \right)^2 \right) \right), \quad (3)$$

where μ is the systemic velocity of the cluster. The standard deviation σ_i for each data point is given by a combination of the standard deviation predicted by the Plummer model and the observational uncertainty:

$$\sigma_i = \sqrt{\sigma(r_i; \{\sigma_0, r_0\})^2 + \sigma_{\rm obs,i}^2}. \quad (4)$$

To carry out Bayesian inference, prior distributions for the parameters must also be defined. We assigned a uniform prior for μ (between -30 km s^{-1} and 30 km s^{-1}). For σ_0, we assigned Jeffreys' scale-invariant prior $p(\sigma_0) \propto 1/\sigma_0$ for σ_0 in the range 0.1–100 km s^{-1}. Finally, r_0 was assigned the Jeffreys' prior $p(r_0) \propto 1/r_0$ for r_0 in the range 0.2–220 pc. These three prior distributions were all chosen to be independent and to cover the approximate range of values that we expect the parameters to take.

2.2. Double Plummer Model

The double Plummer model is a simple extension of the Plummer model. The stars are hypothesized to come from two distinct populations, each having its own Plummer profile parameters (but with a common systemic velocity μ). Thus, at any radius r from the cluster center, we model the velocity distribution as a mixture (weighted sum) of two Gaussians. From previous work (Lane et al. 2010a), we also expect the inner regions of the cluster to be well fitted by a single Plummer profile, so the weight of the second population of stars should become more significant at larger radii.

Thus, instead of having a single σ_0 parameter and a single r_0 parameter, there are now two of each. The probability distribution for the data given the parameters is then the weighted sum of two Gaussians:

$$\begin{aligned} p(\mathbf{v}|\mu, \{\sigma_0\}, \{r_0\}, w(r)) &= \prod_{i=1}^{N} \left(\frac{w(r_i)}{\sqrt{2\pi\sigma_{i,1}^2}} \exp\left(-\frac{1}{2} \left(\frac{v_i - \mu}{\sigma_{i,1}} \right)^2 \right) \right. \\ &\quad \left. + \frac{1 - w(r_i)}{\sqrt{2\pi\sigma_{i,2}^2}} \exp\left(-\frac{1}{2} \left(\frac{v_i - \mu}{\sigma_{i,2}} \right)^2 \right) \right). \end{aligned} \quad (5)$$

Here, $w(r)$ is a weight function that determines the relative strength of one Plummer profile with respect to the other, as a function of radius. We expect one component to dominate at smaller radii and to eventually fade away as the second component becomes dominant. Hence, we parameterize the function $w(r)$ as

$$w(r) = \frac{\exp(u(r))}{1 + \exp(u(r))}, \quad (6)$$

where

$$u(r) = u_\alpha + \frac{r - r_{\rm min}}{r_{\rm max} - r_{\rm min}}(u_\beta - u_\alpha). \quad (7)$$

That is, the log of the relative weight between one Plummer component and the other increases linearly over the range of radii spanned by the data, starting at u_α and ending at a value u_β. Parameterizing w via u makes it easier to enforce the condition that $w(r)$ must be in the range 0–1 for all r. The prior distributions for u_α and u_β were chosen to be Gaussian with mean zero and standard deviation 3. This implies that $w(r)$ will probably lie between 0.05 and 0.95, with a small but not negligible chance of extending lower than 0.001 or above 0.999.

The standard deviations of the two Gaussians at each data point are given by a combination of that predicted by the Plummer model and the observational uncertainty:

$$\sigma_{i,1} = \sqrt{\sigma(r_i; \{\sigma_0, r_0\}_1)^2 + \sigma_{\rm obs,i}^2} \quad (8)$$

$$\sigma_{i,2} = \sqrt{\sigma(r_i; \{\sigma_0, r_0\}_2)^2 + \sigma_{\rm obs,i}^2}. \quad (9)$$

The priors for all the parameters μ, $\{\sigma_0, r_0\}$ were chosen to be the same as in the single Plummer case.

3. RESULTS

An obvious rise in the velocity dispersion of 47 Tuc was described by Lane et al. (2010a, their Figure 11) at approximately half the tidal radius (~28 pc). The tidal radius is ~56 pc (Harris 1996). To confirm the reality of this rise, several tests were performed, including resizing the bins and shifting the bin centers, as described by Lane et al. (2010a). No difference in the overall shape of the dispersion profile was found during any tests.

We used a variant (Brewer et al. 2009) of nested sampling (Skilling 2006) to sample the posterior distributions for the parameters and to calculate the evidence values for the single and double Plummer models. The results are listed in Table 1. The double Plummer model is favored by a factor of $\sim 3 \times 10^7$ and consists of a dominant Plummer profile that fits the inner parts of the radial velocity data (Figure 1) and a second, wider profile that models the stars at large radius.

As a test of the veracity of our model, we altered the model so that $w(r)$ was linear (with endpoints in the range 0–1 and

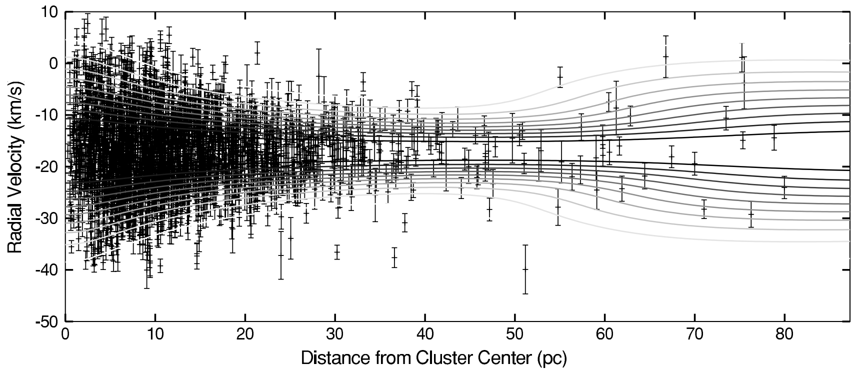

Figure 1. Radial velocities of stars in 47 Tuc together with the best-fit double Plummer model for the velocity distribution as a function of radius. The inner part of the cluster is well modeled by the dominant Plummer profile, while at larger radii, the second plummer profile dominates. The radius at which the two profiles have equal weight is 55 pc.

Table 1
Inferred Parameter Values for the Single Plummer and the Double Plummer Fits to the 47 Tuc Data

Parameter	Value
Single Plummer Profile	
μ	-16.87 ± 0.17 km s^{-1}
σ_0	9.37 ± 0.32 km s^{-1}
r_0	9.27 ± 0.98 pc
log(evidence)	-7759.5
Double Plummer Profile	
μ	-16.94 ± 0.12 km s^{-1}
σ_0	9.93 ± 0.43 km s^{-1}
	[5.70, 13.51] $\pm$ km s^{-1}
r_0	6.76 ± 0.94 pc
	[53.6, 4560] pc
u_α	6.30 ± 1.30
u_β	-2.30 ± 1.12
log(evidence)	-7742.2

Notes. The values quoted are the posterior mean $\pm$ the posterior standard deviation, when the marginal posterior distributions were sufficiently symmetric for this to be a reasonable summary. For the few parameters with asymmetric posterior distributions, we instead give the symmetric 68% credible interval. The evidence values imply that if the two models were equally likely before taking into account the data, the data make the double Plummer model more likely by a factor of $e^{17.3} \approx 3 \times 10^7$. For the double Plummer model, the first value listed is for the component that dominates at $r = 0$.

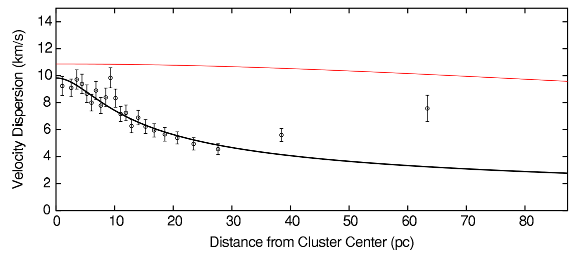

Figure 2. Binned velocity dispersion as a function of radius (from Lane et al. 2010a), with the radial velocity profiles of the two stellar populations from the best-fit double Plummer model. The Plummer profile that dominates at small radii is shown as the thick (black) curve; the thin (red) curve shows the Plummer profile for the stellar population that dominates at large radii.

(A color version of this figure is available in the online journal.)

with a uniform prior) rather than $u(r)$ being linear. This had the effect of reducing the log evidence to ≈ -7748, so in this case the double Plummer model is favored by a factor of $\sim 10^5$. This best-fit model has a more subtle increase in width at large radii, when compared with Figure 1. Presumably this is because $w(r)$ being linear prevents more rapid fade-outs. Correspondingly, the Plummer profile represented by the thin curve in Figure 2 was shifted slightly lower. Note that the model in Figure 1 is narrower than the spread of the data, because the spread also arises partly from observational errors. The most extreme points at large radii are likely to be those for which the intrinsic velocity dispersion is large *and* the observational errors have pushed the points further away from the mean. In Figure 2, the Plummer profiles of the two population components are shown. The inner component is a good fit to the binned velocity dispersions by Lane et al. (2010a). We now discuss possible explanations for this two-component population and calculate an upper limit on when the second component was introduced.

3.1. Evaporation

Drukier et al. (2007) carried out N-body simulations of GCs through core collapse and into post-core-collapse. They showed that the evaporation of low-mass stars due to two-body interactions during these phases alters the velocity dispersion profiles in predictable ways. At approximately half the tidal radius ($r_t/2$), the velocity dispersion reaches a minimum of $\sim$40% of the central dispersion, then rises to $\sim$60% of the central level at r_t. These criteria are certainly met within 47 Tuc (again, see Figure 11 of Lane et al. 2010a). Furthermore, Lane et al. (2010a) conclude that the rise in velocity dispersion could be explained by evaporation due to the core collapsing, and the Fokker–Planck models by Behler et al. (2003) show that 47 Tuc is nearing core collapse.

This appears to be reasonable evidence that 47 Tuc is evaporating. However, based on the conclusions drawn by Drukier et al. (2007) and Lane et al. (2010b), it is unclear how much Galactic tidal fields affect the outer regions of Galactic GCs, and what effect this has on the external velocity dispersion profile. While our best-fit double Plummer model matches the overall form of the trend shown by Drukier et al. (2007) reasonably well (see Figure 1), this scenario does not explain its multiple stellar populations (although these might be explained by chemical anomalies, e.g., Piotto et al. 2007, and references therein), nor its low M/L_V in comparison with its mass (see Figure 6 of Lane et al. 2010b), or its extreme rotation. In addition, the extra-tidal stars are spread uniformly across all regions of the color–magnitude diagram (see Figure 3 of Lane et al. 2010a), which is inconsistent with the two-component population being a consequence of evaporating low-mass stars. We cannot, however, completely discount evaporation without detailed chemical abundance information.

3.2. Merger

Another scenario, which appears to explain most of the unusual properties of 47 Tuc, is that it has undergone a merger in its past (note that this is not the first evidence for such a merger within Galactic GCs; see Ferraro et al. 2002). Several observed quantities can be explained by this hypothesis: (1) the bimodality of the carbon and nitrogen line strengths, (2) the mixed stellar populations, (3) the large rotational velocity, (4) the low M/L_V compared with total mass, and (5) the increase in velocity dispersion in the outskirts of the cluster.

In addition to our evidence for two kinematically distinct stellar populations, Anderson et al. (2009) showed that 47 Tuc also has two distinct sub-giant branches, one of which is much broader than the other, as well as a broad main sequence. The authors determined that this broadening may be due to a combination of metallicities and ages, and it is known from previous studies (e.g., Harbeck et al. 2003) that 47 Tuc has a bimodality in its carbon and nitrogen line strengths. While this bimodality is not unique, a merger could explain its origin. Therefore, another possible scenario, which explains many of the properties of 47 Tuc, is a past merger event.

While it might seem unlikely that this is the remnant of a merger, extant kinematic signatures of subgalactic scale hierarchical merging do exist (e.g., within ω Centauri; Ferraro et al. 2002), and there have been hints that the distinct photometric populations in 47 Tuc might be remnants of a past merger (e.g., Anderson et al. 2009). A possible explanation for this merger hypothesis is given in Section 3.3.

3.3. Initial Formation

The two components may have formed at the same epoch, and the distinct kinematic populations are, therefore, extant remnants from the formation of the cluster itself. If GCs form from a single cloud (see Kalirai & Richer 2010, for a discussion of GCs as simple stellar populations), it is possible for the proto-cluster cloud to initially contain two overdensities undergoing star formation independently at almost the same time. In this case, the two proto-clusters, which would inevitably be in mutual orbit due to the initially bound nature of the proto-cluster cloud, eventually coalesced through the loss of angular momentum due to dynamical friction.

Note that this scenario is similar to the capture of a satellite described by Ferraro et al. (2002) to explain the merger hypothesis for ω Centauri and explains the two kinematic and photometric populations, and the high rotation rate assuming the proto-cluster cloud initially had a large angular momentum. It might also explain the low M/L_V of this cluster.

Interestingly, Vesperini et al. (2009) show that clusters with initially segregated masses evolve more slowly than non-segregated clusters, having looser cores and reaching core collapse much later. Because the core of 47 Tuc is highly concentrated and near core collapse (e.g., Behler et al. 2003), it must be very old if it was initially mass-segregated. 47 Tuc is thought to be 11–14 Gyr old (e.g., Gratton et al. 2003; Kaluzny et al. 2007), hence initial mass segregation is plausible. However, even if 47 Tuc is ~11 Gyr old the original populations would be kinematically indistinguishable at the present epoch (Section 3.5) indicating that some other process was the cause of the two extant populations described in this Letter. Furthermore, Milky Way GC formation ended about 10.8 Gyr ago (e.g., Gratton et al. 2003), long before the upper limit for the initial mixing of the two populations derived in Section 3.5.

3.4. Multiple Star Formation Epochs

Two star formation epochs in GCs result in the radial separation of the two populations, with the second generation initially concentrated in the core (e.g., D'Ercole et al. 2008, and references therein). Furthermore, the kinematics of the second generation are virtually independent of that of the first generation, and the second generation contain chemical anomalies which are consistent with having arisen in the envelopes of the first generation (e.g., Decressin et al. 2007; D'Ercole et al. 2008).

This scenario might explain the two kinematic populations and chemical anomalies of 47 Tuc; however, it is unclear how this would cause the extreme rotation or the anomalous M/L_V.

3.5. Timescale for the Initial Mixing of the Second Population

The scenarios described in Sections 3.2, 3.3, and 3.4 require a second population beginning to mix with an initial population at a particular epoch. Decressin et al. (2008) performed detailed N-body simulations of GCs containing two distinct populations of stars to determine their dynamical mixing time via two-body relaxation. They concluded that ~2 relaxation times are required to completely homogenize the populations, a timescale that is virtually independent of the number of stars in the cluster. They also concluded that the information on the stellar orbital angular momenta of the two populations is lost on a similar timescale. Since we observe two distinct, extant kinematic populations, an upper limit can be placed on when the two populations began to mix.

Decressin et al. (2008) showed that the relaxation time (t_{rh}) of a GC decreases by $\sim 0.29 t_{rh}$ for each consecutive relaxation time, i.e., $t_{rh}(i) \sim 0.71 t_{rh}(i+1)$. Because the two populations are kinematically distinct at the present epoch and the current relaxation time of 47 Tuc is $t_{rh} \approx 3.02$ Gyr (Harris 1996), an upper limit on when the two populations began to mix is 7.3 ± 1.5 Gyr ago. Note that the scenarios discussed in Sections 3.2 and 3.3 can be temporally assessed in this way only if the merger did not disrupt the core of the larger component. This is true for minor mergers in blue compact dwarf galaxies (Sung et al. 2002), therefore, if we assume a merger between objects with a mass ratio of 9:1 (Anderson et al. 2009, show the ratio of the number densities on the two sub-giant branches of 47 Tuc is ~9:1), this is also likely to hold for 47 Tuc.

4. CONCLUSIONS

With a Bayesian analysis of the velocity distribution of 47 Tuc, we conclude that the scenario which best explains the observed properties of 47 Tuc is that we are seeing the first kinematic evidence of a merger in 47 Tuc, which occurred $\lesssim 7.3 \pm 1.5$ Gyr ago. Extant kinematic populations from the merger of formation remnants are a plausible explanation as to the reason for this merger, assuming the two components evolved separately and merged $\lesssim 7.3 \pm 1.5$ Gyr ago. This scenario could explain the two-component population, its extreme rotational velocity, mixed stellar populations, and low M/L_V compared with its mass.

All the other explanations for this two-component population are less plausible than the merger hypothesis. Evaporation of low-mass stars is unlikely due to the various stellar types that are found beyond the tidal radius, and this also cannot explain its low M/L_V. The possibility of multiple star formation epochs does not explain the large rotational velocity, nor the low M/L_V.

Detailed chemical abundances and high resolution N-body simulations of merging GCs are now required to further analyze the merger scenario. Several observed quantities need to be addressed, namely, how much angular momentum can be imparted through a 9:1 merger, what consequence it has on the velocity dispersion in the outer regions of the cluster over dynamical timescales, and what effect it would have on the global M/L_V.

Of course, alternative explanations exist for the observed rise in dispersion. For example, if GCs form in a similar fashion to Ultra Compact Dwarf galaxies, there may be a large quantity of dark matter in the outskirts of the cluster as discussed by Baumgardt & Mieske (2008). However, no evidence exists supporting GCs forming in this manner and GCs do not appear to have significant dark matter components (e.g., Lane et al. 2009, 2010a, 2010b).

This project has been supported by the University of Sydney, the Anglo-Australian Observatory, the Australian Research Council, the Hungarian OTKA grant K76816, and the Lendület Young Researchers Program of the Hungarian Academy of Sciences. Gy.M.Sz. acknowledges the Bolyai Fellowship of the HAS. R.R.L. thanks Martine L. Wilson for everything.

REFERENCES

Anderson, J., & King, I. R. 2003, AJ, 126, 772
Anderson, J., Piotto, G., King, I. R., Bedin, L. R., & Guhathakurta, P. 2009, ApJ, 697, L58
Baumgardt, H., & Mieske, S. 2008, MNRAS, 391, 942
Behler, R. H., Murphy, B. W., Cohn, H. N., & Lugger, P. M. 2003, BAAS, 35, 1289
Bono, G., et al. 2008, ApJ, 686, L87
Brewer, B. J., Pártay, L. B., & Csányi, G. 2009, arXiv:0912.2380
Decressin, T., Baumgardt, H., & Kroupa, P. 2008, A&A, 492, 101
Decressin, T., Meynet, G., Charbonnel, C., Prantzos, N., & Ekström, S. 2007, A&A, 464, 1029
Dejonghe, H. 1987, MNRAS, 224, 13
D'Ercole, A., Vesperini, E., D'Antona, F., McMillan, S. L. W., & Recchi, S. 2008, MNRAS, 391, 825
Drukier, G. A., Cohn, H. N., Lugger, P. M., Slavin, S. D., Berrington, R. C., & Murphy, B. W. 2007, AJ, 133, 1041
Ferraro, F. R., Bellazzini, M., & Pancino, E. 2002, ApJ, 573, L95
Ferraro, F. R., et al. 2009, Nature, 462, 483
Gratton, R. G., Bragaglia, A., Carretta, E., Clementini, G., Desidera, S., Grundahl, F., & Lucatello, S. 2003, A&A, 408, 529
Gratton, R., Sneden, C., & Carretta, E. 2004, ARA&A, 42, 385
Harbeck, D., Smith, G. H., & Grebel, E. K. 2003, AJ, 125, 197
Harris, W. E. 1996, AJ, 112, 1487
Kalirai, J. S., & Richer, H. B. 2010, Phil. Trans. R. Soc. A, 368, 755
Kaluzny, J., Thompson, I. B., Rucinski, S. M., Pych, W., Stachowski, G., Krzeminski, W., & Burley, G. S. 2007, AJ, 134, 541
Kruijssen, J. M. D. 2008, A&A, 486, L21
Lane, R. R., Kiss, L. L., Lewis, G. F., Ibata, R. A., Siebert, A., Bedding, T. R., & Székely, P. 2009, MNRAS, 400, 917
Lane, R. R., Kiss, L. L., Lewis, G. F., Ibata, R. A., Siebert, A., Bedding, T. R., & Székely, P. 2010a, MNRAS, 401, 2521
Lane, R. R., et al. 2010b, MNRAS, submitted
Lee, J.-W., Kang, Y.-W., Lee, J., & Lee, Y.-W. 2009, Nature, 462, 480
McWilliam, A., & Bernstein, R. A. 2008, ApJ, 684, 326
Merritt, D., Meylan, G., & Mayor, M. 1997, AJ, 114, 1074
Piotto, G., et al. 2007, ApJ, 661, L53
Plummer, H. C. 1911, MNRAS, 71, 460
Rejkuba, M., Dubath, P., Minniti, D., & Meylan, G. 2007, A&A, 469, 147
Salaris, M., Held, E. V., Ortolani, S., Gullieuszik, M., & Momany, Y. 2007, A&A, 476, 243
Sivia, D. S., & Skilling, J. 2006, Data Analysis: A Bayesian Tutorial (2nd ed.; Oxford: Oxford Univ. Press)
Skilling, J. 2006, Nested Sampling for General Bayesian Computation, Bayesian Analysis, 4, 833
Sung, E.-C., Chun, M.-S., Freeman, K. C., & Chaboyer, B. 2002, in ASP Conf. Ser. 273, The Dynamics, Structure & History of Galaxies, ed. G. S. Da Costa & H. Jerjen (San Francisco, CA: ASP), 341
Vesperini, E., McMillan, S. L. W., & Portegies Zwart, S. 2009, ApJ, 698, 615

Chapter 3

The Monoceros Ring

(One ring to rule them all, one ring to find them, one ring to bring them all, and in the darkness bind them.)

- J.R.R. Tolkien

3.1 The AAT/WFI Survey of the Monoceros Ring and Canis Major Dwarf Galaxy - I. From $l = (193 - 276)^{\circ}$

Blair C. Conn, **Richard R. Lane**, Geraint F. Lewis, Rodrigo Gil-Merino, Mike J. Irwin, Rodrigo A. Ibata, Nicolas F. Martin, Michele Bellazzini, Robert Sharp, Artem V. Tuntsov and Annette M. N. Ferguson, 2007, *Monthly Notices of the Royal Astronomical Society 376, 939-959*

The debate over whether the MRi and Canis Major overdensity (CMa) are of Galactic or extra-Galactic origin is addressed in the following paper. If the MRi is the result of an accretion event, the most credible progenitor candidate is the CMa dwarf (Martin *et al.*, 2004, 2005). However, it is unclear what the CMa structure actually is; debate has surrounded the nature of this object since its discovery. Several explanations for this stellar overdensity have been proposed; it may be a line-of-sight effect of the Galactic warp (Momany *et al.*, 2004) or outer spiral arm (Carraro *et al.*, 2005; Moitinho *et al.*, 2006). It has also been claimed that the MRi is explained by the flaring of the Disc (Momany *et al.*, 2006). In this paper several new detections of the MRi are reported, expanding its known extent to more than $\sim 180^{\circ}$ of the sky. Comparisons to the Besançon Galaxy model are used to highlight the detections, or otherwise, of the MRi at each location. The claims of the MRi being due to the Flare, and those of the CMa overdensity being due to the Warp or spiral arm, are investigated in detail with the addition of these new data.

Assuming that the MRi is the tidal remnants of a dwarf galaxy, immediate tidal tails should be detectable near the CMa structure itself as overdense coherent stellar systems radiating from the body of the CMa overdensity. Although the Martin *et al.* (2005) model is not a perfect representation of the MRi (neither of the two available MRi models are perfect, as discussed in Section 1.2.3), it is preferred over the Peñarrubia *et al.* (2005) model because only the Martin model shows the CMa overdensity in its current location on the sky. Therefore, in light of predictions from the Martin *et al.* (2005) model, a new interpretation of several of the MRi detections is given with regard to the immediate tidal tails of the CMa structure.

The data analysed in this paper were obtained, and reduced, by collaborators. The code to calculate the data completeness (the fraction of stars detected at any particular magnitude; Section 4.4.1) was written by myself (RRL). While I did not directly contribute heavily to the writing of the manuscript itself, I was involved at every stage of the intellectual process in the development of the manuscript and the conclusions drawn from the data analysis.

Mon. Not. R. Astron. Soc. **376,** 939–959 (2007) doi:10.1111/j.1365-2966.2007.11503.x

The AAT/WFI survey of the Monoceros Ring and Canis Major dwarf galaxy – I. From $l = (193–276)°$

Blair C. Conn,[1,2★] Richard R. Lane,[1] Geraint F. Lewis,[1] Rodrigo Gil-Merino,[1] Mike J. Irwin,[3] Rodrigo A. Ibata,[4] Nicolas F. Martin,[4] Michele Bellazzini,[5] Robert Sharp,[6] Artem V. Tuntsov[1] and Annette M. N. Ferguson[7]

[1] *Institute of Astronomy, School of Physics, A29 University of Sydney, NSW 2006, Australia*
[2] *European Southern Observatory, Alonso de Cordova 3107, Vitacura, Santiago, Chile*
[3] *Institute of Astronomy, Madingley Road, Cambridge CB3 0HA*
[4] *Observatoire de Strasbourg, 11 rue de l'Université, F-67000 Strasbourg, France*
[5] *INAF – Osservatorio Astronomico di Bologna, Via Ranzani 1, 40127 Bologna, Italy*
[6] *Anglo-Australian Observatory, Epping, NSW 1710, Australia*
[7] *Institute for Astronomy, University of Edinburgh, Royal Observatory, Blackford Hill, Edinburgh EH9 3HJ*

Accepted 2007 January 15. Received 2007 January 12; in original form 2006 October 13

ABSTRACT

We present the results of an Anglo-Australian Telescope (AAT) wide field camera survey of the stars in the Monoceros Ring (MRi) and purported Canis Major (CMa) overdensity in the Galactic longitudes of $l = (193–276)°$. Current numerical simulations suggest that both of these structures are the result of a single on-going accretion event, although an alternative solution is that the warped and flared disc of the Galaxy can explain the origin of both of these structures. Our results show that, with regards the MRi, the warped and flared disc is unable to reproduce the locations and strengths of the detections observed around the Galaxy. This supports a non-Galactic origin for this structure. We report eight new detections and two tentative detections of the MRi in this survey. The exact nature of the CMa overdensity is still unresolved, although this survey provides evidence that invoking the Galactic warp is not a sufficient solution when compared with observation. Several fields in this survey are highly inconsistent with the current Galactic disc models that include a warp and flare, to such an extent that explaining their origins with these structures is problematic. We also report that the blue plume stars previously invoked to support the dwarf galaxy hypothesis are unfounded, and associating them with an outer spiral arm is equally problematic. Standard Galactic models are unable to accommodate all the observations of these new structures, leading away from a warped/flared disc explanation for their origins and more toward a non-Galactic source. Additionally, evidence is presented in favour of a detection of the CMa dwarf stream away from the CMa region. As the outer reaches of the Galactic disc continue to be probed, the fascinating structures that are the MRi and CMa overdensity will no doubt continue to inform us of the unique structure and formation of the Milky Way.

Key words: Galaxy: formation – Galaxy: structure – galaxies: interactions.

1 INTRODUCTION

Recent deep optical/infrared (IR) surveys, such as the Sloan Digital Sky Survey (SDSS) (Adelman-McCarthy et al. 2006) and the Two-Micron All Sky Survey (2MASS) (Skrutskie et al. 2006), are revealing increasingly complex structures in the halo of the Milky Way (MW). Among these, several new dwarf galaxies and tidal streams have been uncovered, but do these results favour the current galaxy formation paradigm? Can we consider these new structures as supporting the Λ cold dark matter theories (Abadi et al. 2003a,b) of galaxy formation? Are these the low-mass satellites which will be gradually accreted over time, and do they resolve previous issues such as the missing satellite problem?

While it may be a little premature to answer these questions with the current knowledge of Local Group environment, there is still little direct evidence to support the idea of a merger history for the MW. The Sagittarius dwarf galaxy (Ibata, Gilmore & Irwin 1994)

★E-mail: bconn@physics.usyd.edu.au

has shown that such accretion does occur and is in fact on-going but there are still too few nearby tidal stream remnants to confirm it as the primary Galaxy formation mechanism. However, analyses of these large surveys are uncovering new dwarf galaxies and tidal streams in the inner halo of the MW. For example, the discovery of tidal debris covering 60° of the sky only 20 kpc from the Sun, along with a new dwarf galaxy and other tidal debris is presented by Grillmair (2006a), Grillmair & Dionatos (2006a,b) and Grillmair & Johnson (2006). (Willman et al. 2005a,b) have uncovered a new dwarf galaxy in Ursa Major along with the tiny Willman I object, which is on the border between globular clusters and dwarf galaxies. Even closer satellite galaxies have been found with Belokurov et al. (2006b) and Zucker et al. (2006) presenting the discovery of another two dwarf galaxies using the SDSS data base. These two in Boötes and Canes Venatici are located heliocentrically at ∼60 and 220 kpc, respectively, and are, with the Ursa Major dwarf galaxy, pointing to a possible resolution of the missing Galactic satellites problem outlined in Klypin et al. (1999). Further structure is also highlighted in the discussion by Belokurov et al. (2006a) on the presence of tidal arms in the nearby globular cluster NGC 5466.

Our nearest spiral neighbour, M31, also shows a complicated formation history as Ferguson et al. (2002) have revealed in the Isaac Newton Telescope Wide Field Camera (INT/WFC) Survey. M31 was long thought to have been a relatively quiet spiral galaxy with a well-defined edge, but a faint diffuse outer disc, riddled with substructure, is now visible. Within this substructure, a giant stellar stream (Ibata et al. 2001), a new class of stellar cluster (Huxor et al. 2005) and the new dwarf galaxy, Andromeda IX (Lewis et al. 2004; Zucker et al. 2004), have been discovered. As we probe our own Galaxy to similar depths, will we uncover similar structure? The results coming from the SDSS and 2MASS surveys are suggestive of this. The MW, however, does seem to be a less complex system. Although the MW shows evidence of tidal debris in the halo, within the disc of the Galaxy a major change in recent years has been the discovery of the Monoceros Ring (MRi) by Newberg et al. (2002) and its purported progenitor, the Canis Major (CMa) dwarf galaxy (Martin et al. 2004a). The alternative source of the excess stars in CMa is the Argo star system as discussed in Rocha-Pinto et al. (2006).

The focus of the survey presented here has been to extend the INT/WFC survey of the MRi (Conn et al. 2005a) around the Galactic plane, as well as surveying around the CMa region to provide insight into the possibility of locating a dwarf galaxy there. The present survey has also attempted to investigate the Triangulum–Andromedae overdensity (Rocha-Pinto et al. 2004) and the Virgo overdensity (Jurić et al. 2005). These results will be presented elsewhere.

The layout of this paper is as follows: Section 2 summarizes the discovery of the MRi and the CMa dwarf galaxy; Section 3 describes the observational procedure and data reduction. Section 4 outlines the method employed to analyse the data, the use of a synthetic Galaxy model for comparison and the procedures for determining distances and completeness. Section 5 presents the data and the discussion and conclusions of this study are found in Sections 6 and 7.

2 THE MONOCEROS RING AND THE CANIS MAJOR DWARF GALAXY

Discovering the MRi via an overdensity of colour selected F-stars in the SDSS data set, Newberg et al. (2002) described its original extent from $l = (170–220)°$. Subsequent surveys in 2MASS (Rocha-Pinto et al. 2003; Martin et al. 2004a) and the INT/WFC (Ibata et al. 2003; Conn et al. 2005a) extended the MRi detections back towards the Galactic Centre with some tentative detections in the fields $(l, b) = (61, \pm15)°$ and $(75, +15)°$. More recently, Belokurov et al. (2006a), while tracing the Sagittarius stream with SDSS, notes the presence of the MRi in two bands at latitudes of $b = (20–30)°$. Additionally, Grillmair (2006b) discusses substructure in the MRi, again revealed in the SDSS catalogue. Consistently, the MRi is found on both sides of the plane of the Galaxy at galactocentric distances of ∼17 kpc.

Revealing an overdensity in the 2MASS data, Martin et al. (2004a) fulfilled a prediction by Newberg et al. (2002) that a potential progenitor of the MRi could lie in the nearby CMa constellation. Nestled under the Galactic disc, this overdensity, dubbed the CMa dwarf galaxy, can be found at $(l, b) = (240, -9)°$ and ∼7 kpc from the Sun. Its close proximity to the Galactic disc led Momany et al. (2004) to argue that the overdensity was simply a consequence of the Galactic warp. In response to this interpretation, Martin et al. (2005) presented results from a 2-degree field (2dF) spectrographic radial velocity survey taken at the Anglo-Australian Telescope (AAT). The initial results were complicated through difficulties in removing the instrumental signature from the data, but after resolving these issues Martin et al. (2005) maintained an interesting population of stars with a velocity anomalous to the Galactic disc. Additionally, Conn et al. (2005b) showed that in the background of CMa, the MRi was present at a distance of ∼13.5 kpc, with a velocity of ∼133 km s^{-1} and a dispersion of 23 km s^{-1}. Finally, using radial velocity data of the Carina dwarf and Andromeda galaxies, the MRi was revealed in the foreground of these objects (Martin et al. 2006). In front of the Carina dwarf, it has properties of $\langle V_r \langle = 145 \pm 5$ km s^{-1} with a velocity dispersion of only 17 ± 5 km s^{-1}. In front of the Andromeda galaxy, with stars taken from the 'One Ring' field $(l, b) = (123, -19)°$, it has properties of $\langle V_r \rangle = -75 \pm 4$ km s^{-1} and a dispersion of 26 ± 3 km s^{-1}. Slowly, both a velocity and spatial distribution of the MRi is being revealed.

The three main sources of evidence for the CMa dwarf are (in order of significance) the overabundance of red clump and red giant branch (RGB) stars in this region as seen in the 2MASS catalogue (Bellazzini et al. 2006); the additional velocity component as seen in the 2dF survey of the CMa region and the presence of a strong blue plume (BP) population as can be seen in fig. 1 of Martínez-Delgado et al. (2005). Recently, the origins of the BP population has been brought into question by Carraro et al. (2005) and Moitinho et al. (2006), who do not associate these stars with the foreground overdensity, but rather part of a more distant population of stars. This distant population is claimed to be the extension of the Norma–Cygnus spiral arm into the CMa region; and so these stars now require greater scrutiny in light of this new interpretation. Momany et al. (2006) have also produced a more complete study of their warp scenario, in which they confront the first and second sources of evidence for CMa. They argue that not only can the CMa overdensity be explained by the warp, but that the velocity dispersion as presented by Martin et al. (2005) is expected by current Galaxy models and shows nothing new. In studying the outer disc they suggest the MRi is not a tidal arm from an accretion event but rather the extension of the flare of the disc into those latitudes. In short, they claim all of the new structures in the disc of the MW are simply explained in terms of known Galactic structure. López-Corredoira (2006) concludes on the 'Galactic warp versus dwarf galaxy' debate with the statement that the warp can be formed by such a wide variety of causes that neither radial velocity or photographic surveys can disentangle their origins. This is maybe the case, although a systematic survey of the ages, metallicities, distances and abnormal velocity profiles in this region should provide strong indications if a dwarf galaxy resides in the plane or not. The warp is an important part of the puzzle but should not stop progress in resolving this issue.

Although the results from this paper are unable to answer questions regarding the velocity profile of these outer disc objects, it will attempt to understand those of the CMa and MRi overdensities with regard to their distance and position in the Galaxy. In our discussion, we comment on the likelihood of the proposals put forward by Momany et al. (2006) in explaining the MRi in terms of the outer disc and whether the warp satisfactorily describes the CMa overdensity.

3 OBSERVATIONS AND REDUCTION

The data were obtained using the AAT Wide Field Imager (AAT/WFI) at Siding Spring Observatory (SSO) in New South Wales, Australia. Mounted at the telescope prime focus, the camera consisting of eight 4×2 k CCDs with 0.2295 arcsec pixel^{-1}, covers a field of view approximately 33×33 arcmin^2 per pointing.

The observations were taken over four observing runs, the first on the 2004 January 22–25, the second on 2004 January 30–February 1, the third on the 2004 August 14–16 and the fourth on the 2006 February 1–5. All of the fields were observed with the *g* (WFI SDSS #90) and *r* (WFI SDSS #91) filters. These were chosen to minimize the fringing effects that can be present when observing with other filters. Each exposure consisted of a single 600-s exposure with the *g* filter and two 450-s exposures with the *r* filter. Two exposures were performed in *r* so as to avoid preserving cosmic rays and overexposing the brighter stars when using a single 900-s exposure. Each night, twilight flats were taken along with bias and dark frames for calibration and the closest Landolt standard star field to our target was observed every 2 h. In this manner, the removal of instrumental signatures and precise photometric calibration could be achieved. The seeing at the SSO can vary from 0.9 to 3.0 arcsec thus heavily affecting the limiting magnitude of the data. Although some fields were lost due to poor weather conditions, only the fields with the best photometry have been presented here.

The present survey was designed as a continuation of the MRi survey observed with the INT/WFC (Conn et al. 2005a). The fields were chosen to be roughly separated by 20° in Galactic longitude with adjustments made on the final location to ensure that the field was placed to ensure minimal dust extinction. Altogether the present survey has observed fields from $l = (193–25)°$, across the Galactic bulge; this paper reports only on the results of those fields in the region $l = (193–276)°$.

This part of the survey consists of 16 fields. Most fields are approximately 1 deg^2 in size (four WFI pointings). However, some fields are a combination of one, two or three pointings depending on the time available and quality of data obtained. The single pointing fields make up a strip of observations linking (240, −9)° with (240, +10)°. A summary of the field locations and area of the sky observed with the preliminary results of this survey is shown in Fig. 1 and Table 1.

A specialized version of the Cambridge Astronomy Survey Unit (CASU) data reduction pipeline (Irwin & Lewis 2001) was used to perform the debiasing and trimming, vignetting correction, astrometry and photometry. The flat fielding of the science frames used a master twilight flat generated over each entire observing run. To account for the dust extinction in the fields the DUST_GETVAL.C program supplied by Schlegel[1] was used to determine the extinction

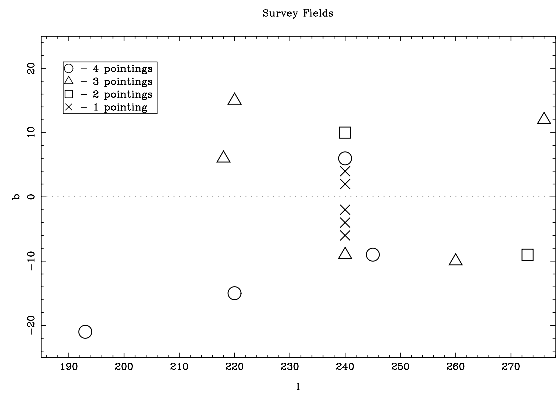

Figure 1. The location of the survey fields in the region $(l, b) = (193–276)°$. The symbols denote the number of pointings per field. The resultant fields have been selected based on data quality and while ideally four pointings would correspond to about 1 deg^2 of sky, observations undertaken during 2006 February had only seven out of eight CCDs available in the array.

for each star. This program interpolates the extinction from the dust maps of Schlegel, Finkbeiner & Davis (1998). Using the several standard fields observed per night provides a comparison for the calibration of the photometry to be determined. The standards are used to derive the CCD zero-points from which all the magnitudes are determined (Irwin & Lewis 2001). A catalogue of each colour band is produced by the pipeline for each paired exposure of *g* and *r*. Non-stellar images are rejected; however, near the limiting magnitude, galaxies begin to appear stellar like and thus become a source of contamination in the data set.

4 DATA PREPARATION

4.1 Detecting non-galactic structure

Searching for additional structure within the colour–magnitude diagrams (CMDs) of the AAT/WFI survey requires an understanding of the inherent structures present when observing through the Galactic disc. The MW can be roughly divided into four components: thin disc, thick disc, halo and bulge. The thin disc is essentially the plane of the Galaxy containing the majority of the stars and is where the spiral structure is also present. The thick disc is less dense than the thin disc and has a greater scaleheight out of the plane. The halo is considered to be a smooth spherical distribution of stars around the centre of gravity of the Galaxy and extends out beyond 20–30 kpc. The bulge is the central region of the Galaxy, including the bar, and contains a very dense old stellar population. The Besançon synthetic Galaxy model[2] (Robin et al. 2003) allows for these components to be considered separately as shown in Fig. 2. Each component is revealed in a distinct region of the CMD, allowing for at least a preliminary estimate of its origins when interpreting the CMDs from the observational data. It should be noted that the Besançon model employs a thin disc cut-off at ∼14 kpc from the Galactic Centre. The validity of such a cut-off is disputed in López-Corredoira (2006).

As an example, Fig. 2 shows the breakdown of the Galactic components as seen in two 1 deg^2 fields at (240, −2)° and (193, −21)°.

[1] http://www.astro.princeton.edu/∼schlegel/dust/data/data.html

[2] http://www.obs-besancon.fr/www/modele

Table 1. Summary of the observations of CMa tidal stream with the AAT/WFI, ordered in ascending Galactic longitude (l). The variation between the total area calculations of 2004 and 2006 is due to failed CCDs in the array shrinking the field of view.

Fields $(l, b)^{\circ}$	Regions per field	Average seeing (arcsec)	Total area ($\deg^2$)	MRi	Average $E(B-V)$	Date
$(193, -21)^{\circ}$	4	1.3	1.21	Maybe	0.08	2004 January 30
$(218, +6)^{\circ}$	3	1.3	0.8	Yes	0.01	2006 February 3
$(220, -15)^{\circ}$	4	1.0	1.21	Yes	0.22	2004 January 31
$(220, +15)^{\circ}$	3	1.3	0.91	Yes	0.04	2004 January 25
$(240, -9)^{\circ}$	3	1.0	0.91	Yes	0.18	2004 January 24
$(240, -6)^{\circ}$	1	1.0	0.3	No	0.40	2004 January 31
$(240, -4)^{\circ}$	1	1.0	0.3	No	0.99	2004 January 31
$(240, -2)^{\circ}$	1	1.0	0.3	No	1.10	2004 January 31
$(240, +2)^{\circ}$	1	1.0	0.3	No	0.79	2004 January 31
$(240, +4)^{\circ}$	1	1.0	0.3	Yes	0.28	2004 January 31
$(240, +6)^{\circ}$	4	1.2	1.21	Yes	0.13	2004 January 31
$(240, +10)^{\circ}$	2	1.3	0.61	Yes	0.10	2004 February 1
$(245, -9)^{\circ}$	4	1.6	1.21	Yes	0.14	2004 January 30
$(260, -10)^{\circ}$	3	1.3	0.91	No	0.21	2004 February 1
$(273, -9)^{\circ}$	2	1.4	0.53	No	0.29	2006 February 3
$(276, +12)^{\circ}$	3	1.1	0.8	Yes	0.09	2006 February 1

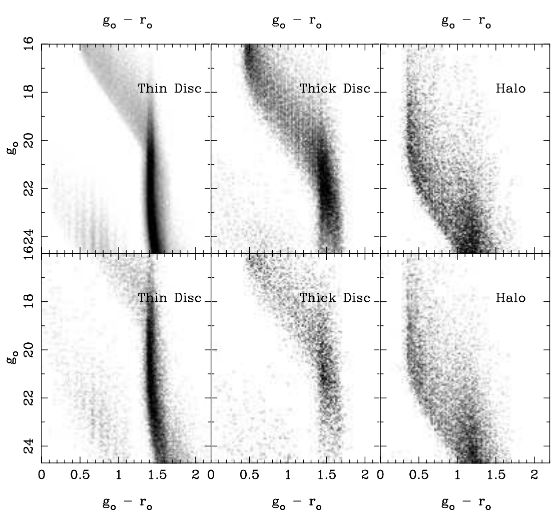

Figure 2. The top panels show the Hess plots (a pixelated CMD in which the resultant image is the square root of the number density) of $(240, -2)^{\circ}$ field from the synthetic model of the Galaxy by Robin et al. (2003) being split into its various Galactic components – thin disc, thick disc and halo. This illustrates where the various components of the galaxy lie on the CMD. The lower panels are from the model field $(193, -21)^{\circ}$ and show how the components vary further away from the plane of the Galaxy.

Analysing Fig. 2 reveals that, as expected, fields closer to the plane have more stars than those away from the plane. This manifests in the smoother CMDs in the top panels, with the bottom panels containing fewer thin and thick disc stars. The structure of each component is due to the homogeneity of the Galaxy and as a result a main sequence forms at every distance increment along that line-of-sight. So as the MW is probed deeper, the collective weight of the main sequences sum to form the CMDs that are observed. The closest main sequences, being brighter in apparent magnitude, form at the top of the CMDs with the subsequent main sequences, being fainter, forming lower down on the CMDs. The different stellar components of the thin and thick disc show the significant change in density between the two, giving them different characteristics in the CMDs. The thin disc being narrow and dense has a smaller scale-height (typically estimated at several hundred parsecs thick) which forms a much tighter sequence in the CMD. The more diffuse thick disc being more extended out of the plane (several kiloparsecs thick) forms a broader sequence. Comparing the top and bottom panels in Fig. 2 also shows the importance of the angle of the observations with regard the Galactic plane.

Detecting non-Galactic components then involves visually comparing the strong sequences detected in the observations with what is expected from the models. The MRi is located beyond the edge of the thick disc, and thus should be seen as a coherent sequence below the last sequence of the thick disc, as can be seen in fig. 12 of Newberg et al. (2002). Differentiating it from the halo component is simpler due to the halo not having any strong main sequences present below the thick disc in the range of our CMDs. So, any strong sequence below the thick disc will most likely be of non-Galactic origins. Although given the recent hypothesis on the MRi being attributed to the flare of the disc, this will also need to be considered. Another possibility is that a non-spherical halo could be misinterpreted as a 'non-Galactic' feature in the outer thick disc. Comparisons with the Besançon synthetic galaxy model reveals that their spheroid density distribution has a flattening of 0.76 and a power index of 2.44 (Robin, Reylé & Crézé 2000) which is moderately non-spherical. They note a significant degeneracy between these parameters which could allow for spheroids with a (c/a) of 0.85 (close to spherical) or 0.6 (quite oblate). As discussed in the following sections, the synthetic galaxy model does not introduce structures into the outer thick disc and so the influence of a non-spherical halo can be assumed to be minimal. The existence of the CMa dwarf galaxy is currently being scrutinized and so the CMDs of the CMa region will be used to investigate the influence of the Galactic warp on the stellar populations present there and whether it is a viable solution to resolving the dwarf galaxy debate.

The synthetic CMDs from the Besançon model data are considered out to 100 kpc (heliocentric distance, R_{HC}) which ensures that

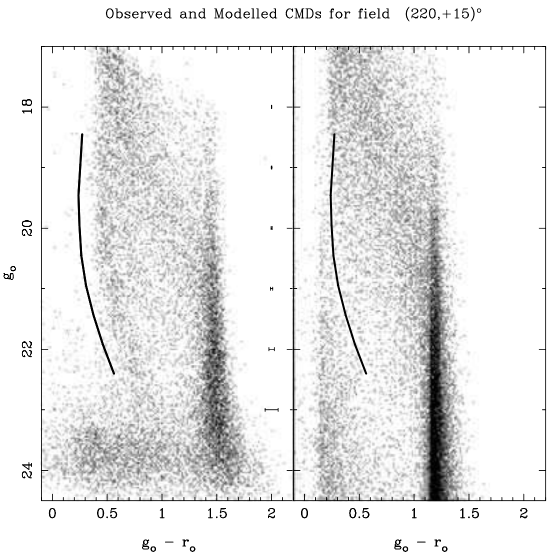

Figure 3. On the left is the AAT/WFI CMD of the field $(l, b) = (220, +15)^{\circ}$, and on the right is the same field as produced by the Besançon synthetic Galaxy model. The model outputs are CFHTLS-Megacam (AB) photometric system converted to Sloan g' and r' using equation (1). The fiducial sequence is placed with zero offset and uses the raw SDSS data (Newberg et al. 2002) from which the fiducial was created.

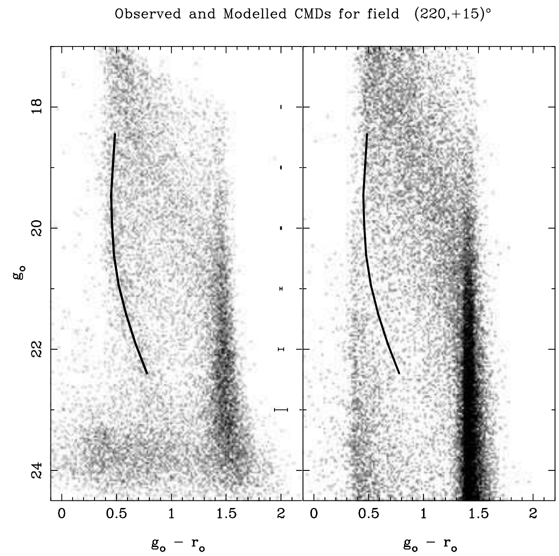

Figure 4. On the left is the AAT/WFI CMD of the field $(l, b) = (220, +15)^{\circ}$, and on the right is the same field as produced by the Besançon synthetic Galaxy model. The model is now the Sloan g' and r' in the AB system converted to the INT/WFC g and r in the Vega photometric system via equation (2). The fiducial sequence has also undergone the same colour conversion.

the halo population extends below the magnitude cut-off of the data and hence does not introduce additional structure. The synthetic fields contain a broad magnitude range (−99, 99) for each passband with zero extinction and the inclusion of all ages/populations and luminosity classes. This then provides as complete a picture of the region of interest as the model can supply. It also allows us to apply colour and distance cuts at our discretion. The model can output directly to the bands g_{CFHT} and r_{CFHT} in the Canada–France–Hawaii Telescope Legacy Survey/Megacam (CFHTLS-Megacam) (AB)[3] photometric system which need to be converted to the SDSS (g', r') system via equation (1):

$$r' = r_{\mathrm{CFHT}},$$
$$g' = \frac{g_{\mathrm{CFHT}} - 0.1480\, r_{\mathrm{CFHT}}}{1 - 0.1480}. \tag{1}$$

Frei & Gunn (1994) report that no conversion is needed between SDSS passbands (g', r') in the AB system to SDSS (g', r') in the Vega system. However, Fig. 3 shows that when using only AB magnitudes, the AAT/WFI data in the Vega system does not match the model in the AB system. A fiducial of the ridgeline from the original SDSS detection of the MRi by Newberg et al. (2002) can be seen to lie blue ward of the bluest edge of the data (see Section 4.1.2). So, using the results of Ibata et al. (2003), who compared overlapping INT and SDSS fields to determine a colour conversion between the two systems, the model is now shifted to the Vega system in this way. This is applicable to our data as both the INT data set and our AAT data set have been reduced using the same pipeline (with small modifications to allow for differences between the telescopes) and no such study has been undertaken with the AAT/WFI instrument. The resultant colour transformation to the INT (g, r) is

$$(g - r) = 0.21 + 0.86\,(g' - r'),$$
$$g = g' + 0.15 - 0.16\,(g - r). \tag{2}$$

The effect of this transformation can be seen in Fig. 4. The converted SDSS fiducial, corrected via equation (2), is now an excellent fit to the strong sequence in these data. The photometric system of the model CMD is now the same as the AAT/WFI CMD and no further changes have been applied to the model or data. All figures in this paper will be shown in the same format as Fig. 4, utilizing equations (1) and (2), with the resultant (g, r) from the synthetic Galaxy model considered the same as the extinction corrected observational data set $(g_{\circ}, r_{\circ})$. The Besançon synthetic Galaxy model employs different density profiles for each component of the Galaxy. These have been outlined in Conn et al. (2005a) and in more detail in Robin & Creze (1986), Robin et al. (1996, 2000) and Reylé & Robin (2001).

4.1.1 Magnitude completeness

Most of the fields presented here, consist of several overlapping subfields, see column 2, Table 1. The completeness of this sample is determined in a similar manner to that of the 2MASS All-Sky Point Source Catalogue (Skrutskie et al. 2006). This approach determines the fraction of stars that are detected in both overlapping images as a function of magnitude. So by matching the stars within those overlapping regions and calculating the proportion of matched stars in each magnitude bin with respect to the total number of stars observed, an estimate of the completeness is made. This produces a photometric completeness curve which can fit approximately by

[3] http://www.cfht.hawaii.edu/Instruments/Imaging/MegaPrime/

Table 2. Parameters used to model the completeness of each field, ordered in ascending Galactic longitude (l). m_c is the estimated 50 per cent completeness level for each filter with λ describing the width of the rollover function (equation 3).

Fields (l, b)	m_c ($g_\circ$)	m_c ($r_\circ$)	λ
$(193, -21)^\circ$	22.40	21.80	0.40
$(218, +6)^\circ$	23.40	22.40	0.50
$(220, -15)^\circ$	22.90	21.90	0.30
$(220, +15)^\circ$	23.60	22.60	0.30
$(240, -9)^\circ$	23.60	22.50	0.40
$(240, +6)^\circ$	24.00	22.70	0.40
$(240, +10)^\circ$	22.65	21.70	0.25
$(245, -9)^\circ$	23.30	22.20	0.60
$(260, -10)^\circ$	22.80	21.80	0.40
$(273, -9)^\circ$	23.40	22.20	0.50
$(276, +12)^\circ$	23.70	22.50	0.40

the equation

$$\mathrm{CF} = \frac{1}{1 + \mathrm{e}^{(m-m_c)/\lambda}}, \quad (3)$$

where m is the magnitude of the star, m_c is the magnitude at 50 per cent completeness and λ is the width of the rollover from 100 to 0 per cent completeness. The values used to model each field can be found in Table 2.

Although the completeness of our survey is not a key problem, attempting to characterize it does provide a manner in which we can compare the data quality of the various fields. In general, this allows an estimate of the magnitude at which the data becomes untrustworthy. Additionally, since the model is mostly used to help identify the major structures in the CMDs, it is unnecessary to apply the completeness function to the model. This is because those structures are typically well away from the 50 per cent completeness limit. It is also important to note that while this method does not account for stars in crowded fields, none of our survey fields can be considered crowded and so this approach is valid for the entire data set.

4.1.2 Estimating the distance and additional calibration

Determining the distance to the CMa and MRi sequences is achieved by taking the ridge line of the detection in the SDSS S223+20 field (Newberg et al. 2002, fig. 12) and creating a fiducial sequence. The AAT/WFI uses SDSS filters and so the fiducial sequence can be directly used on the data with the colour transformations described in equation (2).

The heliocentric distance estimate of the SDSS S223+20 detection is assumed to be 11.0 kpc (Newberg et al. 2002), this then is the zero offset distance. Since the fields have been extinction corrected it is assumed that only distance variations are the cause for any deviation in magnitude from this location. This method does not account for possible differences in age or metallicity between main sequences. The heliocentric distance is calculated using equation (4) and assuming the Sun is 8.0 kpc from the Galactic Centre, the galactocentric distance is found from simple trigonometry:

$$R_{\mathrm{HC}} = 11.0 \times (10^{\mathrm{offset}/5.0}). \quad (4)$$

Determining a value for the error associated with such a measurement is dependent on several factors. Most predominant of these is whether the fields have been correctly calibrated with regard to their photometry and taking into account the dust extinction present within the fields. The dust correction for this data will always overcorrect for stars within the Galaxy, because the dust value is based on the entire cumulative impact of the dust along that line-of-sight (Schlegel et al. 1998). The stars in this survey do not reside at the end of that line-of-sight and so will be overcorrected in the dust extinction process. In most of the fields, the levels of dust are sufficiently low that the difference between the dust value used and the 'correct' value should be small, see Table 1.

To determine whether the colour transformations applied to the data set correspond to reliable distance estimates, three fields to which there are distance estimates to these structures from other surveys have been analysed. Those are $(l, b) = (220, +15)^\circ$, $(240, -9)^\circ$ and $(245, -9)^\circ$. The first field is very close to the original MRi detection of Newberg et al. (2002) and the second and third are part of the CMa detection fields of Martin et al. (2005). The MRi is known to have a distance of 11.0 kpc in the Newberg et al. (2002) field, at $(220, +15)^\circ$ it is also located at 11.0 kpc. For the CMa fields, the distance determined by Martin et al. (2005) is about 7.2 kpc. The present survey locates the centre of the strong sequence at 7.3 kpc or -0.9 mag of offset. Importantly then, each distance estimate here is consistent with independent measurements of those structures.

Having understood the errors involved in both the determination of the photometry, extinction correction and the fiducial sequence, manually placing this fiducial at the centre and two extremes of an acceptable fit 'by-eye' provides a range of distances over which this structure resides. Given the large errors involved, these distances can only be considered indicative of the true distance. However, the range of magnitude offsets defining the extremes does give a sense of the width of the structure. Several fields have only one distance estimate, as locating the extremes is not possible due to the data quality or the narrowness of the sequence. The dominant strong sequence in each field, which could be attributed to either the thin/thick disc or CMa overdensity has only a single distance estimate, corresponding to the faintest edge of that feature. This is due, in general, to the lack of a definite upper edge, see Table 3.

4.1.3 Signal-to-noise ratio estimation technique

Estimating the signal-to-noise (S/N) ratio of the MRi main sequence found in the data has been attempted for several fields. The criterion for S/N ratio determination is that the MRi main sequence is sufficiently distinct from the CMa/disc sequence to avoid potential contamination. The model field is assumed to represent the properties of the background Galactic stars which should be removed to highlight the additional MRi main sequence. The model needs to be adjusted first to more accurately reflect the properties of the data and then subtracted to reveal the excess MRi stars. Before subtraction the model is degraded to match both the completeness profile of the data as shown in Table 2 and the relevant magnitude error properties. To ensure that similar numbers of stars are present in both the data and model prior to subtraction an additional scaling factor is applied. These processes result in the data and the model being essentially identical with the exclusion of the additional MRi main sequence. The S/N ratio is estimated by dividing the number of stars in the feature by the Poisson noise due to the modelled number of stars in the region.[4] Only five fields have been suitable for this estimate namely $(l, b)^\circ = (218, +6)^\circ$, $(220, +15)^\circ$, $(220, -15)^\circ$, $(240, +10)^\circ$ and $(276, +12)^\circ$, see Table 3. These fields have

[4] Parameters available on request: bconn@eso.org

Table 3. Summary of the observations of CMa tidal stream with the AAT/WFI, ordered in ascending Galactic longitude (l).

Fields $(l, b)^\circ$	MRi offset and width (mag)	MRi dist and width (kpc)	MRi S/N ratio estimate	MW/CMa offset lower edge (mag)	MW/CMa dist (kpc)
$(193, -21)^\circ$	0.5	13.8	–	−1.2	6.3
$(218, +6)^\circ$	$0.0^{+0.35}_{-0.3}$	$11.0^{+1.9}_{-1.4}$	~34	−1.5	5.5
$(220, -15)^\circ$	$0.2^{+0.3}_{-0.3}$	$12.1^{+1.7}_{-1.6}$	~32	−1.4	5.8
$(220, +15)^\circ$	$0.0^{+0.3}_{-0.35}$	$11.0^{+1.6}_{-1.6}$	~14	−2.5	3.5
$(240, -9)^\circ$	0.4	13.2	–	−0.6	8.3
$(240, -6)^\circ$	–	-	–	–	–
$(240, -4)^\circ$	–	–	–	–	–
$(240, -2)^\circ$	–	–	–	–	–
$(240, +2)^\circ$	–	–	–	–	–
$(240, +4)^\circ$	0.1	11.5	–	−1.4	5.8
$(240, +6)^\circ$	$0.3^{+0.3}_{-0.3}$	$12.6^{+1.9}_{-1.6}$	–	−1.2	6.3
$(240, +10)^\circ$	$0.5^{+0.3}_{-0.3}$	$13.8^{+2.1}_{-1.7}$	~22	−2.2	4.0
$(245, -9)^\circ$	0.5	13.8	–	−0.6	8.3
$(260, -10)^\circ$	–	–	–	−0.3	9.6
$(273, -9)^\circ$	–	–	–	−0.3	9.6
$(276, +12)^\circ$	0.3	12.6	~26	−2.0	4.4

MRi detections which are easily distinguished from the dominant main sequences in the CMD and thus are suitable for this technique. The remaining detections are too close to the CMa/disc population to easily measure their S/N ratio with this method.

5 SURVEY FIELDS

The location of each field is shown graphically in Fig. 1. Each field presented in this section shows the CMDs with the appropriate fiducial sequence taken from the original Newberg et al. (2002) detection as described in the previous section. The CMDs that we have used are density maps of the underlying distribution with the square root of the number of stars per pixel being presented in all of the CMDs in this paper, called a Hess diagram. This method provides better contrast of the structures especially in high star density regions. In the following sections, the distance estimates to the major features present in each CMD are provided with an analysis of these results in Section 6. The principal features of the CMD have been identified by visual comparison with the Besançon model. The MRi main sequence is evident by its absence in the model and the CMa main sequence is inferred to be associated with the strongest main sequence in the CMD. The fiducial is then placed on the CMD and shifted in magnitude to be aligned 'by-eye' with the respective features. A more accurate technique is unnecessary given the inherent uncertainties already present in a distance estimate of this kind. It is important to note that the fiducials placed on the dominant features of the CMD are not necessarily considered detections, but rather placed to provide insight into all the features present in the CMDs. For the dominant and strongest sequence in each CMD, only the fainter edge has been fit with the fiducial sequence providing a single distance estimate. For the fainter coherent sequences, both the upper and lower extremes have been fitted giving a range of distances to that structure, see Fig. 5. The complete list of the magnitude offsets and distance estimates is contained in Table 3. The brighter, nearer or more dominant sequence has been listed under the heading MW/CMa to illustrate that differentiating between the two is not straightforward when using CMDs. Although some

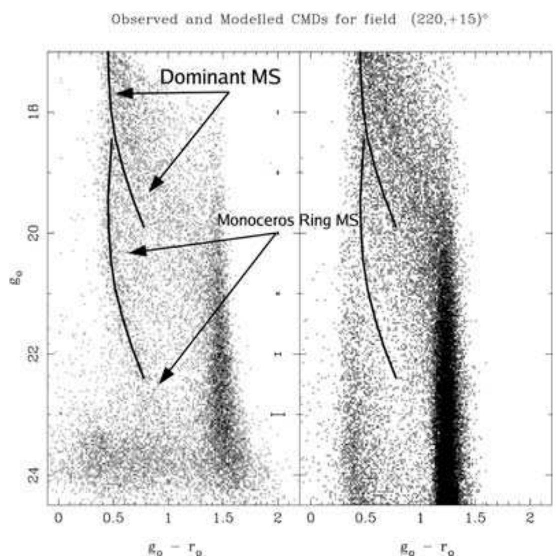

Figure 5. Hess plot (a pixelated CMD where the grey-scale is the square root of the number density for that pixel) of $(l, b)^\circ = (220, +15)^\circ$ (left) and the corresponding Besançon model (right). This figure illustrates the alignment of the fiducial with both the dominant main sequence in the CMD associated with brighter nearby stars and the fiducial aligned with the MRi feature. As illustrated, the dominant main sequence is only defined by its fainter edge while the MRi feature is located along the centre of the main sequence. For this feature the offsets employed are −2.5 and 0.0 mag. To avoid unnecessarily cluttering the data CMDs, the following figures only show the placement of the fiducial on the model. This allows a direct comparison with model and highlights where the new features lie with respect to the expected Galactic components.

fields are most likely to contain only MW stars, there are several that are possibly a mix, or completely dominated by CMa stars. For this reason, this structure is left ambiguously identified in Table 3. The fainter, more distant or less dominant sequence is listed under the heading MRi. To understand the widths of the structures and hence an estimation of the errors for each field, this table should be referenced. The final structure of interest are the BP stars which are located around 18 mag and in the colour range $(g - r) = 0.0$–0.3. These stars can be seen clearly in Fig. 10 and are discussed further in Section 6.2.2.

5.1 Monoceros region

The four fields presented here are in close proximity to the original detections of the MRi as presented in Newberg et al. (2002). Importantly, the present survey has sampled both sides of the plane, finding the MRi to be present across the Galactic plane. This has implications regarding whether the MRi could be a phenomena related to the Galactic warp and flare.

5.1.1 Fields at (193, −21)°

This is the furthest field west from CMa (towards the anticentre direction) that is included in this survey (Fig. 6). Despite the good seeing and area covered in this field, many of the fainter stars have been lost due to the relative proximity of the Moon. This has removed a lot of the detail present in other fields of similar size. Using the fiducial sequence on the two main features in this CMD, we obtain two distance estimates. The first using an offset of −1.2 mag corresponding to a heliocentric distance of ∼6.3 kpc. The second more distant feature, somewhat more tentative, is found at an offset of 0.5 mag, or $R_{\mathrm{HC}} \sim 13.8$ kpc. Given the lack of clarity regarding the potential MRi feature in the data, no attempt has been made to measure the spread of distances over which it is visible. Indeed, it is uncertain whether this is simply the strong overdensity of stars seen at the faint blue end of the model CMD. The stars located at the faint blue end of the CMD are most likely misclassified galaxies and are unlikely to represent any real Galactic structure, they have a considerable error in colour as can be seen by the error bars on the right-hand side of the panel. The 50 per cent completeness in $g_\circ$ for this CMD is 22.4 mag.

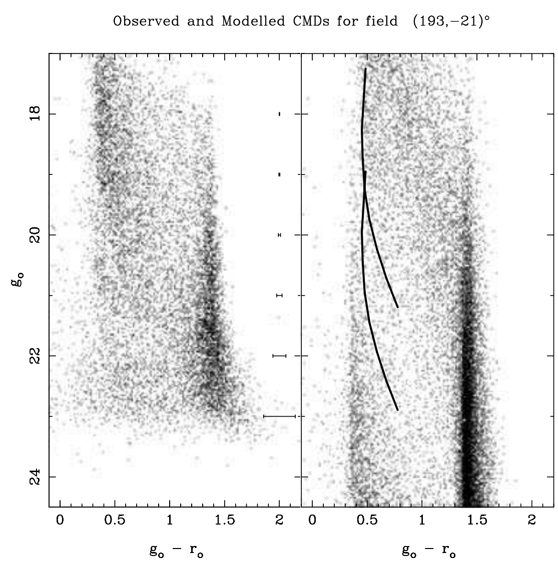

Figure 6. Hess plot (a pixelated CMD where the grey-scale is the square root of the number density for that pixel) of $(l, b) = (193, -21)°$ (left) and the corresponding Besançon model (right). The synthetic Galaxy model is taken from the Besançon online galaxy model website. The model has a distance interval of 100 kpc from the sun to ensure no artificial cuts enter into the CMDs. The model is selected in U band and then converted to g, r using colour corrections from the INT/WFC website. There are two structures in this field, the strong sequence beginning at $g_\circ \sim 19.0$ and a fainter coherent sequence at about 20–21 mag. The offsets required to fit the fiducial sequence from Newberg et al. (2002) are −1.2 and 0.5 mag. Heliocentrically, this corresponds to 6.3 and 13.8 kpc. The 50 per cent completeness in $g_\circ$ for this CMD is 22.4 mag.

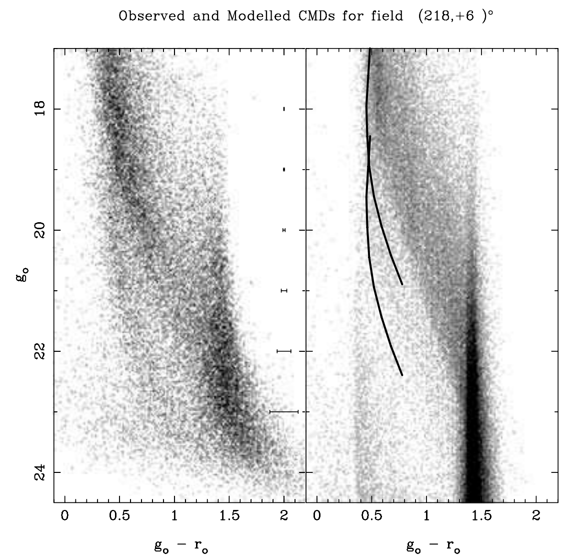

Figure 7. Hess plot of $(l, b)° = (218, +6)°$ (left) and the corresponding Besançon model (right). The figure is otherwise the same as Fig. 6. The sequences fitted here are offset by −1.5 and $0.0^{+0.35}_{-0.3}$ mag. The heliocentric distance of these offsets are ∼5.5 and $11.0^{+1.9}_{-1.4}$ kpc. The CMD is 50 per cent complete at $g_\circ = 23.4$ mag.

5.1.2 Fields at (218, +6)°

At the same Galactic longitude as the original MRi detection made by Newberg et al. (2002), the CMD is presented in Fig. 7. The two fiducials are offset by −1.5 mag for the brighter sequence and $0.0^{+0.35}_{-0.3}$ mag for the fainter coherent sequence. These result in distance estimates of ∼5.5 and $\sim 11.0^{+1.9}_{-1.4}$ kpc, respectively. The CMD is 50 per cent complete at $g_\circ = 23.4$ mag. Given the broad nature of the MW sequence, only the distance to the lower boundary is stated. The S/N ratio estimate for the MRi in this field is ∼34. This value is higher than expected, probably due to the close proximity of the dominant main sequence. The model does not cleanly subtract this feature and so some counts remain to boost the S/N ratio estimate.

5.1.3 Fields at (220, −15)°

As the southern counterpart for the original MRi detection made by Newberg et al. (2002), the CMD for (220, −15)° is presented

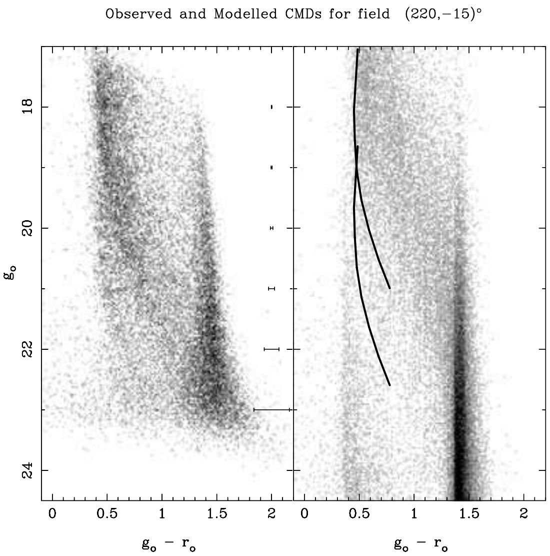

Figure 8. Hess plot of $(l, b)^\circ = (220, -15)^\circ$ (left) and the corresponding Besançon model (right). The figure is otherwise the same as Fig. 6. The sequences fitted here are offset by −1.4 and $0.2^{+0.3}_{-0.3}$ mag. The heliocentric distance of these offsets are 5.8 and $12.1^{+1.7}_{-1.6}$ kpc. At $g_\circ = 22.9$ mag, the CMD is 50 per cent complete.

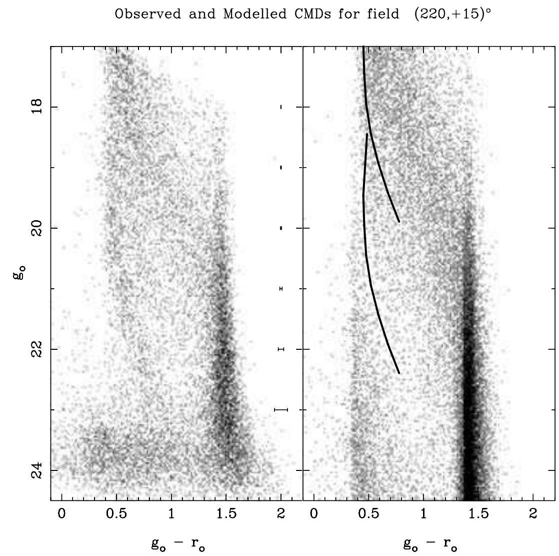

Figure 9. Hess plot of $(l, b)^\circ = (220, +15)^\circ$ (left) and the corresponding Besançon model (right). The figure is otherwise the same as Fig. 6. The sequences fitted here are offset by −2.5 and $0.0^{+0.3}_{-0.35}$ mag. The heliocentric distance of these offsets are 3.5 and $11.0^{+1.6}_{-1.6}$ kpc. The 50 per cent completeness in $g_\circ$ for this CMD is 23.6 mag.

in Fig. 8. The two fiducials are offset by −1.4 mag for the brighter stronger sequence and $0.2^{+0.3}_{-0.3}$ mag for the fainter coherent sequence. These result in distance estimates of ∼5.8 and $\sim 12.1^{+1.7}_{-1.6}$ kpc, respectively. At $g_\circ = 22.9$ mag, the CMD is 50 per cent complete. The fainter sequence is found to have a S/N ratio ∼ 32, although this estimate is probably contaminated by the nearby brighter main sequence.

5.1.4 *Fields at* (220, +15)°

This field, Fig. 9, is the closest to the original MRi detection made by Newberg et al. (2002) taken during the present survey. The two fiducials are offset by −2.5 mag for the brighter stronger sequence and $0.0^{+0.3}_{-0.35}$ mag for the fainter sequence. These result in distance estimates of ∼3.5 and $\sim 11.0^{+1.6}_{-1.6}$ kpc, respectively. Being only 5° from the fields presented in Newberg et al. (2002), the distance to the MRi here is the same as their distance estimate of 11 kpc. The 50 per cent completeness in $g_\circ$ for this CMD is 23.6 mag. A S/N ratio ∼ 14 is found for the fainter sequence.

5.2 Canis Major region

The following fields are part of a strip of observations linking (240, −9)° to (240, +10)°. The fields from $b = -6°$ to +4° are single pointings, while (240, +6)° has four pointings filling out a ∼1° × 1° field and (240, +10)° has two pointings. These observations provide a glimpse as to how the Galaxy profile changes across the Galactic plane. The high dust extinction of the lower Galactic latitudes has distorted the CMDs; however, there is still information in these fields and for this reason they have been left in. The dust is more prominent in the southern fields as characterized by the lesser distortion of the CMDs in the northern fields. All of the fields from $b = -6°$ to +6° were observed under the same conditions with the (240, + 10)° field observed the following night.

5.2.1 *Fields at* (240, −9)°

This field is centred on the location of the putative core of the CMa dwarf galaxy (Fig. 10). The very strong sequence running the length of the CMD can be fit along the faint edge with a fiducial offset by −0.6 mag which corresponds to ∼8.3 kpc. Placing it roughly along the centre of the feature requires an offset of −0.9 mag or ∼7.6 kpc. In Conn et al. (2005b), the presence of the MRi in the background of the CMa overdensity was revealed. This was determined to be at a distance of 13.5 ± 0.3 kpc. Indeed, just below the sequence dominating the CMD there does seem to be an excess of stars which may be another coherent sequence, its contrast is low due to the dominating effect of the CMa sequence. An offset of 0.4 mag is needed to align the fiducial with this feature, corresponding to a heliocentric distance of 13.2 kpc. Given the match this makes with the AAT/2dF detection this is considered a tentative detection. The CMD is 50 per cent complete at $g_\circ = 23.6$ mag.

5.2.2 *Fields at* (240, −6)°

In Fig. 11, the strong sequence is still present in this field although distorted by the increased level of dust and possible non-photometric conditions. The BP stars (see Section 6.2.2) are still easily visible and while there is contention over their origins, they are still indicative that the general structures present here are unchanged from the previous field. Consisting of only one exposure, the 50 per cent completeness level has not been calculated.

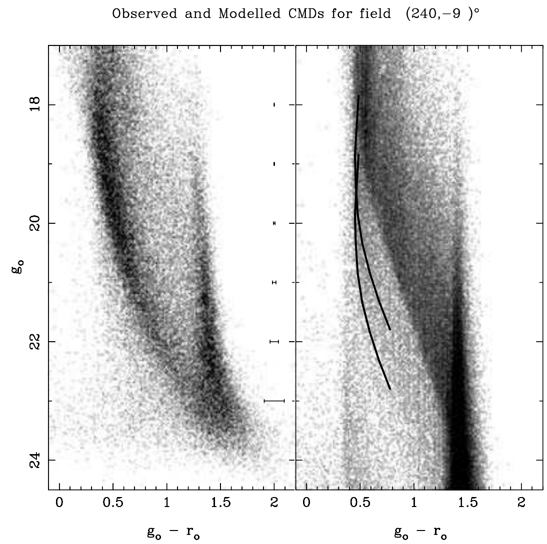

Figure 10. Hess plot of $(l, b) = (240, -9)°$ (left) and the corresponding Besançon model (right). The figure is otherwise the same as Fig. 6. The strong sequence in this field is determined to be at ∼8.3 kpc from an offset of −0.6 mag with the fiducial sequence. Below this strong sequence is an excess of stars at a $g_\circ = 20$–21 mag and $(g_\circ - r_\circ) \sim 0.5$. This excess follows below the strong sequence as it increases in colour. Fitting a fiducial to this excess at an offset of 0.4 mag a distance of 13.2 kpc is obtained. This in excellent agreement with estimated distance to the MRi of 13.5 kpc as derived in the AAT/2dF survey of Conn et al. (2005b). This is deemed a tentative detection of the MRi in this field. The CMD is 50 per cent complete at $g_\circ = 23.6$ mag. Note the presence of BP stars at $g_\circ \lesssim 18$.

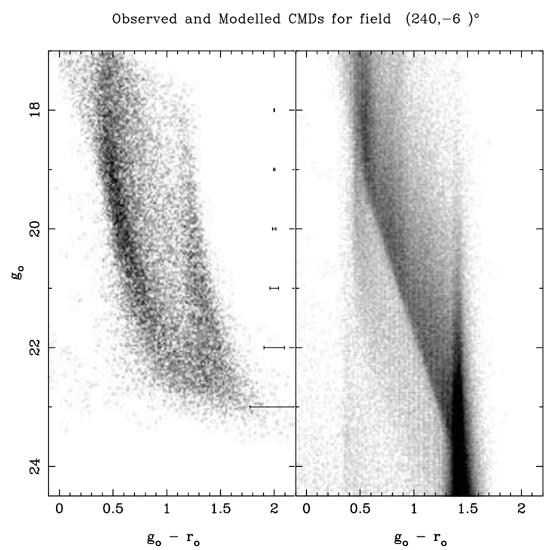

Figure 11. Same as Fig. 6, Hess plot of $(l, b) = (240, -6)°$ (left) and the corresponding Besançon model (right). No offset is placed on this CMD due to the obvious distortion present which is most likely due to the increase in dust and non-photometric conditions. The CMD does show all the same features as present in the (240, −9)° field. Consisting of only one exposure, the 50 per cent completeness level has not been calculated.

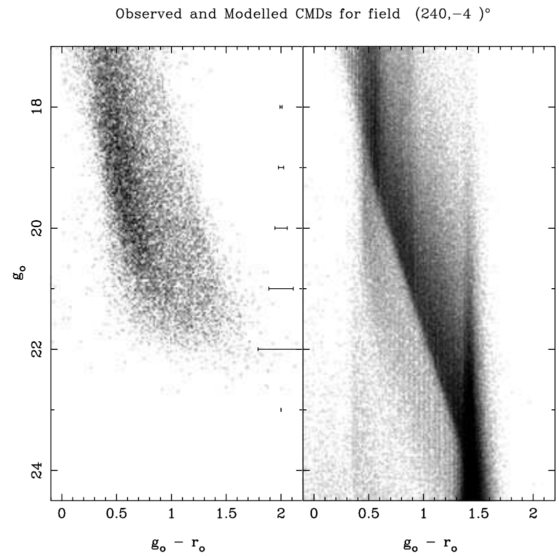

Figure 12. Hess plots of $(l, b) = (240, -4)°$ (left) and the corresponding Besançon model (right). The high dust levels in this field $E(B - V) \sim 1.4$ has distorted the resultant CMD. Although the exact features of the CMD are indistinguishable, the presence of the BP stars remains obvious, although seemingly weaker than the (240, −6)° field. No completeness estimate has been made for this field.

5.2.3 *Fields at* (240, −4)°

This field (Fig. 12), as with those closest to plane, is heavily affected by dust extinction. In particular, it has the second highest dust levels in our survey, where $E(B - V)$ is typically around 0.99. Again, despite the loss of structure in this field, the CMD still shows evidence for a BP population although it appears a little weaker than the preceding (240, −6)° field. The CMD has been left in the location as determined by the calibration process of the CASU pipeline. The high dust levels are the most likely cause for the distortion on the main sequences present in the CMD. No completeness estimate has been made for this field.

5.2.4 *Fields at* (240, −2)°

The dust extinction in this field, Fig. 13, is extremely high, typically around an $E(B - V) \sim 1.1$. There is a faint suggestion of the presence of BP stars, although less so than in the previous field. The strong sequence visible in this region of sky is still apparent. However, it is impossible to provide a distance estimate to this structure. The limiting magnitude of this field is most likely heavily affected by the dust accounting for its position with regard the CMDs in the remaining survey locations. As for the two previous fields, there is only one pointing in this direction and so no completeness estimate has been made.

5.2.5 *Fields at* (240, +2)°

This field, Fig. 14, begins to re-emerge from the dust problems below the plane, showing a strong sequence across the CMD. Unfortunately, due to the distortion effects of the dust, an estimate of the distance to this structure is still not possible. It is difficult to

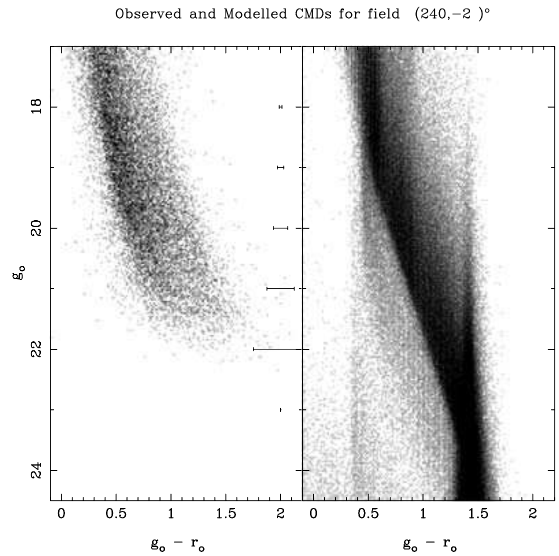

Figure 13. Hess plots of $(l, b) = (240, -2)^\circ$ (left) and its counterpart synthetic CMD (right). The dust here again is heavily distorting the main sequences, allowing only the weak presence of the BP stars to be visible. As for the two previous fields, there is only one pointing in this direction and so no completeness estimate has been made.

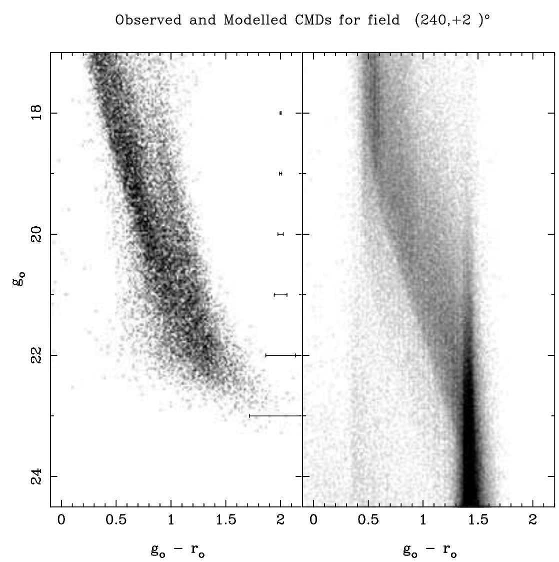

Figure 14. Hess plots of $(l, b) = (240, +2)^\circ$ (left) and its counterpart synthetic CMD (right). Although heavily affected by dust, the dominant main sequence is now clearly visible. The BP population seems to have disappeared or become too bright, leaving what may be solely Galactic stars behind. No distance estimate has been attempted for this field. Despite the distortion, there is obviously a very strong sequence present in this field. Continuing the strip of single pointings above the plane, this field also has no completeness estimate.

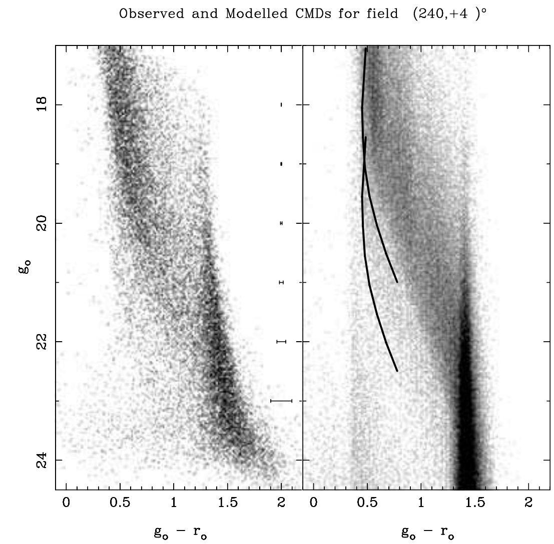

Figure 15. Hess plots of $(l, b) = (240, +4)^\circ$ (left). The fiducial sequences plotted on top of the Besançon model (right) are at offsets of -1.4 and 0.1 mag. These are at ∼5.8 and 11.5 kpc, respectively. This field with a single pointing has no completeness estimate.

judge whether the sequence feature seen here is created by the same structure detected below the plane. The BP population is no longer present, which may indicate these are purely Galactic stars or that it has shifted to brighter magnitudes which are saturated in this survey. Continuing the strip of single pointing above the plane, this field also has no completeness estimate.

5.2.6 Fields at (240, +4)°

Here the main components present in the CMD, Fig. 15, can be fit with fiducials at magnitude offsets of -1.4 and 0.1 mag. The distances then to these features are 5.8 and 11.5 kpc, heliocentric. This field with a single pointing has no completeness estimate.

5.2.7 Fields at (240, +6)°

Consisting of four pointings, this field is the largest of the CMa region targets above the plane (Fig. 16). The strong sequence here corresponds to a magnitude offset of -1.2 mag, or ∼6.3 kpc. With the lower sequence residing at $\sim 12.6^{+1.9}_{-1.6}$ kpc or $0.3^{+0.3}_{-0.3}$ mag of offset. A 50 per cent completeness in this CMD is found at $g_\circ = 24.0$.

5.2.8 Fields at (240, +10)°

Two pointings make up this field (Fig. 17), and again two sequences are clearly visible in the CMD. The closer of the two is at -2.2 mag of offset, or 4.0 kpc. The more distant sequence is offset at $0.5^{+0.3}_{-0.3}$ mag, or $13.8^{+2.1}_{-1.7}$ kpc, heliocentric. This field has a 50 per cent completeness in $g_\circ$ at 22.65. The S/N ratio of the fainter feature is estimated to be ∼22.

5.2.9 Fields at (245, −9)°

This field, presented in Fig. 18, was chosen to probe the lateral extent of the CMa dwarf/overdensity. Being 5° east in longitude,

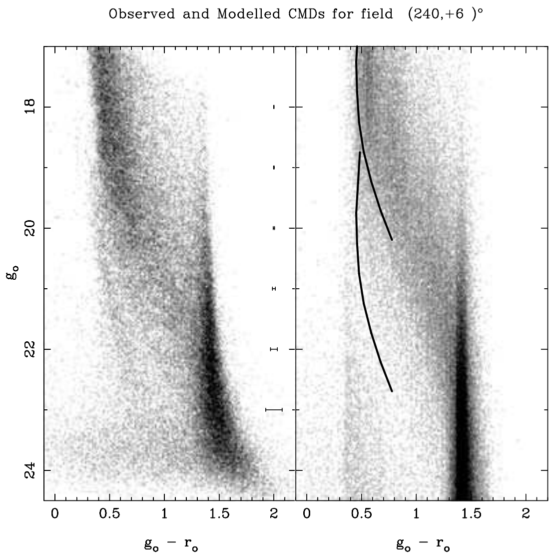

Figure 16. Hess plots of $(l, b) = (240, +6)^\circ$ (left) and its counterpart synthetic CMD (right). The figure is otherwise the same as Fig. 6. The two fiducials are placed at offsets of -1.2 and $0.3^{+0.3}_{-0.3}$ mag, aligning with the features in the data. The heliocentric distance is 6.3 and $12.6^{+1.9}_{-1.6}$ kpc, respectively. A 50 per cent completeness in this CMD is found at $g_\circ = 24.0$.

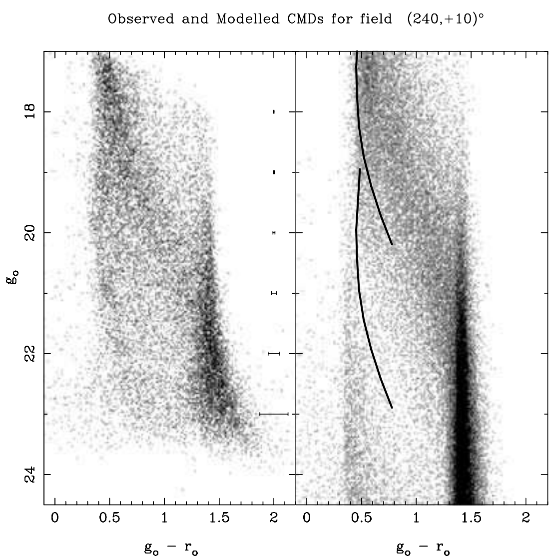

Figure 17. Hess plots of $(l, b) = (240, +10)^\circ$ (left) and its counterpart synthetic CMD (right). The figure is otherwise the same as Fig. 6. There are two structures present in the data for which the fiducial sequences are placed on to the model. The brighter of the two is at a magnitude offset of -2.2 mag, or $\sim$4.0 kpc, and the fainter fiducial with an offset of $0.5^{+0.3}_{-0.3}$ mag, or $13.8^{+2.1}_{-1.7}$ kpc. This field has a 50 per cent completeness in $g_\circ$ at 22.65.

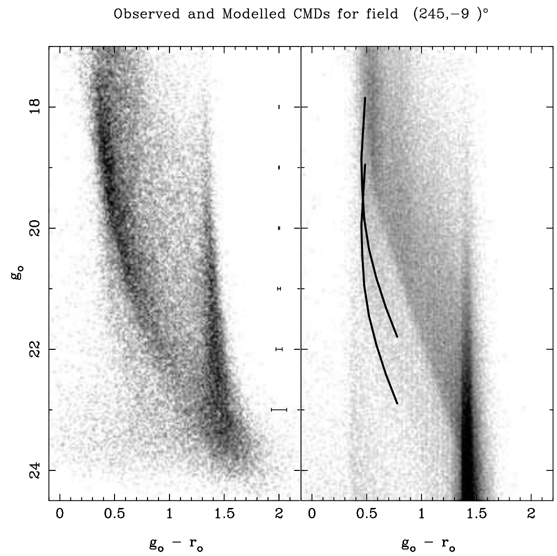

Figure 18. Hess plot of $(l, b) = (245, -9)^\circ$ (left) and the corresponding Besançon model (right). The figure is otherwise the same as Fig. 6. As for the field $(240, -9)^\circ$, this field contains a very strong sequence and is fit by the same offset of -0.6 mag or 8.3 kpc. The presence of a fainter more distant sequence can be seen below the strong sequence and is fit with an offset of 0.5 mag at a heliocentric distance of 13.8 kpc. At 23.3 mag in $g_\circ$, the CMD is 50 per cent complete. Note the presence of BP stars at $g_\circ \lesssim 18$.

the dominant sequence in this region of sky is still very strong. The fiducial sequence has been fitted with an offset of -0.6 mag. This offset corresponds to a distance of $\sim$8.3 kpc. As with the field $(240, -9)^\circ$, a fiducial closer to the centre of this feature is offset by -0.9 mag, or 7.3 kpc. This value matches the distance to dwarf galaxy as reported by Martin et al. (2004b). A fiducial has been fitted to the faint MRi population just below the strong sequence. The offset of 0.5 mag corresponds to 13.8 kpc, heliocentrically. At 23.3 mag in $g_\circ$, the CMD is 50 per cent complete.

5.3 Maximum warp region

The remaining fields in this part of the survey occupy the part of the Galaxy which is most affected by the Galactic warp. Because of predominantly poor weather, only three fields of this region are presented. However, they do contain information regarding the MRi and the CMa dwarf and also continue the Galactic plane survey into the fourth quadrant.

5.3.1 *Fields at* $(260, -10)^\circ$

This field is located 20° from the CMa dwarf/overdensity and although the BP stars have maintained their location on the CMD, the strong sequence has shifted to fainter magnitudes (Fig. 19). The fiducial sequence has been fitted with an offset of -0.3 mag. This offset corresponds to a distance of $\sim$9.6 kpc. There is no clear evidence of the MRi in this field, which would reside below the strong sequence close to the limiting magnitude of this data. The 50 per cent completeness level in $g_\circ$ is found at 22.8 mag for this field. Martin et al. (2006) report on the detection of the MRi 12° further in latitude

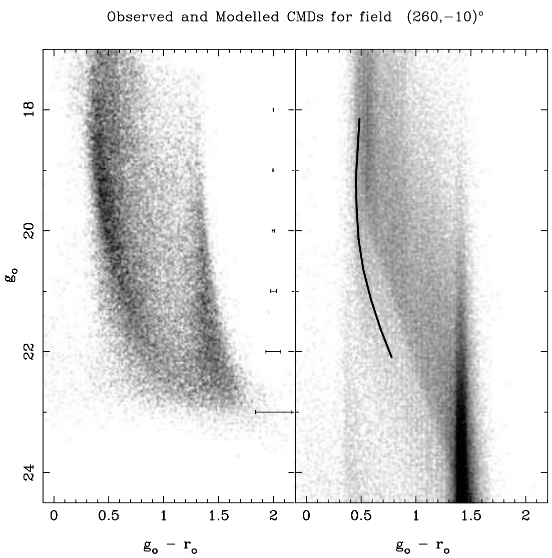

Figure 19. Hess plot of $(l, b) = (260, -10)°$ (left) and the corresponding Besançon model (right). The figure is otherwise the same as Fig. 6. As for the fields nearer the $(240, -9)°$ field, this field contains a very strong sequence and is fit by the an offset of −0.3 mag or 9.6 kpc. The MRi cannot be seen in this field. The 50 per cent completeness level in $g_\circ$ is found at 22.8 mag for this field.

from this field, in front of the Carina dwarf galaxy. This detection was made in velocity space and currently there is no firm estimate of the distance to the MRi at this longitude. Until observations in this region are extended to fainter magnitudes no detection of the MRi can be reported in this field.

5.3.2 *Fields at* (273, −9)°

This field is at the same latitude as the CMa dwarf/overdensity and, as seen in the previous field, the strong sequence in this field has shifted to fainter magnitudes (Fig. 20). The dominant sequence remains very strong and is fitted with a fiducial with an offset of −0.3 mag. This offset corresponds to a distance of ∼9.6 kpc. The CMD is 50 per cent complete at $g_\circ = 23.4$ mag. This field shows some distortion at its faintest extremes, most likely due to a combination of the levels of dust in the region and/or changing conditions during the observations. While the fiducial has been fitted to the data, it is clear that the distortion inhibits the ability to accurately locate the distance. Of most importance is the presence of the strong sequence in this field and the BP stars which reside in the same location as the fields at different longitudes.

5.3.3 *Fields at* (276, +12)°

In Fig. 21, the field shows clear evidence for the MRi. The fiducial sequence has been fitted to the MRi with an offset of 0.3 mag. This offset corresponds to a distance of ∼12.6 kpc. The MW/dominant sequence is found with a fiducials corresponding to −2.0 mag or 4.4 kpc, heliocentric. This CMD is 50 per cent complete at $g_\circ = 23.7$ mag. The fainter sequence is estimated to have S/N ratio ∼ 26.

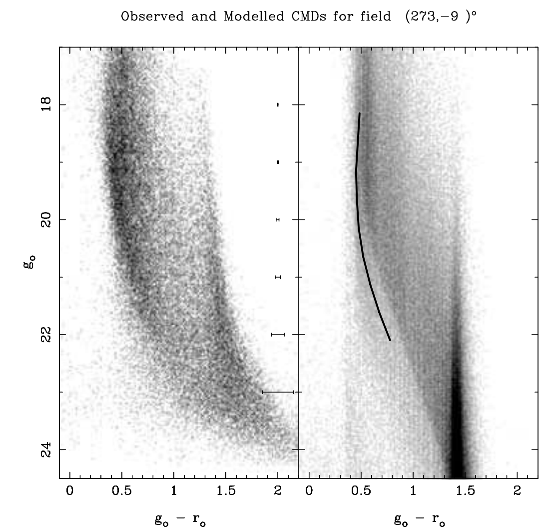

Figure 20. Hess plot of $(l, b) = (273, -9)°$ (left) and the corresponding Besançon model (right). The figure is otherwise the same as Fig. 6. As for the field $(260, -10)°$, this field contains a very strong sequence and is fit by a similar offset of −0.3 mag or ∼9.6 kpc. The CMD is 50 per cent complete at $g_\circ = 23.4$ mag. The distortion of this field due to dust means the fiducial cannot be fitted accurately.

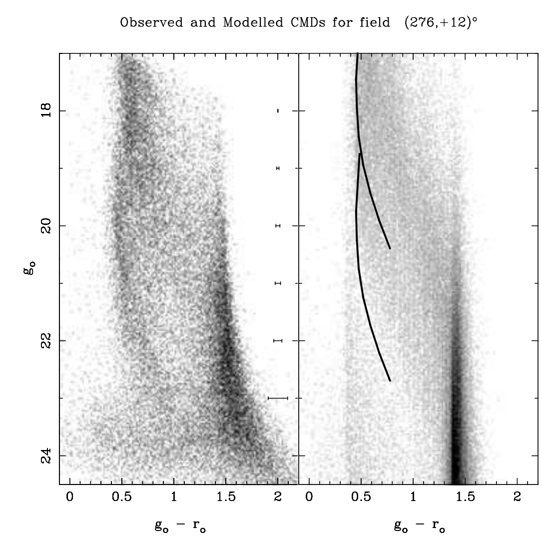

Figure 21. Hess plot of $(l, b) = (276, +12)°$ (left) and the corresponding Besançon model (right). The figure is otherwise the same as Fig. 6. As for the field $(260, -10)°$, this field contains a very strong sequence and is fit by a similar offset of 0.3 mag or ∼12.6 kpc. The MW/dominant sequence is found at 4.4 kpc through an offset of −2.0 mag. This CMD is 50 per cent complete at $g_\circ = 23.7$ mag.

6 ANALYSIS AND DISCUSSION

This section discusses the detections of the MRi and those in the CMa region. This is done separately as there is no consensus on either the origin of these structures or their connectedness.

6.1 The Monoceros Ring

From this survey, we interpret the presence of apparent coherent sequences beyond the edge of the thin/thick disc as the MRi. This results in 10 detections across the entire longitude range of this survey and on both sides of the Galactic plane. Importantly, these results show that the MRi cannot be reproduced by a warped disc scenario leaving only the Galactic flare or a non-Galactic origin for these stars. Fig. 22 shows all the previous MRi detections as projected on to the Galactic plane. The star symbols are the detections outlined in Table 3 and so those star symbols close to the Sun are MW/CMa sequence distances, while those further away are the MRi. Fields above the plane are filled symbols and those below the plane are empty symbols.

The circles at $(61, \pm15)°$ and $(75, +15)°$ from Conn et al. (2005a) are included here as detections. A review of these fields during the preparation of this paper has found them to be detections of the MRi. The previous use of the Besançon synthetic Galaxy model out to only 50 kpc introduced a turn-off in the halo population near these MRi sequences. This added confusion to the identification of the MRi in these fields but increasing the model distance limits to 100 kpc removed this turn-off and showed these features to be truly MRi detections.

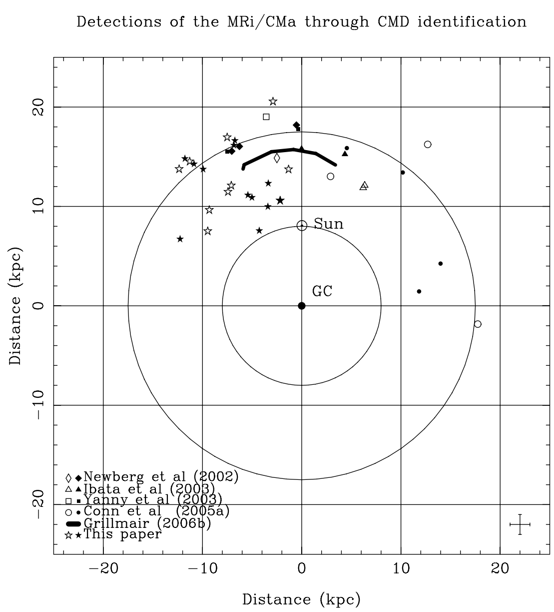

Figure 22. Location of all of the detections of the MRi (to date) and CMa dwarf (from this paper) projected on to the Galactic plane. The symbols denote the source of the distances and locations presented here. Filled symbols are detections made above the plane of the Galaxy, with empty symbols for those fields below the Galactic plane. Approximate locations of the MRi stream (above the plane) seen in Grillmair (2006b) are illustrated with the solid line. The stars (filled and empty) are those detections outlined in this survey. A ±1 kpc error bar in the lower right corner is indicative of the accuracy of these detections. The strip of observations at $l = 240°$ is clearly evident with the fields below the plane (open stars) at the distance of the CMa overdensity and the fields above the plane (filled stars) at the MRi distance. Since each field in the survey has been fit with two fiducial sequences, each is present here to illustrate their location with regard the other detections.

The previous detections of the MRi from CMDs, seen in Fig. 22, show the distance estimates do not form a neat coherent picture of the structure. Rather, there are many gaps between detections which limit our understanding of the overall shape of this feature. Our results seem to show a slight systematic preference for fields below the plane being further away than those above the plane. The fields above the plane from about $l = (118–240)°$ do seem to maintain a consistent galactocentric distance of about 16–17 kpc. There are also a few detections below the plane which consistently fall outside of the 16-kpc circle.

The difficulty with Fig. 22 is that while it distinguishes between those fields above and below the plane, it does not fully convey how far apart those fields truly are. For instance, in the $l = 220°$ direction, the original detection by Newberg et al. (2002), the $(218, +6)°$ field and the $(220, +15)°$ reside at the same distance. The $(220, -15)°$ field with $\sim30°$ of latitude between it and the Newberg et al. (2002) detection is found slightly further away at ~12.1 kpc. This is same structure present on both sides of the plane and with no young stars forming part of the MRi it is unlikely to have been caused by perturbations within the disc.

6.1.1 *Can the flare explain the ring?*

Momany et al. (2006) present a possible explanation for the existence of the MRi in terms of the flaring of the Galactic disc. The flare in the disc is in addition to the warp and represents a gradual widening of the disc with increasing Galactic radii. They present several figures showing the location of the previous MRi detections, from both the Newberg et al. (2002) and Conn et al. (2005a), as intersecting the flare in the Yusifov (2004) model. Fig. 23 shows the Yusifov models' prediction for the stellar density profile of the Galaxy in direction of $l = 123°$, a field which contains two detections of the MRi in the same direction, namely $b = -19°$. The warp in this part of the Galaxy extends north as seen here and because of the flare, the width of the Galaxy grows with increasing distance. The Sun is located at the origin. The stellar density can be seen to decrease in both the radial and the perpendicular directions. The distance estimates to the detections found in this field, from Conn et al. (2005a),

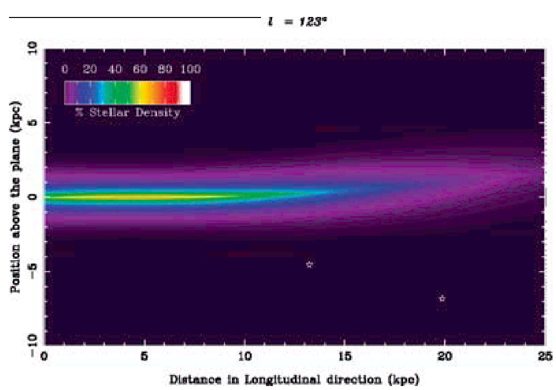

Figure 23. Stellar density profile of the Galaxy as described by Yusifov (2004), in the direction of $l = 123°$. It covers all Galactic latitudes from $-90° < b < 90°$. The star symbols denote the location of the MRi detections as presented in Conn et al. (2005a). The colour scale corresponds to the stellar density of a given coordinate divided by the maximum density for the region. The Galactic plane is seen clearly as the region of high density and it shifts above the plane with increasing distance in correspondence with the properties of the northern warp.

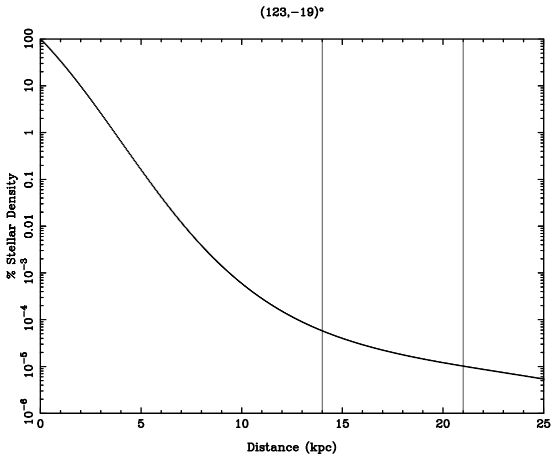

Figure 24. Line-of-sight stellar density profile from the Yusifov (2004) model for $(123, -19)^\circ$. The location of the two vertical lines corresponds to the distances of the two MRi detections in this direction. The first is located at 14 kpc with the second at 21 kpc. This shows that the expected stellar density contribution due to the warp and flare is 10^{-4} times smaller than the maximum stellar density along that line-of-sight. There is also no increase in density to account for the presence of the MRi at these distances in this direction.

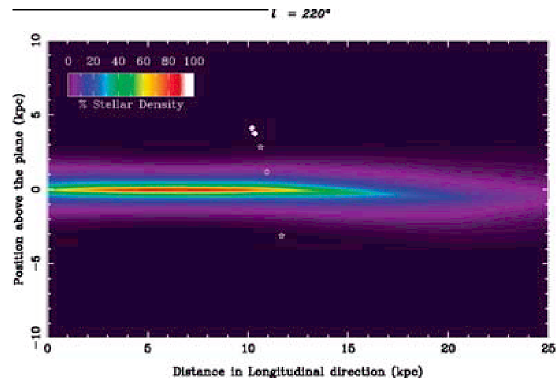

Figure 25. Same as Fig. 23, this is the stellar density profile of the Galaxy in the direction $l = 220^\circ$. The star symbols corresponds the detections of the MRi as outlined in this paper, while the diamonds are from Newberg et al. (2002).

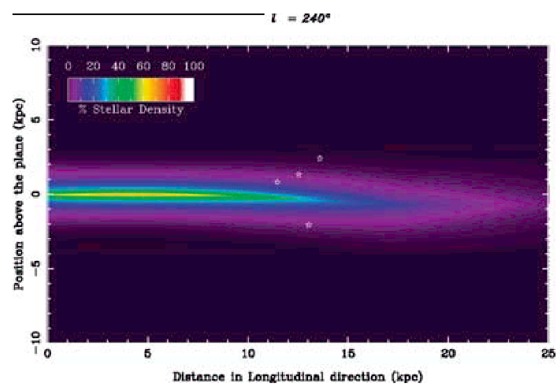

Figure 26. Same as Fig. 23, this is the stellar density profile of the Galaxy in the direction $l = 240^\circ$. The star symbols corresponds the detections of the MRi as outlined in this paper.

are shown as stars. There is an error of at least 10 per cent on their location, as explained in that paper, and in Fig. 23, this error aligns itself with the line joining the location of the symbol and the origin. This figure clearly shows that density in the region of the detections is below 0.5 per cent of the maximum stellar density in this direction. Attributing this feature to the warp is not feasible since a warp would only produce a single smooth main sequence. The flare also does not introduce any structures or boundaries of significance in the entire region and does not seem suitable for explaining the MRi in this direction. To investigate this further, Fig. 24 shows the line-of-sight density profile for the $(123, -19)^\circ$ field from the model. The two vertical lines are placed at the distances of the two detections. It is evident that the model does not show any increase in density with increasing distance from the Sun and that the flare cannot explain the presence of the MRi here.

Two other regions of interest when interpreting the MRi are at $l = 220^\circ$ and 240°. In both cases, the MRi has been detected above and below the plane at the same longitude. The stellar density predictions from the Yusifov model are shown in Figs 25 and 26. In Fig. 25, the diamond symbols are from Newberg et al. (2002), while the star symbols are from this paper and altogether they show that the MRi in this region is an extended vertical structure in the disc. Although it is unsure whether the detections on either side of the plane are of the same origin, the coincidence in their distances should be noted. It is also apparent that known Galactic structure is unable to account for an overdensity at this distance. Could the density profile seen in Fig. 24 be peculiar to that direction? Fig. 27 presents the line-of-sight density for all the detections seen in Fig. 25. The two vertical lines delimit the minimum and maximum MRi distance estimates for these fields. Again, it can be seen that the stellar density profile is unable to reproduce an increase in stellar density which could explain the MRi. The MRi detections here are found within a variety of stellar densities and so neither the warp nor the flare can be invoked to justify their presence. At $l = 240^\circ$, the northern detections range from ∼11.5 kpc at $(240, +4)^\circ$ to ∼13.8 kpc at $(240, +10)^\circ$. Below the plane, the field $(240, -9)^\circ$ is also found at ∼13.8 kpc which is consistent with the results of Conn et al. (2005b). While there is not the neat correlation between the northern and southern detections in this region, as with the $l = 220^\circ$ fields, it does confirm again that the smooth stellar density distributions are unable to account for the overdensity of stars contained in the MRi. The warped flared MW does not contribute significantly at the locations of the MRi, as claimed by Momany et al. (2006).

There is no neat coherent picture of the MRi structure even considering the many detections of it, primarily due to relatively small areas of sky surveyed, combined with rough distance estimates. However, regardless of this, the Galactic flare is not a likely source for this overdensity of stars. Furthermore, while this has only been tested on the Yusifov model, the similarities between the various models make it unlikely that any of them will be able to generate a significant overdensity of stars at the distances found in the data. Additionally, even the possibility of it being a distant spiral arm, it is countered by the vertical extent of the MRi out of the plane. For those dissatisfied with a tidal stream origin for the MRi, other mechanisms will have to be invoked. In the meantime, the best

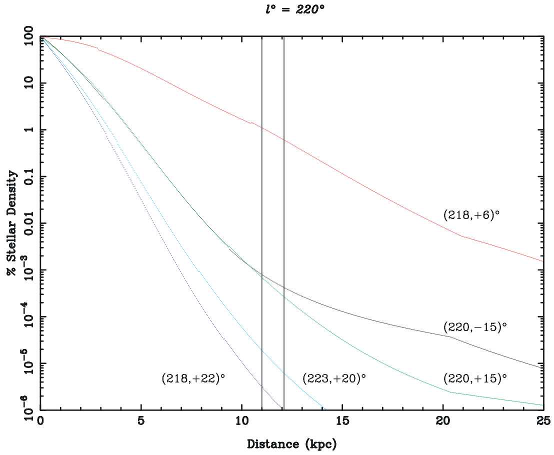

Figure 27. Line-of-sight stellar densities for each detection around $l = 220°$. The two vertical line delimit the maximum and minimum distance estimates for the MRi in this region. Same as Fig. 24, the overdensity of stars belonging to the MRi do not originate from the warp or flare of the Galaxy.

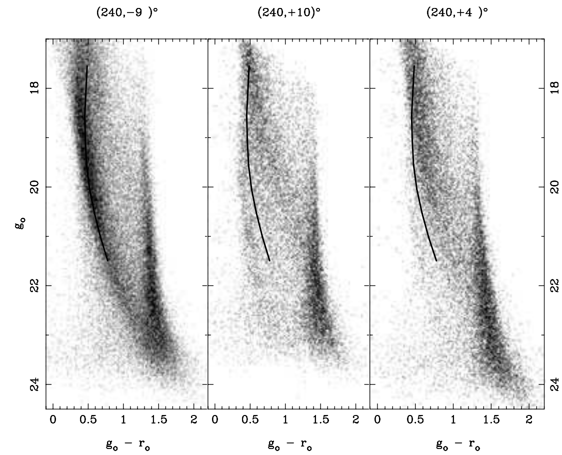

Figure 28. CMDs of (240, −9)° (left), (240, +10)° (centre) and (240, +4)° (right). The fiducial sequence placed on each figure is for the distance of 7.2 kpc. If there was no warp in the disc of the MW then the (240, −9)° and (240, +10)° should be similar due the approximate symmetry of the disc. However, if the MW is warped by ∼3° as suggested by Momany et al. (2006) then (240, −9)° and (240, +4)° should be similar. Given that the two fields will differ with increasing heliocentric radius, the fiducial is placed at the same distance to highlight where they should be the same.

explanation is a tidal stream scenario and so given that, where then is the progenitor?

6.2 The Canis Major dwarf

The existence of the CMa dwarf is debated by Carraro et al. (2005), López-Corredoira (2006), Moitinho et al. (2006) and Momany et al. (2006), who propose either a new warp or spiral arm scenario to explain the presence of the overdensity in this region. While all the issues raised in these papers cannot be addressed here, some qualitative comparisons can provide further insight into this debate.

6.2.1 Warp or dwarf?

The primary source of doubt over the presence of the dwarf galaxy is whether a warp in the disc of the Galaxy is sufficient to explain the overdensity of M giant stars as reported in Martin et al. (2004a). The warp in the Galaxy has been known for a long time and was primarily described through observations of the gas disc, as presented in Burton (1988). Tracing the warp through the stellar populations is more difficult, as only certain types of stars have reliable distance estimate techniques. Yusifov (2004) exploits the pulsar distribution around the Galaxy, while López-Corredoira et al. (2002) use the 2MASS catalogue to trace the warp with the old stellar population (giant stars and red clump stars). The basis of these studies is the assumption that the Galaxy is essentially symmetric above and below the plane. Following the path of the symmetry reveals the warp in the disc and its deviation from the $b = 0°$ plane. Momany et al. (2006) also employ the 2MASS catalogue using the raw counts of RGB and red clump stars above and below the plane to trace the warp. They argue their result shows the mid-plane of the disc is shifted by ∼3° below the plane in the direction of the CMa overdensity at $l \sim 240°$. This result does not elucidate how they account for the presence of dust around the Galaxy and stars at all latitudes and reddening are included. Although this presents a potential flaw in their argument, we can none the less proceed to examine the data in light of their claims. The survey presented here contains a strip of observations at $l \sim 240°$, which provide an excellent opportunity to try to understand the stellar populations of this region. Given that all of the warp models rely solely on symmetric stellar populations around the plane to derive the warp, this can be used to interpret the CMDs presented here. If we consider the field at $(l, b) = (240, -9)°$ as our basis for the warp/dwarf problem, then, by symmetry, there should be a field which is similar on the northern side of the plane. Fig. 28 shows three CMDs from the strip of observations at $l \sim 240°$ chosen to aid our understanding. The field on the left is the observation at $(l, b) = (240, -9)°$, the centre is (240, +10)° and the right CMD is (240, +4)°. Overlaid on each of the CMDs is the fiducial sequence from Newberg et al. (2002) used in the previous sections. It is placed at a magnitude offset corresponding to ∼7.3 kpc and serves as a reference point for all the stars at that distance. If the Galaxy had no warp, then the $b = -9°$ and $+10°$ fields should be, by symmetry, almost identical. Clearly, both the strength and location of the dominant main sequence feature in the south is unmatched in the north. This supports the presence of the warp in this part of the Galaxy. Momany et al. (2006) find the mid-plane of the Galaxy to be offset by ∼3° below the plane at $l \sim 240°$. This implies that the proper corresponding field to compare the (240, −9)° field is not (240, +10)°, but rather (240, +3)°. Unfortunately, this survey does not include a field in this location and so the (240, +4)° is shown instead. The (240, +2)° could also be considered but is affected by too much extinction to be useful in this comparison. Again, the southern field contains many more stars along the entire length of the dominant sequence than its northern counterpart, showing that the symmetry argument is unsuitable for this field. Therefore, the warp is not an adequate explanation for the CMa overdensity. This simple test reveals that these fields are not symmetric around the warped plane. The reasons for supporting the presence of the dwarf galaxy is not to merely substitute it for the warp, but rather to show that there are more stars in this location than can simply be explained

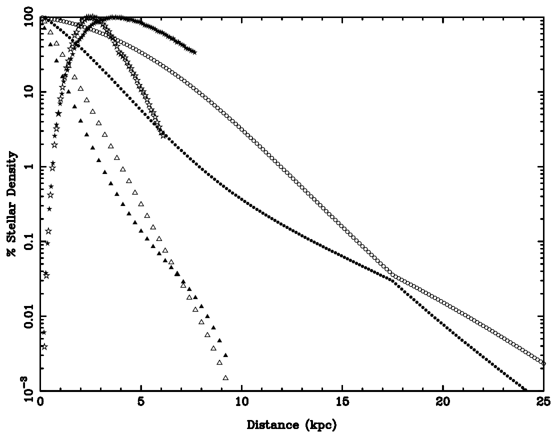

Figure 29. Line-of-sight stellar density for $(l, b) = (240, -9)^\circ$ and $(240, +4)^\circ$ fields. The filled symbols are for the southern field and the empty symbols for the northern fields. The various models are the Besançon synthetic Galaxy model (stars), Yusifov (2004) model (circles) and the López-Corredoira et al. (2002) model (triangles).

by adjusting the warp in the Galactic disc. Comparing the predictions of each model for the fields $(l, b) = (240, -9)^\circ$ and $(240, +4)^\circ$, Fig. 29 shows the stellar density profiles as predicted by the Yusifov (2004) model, the López-Corredoira et al. (2002) model and the Besançon model. The Besançon model's prediction is generated via the histogram of star counts taken from the same data source as the comparison fields generated in Figs 10 and 15. The abrupt cut-off in the Besançon model is from only selecting the thin disc stars in this analysis. The other two models are generated via the density equations presented in their respective papers (López-Corredoira et al. 2002; Yusifov 2004). Fig. 29 clearly shows that none of the models predict any rise in stellar density at the 7.3-kpc distance of the CMa overdensity. Only the Besançon model shows a rolling over of the stellar density at ∼5 kpc for the southern field and ∼3 kpc for the northern field. This does favour higher stellar densities in the south but comparisons with the model, as in Fig. 10, show that there is a clear discrepancy between the model and the data. Although the López-Corredoira et al. (2002) model maintains roughly the same stellar density profile in both hemispheres, at only ∼5 per cent of the maximum stellar density in that direction the density is far too low at the distance of the dwarf to account for the number of stars seen there. The Yusifov (2004) model with different warp parameters predicts more stars in the north than in the south as seen in Fig. 29 at $b = +4^\circ$ and -9°.

The AAT/WFI data presented here do suggest that there is an overdensity of stars below the plane at $l = 240^\circ$, which is still unexplained by the latest warp models. Although the Besançon model can be criticized for introducing a thin disc cut-off and not having the latest estimations of the warp and flare, it does attempt to model the entire set of properties considered to be part of the Galaxy. New parameters of the warp and flare need to be incorporated into the entire picture of the Galaxy to be truly useful when presented with actual data. These additional stars are unexpected in a mostly symmetric Galaxy, but whether they belong to a dwarf galaxy or not are difficult to tell. It is certain though that the standard Galaxy model is inadequate and that a dwarf galaxy could introduce a strong sequence as seen in the CMa region.

6.2.2 *The blue plume star problem*

Investigating the presence of the BP stars in the region of the CMa overdensity has unveiled an interesting problem. The BP stars can be seen in Fig. 10 around 18 mag and in the colour range $(g - r) =$ 0.0–0.3, however, around 0.3 there will be some contamination from main-sequence stars. Recently, these stars have been connected with the disc, the CMa dwarf galaxy and a distant spiral arm. So to which structure do the BP stars belong? The following section will present the arguments for both sides and conclude with a possible course of action to resolve this problem.

The evidence in favour of the dwarf galaxy has relied on the presence of BP stars in the CMa CMDs. Fig. 1 from Martínez-Delgado et al. (2005) has illustrated that a model dwarf galaxy CMD could be consistent with these stars being part of the dwarf galaxy. More recently, Butler et al. (2006) have shown that the BP stars follow a different distribution, more confined to the Galactic plane, than the red clump stars which were used to identify the CMa overdensity. However, as proposed by Carraro et al. (2005) and Moitinho et al. (2006), these stars might be associated with a much more distant structure, an outer spiral arm. The present survey, consisting of only two filters, is unable to confirm the distance estimates of these previous studies, but using the large range of longitudes available it can highlight where the BP stars are visible.

Examination of the data reveals one possible solution to the BP star problem. The BP stars are clearly visible in the two most important fields of the CMa overdensity: $(240, -9)^\circ$ as shown in Fig. 10 and $(245, -9)^\circ$ in Fig. 18. Close inspection of the other fields show that in fact all the fields at $l \geqslant 240^\circ$ *below* the plane have a BP population. Interestingly, none of the fields above the plane shows any evidence of BP stars and those fields below the plane at $l =$ $(193–220)^\circ$ also have no BP stars. So the BP stars in the present survey are visible solely below the plane and at $l > 220^\circ$. Although, the fields $l = (193–220)^\circ$ may be too far out of the plane for the BP stars to be seen. This is not an issue for the northern fields, as the disc is sampled at several latitudes and the BP stars are not present. The only information provided by the present survey on the BP stars is the magnitude at which they are located on the CMD and the direction in which they were observed. A direct measurement of their distance is not possible, but since the distance to the sequences in the CMD can be estimated via fitting of the fiducial, a qualitative approach to the BP distance can be made. The first problem with the BP stars arises here. In each of the AAT/WFI fields containing BP stars, the magnitude at which they are seen is almost constant. Indeed, while the main components of the CMD become fainter with increasing longitude, these stars maintain the same brightness levels. It can be concluded then that these stars are not associated with the strong sequences seen in the CMDs and in turn are not associated with the dwarf galaxy.

The Besançon comparison fields of $(240, -6)^\circ$, $(240, -4)^\circ$ and $(240, -2)^\circ$ (Figs 11, 12 and 13) also contain a BP population at a magnitude comparable with those seen in the data; perhaps then this is not the detection of a new structure, but rather an accepted component of the Galaxy. A breakdown of the BP stars in the Besançon model provides some insight into their origins (see the analysis of the field at $(l, b) = (240, -4)^\circ$ in Fig. 30). The 'age' of the star in Fig. 30 indicates whether it belongs to the thin disc, thick disc, bulge or halo. An age of 1–7 corresponds to thin disc stars, age 8 – thick disc, age 9 – halo, age 10 – bulge. The majority of the stars seen in the BP region are of ages 2 or 3, which is comparable to a population 0.15–1 Gyr old for age 2 and 1–2 Gyr old for age 3. While many BP stars are local, out of the ∼4100 stars plotted here in this

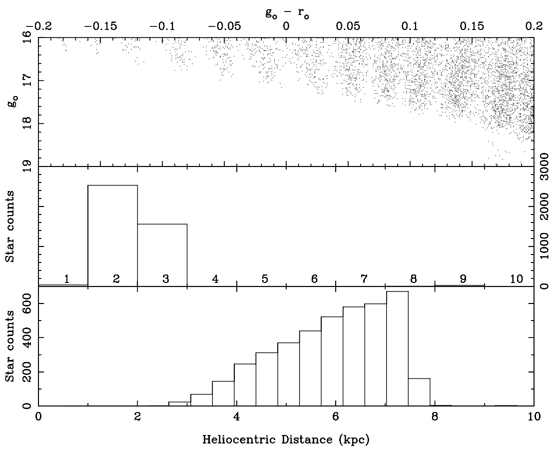

Figure 30. BP stars selected from the Besançon synthetic Galaxy model in the field (240, −4)°. The top panel shows their location on a CMD. The middle panel is their distribution of ages (parametrized into 10 bins), with age 2 corresponding to stars 0.15–1 Gyr old and age 3 being stars 1–2 Gyr old. The lower panel is the heliocentric distance distribution of the stars in kpc. The striation in the top panel is due to the resolution of the model and is not an observable phenomena.

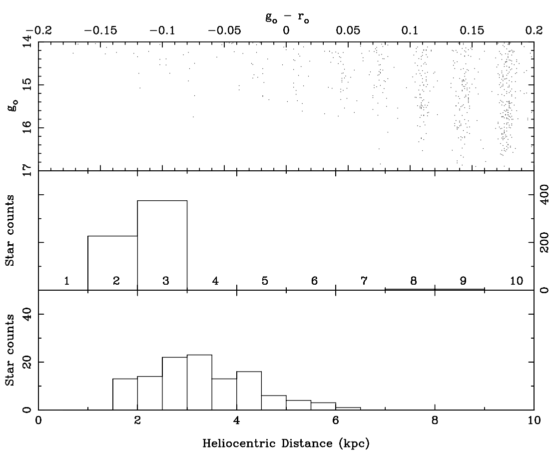

Figure 31. BP stars selected from the Besançon synthetic Galaxy model in the field (240, +4)°. The top panel shows their location on a CMD. The middle panel is their distribution of ages (parametrized into 10 bins), with age 2 corresponding to stars 0.15–1 Gyr old and age 3 being stars 1–2 Gyr old. The lower panel is the heliocentric distance distribution of the stars in kpc. The striation in the top panel is due to the resolution of the model and is not an observable phenomena.

colour–magnitude range, the distribution peaks at ∼7 kpc and drops rapidly to zero by 8 kpc. This is due to cutting through the thin disc in this direction. The missing BP stars in the northern fields of the survey can be explained by the Besançon model shown in Fig. 31. Here, at $(l, b) = (240, +4)°$, the BP stars are found in a magnitude range too bright to be observed at this location, as seen in the data from the present survey. The number of BP stars in this field is approximately a factor of 10 times fewer than those of its southern counterpart. The modelled northern BP stars are also significantly closer at only ∼3 kpc. Both the paucity of BP stars and their proximity lead to the conclusion that these stars belong to the local disc. With the disc being warped, the line-of-sight for the northern field exits the disc earlier, reducing the numbers of BP stars visible. It also ensures the population appears closer; the reverse is true for the south. So when taking into account the predictions of the model, a plausible explanation for the BP stars being part of the disc is found.

6.2.3 *Spiral arms*

It has been conjectured that both the MRi and CMa overdensities can be regarded as part of normal Galactic structure (see Carraro et al. 2005; Moitinho et al. 2006). The MRi is considered to be an extension of the flare into higher latitudes (Momany et al. 2006) and the CMa overdensity a line-of-sight effect close to the maximum Galactic warp (López-Corredoira 2006). To investigate how well the detections of both these structures align with the spiral arms, we have overlaid their locations on fig. 3 of McClure-Griffiths et al. (2004) as shown in Fig. 32. The results of that paper have now been extended in Levine, Blitz & Heiles (2006) revealing the presence of distant gaseous spiral arms out to ∼25 kpc. Fig. 32 consists of a modelled grey-scale density map of the differential H I distribution with the spiral arm models of Cordes & Lazio (2002), overplotted as solid red (grey) lines. On this, the locations of the MRi and putative CMa detections have been included in the same manner as Fig. 22.

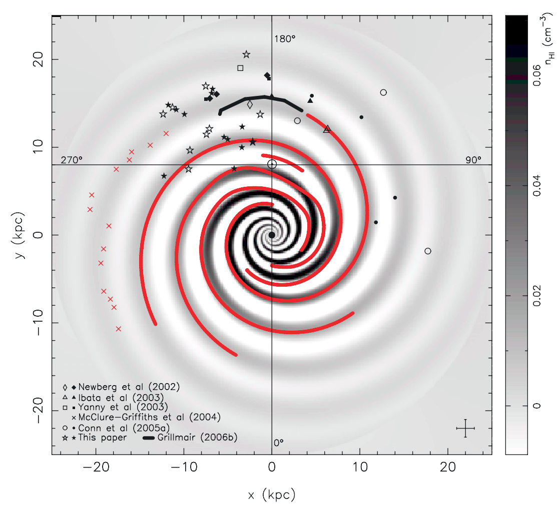

Figure 32. Location of the MRi and CMa detections shown with the grey-scale map of the differential H I density for a simple four-arm MW spiral model, the spiral model of Cordes & Lazio (2002) is overlaid as solid red (grey) lines. This is a reproduction of the left-hand panel of fig. 3 from McClure-Griffiths et al. (2004), who kindly provided their FORTRAN code to allow our points to be overlaid on their figure. The filled symbols represent detections above the plane, with the empty symbols those below. The MRi (above the plane) as discussed in Grillmair (2006b) is shown as a solid black line. Note that this stream my appear as an extension of a Galactic spiral arm, but is, in fact, ∼30° above the Galactic plane. The crosses mark the location of the distant spiral arm detections as mentioned in McClure-Griffiths et al. (2004). The Sun is located at (0.0, 8.0), with the lines intersecting the Sun marking out the Galactic longitudes of 0°, 90°, 180° and 270°. A ±1 kpc error bar in the lower right corner is indicative of the accuracy of these detections.

Do the locations of the MRi detections suggest that it is part of a distant spiral arm? Most of the MRi detections do not seem to correlate with any of the nearby spiral arm locations, with the exception of the Grillmair (2006b) which is the result of the distance estimate of 8.9 ± 0.2 kpc, however, the Grillmair (2006b) portion of the stream outlined here is found between $b = 17^\circ$ and 38°, well above the plane. The remaining points almost seem to align with the gaps between spiral arms more strongly than with the spiral arms themselves. The fields in the first quadrant at $l = 61^\circ$ and 75° are both close to spiral arm overdensities. The difficulty with connecting them to spiral arms is that the northern fields reside at $b = +15^\circ$, and both are at about 15 kpc from the Sun. This places them around 3.7 kpc out of the plane, well outside the warped flared regions in this direction. The field below the plane at $(l, b) = (61, -15)^\circ$ is at 5.4 kpc out of the non-warped plane and so is further from the plane when considering the effect of the northern warp. The detection at $(l, b) = (118, +16)^\circ$ is 3.3 kpc out of the non-warped plane and is again beyond the warped flared disc of the Galaxy. Continuing on around the Galactic plane, the fields at $l = 123^\circ$ have been discussed in Section 6.1.1 and the remaining MRi detections from the various other authors all typically lie between $b = 20^\circ$ and 30° and cannot be associated with a warped and flared disc. For the MRi at least, any alignment with the spiral arms appears purely coincidental, as the density profiles of the disc do not allow for such overdensities to reside well above the plane.

Do the CMa locations follow the spiral arm? The CMa overdensity fields can be seen as the nearby open star symbols from $l = 220^\circ$ to 273° in Fig. 32. The CMa fields are certainly close to the spiral arm, but are the progressively shorter distance estimates to these detections a statistical effect related to the distance estimation technique or does it represent a real change in direction for the overdensity? If the field at $(l, b) = (193, -21)^\circ$ is part of the overdensity, then CMa would be seen as an addition to the disc component. This is because the location of the dominant sequence in that field is further below the plane than is expected. At ∼5.8 kpc from the Sun, it is 2.1 kpc below the plane, much further than the 1.0 kpc predicted by the Besançon synthetic Galaxy model. If this is not an isolated overdensity of stars, then perhaps it is the CMa overdensity extended to these longitudes. Disentangling the CMa overdensity from the disc is not simple, but fields contained in the present survey suggest that a pure warp scenario and hence a spiral arm theory cannot explain all of the observations. Indeed spiral arms seem not to be an identifiable feature within the CMDs. The INT/WFC fields at $(l, b) = (61, \pm 15)^\circ$ cross two–three spiral arms and there is no distinguishable sign of these features in the CMDs. The spiral arms are not visible in the old main-sequence stellar populations which are used to characterize both the MRi and CMa detections. The overdensity in CMa therefore cannot be considered a 'normal' or additional spiral arm. A more detailed study of this region is imperative to resolve all these issues.

6.2.4 *The Canis Major stream*

Given the interest in the Monoceros stream and the subsequent proposal of a dwarf galaxy in CMa, it seems obvious to ask where the immediate tidal tails of the dwarf are to be found. The presence of an obvious tidal feature associated with the overdensity would strengthen the idea that it is a dwarf galaxy. To date, there have only been two simulations of the MRi/CMa system. The simulation from Martin et al. (2005) uses kinematics of the CMa overdensity as constraints on the model, while Peñarrubia et al. (2005) construct their simulation with data from the MRi. Although both simulations predict the progenitor to be in the CMa region, only the Martin et al. (2005) simulation places it in its currently accepted location. Given that this was the criteria for the Martin et al. (2005) model this result is unsurprising, but searching for the CMa stream with the Peñarrubia et al. (2005) model is not feasible given it does not coincide with current observations. The following discussion will focus on the distance estimates to both the MRi sequence in the various fields and also to the distance of the dominant main sequence in the CMDs. It is important to understand though that the dominant sequence could be either a pure disc population, a pure CMa population or a mixture of both and although distinguishing between them is not possible the result is compared with the Martin et al. (2005) model.

Fig. 33 shows the results of the numerical simulation of Martin et al. (2005) with the locations of the currently known detections of both the MRi and CMa. This is an extension of Fig. 20 as seen in Bellazzini et al. (2007). First, it should be noted that the CMa dwarf galaxy is located at $(l, b) \sim (240, -9)^\circ$, as can be seen in the overdensity of points in that location (lower panel) with the CMa stream arcing into the Northern hemisphere around $l = 200^\circ$. The top panel shows the heliocentric distance to the points, with those below the plane in red and those above in green. CMa is located at its accepted distance of ∼7 kpc. The other symbols are described in the figure caption. A key feature of the Martin et al. (2005) and Peñarrubia et al. (2005) models is that the MRi is simply a wrapped tidal arm of the CMa accretion event. In this manner, the structures described within Newberg et al. (2002), Ibata et al. (2003), Yanny et al. (2003) and Grillmair (2006b) conform to this idea of sampling a wrapped tidal arm. Their detections are in general more distant and less dense than the immediate CMa stream as predicted by the Martin et al. (2005) model. Some observations in both the present paper and Conn et al. (2005a) do seem to coincide with the predicted spatial location of the CMa stream on the sky.[5] In particular, the fields at $(l, b) = (118, +16)^\circ, (150, +15)^\circ, (218, +6)^\circ, (260, -10)^\circ$ and $(273, -9)^\circ$ are located within the modelled CMa stream as it is seen on the sky (lower panel). Indeed, when considering the distance estimates to the features in those fields there is a good correspondence with the predictions of the model. In the fields at $(l, b) = (118, +16)^\circ$ and $(150, +15)^\circ$, the features are only a few kpc more distant than the model but it is only constrained in the CMa region, so this difference is not unexpected. At $(l, b) = (218, +6)^\circ$, the distance estimate to the CMa/disc feature is consistent with the model predictions, as is also the case for the $(l, b) = (260, -10)^\circ$ field; the $(l, b) = (273, -9)^\circ$ detection is found on the edge of the predicted distance estimate of the stream. For those fields in the CMa region, an interesting interpretation can be made. The detections below the plane (crosses) seem to demarcate the far edge of the dwarf, while the detections above the plane (plus signs) demarcate the near side. This can be seen in the location of these detections in the top panel. Could this be inferring the orientation of the dwarf?

Although this rudimentary coincidence of the observations of the MRi/CMa fields with the Martin et al. (2005) model does not validate this model. It does suggest that previous observations termed MRi detections could be reinterpreted as CMa stream detections. In particular, both the $(l, b) = (118, +16)^\circ$ and $(150, +15)^\circ$ fields from Conn et al. (2005a) would fit this new scenario. The fields from the present paper which align with the CMa stream also support this

[5] Bellazzini et al. (2007) contains additional observations, not included here, which also intersect with the predicted location of the CMa stream.

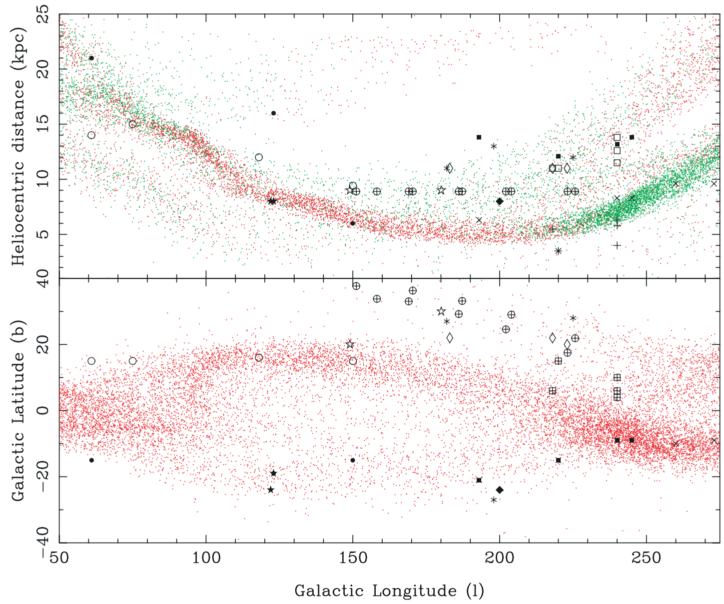

Figure 33. Location of the MRi and CMa detections shown with the numerical simulation of the CMa dwarf galaxy as presented in Martin et al. (2005). The symbols are as follows: in the top panel the simulation is shown with red (dark grey) dots representing stars below the plane and green (light grey) above the plane. Filled symbols represent observations below the plane and open symbols are observations above the plane. The circles are from Conn et al. (2005a); the stars are from Ibata et al. (2003); the diamonds are from Newberg et al. (2002); the asterisks are from Yanny et al. (2003); the squares are from the present paper with the plus (+) symbols for the CMa/Disc distance in the northern fields and the cross (×) symbols for the CMa/Disc distance in the southern field. The outline of the stream described in Grillmair (2006b) is shown with the circles containing the plus signs.

conclusion. Unfortunately, there are too few observations between $l = 100°$ and 180° to further test the model in these regions. With the CMa stream predicted to be relatively nearby, testing these predictions at latitudes around $b = 20°$ should be fairly straightforward.

7 CONCLUSION

The survey presented here consists of 16 fields from $l = (193–276)°$, all observed with the AAT/WFI between 2004 and 2006, providing strong evidence that the MRi cannot be considered part of the normal warp/flare profile of the Galactic disc. Of the 16 fields, eight have a strong sequence beyond the normal disc component which have been interpreted as the MRi; two others are presented as tentative discoveries. Resolving the origins of the putative CMa dwarf galaxy is extremely difficult with a survey of this kind, but the conclusions reached are that by symmetry around the warped Galactic plane, there is no field above the plane which matches the properties of those in the overdensity. Also, there is no appreciable change in the density profiles of the various Galactic disc models to explain an overdensity of stars at that distance in CMa. The origins of the BP stars reveal two contradictory scenarios. From one view they are part of the Galactic disc and from another they are not. Although a more detailed survey is needed to resolve this issue, they can no longer be associated with CMa overdensity stars. Searching for a spiral arm explanation to the MRi and CMa detections are mostly excluded on the basis of their distance out of the plane. The CMa detections are close to the plane and partially mixed in with known Galactic components. This makes disentangling them very difficult. However, since spiral arms are not visible in the basic structure of CMDs, which are comprised mainly of old main-sequence stars, attributing the putative dwarf to an outer spiral arm is not possible with the data in hand. Importantly, the location of the dominant sequence in the $(l, b) = (193, -21)°$ field is highly inconsistent with current Galaxy models and may represent and extension of the CMa overdensity into this field. This field differs the most from the Besançon synthetic Galaxy model and may indicate a location where the CMa dwarf can be analysed away from the disc. A study to fill the gaps in the entire CMa region is required to determine the origins of these disputed structures. Furthermore, the existence of a CMa stream can now be considered a possibility with previous detections labelled as MRi detections now potentially associated with the CMa stream. Further sampling of the predicted locations of the CMa stream is necessary to resolve the uncertainties presented here. Although many properties of the MRi and the CMa/isc features are unknown, there is now a growing pool of evidence supporting a merger event in the Galaxy. Continued study will undoubtedly reveal their true impact on the formation and evolutionary scenarios of the MW.

ACKNOWLEDGMENTS

Many thanks to the referee for their thorough review which has improved the quality of this paper. We would also like to thank Naomi McClure-Griffiths for her assistance with the spiral arm comparisons. BCC would like to thank the University of Sydney for its UPA Scholarship and ESO for their Postdoctoral Fellowship without them he would not be able to listen to the cricket from a telescope on the other side of the world. RRL thanks both LKN and MK for their financial and on-going support. GFL acknowledges the support of the Discovery Project grant DP0343508. The research of AMNF has been supported by a Marie Curie Fellowship of the European Community under contract number HPMF-CT-2002-01758.

REFERENCES

Abadi M. G., Navarro J. F., Steinmetz M., Eke V. R., 2003a, ApJ, 591, 499
Abadi M. G., Navarro J. F., Steinmetz M., Eke V. R., 2003b, ApJ, 597, 21
Adelman-McCarthy J. K. et al., 2006, ApJ, 162, 38
Bellazzini M., Ibata R., Martin N., Lewis G. F., Conn B. C., Irwin M. J., 2006, MNRAS, 366, 865
Bellazzini M., Kalirai J., Ibata R. A., Martin N. F., Lewis G. F., Conn B. C., Irwin M. J. 2007, MNRAS, submitted
Belokurov V., Evans N. W., Irwin M. J., Hewett P. C., Wilkinson M. I., 2006a, ApJ, 637, L29
Belokurov V. et al., 2006b, ApJ, 647, L111
Burton W. B., 1988, Galactic and Extragalactic Radio Astronomy. Springer, Berlin, p. 295
Butler D. J., Martinez-Delgado D., Rix H., Penarrubia J., de Jong J. T. A., 2006, preprint (astro-ph/0609316)
Carraro G., Vázquez R. A., Moitinho A., Baume G., 2005, ApJ, 630, L153
Conn B. C., Lewis G. F., Irwin M. J., Ibata R. A., Ferguson A. M. N., Tanvir N., Irwin J. M., 2005a, MNRAS, 362, 475
Conn B. C., Martin N. F., Lewis G. F., Ibata R. A., Bellazzini M., Irwin M. J., 2005b, MNRAS, 364, L13
Cordes J. M., Lazio T. J. W., 2002, preprint (astro-ph/0207156)
Ferguson A. M. N., Irwin M. J., Ibata R. A., Lewis G. F., Tanvir N. R., 2002, AJ, 124, 1452
Frei Z., Gunn J. E., 1994, AJ, 108, 1476
Grillmair C. J., 2006a, ApJ, 645, L37
Grillmair C. J., 2006b, ApJ, 651, L29
Grillmair C. J., Dionatos O., 2006a, ApJ, 641, L37
Grillmair C. J., Dionatos O., 2006b, ApJ, 643, L17
Grillmair C. J., Johnson R., 2006, ApJ, 639, L17
Huxor A. P., Tanvir N. R., Irwin M. J., Ibata R., Collett J. L., Ferguson A. M. N., Bridges T., Lewis G. F., 2005, MNRAS, 360, 1007
Ibata R. A., Gilmore G., Irwin M. J., 1994, Nat, 370, 194
Ibata R., Irwin M., Lewis G., Ferguson A. M. N., Tanvir N., 2001, Nat, 412, 49
Ibata R. A., Irwin M. J., Lewis G. F., Ferguson A. M. N., Tanvir N., 2003, MNRAS, 340, L21
Irwin M., Lewis J., 2001, New Astron., 45, 105
Jurić M. et al., 2005, preprint (astro-ph/0510520)
Klypin A., Kravtsov A. V., Valenzuela O., Prada F., 1999, ApJ, 522, 82
Levine E. S., Blitz L., Heiles C., 2006, Sci, 312, 1773
Lewis G. F., Ibata R. A., Chapman S. C., Ferguson A. M. N., McConnachie A. W., Irwin M. J., Tanvir N., 2004, Publ. Astron. Soc. Aust., 21, 203
López-Corredoira M., 2006, MNRAS, 369, 1911
López-Corredoira M., Cabrera-Lavers A., Garzón F., Hammersley P. L., 2002, A&A, 394, 883
McClure-Griffiths N. M., Dickey J. M., Gaensler B. M., Green A. J., 2004, ApJ, 607, L127
Martin N. F., Ibata R. A., Bellazzini M., Irwin M. J., Lewis G. F., Dehnen W., 2004a, MNRAS, 348, 12
Martin N. F., Ibata R. A., Conn B. C., Lewis G. F., Bellazzini M., Irwin M. J., McConnachie A. W., 2004b, MNRAS, 355, L33
Martin N. F., Ibata R. A., Conn B. C., Lewis G. F., Bellazzini M., Irwin M. J., 2005, MNRAS, 362, 906
Martin N. F., Irwin M. J., Ibata R. A., Conn B. C., Lewis G. F., Bellazzini M., Chapman S., Tanvir N., 2006, MNRAS, 367, L69
Martínez-Delgado D., Butler D. J., Rix H.-W., Franco Y. I., Peñarrubia J., Alfaro E. J., Dinescu D. I., 2005, ApJ, 633, 205
Moitinho A., Vázquez R. A., Carraro G., Baume G., Giorgi E. E., Lyra W., 2006, MNRAS, 368, L77
Momany Y., Zaggia S. R., Bonifacio P., Piotto G., De Angeli F., Bedin L. R., Carraro G., 2004, A&A, 421, L29
Momany Y., Zaggia S., Gilmore G., Piotto G., Carraro G., Bedin L. R., de Angeli F., 2006, A&A, 451, 515
Newberg H. J. et al., 2002, ApJ, 569, 245
Peñarrubia J. et al., 2005, ApJ, 626, 128
Reylé C., Robin A. C., 2001, A&A, 373, 886
Robin A., Creze M., 1986, A&A, 157, 71
Robin A. C., Haywood M., Creze M., Ojha D. K., Bienayme O., 1996, A&A, 305, 125
Robin A. C., Reylé C., Crézé M., 2000, A&A, 359, 103
Robin A. C., Reylé C., Derrière S., Picaud S., 2003, A&A, 409, 523
Rocha-Pinto H. J., Majewski S. R., Skrutskie M. F., Crane J. D., 2003, ApJ, 594, L115
Rocha-Pinto H. J., Majewski S. R., Skrutskie M. F., Crane J. D., Patterson R. J., 2004, ApJ, 615, 732
Rocha-Pinto H. J., Majewski S. R., Skrutskie M. F., Patterson R. J., Nakanishi H., Muñoz R. R., Sofue Y., 2006, ApJ, 640, L147
Schlegel D. J., Finkbeiner D. P., Davis M., 1998, ApJ, 500, 525
Skrutskie M. F. et al., 2006, AJ, 131, 1163
Willman B. et al., 2005a, AJ, 129, 2692
Willman B. et al., 2005b, ApJ, 626, L85
Yanny B. et al., 2003, ApJ, 588, 824
Yusifov I., 2004, preprint (astro-ph/0405517)
Zucker D. B. et al., 2004, ApJ, 612, L121
Zucker D. B. et al., 2006, ApJ, 643, L103

This paper has been typeset from a TEX/LATEX file prepared by the author.

3.2 The Anglo-Australian Telescope/Wide Field Imager Survey of the Monoceros Ring and Canis Major Dwarf Galaxy - II. From $l = (280 - 025)^\circ$

Blair C. Conn, **Richard R. Lane**, Geraint F. Lewis, Mike J. Irwin, Rodrigo A. Ibata, Nicolas F. Martin, Michele Bellazzini and Artem V. Tuntsov, 2008, *Monthly Notices of the Royal Astronomical Society 390, 1388-1398*

This paper continues the search for the MRi and CMa overdensity at various locations around the Galaxy. Again, the work presented here is the product of a pinhole survey of the outer Disc and Halo. The analysis of the data from this survey has produced two further detections of the MRi at previously unknown locations, bringing the known extent of the MRi to $\sim 240^\circ$ of the sky. No detections were found in the Bulge, however, this is unsurprising due to the stellar density of the Galaxy at those locations; disentangling MRi stars from Bulge stars is an extremely difficult task.

A region close to the maximum of the Warp, South of the Plane, is analysed here to further constrain the likelihood that the Canis Major overdensity is simply a line-of-sight effect of the Galactic warp. If the overdensity is a *physical* overdensity of stars, the remnants of a dwarf galaxy, it is imperative to trace its path through the Galaxy to determine its role in the evolution of the Milky Way. Can the detections of the CMa overdensity in this region be fully explained by the Warp? It is important to take into account the expected distance to the warped part of the Disc we are looking through to be able to distinguish between the two scenarios. The Besançon Synthetic Galaxy model is again used for comparison with all observed fields and no obvious deviation from the model can be inferred in those fields in which the MRi/CMa is absent, a good indication of the veracity of the model for work such as that presented in this paper.

In addition, the density and breadth of the MRi is compared above and below the Plane. With the inclusion of these new data the accuracies of the two N-body models of the tidal destruction of the Canis Major dwarf galaxy are compared. These new data again show that neither are perfect, although the Martin *et al.* (2005) model is the better of the two in comparison with this dataset. What is clear, therefore, is that there is a requirement for further modelling of these important structures to determine the exact nature of the MRi and the location of its progenitor. An important task in understanding the Galaxy.

Again, the data analysed in this paper were obtained, and reduced, by collaborators. The code to calculate the data completeness (Section 3) was written by myself (RRL). While I did not directly contribute heavily to the writing of the manuscript itself, I was involved at every stage of the intellectual process in the development of the manuscript and the conclusions drawn from the data analysis.

Mon. Not. R. Astron. Soc. **390,** 1388–1398 (2008) doi:10.1111/j.1365-2966.2008.13847.x

The Anglo-Australian Telescope/Wide Field Imager survey of the Monoceros Ring and Canis Major dwarf galaxy – II. From $l = (280–025)°$

Blair C. Conn,[1,2*] Richard R. Lane,[1] Geraint F. Lewis,[1] Mike J. Irwin,[3]
Rodrigo A. Ibata,[4] Nicolas F. Martin,[4] Michele Bellazzini[5] and Artem V. Tuntsov[1,6]

[1] *Institute of Astronomy, School of Physics, A29, University of Sydney, NSW 2006, Australia*
[2] *European Southern Observatory, Alonso de Cordova 3107, Vitacura, Santiago, Chile*
[3] *Institute of Astronomy, Madingley Road, Cambridge CB3 0HA*
[4] *Observatoire de Strasbourg, 11, rue de l'Université, F-67000, Strasbourg, France*
[5] *INAF–Osservatorio Astronomico di Bologna, Via Ranzani 1, 40127, Bologna, Italy*
[6] *Sterberg Astronomical Institute, Moscow, Russia*

Accepted 2008 August 15. Received 2008 August 14; in original form 2007 December 23

ABSTRACT

This paper concludes a systematic search for evidence of the Monoceros Ring and Canis Major dwarf galaxy around the Galactic plane. Presented here are the results for the Galactic longitude range of $l = (280–025)°$. Testing the claim that the Monoceros Ring encircles the entire Galaxy, this survey attempts to document the position of the Monoceros Ring with increasing Galactic longitude. Additionally, with the discovery of the purported Canis Major dwarf galaxy, searching for more evidence of its interaction is imperative for tracing its path through the Galaxy and understanding its role in the evolution of the Milky Way. Two new detections of the Monoceros Ring have been found at $(l, b) = (280, +15)°$ and $(300, +10)°$. Interestingly, in general, there seem to be more detections above the plane than below it; in this survey, around 2/3 of the firm Monoceros Ring detections are in the north. This coincides with the northern detections appearing to be qualitatively denser and broader than their southern counterparts. The maximum of the Galactic warp in the south is also probed in this survey. It is found that these fields do not resemble those in the Canis Major region suggesting that the warp does not change the shape of the colour–magnitude diagram as is witnessed around Canis Major. The origins and morphology of the Monoceros Ring are still elusive primarily due to its enormous extent on the sky. Continued probing of the Galactic Outer Disc is needed before a consensus can be reached on its nature.

Key words: Galaxy: formation – Galaxy: structure – galaxies: interactions.

1 INTRODUCTION

The Monoceros Ring (MRi), discovered in 2002 (Newberg et al. 2002), has now been traced around the Galaxy from $l = 75–260°$, as shown through the Sloan Digital Sky Survey (SDSS; Newberg et al. 2002), Two Micron All Sky Survey (Rocha-Pinto et al. 2003), Isaac Newton Telescope Wide Field Camera Survey (Ibata et al. 2003) and the Anglo-Australian Telescope Wide Field Imager Survey (Conn et al. 2005a). Continuing around the Galactic plane, this survey extends these previous results to complete the first Wide Field Imager survey of the MRi around the Galaxy that began with the Isaac Newton Telescope/Wide Field Camera (INT/WFC) in Conn et al. (2005a). Studies into this structure have been discussed in Paper I of this series (Conn et al. 2007, hereafter Paper I), and references therein. In addition to this, an RR Lyrae survey of the Galactic halo using QUEST data has also revealed the presence of the MRi and investigated the overdensity in Canis Major (Vivas & Zinn 2006; Mateu et al. 2007).

Residing in the thick disc of the Milky Way (MW), the MRi is revealed only by obtaining deep photometry of large patches of sky, typically greater than 1 deg^2. In this preliminary first pass of the MW, the thick disc was sampled at Galactic latitudes nominally between $b = \pm10°–20°$ and about every 20° in Galactic longitude. To date, the entire survey has strong detections of the MRi in 14 regions with three additional tentative detections out of 25 regions observed. It has been found on both sides of the Galactic plane at Galactic latitudes from 4° to 20°, and its extent away from the plane is as yet undetermined although SDSS results suggest that it could be as high as +30° (Belokurov et al. 2007). Numerical

*E-mail: bconn@eso.org

simulations of the MRi as a tidal stream predict it to have multiple wraps around MW, although the current data set cannot distinguish between different aspects of the stream or whether the different detections are part of a coherent structure. Fig. 1 shows the previous detections of the MRi as reported in Conn et al. (2005a) and Paper I. Fig. 2 of Paper I shows how these colour–magnitude diagrams (CMDs) can be interpreted by showing the approximate location of the thin, thick and halo stars in the field. Fig. 5 of Paper I illustrates which components are being referenced when discussed in the text. Each of the fields in this figure is pixelated CMD. The pixel values represent the square root of the number of stars in that pixel. Ordered by increasing Galactic longitude, Fig. 1 tentatively shows the changing strength and thickness of the MRi around the plane. Qualitatively, the strength of the MRi can be seen in comparison with the MW components. Additionally, the only apparent difference between northern and southern detections is perhaps that the southern MRi features appear qualitatively narrower than their northern counterparts. There is no clear explanation as to why this is the case.

While there is more and more evidence regarding the true extent of this structure, there is very little information concerning many of its generic properties. As such, no direct measurement of the density profile of any part of the stream around the sky, nor a complete survey of its true extent on the sky, has been attempted. In the region covered by the SDSS, Jurić et al. (2008) and Ivezic et al. (2008) reported on the presence of the MRi with regard to its number density, metallicity and kinematics. A clear overdensity of stars can be seen at a distance of 16 kpc (Jurić et al. 2008), and Ivezic et al. (2008) reported a mean metallicity of [Fe/H] = −0.95 with a scatter of around 0.15 dex. Kinematically, they show a spread of velocities rotating consistently faster than the local standard of the rest and in accordance with the predictions of Peñarrubia et al. (2005).

The only possible candidate for the stream's progenitor is an overdensity of stars found in Canis Major, but possible confusion with the Galactic warp has created doubts on this detection. Numerical simulations created using the properties of these stars have predicted the location and extent of the MRi with good accuracy and so add support to the dwarf galaxy scenario. This ongoing debate centres on whether observations of the Canis Major overdensity conform to known Galactic structure, such as the warp, or can be considered truly additional. Paper I outlines some of the possible inconsistencies between predicted properties of the Galactic warp and direct observations of these structures. In response to this, López-Corredoira et al. (2007) have presented an explanation relying on only first-order Galactic structure. Further refinement of the properties of the MRi is needed to determine whether Canis Major (CMa) is the most likely candidate as its progenitor.

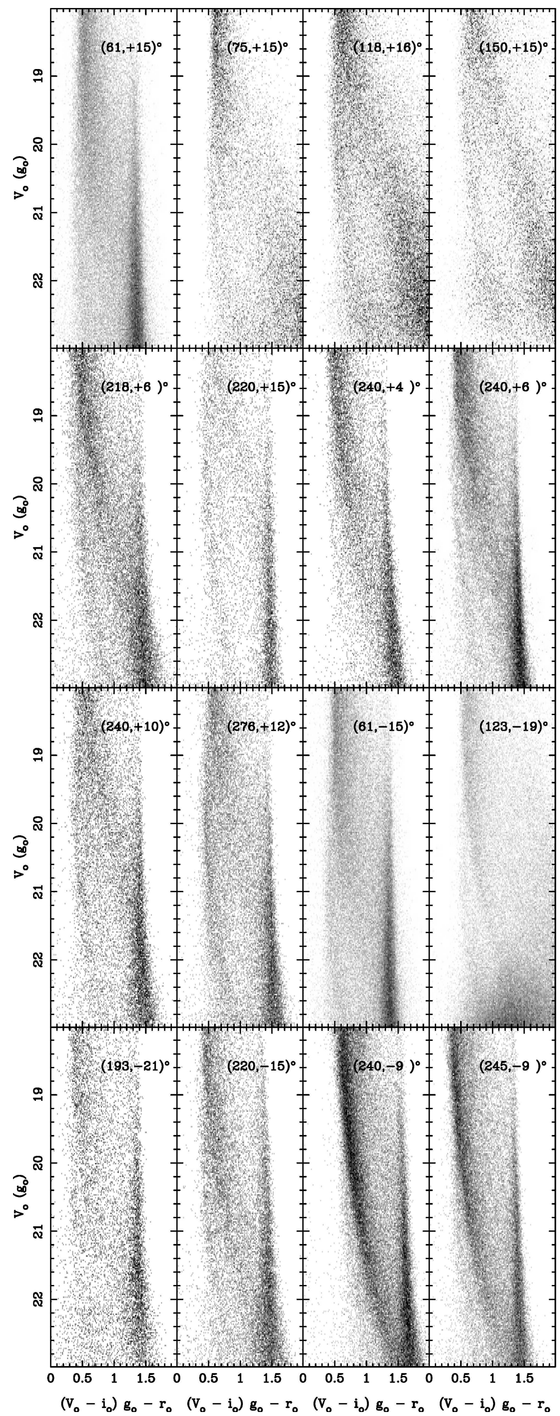

Figure 1. Visual summary of all the previous MRi detections from the INT/WFC survey (Conn et al. 2005a) and AAT/WFI survey (Paper I) of the outer disc. The CMDs are of two types *V*, *i* and *g*, *r*. For more detailed analysis of these fields and the reported detections, see the relevant articles.

2 OBSERVATIONS AND REDUCTION

The Anglo-Australian Telescope/Wide Field Imager (AAT/WFI) at Siding Spring Observatory in New South Wales, Australia, was used to conduct the current survey. The AAT/WFI is mounted at prime focus with a field of view of approximately 33 arcmin on a side. It consists of eight 4 × 2k CCDs with a pixel scale of 0.2295 arcsec per pixel.

The observations were taken over three observing runs, the first on the 2004 January 22–25, the second on 2004 January 30, 31 and February 01, and the third on the 2004 August 14, 15 and 16. To

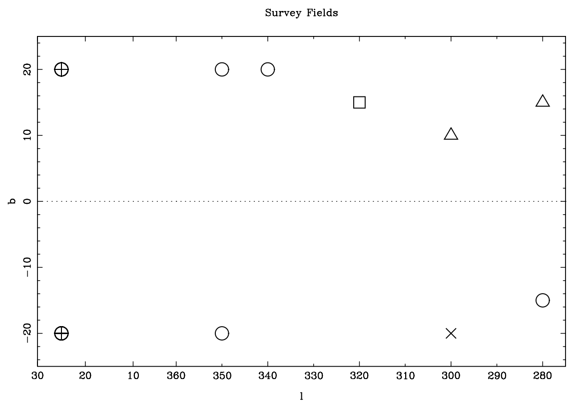

Figure 2. This figure shows the location of the survey fields presented in this paper. The symbols denote the number of pointings per field. The circles with plus signs represent five pointings; the empty circles, four pointings; the triangles, three pointings; the square, two pointings and the cross, one pointing. Each field was intended to have four to five pointings, however weather and time constraints have resulted in many fields containing less. The survey was originally designed to contain a more complete coverage of the Galactic plane, however weather again significantly limited the number of photometric or near-photometric fields with useful data. The resultant fields have been selected based on data quality and information content. While ideally four pointings would correspond to about 1 deg^2 of sky, observations undertaken during 2004 August had only six of eight CCDs available, and those taken during 2006 February had only seven of eight CCDs available. This has limited the amount of sky surveyed, despite attempts to reduce its impact. The actual field of view observed can be found in Table 1 under the Total Area column.

minimize the fringing effects that are present when observing with other filters, we employed the *g* (WFI SDSS 90) and *r* (WFI SDSS 91) filters. Exposure times used were a single 600 s exposure in *g* and two 450 s exposures in *r*. Twilight flats along with bias and dark frames were used for calibration, and Landolt Standard Star fields were observed roughly every two hours. Data reduction was performed using the Cambridge Astronomical Survey Unit pipeline (Irwin & Lewis 2001); a thorough description of this process and the necessary calibrations are outlined in Paper I.

This paper presents the final section of the survey using the AAT/WFI which observed fields from $l = (280\text{–}25)^\circ$ across the Galactic bulge. This is in addition to Paper I which covered fields in the regions $l = (195\text{–}276)^\circ$. Nine fields have been observed, and in general each field is approximately 1 deg^2 or four WFI pointings. A summary of the results of this survey is shown in Table 1.

3 ANALYSIS

The magnitude completeness of the data has been estimated in the same manner as described in Paper I. In essence, this involves using overlapping regions of the observed fields to determine the completeness. The field at $(l, b) = (300, -20)^\circ$ has only one pointing and so with this approach no completeness estimate is possible. Table 2 presents the completeness profiles of each field based on the equation

$$\mathrm{CF} = \frac{1}{1 + \mathrm{e}^{(m-m_c)/\lambda}}. \tag{1}$$

Estimating the completeness provides a way to evaluate the quality of the data and helps to determine the reliability of the detections in the faint end of the CMD. While in Paper I the completeness profile was used when making signal-to-noise ratio estimates of the stream, the data here are not of sufficient quality to allow such a measurement. This is because many of these fields only have two or three pointings per region (fewer stars) coupled with poor seeing leading to a relatively bright limiting magnitude. With these factors, the MRi is not seen as clearly above the noise as in Paper I.

Following the method used by Ibata et al. (2003), Conn et al. (2005a) and Paper I, we have used a main-sequence fiducial to estimate the distance to the features seen in the CMDs. For a complete explanation of the process and errors involved, see section 4.1.2 of Paper I. The furthest distance to which this method can find the MRi is difficult to estimate. The number density of MRi stars per field and the distance to the MRi are obviously important to whether a detection is found. Additionally, the quality of the data in those fields will again directly influence the likelihood of a detection. Poor seeing and insufficient sky coverage could easily affect the ability of this method to make a successful detection. The findings of this survey suggest that if the MRi is within ∼20 kpc, it will be detectable. Beyond this, it is highly dependent on the strength of MRi in the CMD and only one field has the MRi placed greater than 20 kpc. A possible reason for this is that a detection at a distance of 20–30 kpc involves a shift of 1.5–2.2 mag from the base position at 11 kpc ($g = 19.5$). The turn-off of the shifted main sequence is now located at ∼22 mag where the photometric errors are starting to increase and thereby spread out the main sequence. In the absence of very deep or wide surveys, this apparent limit of ∼20 kpc may remain the practical limit for finding the MRi.

3.1 Comparisons with the Besançon model

The basic methodology we have employed when searching for additional structures in the outer disc of the Galaxy is to make direct comparisons with the Besançon model, which purports to predict

Table 1. Summary of the observations of MRi/Canis Major tidal stream with the AAT/WFI, ordered in ascending Galactic longitude (*l*). The number of CCDs available during the different runs vary and thus has affected the total area or field of view observed.

Fields $(l, b)^\circ$	Regions per field	Average seeing (arcsec)	Total area (deg^2)	Mri	Average $E(B-V)$	Date (dd/mm/yy)
$(280, -15)^\circ$	4	1.3	1.21	No	0.128	01/02/04
$(280, +15)^\circ$	3	1.0	0.93	Yes	0.083	25,30/01/04
$(300, -20)^\circ$	1	1.3	0.3	No	0.109	31/01/04
$(300, +10)^\circ$	3	1.2	0.93	Yes	0.171	25/01/04
$(340, +20)^\circ$	4	2.8,1.6	0.91	No	0.095	15-16/08/05
$(350, -20)^\circ$	4	2.2	0.91	No	0.055	15/08/05
$(350, +20)^\circ$	4	1.4	0.91	No	0.112	16/08/05
$(025, -20)^\circ$	5	2.0	1.14	No	0.137	15-16/08/05
$(025, +20)^\circ$	5	2.0	1.14	No	0.098	15-16/08/05

Table 2. Parameters used to model the completeness of each field, ordered in ascending Galactic longitude (l). m_c is the estimated 50 per cent completeness level for each filter with λ describing the width of the rollover function (see equation 1 and further details in Paper I).

Fields $(l, b)^\circ$	$m_c\ (g_\circ)$	$m_c\ (r_\circ)$	λ
$(280, -15)^\circ$	22.40	21.40	0.55
$(280, +15)^\circ$	23.85	22.60	0.60
$(300, -20)^\circ$		No estimate possible	
$(300, +10)^\circ$	23.30	22.40	0.30
$(340, +20)^\circ$	21.80	20.70	0.45
$(350, -20)^\circ$	23.10	22.30	0.30
$(350, +20)^\circ$	23.40	22.40	0.75
$(025, -20)^\circ$	22.60	21.70	0.60
$(025, +20)^\circ$	22.60	21.70	0.60

Table 3. Summary of the observations of MRi/Canis Major tidal stream with the AAT/WFI, ordered in ascending Galactic longitude (l). The offset is measured in magnitudes from the zero offset position of the Newberg et al. (2002) detections at 11 kpc.

Fields $(l, b)^\circ$	MRi offset (mag)	MRi dist (kpc)	MW/CMa offset (mag)	MW/CMa dist (kpc)
$(280, -15)^\circ$	–	–	–	–
$(280, +15)^\circ$	0.0	11.0	–	–
$(300, -20)^\circ$	–	–	−0.8	7.6
$(300, +10)^\circ$	0.8	15.9	−0.8	7.6
$(340, +20)^\circ$	–	–	−0.2	10.0
$(350, -20)^\circ$	–	–	−0.5	8.7
$(350, +20)^\circ$	–	–	+0.2	12.1
$(025, -20)^\circ$	–	–	−2.0	4.4
$(025, +20)^\circ$	–	–	−2.2	4.0

its properties. While this approach is not favoured by some, it has a few advantages. First, and quite importantly, it allowed the survey to be completed in a reasonable time frame. Adding an extra filter, such as a U- or i-band filter, would have dramatically increased the time needed. Secondly, the dynamic range of the survey means that the brighter end of the survey can test the predicted properties of the bulk MW components while the fainter end tests the outer disc region. Since the MRi is only distinguishable in the thick disc/halo part of the CMD, searching for its presence relies on looking at the fainter end of the CMD. The Canis Major dwarf galaxy feature, as discussed in Paper I, is located more or less in the thin disc component. Indeed, since most of the debate concerning CMa revolves around whether the CMDs observed in the CMa region are explainable in terms of purely disc components or whether an extra component exists in the same colour–magnitude space; it is for the latter possibility that the distance to the edge of the thin disc component has been determined for the fields in this part of the survey. Checking their position with respect to the model provides an opportunity to assess whether it is different and perhaps could be related to the CMa overdensity. For some fields, measuring the faint edge of the thin disc cut-off has not been possible due to the CMDs not showing a clear edge. For these fields, the distance to the bright edge of the thin disc region has been found. So, for each field there are three possible structures to be examined: the faint MRi component, which may represent additional MW substructure; the faint edge of the thin disc, which may represent a misidentified CMa-type population as per Paper I or the upper edge of the thin disc, which tests the model in these directions. The results of these parameters are presented in Table 3.

3.2 Survey fields

The location of each field in Galactic coordinates is shown graphically in Fig. 2. Each field is presented in the following sections showing the CMDs with the appropriate main-sequence-type overlay as taken from the original Newberg et al. (2002) detection and described in Paper I. All magnitude offsets of the main-sequence overlay are with respect to this Newberg et al. (2002) detection at 11.0 kpc. Table 3 summarizes the outcome of this study and uses the same formatting as in Paper I. It should be noted though that this paper does not find evidence of the Canis Major dwarf, and the final column of Table 3 simply presents where the fiducial main sequence has been placed. In general, for this part of the survey, the Besançon model is well matched to the data and as such the dominant main sequence is easily attributed to known Galactic structure.

The CMDs that we have used are density maps of the underlying distribution. Each pixel is the square root of the number of stars in that part of the CMD. This method provides better contrast of the structures, especially in regions of high stellar density. A presentation of all the fields from previous AAT and INT surveys in which the MRi is present can be seen in Fig. 1. In the following sections, we will provide the distance estimates to the major features present in each CMD from this part of the survey with an analysis of these results presented in the Discussion (Section 4).

3.2.1 *Fields* $(280, -15)^\circ$

The $(280, -15)^\circ$ field (Fig. 3) is approximately 40° from the purported dwarf galaxy in Canis Major, and the features here seem less defined than in the nearer fields. This is perhaps due to slight differences in the photometric solution for each frame combined with the brighter limiting magnitude. The strong main sequence seen in $(l, b) = (273, -9)^\circ$ (fig. 20 of Paper I) is not seen here although the increase in latitude away from the Galactic plane could account for this change. Deeper imaging of this region is necessary to confirm the lack of the CMa feature and to investigate the slight excess of stars in the region $g_\circ > 21$ and $(g - r)_\circ < 1.0$.

3.2.2 *Fields* $(280, +15)^\circ$

The $(280, +15)^\circ$ field (Fig. 4) is similar to its corresponding field below the plane at $(280, -15)^\circ$. The comparison field from the Besançon model is presented here with the fiducial main sequence at the location of the additional main sequence present in the data. This main sequence has been interpreted as the MRi. Interestingly, the MRi feature in this field is more extended than in others. The stream is perhaps extended or wrapped in this part of the sky or the MW components here have different strengths than the Besançon model predicts. A mix of the two is also possible. The fiducial shown marks the brighter edge of this feature. With only a small shift from the nearby detection at $(276, +12)^\circ$ (see Fig. 1), the offset used for this feature is 0.8 mag corresponding to 15.9 kpc heliocentrically. In comparison to the detection at $(276, +12)^\circ$, this is about 4 kpc further away. The lower edge of this feature is approximately 0.5 mag fainter and thus would be estimated at around 20 kpc. No attempt has been made to estimate the width of this feature.

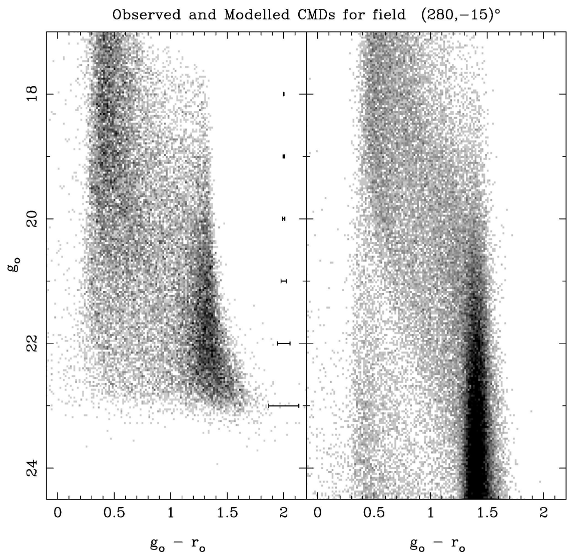

Figure 3. Hess plot of $(l, b) = (280, -15)^\circ$ and the corresponding Besançon model. A Hess plot is created by pixelating the CMD and generating a greyscale on the basis of the square root of the pixel number density. The same process is applied to both the data (left-hand panel) and model (right-hand panel). The synthetic galaxy model was generated via the Besançon online galaxy model web site (http://bison.obs-besancon.fr/modele/). The distance interval applied to the model is a line of sight from the Sun out to 100 kpc. This ensures that no artificial cuts can enter into the CMDs via distance effects. The model is selected in *g*, *r* in the CFHTLS system and is converted to *g*, *r* of the AAT/WFI via the colour conversions discussed in section 4.1 of Paper I.

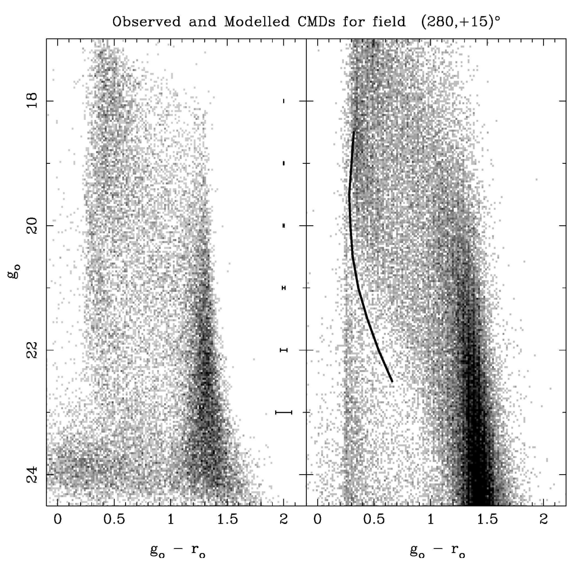

Figure 4. Hess plot of $(l, b) = (280, +15)^\circ$ and the corresponding Besançon model. The figure is otherwise the same as Fig. 3. The main sequence fitted here for the MRi is offset by 0.8 mag. The heliocentric distance related to this offset is then 15.9 kpc. No error or signal-to-noise ratio estimate has been derived for this feature.

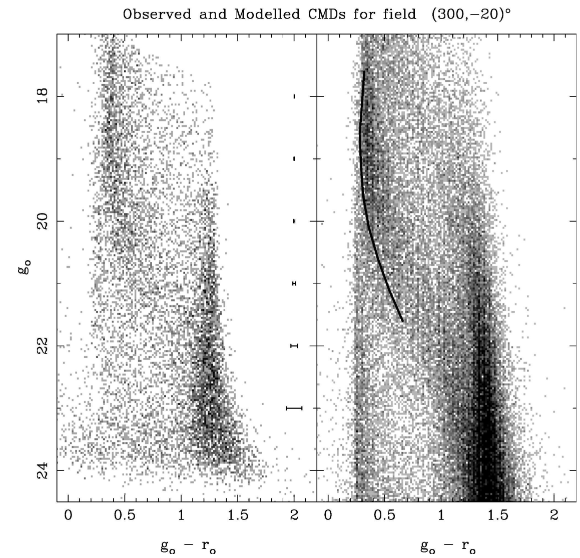

Figure 5. Hess plot of $(l, b) = (300, -20)^\circ$ and the corresponding Besançon model. The figure is in the same format as Fig. 3. The main sequences fitted here are offset by -0.8 mag. The heliocentric distance of this offset is 7.6 kpc. The similarity with the synthetic CMD suggests that this main sequence in the data is associated with Galactic disc.

3.2.3 *Fields* (300, −20)°

At $(300, -20)^\circ$ (Fig. 5), the main-sequence crossing the middle of the CMD is well matched by the synthetic CMD and corresponds to the location of the disc stars seen in the model. The overlay is offset at -0.8 mag or $\sim$7.6 kpc. There is perhaps a main sequence belonging to the MRi at the faint blue end of the CMD; however, the model does indicate that some stars should be expected in that location. Given the overall noisy quality of the CMD, no attempt is made to identify whether those stars may belong to the MRi. The strong main sequence defined by the fiducial is a good match with the model and thus is most likely of Galactic origin.

3.2.4 *Fields* (300, +10)°

The $(300, +10)^\circ$ field (Fig. 6) contains an obvious additional main sequence more distant than the expected MW component. The original data for this field were slightly misaligned in colour after all the photometric calibrations were applied. To try to ensure the smallest shift possible when correcting this, the *r* magnitudes have all been shifted by $+0.1$ mag. Taking the field without any differential extinction and shifting the others to match align the final CMD in the correct colour range and allow the main-sequence overlay to be used to estimate the distance. Of course, shifting the data in this manner weakens the accuracy to which we can determine the distance. While the shift was small, all the distances reported for this field can only be seen as indicative and do not have the accuracy as reported in the other fields of the survey. The two overlays are offset by -0.8 mag for the brighter main sequence and 0.8 mag for the fainter main sequence. These result in distance estimates of $\sim$7.6 and $\sim$15.9 kpc, respectively. The stronger main sequence is clearly related to the Galaxy given the good correlation with the model.

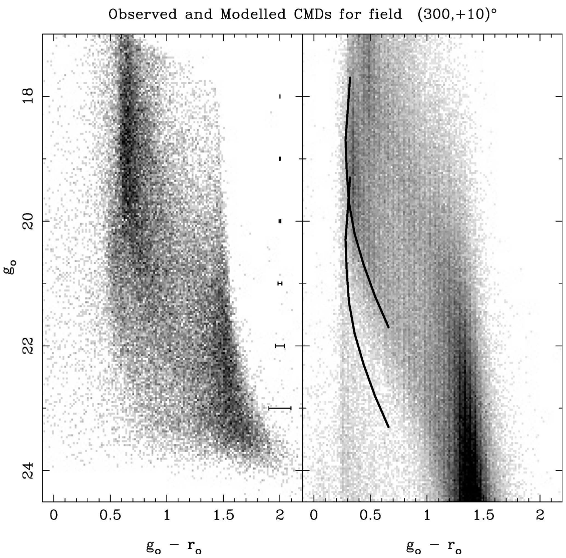

Figure 6. Hess plot of $(l, b) = (300, +10)°$ and the corresponding Besançon model. The figure is otherwise the same as Fig. 3. The main sequences fitted here are offset by −0.8 and 0.8 mag. The heliocentric distance of these offsets are 7.6 and 15.9 kpc. The Galaxy component is related to the closer feature and the MRi to the more distant feature. Due to the data having been shifted by 0.1 mag in r to align the CMD in colour, the distances have an additional source of uncertainty.

3.2.5 Fields (340, +20)°

The data in this field (Fig. 7) are a combination of two pointings which resulted in different limiting magnitude when calibrated. This could partly contribute to the lack of coherence in the data towards the limiting magnitude of the shallower sample ($g_\circ \sim 22.5$). When combining the two data sets, the selection criteria have been tightened; in the other fields, if the object is classified as a star in one filter, and only possibly a star in the other, it is accepted. With this CMD, only if in both filters the object is classified as a star has it been plotted. This was done to try and remove some of the additional noise in the CMD. Additionally, however, an alignment in colour by ∼0.1 mag redward was also required. This will impact the accuracy of any distance estimates of structures within this field. The overlay is fitted to the lower extreme of the MW main sequence and is a good match to the predictions of the model.

3.2.6 Fields (350, −20)°

This field (Fig. 8) shows a broad main sequence with an overlay placed with an offset of −0.5 mag (8.7 kpc heliocentric distance). There is an obvious problem with the predictions of the model. In the following field, this problem was avoided by locating a field nearby which reproduced an acceptable CMD. Unfortunately, there was no nearby field in the model which resembled the data here and so was left as it is. Indeed, comparing with the results of the northern field, it suggests that the data here consist solely of Galactic components.

3.2.7 Fields (350, +20)°

As for the southern field at this Galactic longitude, this field also had a problematic model CMD. However, it was noted that a slight change in coordinates in the model produced a CMD much more similar to the data. So, for this field, the comparison field is (347.5, +20)° rather than (350, +20)° (Fig. 9). The (347.5, +20)° synthetic field is used here due to its similarity with the data. The contrast between the data and the model for the field in the south is deemed a glitch rather than a flaw in the entire model. The overlay here is

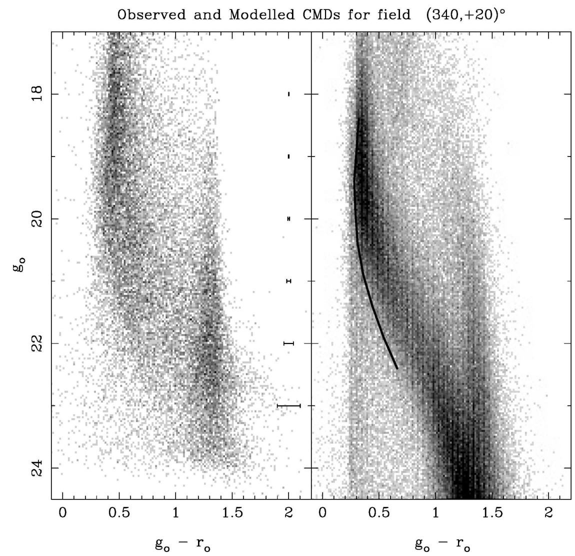

Figure 7. As for Fig. 3, Hess plot of $(l, b) = (340, +20)°$. The offset is placed at −0.2 mag or 10.0 kpc heliocentrically, and is clearly associated with the MW component in the model. The original CMD was slightly offset in colour and this has been corrected with a small shift of 0.1 mag in r towards the red. The distance estimates become less accurate due to this shift.

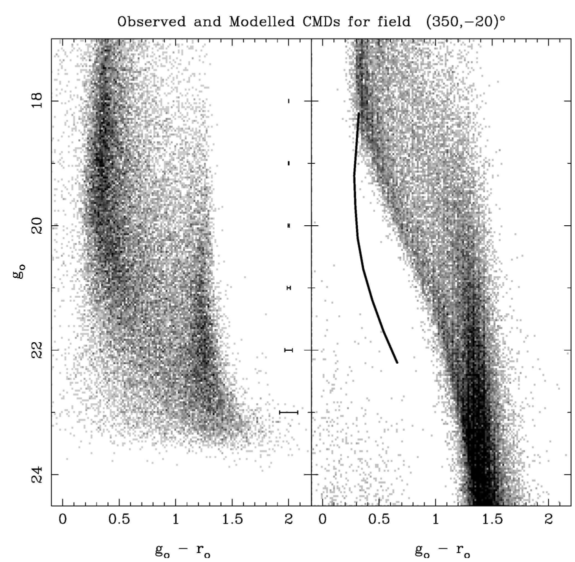

Figure 8. Hess plots of $(l, b) = (350, −20)°$. The overlay is placed at −0.5 mag or 8.7 kpc heliocentrically. The model clearly has problems with this direction on the sky and any differences are not expected to be real. The data do not seem to have an MRi-like component.

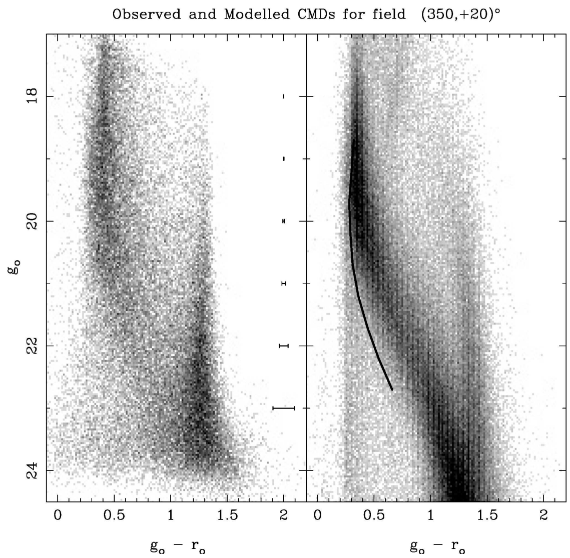

Figure 9. Hess plots of $(l, b) = (350, +20)^\circ$ and its counterpart synthetic CMD. The synthetic CMD used here is actually $(347.5, +20)^\circ$, the model field with the same coordinates is very similar to that seen in Fig. 8. It was found though that with a small shift in longitude, the model retrieves a CMD similar to the data. Since there is no reason to account for such a drastic change in the CMD in this direction, the $(347.5, +20)^\circ$ field is used instead. The overlay here is at 0.2 mag of offset or 12.1 kpc heliocentric distance. The overlay is fitted 'by eye' to the lower extremity of the dominant main sequence and is a good match to the model.

placed at 0.2 mag and corresponds to the fainter edge of the main sequence. It can be found at a heliocentric distance of 12.1 kpc, although, as with the southern field, the main sequence in the model does seem to be stronger than the data. On the whole though, they are much more similar here than in the previous fields.

3.2.8 *Fields* (025, −20)°

This field (Fig. 10) completes the MRi survey below the Galactic plane which began with the INT/WFC survey. Despite having seeing of typically 2 arcsec, the limiting magnitude of the data is still relatively deep. In comparison with the model, the strong main sequence is conspicuously missing from the data. In an attempt to compare the features, the bright end of the weak MW main sequence in the data has been fit with an offset of −2.0 mag. This converts to a distance estimate of 4.4 kpc, which is a reasonable match with the model. It is uncertain why this field lacks a strong thin disc presence in the data.

3.2.9 *Fields* (025, +20)°

The final field of the survey on the northern side of the plane (Fig. 11) is remarkably similar to its southern counterpart. Again, the model predicts strong main sequence for the thin disc component which is not present in the data. To provide some point of comparison, the approximate bright end of the weak MW main sequence has been estimated and is found at an offset of −2.2 or 4.0 kpc. The model also predicts this edge here. There is no evidence of the MRi in this field.

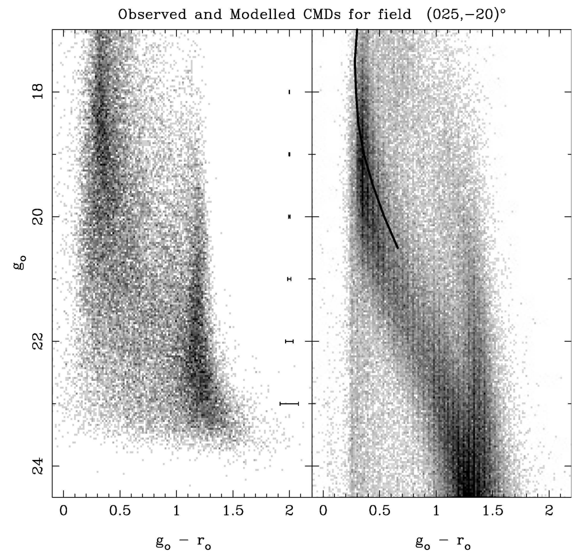

Figure 10. Hess plots of $(l, b) = (025, -20)^\circ$ and its counterpart synthetic CMD. As for Fig. 3. The overlay is placed at an offset of −2.0 mag, aligning with the bright end of the MW main-sequence feature in the data. The $D_\odot$ is 4.4 kpc.

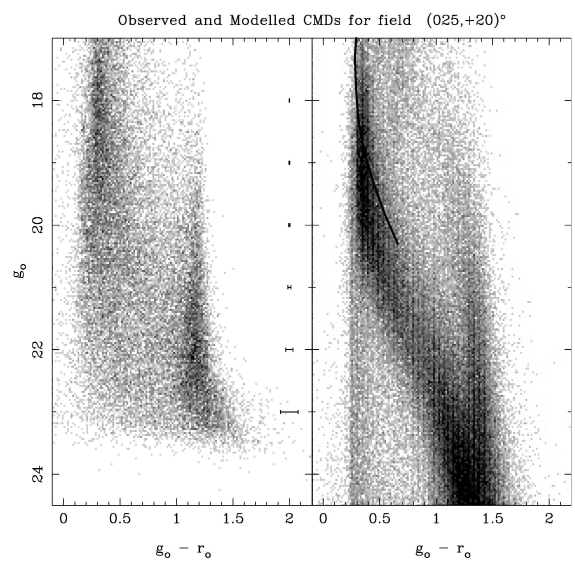

Figure 11. Hess plots of $(l, b) = (025, +20)^\circ$ (left-hand panel) and its counterpart synthetic CMD (right-hand panel). As for Fig. 3. Despite the lack of a strong main sequence in the data, a main-sequence overlay is fitted to what is estimated as the bright end of the MW main sequence. This is at a magnitude offset of −2.2 or $D_\odot \sim 4.0$ kpc, in rough accordance with the model.

4 DISCUSSION

To date, there are only two numerical simulations of the MRi and Canis Major structures; these are from Martin et al. (2005) and Peñarrubia et al. (2005). The primary difference between these two models is that the Martin et al. (2005) model uses the properties of

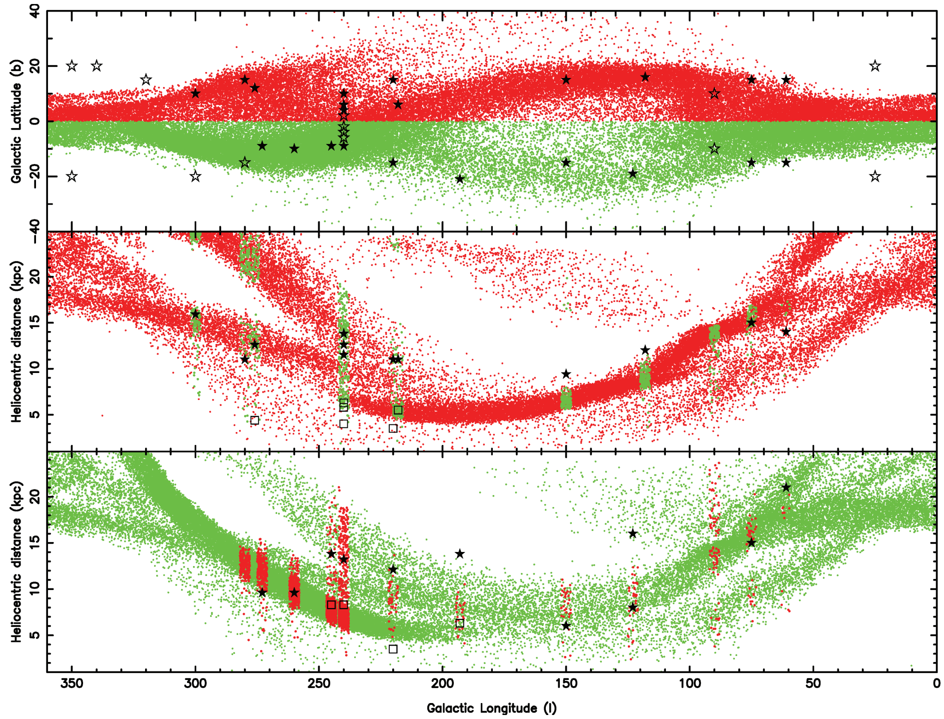

Figure 12. Comparison of the (Martin et al. 2005) numerical simulation of the MRi/Canis Major streams and the locations and distances of the detections (including tentative ones) arising from the survey. The top panel shows the simulation in Galactic coordinates, the centre panel shows only those fields and points from the model above the Galactic plane against heliocentric distance and the lower panel is for those points below the Galactic plane. In the centre and lower panels, the points with the opposite colour (i.e. green instead of red or vice versa) are the predicted distance of the model in the direction of the observed fields. The filled stars show fields with detections of the MRi and empty stars show fields in which the MRi was not detected. Empty squares show the location of the proposed CMa feature at that longitude as per the findings of Paper I.

the Canis Major overdensity as its constraints and the Peñarrubia et al. (2005) model uses the data collected on the MRi up to that time. The following two sections compare the findings of this paper, Paper I and the INT/WFC paper (Conn et al. 2005a) with these models. To make the comparison meaningful, in the next sections the MRi is assumed to be a tidal stream.

4.1 Comparing the observations with the Martin et al. (2005) model

The numerical simulation of Martin et al. (2005) has been plotted with the results from the entire survey [this paper; Paper I; Conn et al. 2005a] in Fig. 12. The top panel shows the model in (l, b) space dividing the points, by colour, for those above and below the Galactic plane. All of the fields from the three papers have been overplotted as either full or open stars. Full stars represent fields with an MRi detection, and open stars are fields without an MRi detection. Tentative detections have been included in this figure.

The middle panel contains only the points above the plane plotted against heliocentric distance. For each field, the prediction of the model for that location (l, b) is shown in green. This then allows direct comparison between the findings of the survey with the prediction of the model. To avoid clutter, the top panel only showed MRi detections but for completeness the CMa detections from Paper I, which reside in the same fields, are plotted as open squares. The fields between $l = (200–300)^\circ$ do seem to correspond well to the model, although there are a spread of distances which are possible. The fields at $(l, b) = (118, +16)^\circ$ and $(150, +15)^\circ$ are at distances greater than the predicted location but they do vary in-step with the model and so could just represent the model stream being too close heliocentrically. At $(l, b) = (90, +10)^\circ$, there is a conspicuous absence of the Mri, while in other fields, the overall data quality or area covered could be a reason for a non-detection, but here there is no such problem. It is unclear why the feature is absent. For the $(l, b) = (75, +15)^\circ$ field, the detection again matches the model while the detection at $(l, b) = (61, +15)^\circ$ does not correspond well. The reasons for this is also uncertain.

The lower panel shows the predictions for the stream model below the plane. Around $l = (240–276)^\circ$, the detections do roughly correspond to the model and from $l = (60–240)^\circ$ the connection is more or less correlated with the general direction of the stream. The two interesting omissions in the south are $(l, b) = (90, -10)^\circ$ and $(l, b) = (280, -15)^\circ$ as both these fields were expected to have MRi components. As per the northern field at $l = 90^\circ$, the data quality in its southern counterpart field is sufficiently high to robustly conclude that no MRi feature is present here. For the $l = 280^\circ$ field, the limiting magnitude is the second worst in the sample but given that the predicted distance is more or less that of the original detection by Newberg et al. (2002), it should be visible. The stream therefore does not pass through this field at the distances suggested by the model.

Non-detections of the stream also provide an opportunity to test the model. In all but a few cases, the non-detections in the data are supported as non-detection regions in the model. The survey is too

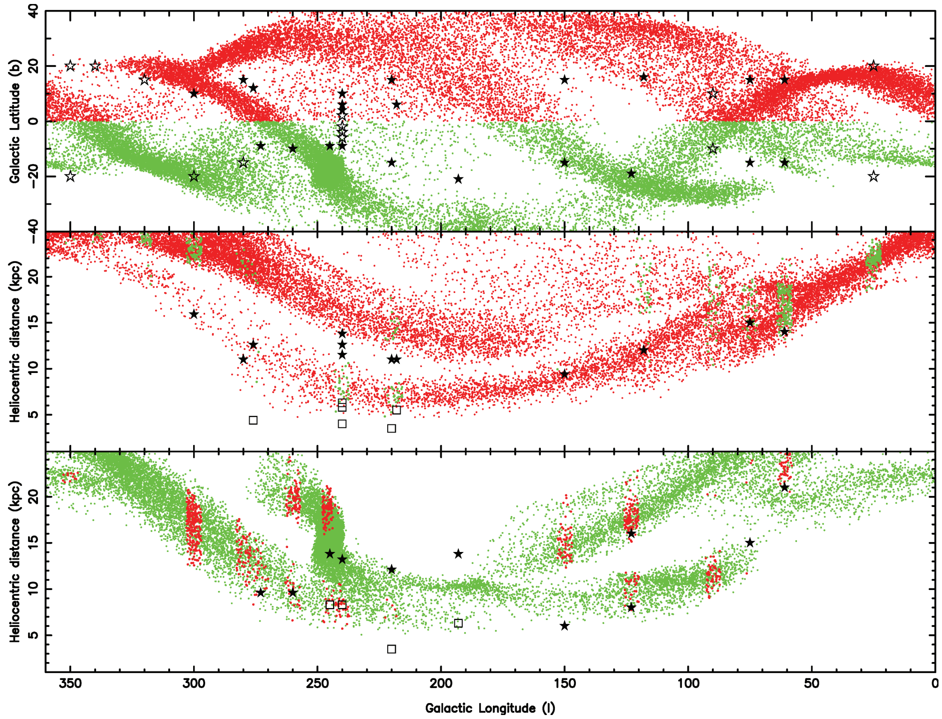

Figure 13. As for Fig. 12, but using the numerical simulation of Peñarrubia et al. (2005). This model is useful for comparison as it uses the MRi detections known at that time as constraints, rather than the overdensity of stars in the Canis Major region as used by Martin et al. (2005).

sparse to draw conclusions as to a potential path for the stream, but it does serve as a basis for future studies and models.

4.2 Comparing the observations with the Peñarrubia et al. (2005) model

Interpretation of the predictions of the Peñarrubia et al. (2005) model has been done in the same way as for the Martin et al. (2005) model, primarily by comparing the locations and distances of the observed structures with those predicted by the model (Fig. 13). The lower two panels show the predicted stream locations from the model in each of the regions surveyed. Given that the Peñarrubia et al. (2005) model uses fewer particles than the Martin et al. (2005) model, a slightly bigger area has been chosen around each field to sample enough model data points. The correspondence with data is seemingly poorer for the Peñarrubia et al. (2005) model and several non-detection regions are supposedly populated by the stream.

For the northern fields, many of the distances do seem to match the predictions of the model. A close inspection of the model shows that the detections are located on the wrong arm. Most of the fields observed are located in sparsely populated regions of the model and do not probe the predicted path of the model to higher latitudes. The field at $l = 25°$ is possibly undetected due to the predicted distance of the stream here. As discussed in Section 3, it is estimated that the technique used is only sensitive to objects less than 20 kpc distant. The fields at $(l, b) = (61–75)°$ could be seen as the confirmation of the stream, however the non-detection at $(l, b)) = (90, +10)°$ is difficult to explain. At $(l, b)) = (118, +16)°$, the detection is at least 5 kpc closer than the distance estimate from the model. For the field centred on $(l, b)) = (150, +15)°$, it resides in an almost empty region of the model, but seemingly, the detected stream here corresponds with the tidal arm at higher latitudes. The discrepancy for this model around the $l = 240°$ region is known and has been commented on by other authors. The fields at longitudes $l = (260–360)°$ are simply unable to observe the stream according to the model. The latitude for these fields is not so much a problem and detections reported in this paper do not match the model at all.

In the south, the match with the model is good around $l = 60°$ and 123° and close to the plane around 250°. The remaining fields occupy regions of low density in the model. A few fields, such as those at $l = 90°$, present real discrepancies with the model. The main difference between the northern fields is that most of the predicted stream locations in the south should have been detectable by the technique used here. In favour of the model though, a significant proportion of the model is not sampled in the survey as it is above a latitude of 20°. Finally, in comparison to the original data used to create the model (see Fig. 2; Peñarrubia et al. 2005), most of the data points there reside between $l = (110–240)°$. This corresponds to a relatively sparse sampling in this survey. Another comparison of this model against the available data is presented in Peñarrubia, Martinez-Delgado & Rix (2007).

4.3 Key locations to test the models

Each model predicts that in key areas of the Galaxy, there are significant changes in the stream which could be used to both test the model and provide further support to the tidal stream scenario as a whole. In particular, these are the regions south of the purported Canis Major dwarf galaxy over the longitude range $l = (200–250)°$ since in this location the two models predict different approaches for the stream into the core. The region $l = (130–220)^\circ$ is where the Martin et al. (2005) model predicts the leading tidal arm of the dwarf galaxy should decrease in latitude and enter into the disc. Finally, in the region $l = (025–050)^\circ$, the stream is predicted to be close to the plane ($b = \pm10^\circ$) in the Martin et al. (2005) model and away from the plane ($b = \pm20^\circ$) in the Peñarrubia et al. (2005) model. Knowledge of the stream around the bulge is needed to constrain its position in all four quadrants of the Galaxy. The bulge presents an additional challenge in that the distance of the targets and the high density of foreground stars will make the MRi difficult to detect. The current data set is unable to detect the MRi at the distances predicted by the Peñarrubia et al. (2005) model (25–30 kpc), and the Martin et al. (2005) model predictions of 15–25 kpc are yet to be tested so close to the plane.

4.4 Insights into the nature of the Galactic warp

One of the key properties of the Galactic disc is the warp. Around $l = 90^\circ$, the disc curves up from the $b = 0^\circ$ position, and around $l = 270^\circ$ it curves down. Studies into the putative Canis Major dwarf galaxy have had to contend with the close proximity of the warp and much debate has been centred on whether the CMDs in this region can be fully explained by the warp or require an additional source of stars. This part of the survey provides an opportunity to understand the impact of the Galactic warp on CMDs through a closer inspection of fields $(l, b) = (280, \pm15)^\circ$ (Figs 3 and 4). At $l = 280^\circ$, these fields are very near the maxima of the southern warp. First, both these fields are well matched by the model and the warp is seen clearly as an excess of stars in the southern field. This manifests both as a general increase in star counts and an obvious thickening of the thin and thick disc components as seen in the southern field. How to identify the different components of the Galaxy in the CMDs is shown in fig. 2 of Paper I. Secondly, we see that the influence of the Galactic warp does not change the shape of the CMD. The northern field at $l = 280^\circ$ is essentially a shifted version of its southern counterpart. This is important because a comparison of almost symmetric fields $(l, b) = (240, +10)^\circ$ and $(l, b) = (240, -9)^\circ$ (see Fig. 1 or figs 10 and 17 from Paper I) is remarkably different. While the fields at $l = 280^\circ$ have more of a sharp edge to thin–thick disc boundary, the Canis Major field shows a true-curving main sequence which is unmatched in the northern field. Since the $l = 280^\circ$ fields show that the warp does not seem to have an impact on the shape of the CMD, the fields in Canis Major must be considered anomalous to the usual Galactic warp scenario. Whether this anomaly is caused by a dwarf galaxy is uncertain; however these qualitative differences in the CMDs should be investigated so that our understanding of this region is more complete.

5 CONCLUSION

This paper reports on two new detections and seven non-detections of the MRi tidal stream. The results presented here conclude a survey tracing this feature around the entire Galactic plane. The previously reported detections of the survey are presented in Fig. 1. Comparing the relative strengths of the MRi and the main MW population, it appears qualitatively that the stream is denser and broader above the plane than below but as such there is no explanation why this would be the case. The part of the overall survey presented here shows no evidence of the strong Canis Major dwarf main sequence in the CMDs. The CMa sequence is historically identified as a shift in the position and shape of the strongest main sequence in the CMD. For the fields presented here, the dominant main-sequence feature in the CMDs is easily attributed to the thin and thick discs. In each instance where the distance has been determined to these structures, it is in accordance with the Besançon synthetic galaxy model predictions. Therefore, they can be confidentially associated with the MW. The only field which might be expected, from the Martin et al. (2005) model, to contain the CMa signature is $(l, b) = (280, -15)^\circ$. This field does not show this CMa-style sequence in the CMD (Fig. 3).

Comparing these new MRi detections with the two current numerical simulations of the stream and putative dwarf galaxy progenitor has led to inconclusive results. The Martin et al. (2005) model north of the Galactic plane roughly traces the locations of the detections. In the south, the correspondence between the model and the detections is adequate with some noted exceptions. Several detections presented in this survey indicate, with reasonable certainty, the locations in which the model is incorrect. For the Peñarrubia et al. (2005) model, there is less correlation between the data points and the predicted stream locations than is seen with the Martin et al. (2005) model. Although some points do seem to represent a better fit, it is important to note though that a significant proportion of the Peñarrubia et al. (2005) model does reside outside a Galactic latitude of $b = \pm20^\circ$. So much of the model has not been sampled by this survey. Indeed, it is easy to see that this survey is too narrow in Galactic latitude in comparison with the data used to construct the model and the predictions it makes. Drawing a conclusion based on these results is inadvisable, but there is little here to strongly support this model. Both models will obviously require reworking to include the new information available along with more observations to test their predictions.

With regard to the Besançon synthetic galaxy model, there is no presence of the MRi as part of natural Galactic structure. In almost all fields in this survey, the bulk MW components of thin, thick disc have been accurately modelled. There is no systematic discrepancy between the model and data even in regions containing the Galactic warp. Only the regions around Canis Major, as discussed in Paper I, show a definite shift from the observational data. Given the data support the predictions of the Besançon model in all but the MRi detections, it is reasonable to assume this structure is indeed additional to the usual Galactic components.

Determining the density profile of this feature around the Galaxy and indeed connecting detections is an important next step in resolving its origins. To date, targeted deep surveys, such as these, have resolved many important questions surrounding this structure. This survey sheds some light on the impact of the Galactic warp on the CMDs showing that it does not affect its morphology significantly and the Besançon model is adequate for most fields. This has implications with regard to how the fields in the Canis Major region are to be interpreted as the fields there have obviously different characteristics. While the nature of the MRi still remains quite elusive, this is primarily due to its large extent on the sky and its location close to the plane. For the time being, both the Galactic origin scenario and the tidal stream hypothesis are still possibilities for this structure. The completed survey, presented here, has shown that a targeted campaign of observations can provide insights on not only this structure but also generic Galactic structures as well.

ACKNOWLEDGMENTS

MB acknowledges the financial support of INAF to this research through the grants PRIN05-CRA 1.06.08.02 and PRIN07-CRA 1.06.10.04. RRL would like to thank LKN for her ongoing support. BCC thanks the referees for their constructive comments and B. Carry for his work with the lighting.

REFERENCES

Belokurov V. et al., 2007, ApJ, 658, 337

Conn B. C., Lewis G. F., Irwin M. J., Ibata R. A., Ferguson A. M. N., Tanvir N., Irwin J. M., 2005a, MNRAS, 362, 475

Conn B. C. et al., 2007, MNRAS, 376, 939 (Paper I)

Ibata R. A., Irwin M. J., Lewis G. F., Ferguson A. M. N., Tanvir N., 2003, MNRAS, 340, L21

Irwin M., Lewis J., 2001, New. Astron. Rev., 45, 105

Ivezic Z. et al., 2008, ApJ, 684, 287

Jurić M. et al., 2008, ApJ, 673, 864

López-Corredoira M., Momany Y., Zaggia S., Cabrera-Lavers A., 2007, A&A, 472, L47

Martin N. F., Ibata R. A., Conn B. C., Lewis G. F., Bellazzini M., Irwin M. J., 2005, MNRAS, 362, 906

Mateu C., Vivas K., Zinn R., Miller L., 2007, in Vazdekis A., Peletier R., eds, Proc. IAU Symp. 241, Stellar Populations as Building Blocks of Galaxies. Cambridge Univ. Press, Cambridge, p. 359

Newberg H. J. et al., 2002, ApJ, 569, 245

Peñarrubia J. et al., 2005, ApJ, 626, 128

Peñarrubia J., Martinez-Delgado D., Rix H. W., 2007, ApJL, submitted (astro-ph/0703601)

Rocha-Pinto H. J., Majewski S. R., Skrutskie M. F., Crane J. D., 2003, ApJ, 594, L115

Vivas A. K., Zinn R., 2006, AJ, 132, 714

This paper has been typeset from a TEX/LATEX file prepared by the author.

3.3 The Subaru and 40-inch Distractions

Two attempts were made to collect data to further analyse the MRi and CMa structures which began with the two previous papers. These consisted of observing runs using the Subaru telescope on Mauna Kea in Hawai'i and the 40-inch (40″) telescope at Siding Spring Observatory in New South Wales, Australia. An observing run using the Subaru telescope was also performed to establish the nature of a recently discovered dwarf galaxy-like object Willman 1 and the Ursa Major dwarf galaxy (UMa), and two follow-up runs were proposed following the failure of the first, the last of which included the newly discovered Canis Venatici dwarf galaxy (CVnI). These five attempted observing runs, including intentions and outcomes, are outlined in the remainder of this Chapter.

Willman 1, UMa and CVnI

In the first instance, we were awarded 5.5 hours on the Subaru telescope as one of only two successful Australian applicants to obtain Subaru time via the new Gemini-Subaru time share agreement which began in Semester 2006B. We were to obtain data on Willman 1 and UMa, using the wide field camera Suprime-Cam in service mode, that is, Subaru staff were to perform the observations for us.

The overarching aim of this project was to gain a better understanding of the low-mass building blocks of the Galaxy. Willman 1, originally reported by Willman *et al.* (2005b), was, at that time, thought to be the least massive dwarf galaxy-like structure in the Galactic halo, with an initial mass estimate of $\sim 120 - 2000\,\mathrm{M}_{\odot}$. This mass estimate seemed very unlikely considering objects of such low mass are not likely to be gravitationally bound, although it was clearly a very small object. Because this structure appeared to be less massive than even the smallest GCs, it would lend invaluable insight to the lowest mass building blocks of galaxies. Indeed, if Willman 1 has such a low mass, what could it be? Certainly not a dwarf galaxy or GC; perhaps a new class of object? Another apparently low-mass Galactic satellite, UMa, had also recently been discovered (Willman *et al.*, 2005a) and reported to be the lowest surface brightness companion known, and to be very distant ($\sim 100\,\mathrm{kpc}$). Because many important attributes of these interesting objects were still unknown, it was vital to our understanding of the fundamental building blocks of the Galaxy to obtain better quality data on both objects. Direct imaging of faint tidal debris, combined with surface brightness measurements, would allow estimates of their tidal radii through profile fitting. Furthermore, we were to calculate their masses, metallicities, surface brightnesses, distances and look for multiple star formation epochs, improving our knowledge significantly.

The observations were performed February 18, 2007, following a substantial delay due to an earthquake. Unfortunately, our efforts were thwarted due to complete cloud cover on the night of the observing run, and the Subaru staff in charge of the observations sent back data of the undersides of the clouds. The initial form of the time-share agreement left us with no course for reobservation so we were left empty-handed. Fortunately, because of the problems we encountered during this scheduled service run, the Subaru-Gemini time-share agreement has now been altered so that these types of problems no longer arise from service observations.

Due to the poor quality of the data, we applied for Subaru time twice more over the next three semesters to observe these same objects, with similar goals. To further our understanding of faint, low-mass Galactic satellites, we included CVnI, one of the lowest mass dwarf satellite galaxies of the MW, in the final proposal (for Semester 2008A). We intended to determine its density profile, look for metallicity gradients using three broadband colours as a metallicity proxy, and determine its star formation history through isochrone fitting. To further constrain the formation history of the Galaxy, we were to use multi-colour matched filtering to detect faint tidal debris. Neither of these proposals were awarded any time.

Recently Discovered Planar Streams and Revisiting the MRi

Two projects were proposed to run concurrently to further constrain the MRi in various locations both above and below the Galactic plane. Time was awarded for both projects, with eight nights on the 40″ telescope and one night on Subaru, both in classical mode, that is, I was to do the observing myself for both projects.

Many Galactic satellites, and associated tidal streams, have recently been discovered in SDSS data (e.g. Grillmair, 2006, and references therein). However, SDSS coverage does not extend over the entire sky, leaving a lot of Galactic substructure unstudied. A hint of one of these structures (the "Eastern Banded Structure", or EBS; Grillmair, 2006) extends into SDSS coverage by only a few degrees (see Figure 3.1), and there is evidence that it may be related to the main stream reported by Grillmair (2006). The EBS also appears to extend toward the Galactic disc. Is it possible that this new structure is also part of the single accretion event that formed the other in-Plane streams, including the MRi? The 40″ survey planned to extend the coverage of the EBS South of SDSS, to validate its existence and reveal its path toward the Galactic plane and main Grillmair (2006) stream. An attempt was to be made to locate the point of contact between these streams, with blue main sequence stars employed as density tracers, revealing the relative luminosity/density of both the EBS and Grillmair streams, as well as the region between the streams. These density maps were designed, in part, to probe the reality of the striations reported in both streams. The density profile would also have been used to constrain the amount of material in each wrap of the stream about the Galaxy and hence constrain the age of the accretion. Very important steps toward a complete understanding of the MRi.

Data in SDSS reaches $u' \sim g' \sim r' \sim 22$ and $i' \sim z' \sim 21$, showing that these streams can be observed at this magnitude limit, although at the very limit of detection; clever exponential *and* fourth order polynomial surface fits had to be subtracted (Grillmair, 2006) before smoothing and weighted summation of the final image revealed these extremely low surface density features. This project had planned to reach ~ 1 mag deeper than SDSS, to avoid systematic effects introduced when analysing very low surface density targets. It had been planned to use the data from the Wide Field Imager[1] on the 40″ telescope to determine the distance, metallicity and further age estimates through isochrone fitting to resulting Colour Magnitude Diagrams (CMDs), however, weather intervened which reduced the survey area covered and the quality of the data collected. We had also planned to use these data to constrain high resolution numerical models of the tidal break-up of dwarf satellite systems to further constrain the in-Plane structures observed, which would have uncovered whether these new streams are indeed other branches of the single accretion event that created the MRi, further revealing the accretion history of the Galactic disc.

During the 40″ observing run, half of the nights had high, thin cloud and strong winds (up to 60 knots), which meant it was not possible to open the dome, and the other half were partly cloudy with very poor seeing (a measure of the stability of the atmosphere; at times it was as bad as $\sim 5''$, effectively rendering the data unusable). This resulted in a dataset covering less than half of the sky coverage originally proposed, to a B magnitude of $\sim 18-19$ rather than the intended 22.7 (see Figure 3.1 for the total sky coverage proposed and Figure 3.2 for an example of the data quality achieved). During reduction of the data[2] it was realised that the headers of the .fits files containing the data from this run were offset from the true pointing position of the telescope. These offsets were usually $< 2'$, but in a random direction, so that we had to realign

[1]For a detailed description of the Wide Field Imager see PhD thesis by Blair C. Conn entitled "New Overdensities in the Thick Disc and Halo: the Interactions of a Newly-Accreted Galaxy".

[2]The data was reduced using the Cambridge Astronomical Survey Unit (CASU) data reduction pipeline (see Irwin & Lewis, 2001, and PhD thesis by Blair C. Conn entitled "New Overdensities in the Thick Disc and Halo: the Interactions of a Newly-Accreted Galaxy" for detailed descriptions of the CASU pipeline) specifically modified to work with the 40″ Wide Field Imager data.

each individual frame by hand to allow the data reduction pipeline to match the imaged stellar positions. Once this was done it was clear that because of the weather and seeing, first, the data did not go to faint enough magnitudes and second, there were insufficient stars to produce useful CMDs. The lack of stars is likely due to the CASU pipeline classifying many of the stars as galaxies due to the poor observing conditions spreading the star light over a large number of pixels of the camera. Figure 3.2 shows a comparison of CMDs from a single 40″ field and one from a recent data acquisition from Subaru at the same latitude and with the same sky coverage (see below for details of the Subaru data). Note that the MRi sequence "turns in" [from blue (negative values of $g-r$) to red (positive values of $g-r$)] at $r \sim 19$ which is also approximately the limiting magnitude of the 40″ data.

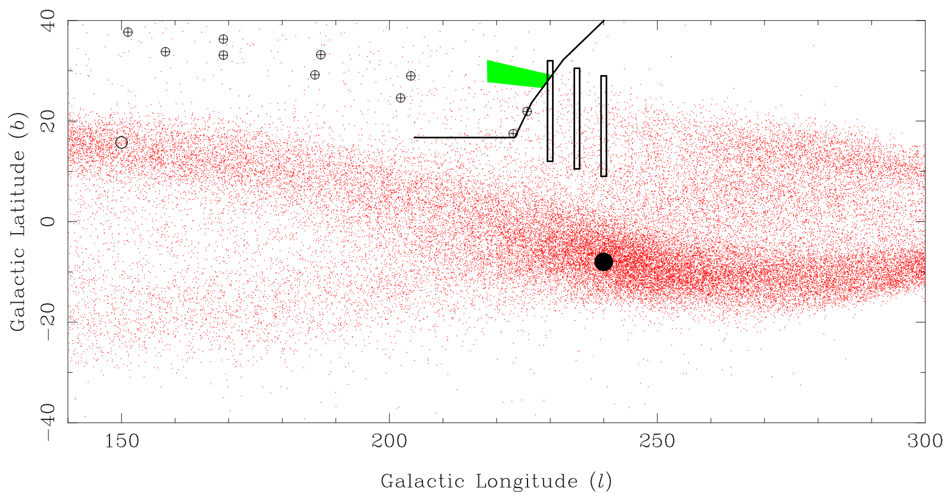

Figure 3.1: The Martin *et al.* (2005) model of the tidal break-up of the CMa dwarf (red dots). Overlaid onto this model are: three rectangles representing the three proposed regions to be covered by the 40″ survey, the core of the Canis Major overdensity (solid circle), the Conn *et al.* (2005) detection of the MRi at $(l, b) = (150, +15)^\circ$ (open circle), the Grillmair (2006) stream (circled plus signs), the approximate known extent of the "Eastern Banded Structure" (green polygon) and the approximate limit of SDSS Data Release 6 coverage (solid black line) with no coverage closer to the Plane or with increased l. Note that SDSS coverage will never extend into these regions.

The Subaru survey was intended to target ~ 10 square degrees of sky, centered on a new detection of the MRi at $(l, b)^\circ = (167.1, -34.7)^\circ$ (Casetti-Dinescu *et al.*, 2008). Importantly, the distance of this detection from the Plane meant greatly reduced Galactic contamination, providing an unobscured view of this structure. This survey would have provided an exquisite opportunity to unravel the nature of this feature and its relation to the Canis Major overdensity.

Casetti-Dinescu *et al.* (2008) identified MRi member stars concurrent with the Peñarrubia *et al.* (2005) model of the break-up of CMa (Figure 3.3). Our survey was to target nine fields in a 3×3 grid, centered on the SA71 region (red circle in Figure 3.3), to determine the distance to, and orientation of, the MRi in this region through the measured density profile of each field and CMD analysis. We planned that each field, spaced five degrees apart, would comprise a mosaic of four pointings, covering ~ 1 square degree per field. In this way, a systematic search for the orientation of the MRi would be performed.

We planned to map each square degree field to g'=26.0 and r'=25.5, > 5 magnitudes below the expected redward trend of the MRi sequence at 9 kpc, providing data far down this sequence, and hence reliable differentiation between it and MW sequences (Figure 3.4). In addition, this would create a more complete sampling of fainter stream stars which are inherently more

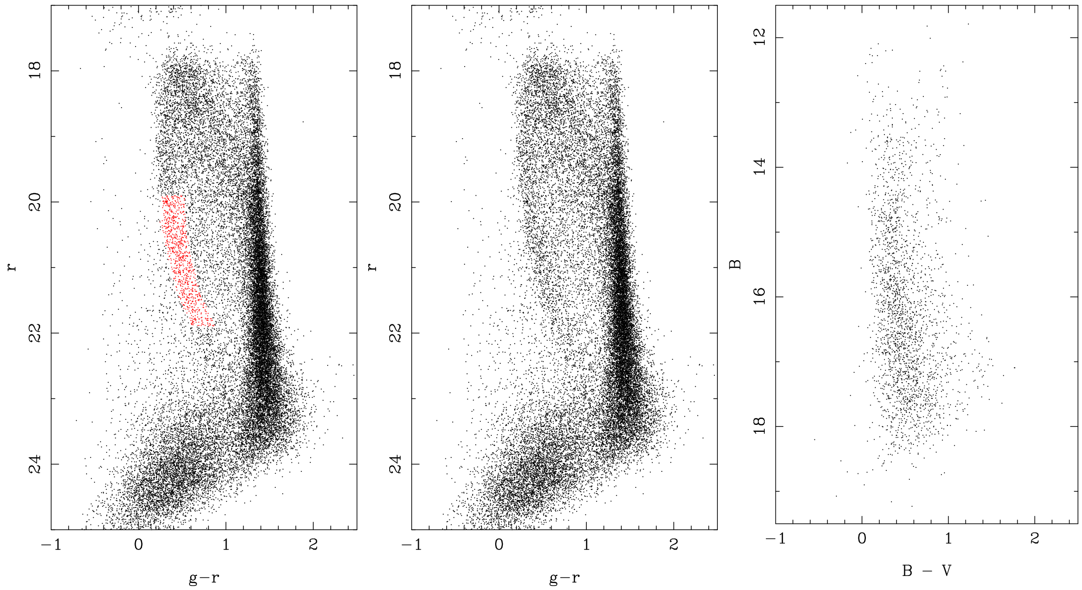

Figure 3.2: Comparison between the quality of the 40″ data and data from the recent Subaru run. *Left:* A CMD produced from $\sim$ 1 square degree of the recently obtained Subaru data centered on $(,b)^\circ \approx(150.0, +14.5)^\circ$. A section of the MRi sequence has been coloured red to highlight the location of the sequence. *Centre:* The same CMD as the left panel without the highlighting of the MRi sequence. *Right:* An example of the data from the 40″ run. This CMD of a single 40″ field centered on $(l,b)^\circ \approx(240.0, +14.5)^\circ$ also covers $\sim$ 1 square degree and is at the same latitude as the Subaru field. Note that the MRi sequence "turns in" at approximately the limiting magnitude of the 40″ data ($r \sim 19$), therefore, the MRi feature is absent in the 40″ data. Note also that the 40″ data does not reach fainter than SDSS. The the vertical scale in the right panel is different to that in the centre and left panels.

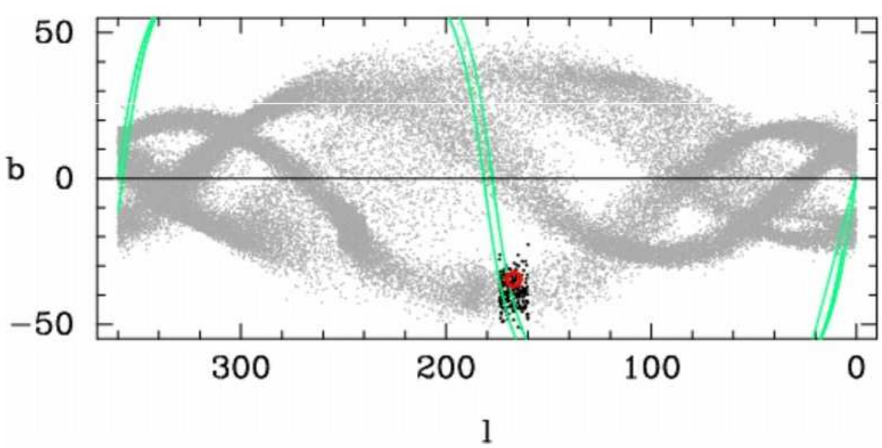

Figure 3.3: The spatial distribution of MRi tidal debris from the Peñarrubia *et al.* (2005) model (grey points) overlaid with MRi stars observed by Casetti-Dinescu *et al.* (2008) (black points). The orbital path of the Sagittarius dwarf galaxy is shown as green parallel lines and the red circle is the SA71 area selected by Casetti-Dinescu *et al.* (2008) for their survey. This was originally published by Casetti-Dinescu *et al.* (2008) as their Figure 7.

numerous; the large number of stars would provide an accurate density profile of the MRi over $\sim$ 10 degrees of latitude, and this would allow the stream to be traced across these fields in both

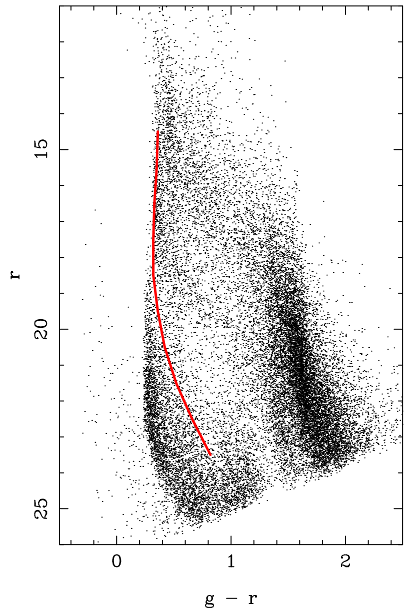

Figure 3.4: A 2.5 square degree field from the Besançon Synthetic Galaxy model centered on the SA71 MRi detection at $(l, b)^\circ = (167.1, -34.7)^\circ$. The solid red line denotes the expected position of the MRi sequence at 9 kpc. Note the redward trend of the MRi sequence at $r \gtrsim 19.0$ and the clear separation between the MRi and Galactic sequences.

latitude and longitude.

In addition to the density profile, the stellar populations present in the MRi would have ages dependent on its formation scenario; it would contain stars with a similar age distribution as the Disc if the origins of the structure truly lie with the Galaxy. These new data, combined with the numerous MRi detections of previous surveys, would have provided parameters for high resolution N-body/Smoothed Particle Hydrodynamics simulations of the stream. These simulations would have necessarily described the most realistic model of the MRi to-date, having tightly constrained final conditions determined by these data. These simulations would likely also have provided: the required evidence for the in-Plane accretion hypothesis (or otherwise), a test for the veracity of the previous models, and would be used as a platform to focus future photometric and spectroscopic surveys of the MRi. On the night of the observations (October 27, 2008) Mauna Kea was completely cloud covered and despite waiting until sunrise for it to clear we were unable to collect any data. One positive outcome from the observing run was that I got to visit Hawai'i and Mauna Kea observatory.

Since then, a new survey has been performed on Subaru with the Suprime-Cam wide field camera, targeting three strips of sky, each $\sim 15^\circ$ long, perpendicular to the Plane at $l = 130^\circ$, 150° and 170° and another strip cutting across the main stream reported by Grillmair (2006) (see left two panels of Figure 3.2 for CMDs from this new survey). We now have a fantastic dataset of four strips of the sky in which the MRi can be traced very well and we are basing a paper on these data (Conn *et al.*, in prep). In this up-coming paper we will reveal the orientation of the MRi over the range of Galactic latitude $130^\circ < l < 170^\circ$, as well as its cut-off North of the Plane (where its density drops to that of the background Galactic field) over that range of latitudes. For the first time the density of MRi will be calculated, as will its overall mass. These new data, along with the data from the two previous papers in this thesis, will form the basis for a new N-body model which we will present in a forthcoming paper. We are slowly edging closer to a full understanding of this structure and its relationship with the Galaxy.

Chapter 4

Conclusions and Further Work

I refuse to answer that question on the grounds that I don't know the answer.

- Douglas Adams

The work presented in this thesis draws on two separate but intimately linked approaches to the problem of hierarchical structure formation at the galactic, and subgalactic scales. The first, that of testing the nature of the gravitational interaction, focuses on our understanding of gravity. If we do not understand the way gravity behaves, does this mean that our best model of Universal structure formation, ΛCDM, is flawed? If ΛCDM is flawed, does this also then mean that the missing satellite problem may be resolved? The second, observations of the MRi and possible progenitor the CMa dwarf, addresses galactic-scale structure formation, with particular focus on galactic discs.

To be able to determine whether the accelerations of stars near the outskirts of GCs is in keeping with Newtonian predictions, it was first necessary to quantify the dark matter content of each GC in the survey. Mass-to-light information was calculated from the projected density profile of each cluster and surface brightness measurements. Due to crowding and confusion effects resulting in a large uncertainty in the mass contained with the cores of GCs, no mass-to-light information can easily be claimed for the cores of GCs. Therefore, the rarely used, but very robust method for calculating the global mass-to-light ratios of GCs was adopted, that of using mass-to-light *profiles*. This means the mass uncertainty in the core can be avoided by only calculating the mass-to-light ratio for radii beyond the core, in this case for radii greater than the Plummer scale radius which is considerably larger than the core radius. In all ten clusters presented here, none show any evidence for significant dark matter components, since all have mass-to-light ratios $\lesssim 5$. The lack of dark matter gives some indication of the formation of GCs. If they formed concurrently with other Galactic components, why are they so dark matter deficient? The paucity of dark matter is indicative of formation outside of the Galaxy, unless there is a mechanism which removes the dark matter and leaves the stellar material behind. If they are formed within the tidal tails of mergers, as has been suggested, this still does not explain the dark matter deficiency.

The globular cluster analysis was performed in a completely homogeneous manner by using the same instrument for data collection, reducing the data with the same reduction pipeline, and all subsequent data analysis being performed in the same way. This homogeneity is very important in such a large study to ensure that all systematics are accounted for coherently. The results presented here *strongly* indicate that Newtonian gravity is a good description of how things really behave, even in the very low acceleration regime (below a_0) at the outskirts of GCs. This is an important result for two reasons. First, it shows that gravity is well understood. Second, this implies that the ΛCDM structure formation model is still our best model for structure formation in the Universe, which then means that the missing satellite problem is still exactly that, problematic. Why ΛCDM predicts so many more satellites for large galaxies is still unclear, although better observations of galactic haloes may eventually resolve this problem through the detection of numerous low-mass halo objects.

In addition to determining the dark matter content of the target GCs and testing Newtonian gravity, several other important results came from this project. (1) The rotations of all ten clusters were measured, with two, namely 47 Tuc and M22, exhibiting very large rotational velocities. A possible explanation for the extreme rotation of 47 Tuc is that it underwent a merger in its past. (2) A known method for calculating the metallicities of GCs, and also for individual stars, was vastly improved by calibrating from the equivalent widths of the calcium triplet lines and the Tip of the Red Giant Branch, rather than the horizontal branch. Because the horizontal branch is approximately five magnitudes fainter than the RGB tip, this method can now be used to calculate the metallicities of much more distant objects where the horizontal branch is not available, and also for objects, such as M55, where the blue horizontal branch stars are too hot to exhibit strong calcium triplet lines. (3) GCs within $\sim 3\,\mathrm{kpc}$ of the Plane are apparently tidally disturbed by the Disc. This may be unsurprising because tidal shocking by galactic discs is well known, however, for all clusters that are not being continuously shocked by the Disc (M4, for example, is on a nearly Planar orbit and so is undergoing continuous tidal stress) their apparent cooling times are far shorter than their relaxation times. It is unclear what cooling mechanism is at work here because two-body relaxation can not occur this quickly in the diffuse outer regions of GCs. (4) It is possible, although highly speculative, that 47 Tuc, M22 and NGC 6752 contain intermediate black holes in their cores. According to the low-mass extension of the M-σ relation, these have masses of $\sim 675\mathrm{M}_{\odot}$, $\sim 170\mathrm{M}_{\odot}$ and $\sim 80\mathrm{M}_{\odot}$ respectively. (5) The lack of tidal heating signatures on GCs in the outer Halo is a weak indication of the non-triaxiality of the dark Halo. (6) Instead of the expected monotonic drop with radius expected for the velocity dispersion profile of 47 Tuc, a marked rise was discovered at radii greater than half the tidal radius. This is a very important result because it shows that this cluster is either quickly evaporating, or more likely, underwent a merger $7.3 \pm 1.5\,\mathrm{Gyr}$ ago. This is only the second kinematic evidence of hierarchical merging at the GC-scale, and a truly rare opportunity to further understand merging at the subgalactic scale.

Constraining the location of the MRi around the Galaxy is an important step in understanding Disc evolution. The research described in this thesis shows conclusively that the MRi entirely encircles the Disc with 10 bona fide and two tentative new detections of the structure. These new data provide strong evidence that the MRi cannot be considered part of the Warp or Flare, and is extra-Galactic in origin. It is also apparent that the Warp can not produce the signatures that are seen in the CMDs near the core of the CMa overdensity, therefore, the structure is not a line-of-sight effect as has been claimed. Due to their enormity, the exact nature of both structures is difficult to determine from this survey alone and large, deep surveys of the outer stellar Halo and thick Disc are required before a consensus can be reached.

Despite several abortive attempts to obtain additional data on the MRi, a fantastic dataset has now been obtained from the Subaru telescope. A manuscript in preparation will further the current knowledge of the MRi and its role in the evolution of the Disc greatly. In this coming manuscript, the first attempt will be made to weigh the MRi, giving tight constraints on the initial mass of the progenitor. The orientation of the MRi above the Plane and over the latitude range $130^{\circ} < l < 170^{\circ}$ will also be presented, as will the northern limit of the stream over those latitudes. These new data will be used to focus a high resolution N-body simulation of the tidal breakup of the MRi progenitor, with the new model to be presented in a subsequent manuscript. This will tell us much about hierarchical merging at subgalactic scales and how these mergers relate to ΛCDM, by adding another branch to the known merger tree of the Galaxy.

My research has paved the way to a greater understanding of the Galaxy, however, there is, of course, more to be done. A brief summary of various directions that can be taken follows.

The formation of GCs is still hotly debated. To fully understand their formation, proper motion studies of their members are required. While some of this information exists for several

GCs, determining the proper motions of all stars which now have publicly available radial velocity information will allow for the three dimensional kinematics to be calculated. It will then be possible, for example, to obtain the three dimensional axes of rotation of these clusters with respect to the Galactic centre. If these can be shown to be correlated in some way, this will be a vital piece of information on the formation history of the Halo GCs. Although it is becoming clear that GCs have negligible dark matter content, the question of *why* GCs are virtually DM free is still unanswered. Interestingly, there is still no consensus on the DM content of tidal dwarf galaxies. Since these may form in concert with GCs (e.g. Bournaud & Emsellem, 2008; Hancock *et al.*, 2009), and because the formation environment is likely to play a crucial role in the DM content of these objects, the dark matter content of tidal dwarfs may also be minimal. Measurements of the DM content of tidal dwarf galaxies is, therefore, another important step in our understanding GC formation.

Ferraro *et al.* (2003) discussed the possibility that the inner 0.08 pc of NGC 6752 has $\mathrm{M/L_V} \sim 6-7$. Since we do not claim any knowledge of the $\mathrm{M/L_V}$ at those radii, but see an increased $\mathrm{M/L_V}$ toward the core, this is a possibility. Interestingly, Leigh *et al.* (2009) have noted an observational correlation which may be useful for accurately estimating the masses of GC cores, and, therefore, may make such core $\mathrm{M/L_V}$ measurements possible. Further research is needed to ensure the technique is valid before this can be done. Explaining the anomalously large $\mathrm{M/L_V}$ for the core of NGC 6752 is not within the scope of this thesis but if it can be corroborated, its cause should be pursued, since no GC has been shown to have such high $\mathrm{M/L_V}$ at any radius (assuming the lower end of our M53 estimate is taken).

The cooling mechanism for the outskirts of GCs discussed above needs to be explored. As mentioned, normal two-body relaxation can not account for such rapid cooling at the stellar densities in these outer regions. One way to address this issue is to perform high resolution N-body simulations of disc shocking in GCs to see if this cooling can be replicated. If similar cooling is observed in these simulations, a mechanism can then be investigated.

Modelling the two-component population of 47 Tuc in this thesis relied exclusively on stellar kinematics. Although Plummer models which are fit solely to GC kinematics can also be good fits to their surface brightness profiles (Lane *et al.*, in prep.), it is important to extend the model to include an extra constraint by forcing such a fit. This new, better constrained model is currently being produced and will form the basis of a forthcoming manuscript. N-body simulations of merging globular clusters are also required to further clarify the merger scenario for 47 Tuc. These simulations will address several observed quantities, namely how much angular momentum can be imparted through a 9:1 merger, what consequence the merger has on the velocity dispersion in the outer regions of the cluster over dynamical timescales, and what effect it has on the global $\mathrm{M/L_V}$. If it can be confirmed that 47 Tuc has recently undergone hierarchical merging, as seems to also be the case with ω Centauri, this provides evidence that small-scale structure formation is much more common than previously believed at the current epoch, which may alleviate the problem of the missing satellites.

Modelling of the MRi and CMa structures is of major importance to their complete comprehension. While there is now general agreement that the MRi is the result of an in-Plane accretion event, the currently available models of this merger are unsatisfactory. Despite the lack of data from several attempted surveys, the new data presented in this thesis, along with that from the Subaru/Suprime-Cam survey mentioned in Section 3.3 will form the basis of the most realistic numerical model of the break-up of the MRi progenitor to-date. With the tight constraints that can now be imposed on the model, it will be of sufficient quality to provide targets for future observations of the MRi. This will hasten advances in the understanding of this structure immensely, and hence of the evolution of the Disc, because regions of specific interest can be quickly targeted.

Bibliography

Abadi M. G., 2009, RMxAC, 35, 177

Anderson, J., Piotto, G., King, I. R., Bedin, L. R., & Guhathakurta, P. 2009, The Astrophysical Journal, Letters, 697, L58

Bassino L. P., 2008, AIPC, 1043, 373

Bekki, K., Yahagi, H., Nagashima, M., & Forbes, D. A. 2007, Royal Astronomical Society, Monthly Notices, 382, L87

Bender, R., & Saglia, R. P. 1999, Galaxy Dynamics - A Rutgers Symposium, 182, 113

Bica E., Bonatto C., Barbuy B., Ortolani S., 2006, A&A, 450, 105

Binney, J., & Merrifield, M. 1998, Galactic astronomy / James Binney and Michael Merrifield. Princeton, NJ : Princeton University Press, 1998. (Princeton series in astrophysics) QB857 .B522 1998

Binney, J., Dehnen, W., & Bertelli, G. 2000, Royal Astronomical Society, Monthly Notices, 318, 658

Bobylev, V. V., Bajkova, A. T., & Stepanishchev, A. S. 2008, Astronomy Letters, 34, 515

Boily, C. M., & Kroupa, P. 2003, Royal Astronomical Society, Monthly Notices, 338, 665

Bournaud, F., Duc, P.-A., & Emsellem, E. 2008, Royal Astronomical Society, Monthly Notices, 389, L8

Buser, R., Rong, J., & Karaali, S. 1999, Astronomy and Astrophysics, 348, 98

Carlberg, R. G. 1984, The Astrophysical Journal, 286, 403

Carney, B. W., Latham, D. W., & Laird, J. B. 1990, The Astronomical Journal, 99, 572

Carollo D., Beers T. C., Lee Y. S., et al., 2007, Natur, 450, 1020

Carraro, G., Vázquez, R. A., Moitinho, A., & Baume, G. 2005, The Astrophysical Journal, Letters, 630, L153

Casetti-Dinescu, D. I., Carlin, J. L., Girard, T. M., Majewski, S. R., Peñarrubia, J., & Patterson, R. J. 2008, The Astronomical Journal, 135, 2013

Castro-Rodríguez, N., López-Corredoira, M., Sánchez-Saavedra, M. L., & Battaner, E. 2002, Astronomy and Astrophysics, 391, 519

Casuso, E., & Beckman, J. E. 2006, Astronomy and Astrophysics, 448, 571

Cen R., Ostriker J. P., Prochaska J. X., Wolfe A. M., 2003, ApJ, 598, 741

Clewley, L., & Warren, S. 2003, The Mass of Galaxies at Low and High Redshift, 6

Conn, B. C., Martin, N. F., Lewis, G. F., Ibata, R. A., Bellazzini, M., & Irwin, M. J. 2005, Royal Astronomical Society, Monthly Notices, 364, L13

Conn, B. C., *et al.* 2007, Royal Astronomical Society, Monthly Notices, 376, 939

Conn, B. C., Lane, R. R., Lewis, G. F., Irwin, M. J., Ibata, R. A., Martin, N. F., Bellazzini, M., & Tuntsov, A. V. 2008, Royal Astronomical Society, Monthly Notices, 390, 1388

Conselice, C. J., Yang, C., & Bluck, A. F. L. 2009, Royal Astronomical Society, Monthly Notices, 361

Courteau, S., de Jong, R. S., & Broeils, A. H. 1996, The Astrophysical Journal, Letters, 457, L73

Crane, J. D., Majewski, S. R., Rocha-Pinto, H. J., Frinchaboy, P. M., Skrutskie, M. F., & Law, D. R. 2003, The Astrophysical Journal, Letters, 594, L119

Dejonghe, H. 1987, MNRAS, 224, 13

de Vaucouleurs, G. 1948, Annales d'Astrophysique, 11, 247

Diemand, J., Kuhlen, M., & Madau, P. 2007, The Astrophysical Journal, 657, 262

Eggen, O. J., Lynden-Bell, D., & Sandage, A. R. 1962, The Astrophysical Journal, 136, 748

Elmegreen, B. G., Bournaud, F., & Elmegreen, D. M. 2008, The Astrophysical Journal, 688, 67

Ferraro, F. R., Bellazzini, M., & Pancino, E. 2002, The Astrophysical Journal, Letters, 573, L95

Ferraro, F. R., Possenti, A., Sabbi, E., Lagani, P., Rood, R. T., D'Amico, N., & Origlia, L. 2003, The Astrophysical Journal, 595, 179

Ferreira, P. G., & Starkman, G. D. 2009, Science, 326, 812

Forbes, D. A., & Spitler, L. 2008, IAU Symposium, 245, 281

Frommert, H. 2007, `http://www.seds.org/~spider/spider/MWGC/mwgc.html`

Gilmore, G., & Reid, N. 1983, Royal Astronomical Society, Monthly Notices, 202, 1025

Grillmair, C. J. 2006, The Astrophysical Journal, Letters, 651, L29

Haghi H., Baumgardt H., Kroupa P., Grebel E. K., Hilker M., Jordi K., 2009, MNRAS, 395, 1549

Han, C., & Ryden, B. S. 1994, The Astrophysical Journal, 433, 80

Hancock, M., Smith, B. J., Struck, C., Giroux, M. L., & Hurlock, S. 2009, The Astronomical Journal, 137, 4643

Harris, W. E. 1996, The Astronomical Journal, 112, 1487

Harris W. E., 2010, RSPTA, 368, 889

Hartwick, F. D. A. 2009, The Astrophysical Journal, 691, 1248

Hasegawa, K., Umemura, M., & Kitayama, T. 2009, Royal Astronomical Society, Monthly Notices, 397, 1338

Helmi A., 2008, A&ARv, 15, 145

Ibata, R. A., Gilmore, G., & Irwin, M. J. 1994, Nature, 370, 194

Ibata R., Irwin M., Lewis G., Ferguson A. M. N., Tanvir N., 2001a, Nature, 412, 49

Ibata, R., Lewis, G. F., Irwin, M., Totten, E., & Quinn, T. 2001b, The Astrophysical Journal, 551, 294

Ibata, R. A., Lewis, G. F., Irwin, M. J., & Quinn, T. 2002, Royal Astronomical Society, Monthly Notices, 332, 915

Ibata, R. A., Irwin, M. J., Lewis, G. F., Ferguson, A. M. N., & Tanvir, N. 2003, Royal Astronomical Society, Monthly Notices, 340, L21

Ibata R., Martin N. F., Irwin M., Chapman S., Ferguson A. M. N., Lewis G. F., McConnachie A. W., 2007, ApJ, 671, 1591

Irwin, M., & Lewis, J. 2001, New Astronomy Review, 45, 105

Jurić, M., *et al.* 2008, The Astrophysical Journal, 673, 864

Kazantzidis, S., Bullock, J. S., Zentner, A. R., Kravtsov, A. V., & Moustakas, L. A. 2008, The Astrophysical Journal, 688, 254

Kazantzidis, S., Zentner, A. R., Kravtsov, A. V., Bullock, J. S., & Debattista, V. P. 2009, arXiv:0902.1983

King I. R., 1966, AJ, 71, 64

Kochanek, C. S. 1996, The Astrophysical Journal, 457, 228

Kong, D.-L., & Zhu, Z. 2008, Chinese Astronomy and Astrophysics, 32, 360

Koposov, S. E., Yoo, J., Rix, H.-W., Weinberg, D. H., Macciò, A. V., & Escudé, J. M. 2009, The Astrophysical Journal, 696, 2179

Kormendy, J., & Kennicutt, R. C., Jr. 2004, Annual Review of Astronomy and Astrophys, 42, 603

Kroupa, P. 1992, IAU Colloq. 135: Complementary Approaches to Double and Multiple Star Research, 32, 228

Larson, R. B. 1974, Royal Astronomical Society, Monthly Notices, 166, 585

Law, D. R., Majewski, S. R., & Johnston, K. V. 2009, The Astrophysical Journal, Letters, 703, L67

Leigh, N., Sills, A., & Knigge, C. 2009, Royal Astronomical Society, Monthly Notices, 399, L179

Łokas, E. L. 2001, Royal Astronomical Society, Monthly Notices, 327, L21

López-Corredoira, M., Cabrera-Lavers, A., Garzón, F., & Hammersley, P. L. 2002, Astronomy and Astrophysics, 394, 883

Lütticke, R., Dettmar, R.-J., & Pohlen, M. 2000a, Astronomy and Astrophysics, Supplement, 145, 405

Lütticke, R., Dettmar, R.-J., & Pohlen, M. 2000b, Astronomy and Astrophysics, 362, 435

MacArthur, L. A., Courteau, S., & Holtzman, J. A. 2003, The Astrophysical Journal, 582, 689

Mandushev, G., Staneva, A., & Spasova, N. 1991, Astronomy and Astrophysics, 252, 94

Martin, N. F., Ibata, R. A., Bellazzini, M., Irwin, M. J., Lewis, G. F., & Dehnen, W. 2004, Royal Astronomical Society, Monthly Notices, 348, 12

Martin, N. F., Ibata, R. A., Conn, B. C., Lewis, G. F., Bellazzini, M., & Irwin, M. J. 2005, Royal Astronomical Society, Monthly Notices, 362, 906

Martin, N. F., Ibata, R. A., Irwin, M. J., Chapman, S., Lewis, G. F., Ferguson, A. M. N., Tanvir, N., & McConnachie, A. W. 2006, Royal Astronomical Society, Monthly Notices, 371, 1983

Martínez-Delgado, D., Pohlen, M., Gabany, R. J., Majewski, S. R., Peñarrubia, J., & Palma, C. 2009, The Astrophysical Journal, 692, 955

Mel'Nik, A. M., & Dambis, A. K. 2009, Royal Astronomical Society, Monthly Notices, 400, 518

McConnachie A. W., Irwin M. J., Ibata R. A., et al., 2009, Nature, 461, 66

McDonald, M., Courteau, S., & Tully, R. B. 2009, Royal Astronomical Society, Monthly Notices, 393, 628

Milgrom, M. 1983, The Astrophysical Journal, 270, 365

Mirabel, I. F. 2001, Astrophysics and Space Science Supplement, 277, 371

Moffat, J. W., & Toth, V. T. 2008, The Astrophysical Journal, 680, 1158

Moitinho, A., Vázquez, R. A., Carraro, G., Baume, G., Giorgi, E. E., & Lyra, W. 2006, Royal Astronomical Society, Monthly Notices, 368, L77

Momany, Y., Zaggia, S. R., Bonifacio, P., Piotto, G., De Angeli, F., Bedin, L. R., & Carraro, G. 2004, Astronomy and Astrophysics, 421, L29

Momany, Y., Zaggia, S., Gilmore, G., Piotto, G., Carraro, G., Bedin, L. R., & de Angeli, F. 2006, Astronomy and Astrophysics, 451, 515

Moore, B. 1996, The Astrophysical Journal, Letters, 461, L13

Moore, B., Governato, F., Quinn, T., Stadel, J., & Lake, G. 1998, The Astrophysical Journal, Letters, 499, L5

Mouhcine M., Ibata R., Rejkuba M., 2010, ApJ, 714, L12

Najarro, F., Figer, D. F., Hillier, D. J., Geballe, T. R., & Kudritzki, R. P. 2009, The Astrophysical Journal, 691, 1816

Navarro, J. F., Frenk, C. S., & White, S. D. M. 1997, The Astrophysical Journal, 490, 493

Newberg, H. J., *et al.* 2002, The Astrophysical Journal, 569, 245

Odenkirchen, M., *et al.* 2001, The Astrophysical Journal, Letters, 548, L165

Ortolani, S., Renzini, A., Gilmozzi, R., Marconi, G., Barbuy, B., Bica, E., & Rich, R. M. 1995, Nature, 377, 701

Parmentier, G., & Grebel, E. K. 2005, Royal Astronomical Society, Monthly Notices, 359, 615

Peñarrubia, J., *et al.* 2005, The Astrophysical Journal, 626, 128

Peñarrubia J., Walker M. G., Gilmore G., 2010, AIPC, 1240, 375

Perets, H. B., & Fabrycky, D. C. 2009, arXiv:0901.4328

Phinney, E. S. 1993, Structure and Dynamics of Globular Clusters, ASPC, 50, 141

Plummer, H. C. 1911, Royal Astronomical Society, Monthly Notices, 71, 460

Reddy, B. E. 2007, IAU Symposium, 241, 209

Renzini, A. 1994, Astronomy and Astrophysics, 285, L5

Robin, A. C., Reylé, C., Derrière, S., & Picaud, S. 2003, Astronomy and Astrophysics, 409, 523

Rocha-Pinto, H. J., Majewski, S. R., Skrutskie, M. F., & Crane, J. D. 2003, The Astrophysical Journal, Letters, 594, L115

Rubin, V. C. 1979, The Large-Scale Characteristics of the Galaxy, 84, 211

Rubin, V. C. 1983, Science, 220, 1339

Ryan, S. G., & Norris, J. E. 1991, The Astronomical Journal, 101, 1865

Scarpa, R., Marconi, G., & Gilmozzi, R. 2003, Astronomy and Astrophysics, 405, L15

Scarpa, R., Marconi, G., & Gilmozzi, R. 2004a, Dark Matter in Galaxies, 220, 215

Scarpa, R., Marconi, G., & Gilmozzi, R. 2004b, in "Baryons in Dark Matter Halos", eds. R. Dettmar *et al.*, SISSA, Proceedings of Science, 55.1, http://pos.sissa.it

Scarpa, R., Marconi, G., Gilmozzi, R., & Carraro, G. 2007, The Messenger, 128, 41

Searle, L., & Zinn, R. 1978, The Astrophysical Journal, 225, 357

Sérsic, J. L. 1968, Cordoba, Argentina: Observatorio Astronomico, 1968

Siebert, A., *et al.* 2008, Royal Astronomical Society, Monthly Notices, 391, 793

Skrutskie, M. F., *et al.* 2006, The Astronomical Journal, 131, 1163

Sollima A., Bellazzini M., Smart R. L., Correnti M., Pancino E., Ferraro F. R., Romano D., 2009, MNRAS, 396, 2183

Starkenburg, E., *et al.* 2009, The Astrophysical Journal, 698, 567

Tollerud, E. J., Bullock, J. S., Strigari, L. E., & Willman, B. 2008, The Astrophysical Journal, 688, 277

Trager, S. C., King, I. R., & Djorgovski, S. 1995, The Astronomical Journal, 109, 218

Valenti, E., Ferraro, F. R., & Origlia, L. 2007, The Astronomical Journal, 133, 1287

Velazquez, H., & White, S. D. M. 1999, Royal Astronomical Society, Monthly Notices, 304, 254

Villalobos, Á., & Helmi, A. 2008, Royal Astronomical Society, Monthly Notices, 391, 1806

von Hippel, T., & Bothun, G. D. 1993, The Astrophysical Journal, 407, 115

Watkins L. L., Evans N. W., An J. H., 2010, MNRAS, 709

Weil M. L., Pudritz R. E., 2002, AAS, 34, 1190

White, S. D. M., & Rees, M. J. 1978, Royal Astronomical Society, Monthly Notices, 183, 341

Willman, B., *et al.* 2005a, The Astrophysical Journal, Letters, 626, L85

Willman, B., *et al.* 2005b, The Astronomical Journal, 129, 2692

Yanny, B., *et al.* 2004, The Astrophysical Journal, 605, 575

York, D. G., *et al.* 2000, The Astronomical Journal, 120, 1579

Yusifov, I. 2004, The Magnetized Interstellar Medium, 165

Zucker, D. B., *et al.* 2006, The Astrophysical Journal, Letters, 643, L103

Zwicky, F. 1933, Helvetica Physica Acta, 6, 110